

Dissertation
submitted to the
Combined Faculties for the Natural Sciences and for Mathematics
of the Ruperto-Carola University of Heidelberg, Germany
for the degree of
Doctor of Natural Sciences

Presented by
M.Sc. Ina Karen Stoeck
Born in Lausanne, Switzerland
Oral Examination: 20.06.2016

The role of cellular lipid homeostasis in the hepatitis C virus replication cycle

**Referees: Prof. Dr. R. Bartenschlager
Prof. Dr. O. Fackler**

Declaration

The applicant, Ina Karen Stoeck, declares that she is the sole author of the submitted dissertation and no other sources for help apart from those specifically referred to have been used. Additionally, the applicant declares that she has not applied for permission to enter examination procedure at another institution and this dissertation has not been presented to another faculty and has not been used in its current or any other form in another examination.

Date

Signature

Acknowledgement

This study was conducted under the supervision of **Prof. Dr. Ralf Bartenschlager** at the Molecular Virology Unit, Department of Infectious Diseases at the University Hospital of Heidelberg. The work was funded by the **Marie-Curie actions „EUVIRNA“, a European Training Network on (+) RNA Virus Replication and Antiviral Drug Development.**

First of all I would like to thank **Ralf** for his encouragement and support throughout my entire PhD. I am very grateful for your constructive input and the freedom that I obtained to develop own ideas. Thank you for being a greatly supportive, enthusiastic, patient and fair supervisor. I would also like to thank **Prof. Dr. Volker Lohmann** for constructive ideas and discussions during lab-meetings and our annual retreats.

In addition I want to thank **Prof. Dr. Oliver T. Fackler** for agreeing to be my second supervisor. Furthermore I wish to thank **PD. Dr. Karin Müller-Decker** and **Dr. Pierre-Yves Lozach** for being part of my PhD Defense Committee.

Furthermore I would like to thank **Dr. Gualtiero Alvisi** that started the LD RNAi screen project and was a kind and helpful supervisor during the first year of my PhD. Thank you for introducing me into the laboratory practice and for being of such a positive nature. Moreover I would like to thank **Prof. Dr. Lars Kaderali and his research group** for their important contribution to this PhD project. In addition I would like to thank **Dr. Vibor Laketa** for his technical assistance, as well as **Inés and David** for their efforts and contributions to the LTP project. In addition I want to thank **Jiji** for her positive spirit and her support regarding the live cell imaging. I further want to thank **Eliana, David** and **Jamie** for their constructive critiques and proofreading activities concerning this manuscript.

During the course of this PhD I faced lots of great moments but also plenty of challenges. I owe it to the **members of the AGB** that I truly enjoyed every day working in this lab. Thank you for creating such a great, open-minded and friendly atmosphere! Indeed I have made lots of friends while working in this group to which I owe that Heidelberg became part of home. Thank you **Eli, Carola, Jiji, Danijela, Hanna** and **Nina** for having become true friends. I enjoyed and appreciate the time spent with you during our city or ski trips, at sports, during holidays, at C. Nerd, at cake times..... and at many more moments. Special thanks go to **Pietro**, for being such a good EUVIRNA travel companion full of funny surprises. I also want to thank my friends **Emma, George, Roman** and **Bebiana** for all the good times we have spent and many more to come! I wish to thank my **friends from Zurich**. Although I have left the city almost 5 years ago you still make me feel like coming home and being part of it. This is true friendship! I furthermore want to thank my **Venice and boulder friends** that always managed to get my mind off work. You are such a fun crowd and I am glad to be part of it!

My deepest gratitude goes to my family. Without the unconditional love and support of **my parents** I would never be where and who I am. I do not take this for granted and know how blessed I am; there are simply no words to express my gratitude to you! I really wish to thank my **brother Christian**, for just being the older brother that takes care, for always having a good advice, for being steady and being a truly good person. I want to thank the rest of my family and wish that my grandparents would have been able to witness me becoming one of the Dr. Stoeck(s).

Summary

With approximately 160 million people being persistently infected with hepatitis C virus (HCV), which bears a high risk of serious liver damage (fibrosis, cirrhosis, hepatocellular carcinoma), infections with HCV represent a major global health burden. Recent advances in the development of HCV-specific direct acting antiviral drugs have substantially improved the success rates of antiviral therapy. Nevertheless major challenges such as high costs, high number of undiagnosed infections and the possibility of reinfection even after therapy-induced virus elimination remain. There is increasing evidence that infections with this hepatotropic virus are tightly linked to lipid metabolism. For instance, lipid droplets (LDs) play an important role in the replication cycle of HCV, but also of the related Dengue virus (DENV). Moreover, HCV induces profound upregulation of lipogenic genes and its replication is attenuated by certain statins, which are known inhibitors of the cholesterol synthesis pathway.

With the overall goal to decipher the role of cellular lipid homeostasis for the HCV replication cycle I have studied two interrelated aspects. The first one aimed at gaining a better insight into the link between HCV and LDs, the cellular lipid storage organelles. By performing a RNAi screen targeting host factors implicated in LD homeostasis the aim was to identify novel candidates involved in the replication cycle of HCV, and for comparative purposes, DENV, as well as genes involved in the regulation of LD-linked pathways. Obtained results highlighted a central role of LDs in the replication cycle of both viruses and revealed the cellular DEAD box RNA helicase 3 (DDX3) as a key factor in the replication cycle of HCV and DENV. By using reverse genetics and biochemical assays I found that DDX3 is recruited to LDs via the HCV core protein, but loss of recruitment had no discernable effect on the viral life cycle. Nevertheless, our results identified a yet unexplored role of DDX3 in the production of infectious HCV.

The second part of this PhD thesis focused on another aspect related to the link between HCV and lipid homeostasis. Similar to other positive-strand RNA viruses, HCV remodels endomembranes to generate viral replication factories. There is increasing evidence that HCV co-opts cellular pathways in order to generate a specific lipid microenvironment that harbors the viral replication machinery. Using a set of microscopy-based approaches I found that HCV reorganizes the distribution of free cholesterol and possibly recruits it from the plasma membrane to the sites of viral replication. To understand the molecular mechanisms responsible for the reshaping of the cholesterol distribution, I performed a small scale RNAi screen targeting a selection of lipid transfer proteins (LTPs) implicated in direct, non-vesicular lipid transport. In this way I identified several LTPs (i.e. Niemann-Pick disease type C1 (NPC1), Oxysterol-binding protein-related protein 1A, StAr-related lipid transfer domain protein 3, membrane associated phosphatidylinositol transfer protein 1) required for HCV replication, highlighting the critical role of endosomal cholesterol transport for efficient virus propagation. Pharmacological inhibition of endosomal cholesterol export induced lipid accumulation in lysosomal vesicles and impaired the transfer of free cholesterol to potential sites of viral replication. Concomitantly, viral RNA replication was impaired, implying that HCV RNA replication depends on the redistribution of plasma membrane unesterified cholesterol through the endosomal pathway. Thus, HCV might usurp LTPs such as NPC1 to allow recruitment of free cholesterol to the viral replication factories.

Zusammenfassung

Man schätzt dass weltweit ca. 160 Millionen Menschen chronisch mit dem Hepatitis C Virus (HCV) infiziert sind. Da diese Infektion die Wahrscheinlichkeit für schwere Leberschäden (Leberfibrose, Leberzirrhose, hepatozelluläres Karzinom) massiv steigert, stellen Infektionen mit dem HCV ein globales Gesundheitsproblem dar. Die Fortschritte in der Entwicklung effektiver und selektiver Wirkstoffe haben in den letzten Jahren maßgeblich zur Verbesserung der antiviralen Therapie beigetragen. Dennoch stellen die damit verbundenen hohen Kosten, die hohe Anzahl an nicht diagnostizierten Infektionen sowie die Möglichkeit der erneuten Infektion nach erfolgreicher antiviraler Therapie weiterhin eine große Herausforderung in der Bekämpfung der HCV Infektion dar. Es deutet immer mehr darauf hin, dass Infektionen mit diesem hepatotropen Virus stark an den Lipid Metabolismus der Wirtszelle gekoppelt sind. So spielen beispielsweise Fett Tröpfchen (LTs) eine wichtige Rolle im Replikationszyklus des HCV, aber auch in dem des verwandten Dengue Virus (DENV). Des Weiteren induziert HCV die Expression von Genen, die im zellulären Lipid-Metabolismus involviert sind. Darüber hinaus beeinträchtigt die Behandlung mit Statinen, welche Inhibitoren des zellulären Cholesterolsynthese Wegs sind, die Virusvermehrung.

Mit dem Ziel die Rolle der zellulären Lipid Homöostase im Vermehrungszyklus des HCV besser zu verstehen habe ich zwei komplementäre Aspekte adressiert. Im ersten Teil meiner Arbeit habe ich versucht einen besseren Einblick in die Funktion der LTs, den zellulären Lipidspeicherorten, im HCV Vermehrungszyklus zu erlangen. Ausgangspunkt war ein RNAi-basierter Suchtest, der zum Ziel hatte zelluläre Faktoren zu identifizieren welche sowohl für die zelluläre LT Homöostase also auch für den HCV und DENV Replikationszyklus relevant sind. Die hierbei erzielten Resultate zeigen, dass LTs von zentraler Bedeutung im Vermehrungszyklus beider Viren sind und deuten auf eine für beide Viren wichtige Funktion der zellulären DEAD box RNA Helikase 3 (DDX3) hin. Aufgrund der Ergebnisse biochemischer Versuche und reverser Genetik konnte ich feststellen, dass DDX3 durch das HCV Kapsidprotein an LTs rekrutiert wird, jedoch der Verlust dieser Rekrutierung keinen erkennbaren Einfluss auf die virale Vermehrung hat. Damit bleibt noch unklar, welche Funktion DDX3 für die Produktion von infektiösen Hepatitis C Viruspartikeln hat.

Im zweiten Teil meiner Doktorarbeit fokussierte ich mich auf einen weiteren Aspekt der Wechselwirkung zwischen HCV und der zellulären Lipid Homöostase. Wie auch schon für andere Plusstrang RNA Viren beobachtet, induzieren die HCV Proteine eine massive Umorganisation intrazellulärer Membranen, die ein wesentliches Element der viralen Vermehrungsfabriken darstellen. Diese Vermehrungsfabriken besitzen eine spezifische Lipidzusammensetzung. Mit Hilfe verschiedener Mikroskopie-basierter Experimente konnte ich feststellen, dass das HCV die Verteilung von unesterifiziertem Cholesterol in der Zelle beeinflusst und dieses Lipid möglicherweise von der Plasmamembran zu den Replikationsorganellen rekrutiert wird. Im nächsten Schritt versuchte ich die molekularen Mechanismen aufzudecken, die es dem Virus erlauben diese Umverteilung von Cholesterol zu induzieren. Zu diesem Zweck habe ich einen RNAi Suchtest durchgeführt mit dem Ziel die für das HCV wichtigen Proteine des direkten Lipid Transports zu identifizieren. Auf diese Weise konnte ich verschiedene Lipid Transport Proteine (LTPs) wie etwa das Niemann-Pick Disease Type C1 Protein, Oxysterol-binding protein-related Protein 1A, StAr-related lipid transfer domain Protein 3 oder das membrane associated phosphatidylinositol transfer protein 1 identifizieren, welche wichtig für die Vermehrung des HCV sind. Diese Ergebnisse deuten auf eine wichtige Rolle des endosomalen Cholesterol Transports im viralen Vermehrungszyklus. So führte die pharmakologische Inhibierung des endosomalen

Cholesterol Transports zu einer Anreicherung von Lipiden in lysosomalen Vesikeln und reduzierte darüber hinaus den Transport von unesterifiziertem Cholesterol zu den viralen Replikationsorganellen. Gleichzeitig konnte ich beobachten, dass die virale RNA Vermehrung reduziert war. Es ist deshalb zu vermuten, dass die Vermehrung der viralen RNA von der Umverteilung und Rekrutierung von Cholesterol von der Plasmamembran durch den endosomalen Weg abhängt. Demzufolge scheint das HCV die Funktion von LTPs wie beispielsweise NPC1 zu nutzen, um unesterifiziertes Cholesterol zu den viralen Vermehrungsfabriken zu rekrutieren.

Table of Content

Declaration	i
Acknowledgements	iii
Summary	iv
Zusammenfassung	v
Table of Content	vii
Figures	x
Tables	xii
Abbreviations	xiii
1 Introduction	1
1.1 General aspects of hepatitis C virus (HCV)	2
1.1.1 Hepatitis	2
1.1.2 Discovery and classification of HCV	2
1.1.3 Epidemiology and treatment	3
1.2 Molecular biology of HCV	5
1.2.1 HCV genome organization and viral proteins	5
1.2.2 Tools to study the HCV replication cycle	10
1.2.3 The viral replication cycle	11
1.2.4 HCV and cellular lipid metabolism	14
1.3 Dengue virus – lipid droplets and the membranous web	17
1.4 The DEAD box RNA helicase 3, X-linked, (DDX3X, DDX3)	18
1.5 Cellular membrane homeostasis	19
1.5.1 Cellular membrane compartmentalization	19
1.6 Intracellular lipid traffic	20
1.6.1 Lipid transfer protein (LTP)-assisted lipid transport	21
1.6.2 Lipid transfer proteins involved in sterol transport	23
1.6.3 Lipid transfer proteins – Niemann-Pick Disease Type C (NPC) 1 (NPC1) protein	25
1.6.4 Sterol transport and sterol homeostasis	26
1.6.5 Lipid droplets	27
1.7 Aim of study	29
2 Materials and Methods	31
2.1 Materials	32
2.1.1 Antibodies and dyes	32
2.1.2 Buffers and solutions	33
2.1.3 Plasmid constructs	34
2.1.4 Chemicals and compounds	36
2.1.5 Media and antibiotics	37
2.1.6 Enzymes and kits	37

2.1.7	DNA and RNA oligonucleotides	38
2.1.8	Instruments	40
2.1.9	Transfection reagents	40
2.1.10	Cell culture	40
2.2	Methods	42
2.2.1	Cell culture	42
2.2.2	Nucleic acid standard methods	42
2.2.3	Standard cloning methods	44
2.2.4	Protein analysis standard methods	46
2.2.5	Virological methods	47
2.2.6	Experimental procedures	48
2.2.7	RNAi screens	51
2.2.8	Biochemical assays	53
2.2.9	Imaging	54
2.2.10	Statistical analysis	56
3	Results	59
3.1	Identification and characterization of novel factors involved in lipid droplet homeostasis and in the replication cycle of HCV and DENV	60
3.1.1	Setup, performance and statistical analysis of the LD-RNAi screen	60
3.1.2	Performance of control siRNAs and hit calling	62
3.1.3	Analysis of the connection of LD-dependent viruses and the lipid storage organelle	65
3.1.4	Bioinformatic analysis of LD RNAi screen	66
3.1.5	Follow-up studies of the LD RNAi screen	68
3.2	Studying the role of LTP-assisted cholesterol traffic in HCV replication	87
3.2.1	Distribution of unesterified cholesterol in HCV infected cells	87
3.2.2	Identification of important Lipid transfer proteins (LTPs) required for the HCV and DENV replication cycle	100
3.2.3	Evaluating the role of the Niemann-Pick Disease Type C1 protein in the HCV replication cycle	107
3.2.4	Studying the effect of U18666A on HCV replication	113
3.2.5	Studying the impact of sterol synthesis inhibitors on sterol homeostasis and HCV replication	117
3.2.6	Elucidating the biological relevance of endosomal lipid traffic in HCV replication	125
4	Discussion	133
4.1	A comparative RNAi screen targeting potential LD-factors to study their implications in the replication cycle of HCV and DENV	134
4.1.1	RNAi screen analysis	134
4.1.2	Potential role of COPI in HCV and DENV particle production as well as LD homeostasis	136
4.1.3	High hit rate of LD RNAi screen indicates central role of the lipid storage organelle in the replication cycles of LD-dependent viruses	138
4.1.4	Studying the role of the DEAD box RNA helicase 3 in the replication cycle of HCV and DENV	140
4.2	Studying the role of lipid transfer protein mediated cholesterol transport in the HCV replication cycle	149
4.2.1	Studying the distribution of free cholesterol in HCV infected cells	149
4.2.2	Evaluating the role of LTPs implicated in direct lipid transfer in the replication cycle of HCV and DENV	152

4.2.3	The role of LTP-assisted cholesterol traffic through the endosomal vesicular pathway in HCV replication	155
5	Conclusion and perspectives	165
6	Supplement	171
6.1	<i>Supplementary Figures</i>	172
6.2	<i>Supplementary Tables</i>	176
6.3	<i>Supplementary Movies</i>	177
7	References	181
8	Publications and presentations	201
8.1	<i>Publications</i>	202
8.2	<i>Oral Presentations</i>	202
8.3	<i>Poster presentations</i>	202

Figures

Figure 1.1	Countries according to their most prevalent HCV genotypes	4
Figure 1.2	Hepatitis C virus genome organization	5
Figure 1.3	Schematic representation of the membrane topology of cleaved HCV proteins	6
Figure 1.4	Schematic representation of the HCV replication cycle	12
Figure 1.5	Scheme of Lipid transfer protein (LTP)-assisted lipid traffic at membrane contact sites	21
Figure 1.6	Model of lipid transfer at the Golgi/ER interface mediated by the membrane associated phosphatidylinositol transfer protein 1 (PITPNM1), the oxysterol-binding protein (OSBP) and the ceramide transfer protein (CERT)	22
Figure 1.7	Scheme of Oxysterol-binding protein (OSBP) mediated cholesterol and phosphatidylinositol-4-phosphate (PtdIns4P) exchange at ER/ Golgi membrane contact sites	24
Figure 3.1	Primary screen setup	61
Figure 3.2	Performance of control siRNAs	63
Figure 3.3	Primary and deconvolution screen results	65
Figure 3.4	Analysis of the relationship of the viral replication cycle and LD biology	66
Figure 3.5	Schematic representation of the subcellular localization of hit candidates identified by the primary screens	67
Figure 3.6	Candidates for follow-up studies	68
Figure 3.7	DDX3 knockdown affects HCV reporter but not DENV reporter virus replication cycle	70
Figure 3.8	Effect of DDX3 gene knockdown on RNA replication of <i>gt1b</i> and <i>gt2a</i> stable <i>Firefly</i> luciferase replicon cell lines	71
Figure 3.9	Effect of DDX3 on later stages of full-length <i>Renilla</i> luciferase reporter virus replication	73
Figure 3.10	Cellular distribution of DDX3 in HCV or DENV infected cells	74
Figure 3.11	Localization of DDX3 to lipid droplets is dependent on the presence of the HCV core protein	75
Figure 3.12	HCV isolate specific differences in DDX3 relocalization efficiency	77
Figure 3.13	Schematic representation of viral constructs used in the subsequent experiments	78
Figure 3.14	Effect of Y35A HCV core point mutation on DDX3 distribution	79
Figure 3.15	Effect of Y35A HCV core point mutation on the full replication cycle of HCV	80
Figure 3.16	Effect of F24A HCV core point mutation on the cellular distribution of DDX3	81
Figure 3.17	Effect of F24A HCV core point mutation on the full replication cycle of HCV	83
Figure 3.18	Effect of core mutation on neutral lipid content of HCV replicating cells	85
Figure 3.19	Sensitivity of <i>wild-type</i> and F24A core mutant virus towards DDX3 gene knockdown	86
Figure 3.20	Distribution of free/ unesterified cholesterol in HCV infected and mock cells	88
Figure 3.21	Pretests for Topfluor-Cholesterol (TFC) live cell imaging	91
Figure 3.22	Experimental setup of live cell imaging of Topfluor-Cholesterol (TFC) added early or late in HCV replication	93
Figure 3.23	Topfluor-Cholesterol (TFC) dynamics at early and late stages of HCV replication	94
Figure 3.24	Topfluor-Cholesterol (TFC) dynamics in the early phase upon TFC addition at early or late stages of HCV replication	96
Figure 3.25	Topfluor-Cholesterol (TFC) and NS5AmCherry trafficking over time	98
Figure 3.26	Topfluor-Cholesterol (TFC) recovery from NS4B-HA mediated DMV purification	99
Figure 3.27	Lipid transfer protein (LTP) RNAi screen setup	102
Figure 3.28	LTP RNAi screen results	103
Figure 3.29	Validation of selected candidates by shRNA-mediated knockdown	106

Figure 3.30	NPC1 gene knockdown reduces HCV RNA replication	109
Figure 3.31	Subcellular localization of NPC1 in HCV infected cells	111
Figure 3.32	Effect of NPC1 gene knockdown on the cellular distribution of free cholesterol	112
Figure 3.33	Effect of U18666A treatment on cellular localization of free cholesterol	114
Figure 3.34	Effect of U18666A treatment on the early phase of HCV replication	116
Figure 3.35	Effect of inhibitors of the sterol synthesis and trafficking pathway on the subcellular distribution of unesterified cholesterol	119
Figure 3.36	Effect of inhibitors of the sterol synthesis and trafficking pathway on the subcellular distribution of the ganglioside GM1	120
Figure 3.37	Effect of sterol synthesis and trafficking inhibitors on established viral genome replication	122
Figure 3.38	Effect of sterol synthesis and trafficking inhibitors on replication of subgenomic replicons of different genotypes	123
Figure 3.39	Effect of sterol synthesis and trafficking inhibitors on transcript levels of HMGCoA reductase, LDLR Receptor (LDLR) and the ATP binding cassette sub-family A member 1 (ABCA1)	125
Figure 3.40	Experimental setup of live cell imaging of Topfluor-Cholesterol (TFC) in U18666A treated cells early or late in HCV replication	126
Figure 3.41	Live cell imaging of Topfluor-Cholesterol (TFC) in U18666A treated cells early or late in HCV replication	127
Figure 3.42	Live cell imaging of Topfluor-Cholesterol (TFC) and NS5AmCherry in U18666A treated cells early or late in HCV replication	129
Figure 3.43	Effect of U18666A on HCV induced membranous web	131
Figure 4.1	Hypothetical model of lipid transfer through the concerted action of lipid transfer proteins at ER/ golgi contact sites	153
Figure 5.1	Hypothetical model of LTP-assisted cholesterol transport through the endocytic pathway to the viral replication sites	168

Tables

Table 2.1	Primary antibodies and dyes used in this study	32
Table 2.2	Secondary antibodies used in this study	33
Table 2.3	Buffers and solutions used for protein work	33
Table 2.4	Buffers and solutions used for nucleic acid work	33
Table 2.5	General buffers and solutions	34
Table 2.6	Buffers and solutions for luciferase activity assays	34
Table 2.7	pTM-based expression constructs	34
Table 2.8	pFK-based viral vectors used in this study	35
Table 2.9	NPC1 expression constructs	36
Table 2.10	Retroviral vectors	36
Table 2.11	Chemicals and reagents	36
Table 2.12	Compounds used in this study	36
Table 2.13	Media	37
Table 2.14	Antibiotics	37
Table 2.15	Enzymes	37
Table 2.16	Kits	37
Table 2.17	DNA oligonucleotides used for cloning	38
Table 2.18	DNA oligonucleotides used for qPCR	38
Table 2.19	shRNA oligonucleotides used in this study	39
Table 2.20	siRNA oligonucleotides used in this study	40
Table 2.21	Instruments relevant for this study	40
Table 2.22	Transfection reagents	40
Table 2.23	Constructs generated in this study with the respective restriction enzymes used for cloning	45
Table 2.24	NPC1 expression plasmids used in this study	46
Table 3.1	LTPs targeted in the RNAi screen	101

Abbreviations

ABCA	ABC transporter subfamily A	PFA	paraformaldehyde
ATP	adenosine triphosphate	p.inf.	post infection
	A, C, G, T, U DNA: cytosine, guanine, adenine, thymine, RNA: uracil	PBS	phosphate buffered saline
cDNA	complementary DNA	PCR	polymerase chain reaction
cplt	complete	PC	phosphatidylcholine
COPI	coat protein complex I	PEG	polyethylene glycol
DDT	Dithiothreitol	PM	plasma membrane
DDX3	DEAD-box helicase 3	Ptdins	phosphatidylinositol
DENV	Dengue virus	PtdSer	phosphatidylserine
DMSO	dimethyl sulfoxide	RC	replication complex
DMV	double membrane vesicle	RdRp	RNA-dependent RNA polymerase
DNA	deoxyribonucleic acid	RLU	relative light units
EE	early endosome	RLuc	<i>Renilla</i> luciferase
epo	electroporation	RNA	ribonucleic acid
ER	endoplasmic reticulum	RT	room temperature
EMCV	encephalomyocarditis virus	SDS	sodium dodecyl sulfate
FASN	fatty acid synthase	siRNA	small interfering RNA
FLuc	<i>Firefly</i> luciferase	shRNA	small hairpin RNA
gt	genotype	SR-BI	scavenger receptor BI
HA	hemagglutinin	START	StAR-related lipid transfer
HCV	hepatitis C virus	SMV	single membrane vesicle
HIV	human immunodeficiency virus	SVR	sustained viral response
HRP	horseradish peroxidase	TAG	triacylglycerol/triacylglyceride
IF	immunofluorescence	TCID ₅₀	tissue culture infectious dose 50
IFN	interferon	TFC	Topfluor-Cholesterol
IP	immunoprecipitation	UTR	untranslated regions
IRES	internal ribosome entry site	v/v	volume/volume
JFH1	Japanese fulminant hepatitis- 1	VLDL	very-low density lipoprotein
Kb	kilo base	w/v	weight/ volume
kDa	kilo Dalton	VSV	vesicular stomatitis virus
LB	lysogeny broth	vRNA	viral RNA
LD	lipid droplet	WB	Western Blot
LE	late endosome		
LDL	low density lipoprotein		
LDLR	low density lipoprotein receptor		
LTP	lipid transfer protein		
LY	lysosome		
LVP	lipovirion particle		
miRNA	micro RNA		
MMV	multimembrane vesicle		
ms	millisecond		
NPC	Niemann-Pick Disease Type C		
NS	non-structural proteins		
NT	non-targeting		
OSBPL	oxysterol-binding protein like		
PAGE	polyacrylamide gel electrophoresis		

1 Introduction

1.1 General aspects of hepatitis C virus (HCV)

1.1.1 Hepatitis

The term „**hepatitis**“ originates from the Greek *hēpar* = liver + *itis* = inflammation, which describes the inflammation of the liver. Hepatitis may result from several causes, such as prolonged abuse of alcohol or certain drugs, autoimmune or metabolic diseases, but also infectious agents such as bacteria or viruses [1]. The most common cause of hepatitis is the infection with either one of the five hepatitis viruses: hepatitis A virus (HAV), HBV, HCV, HDV and HEV. Due to their divergent molecular biology these viruses belong to different virus families, however all of them are strongly liver-tropic, causing liver inflammation. Acute infections with either virus might be asymptomatic or cause flu-like symptoms, jaundice (yellowing of the eyes and skin) abdominal pain, extreme fatigue, vomiting or nausea. While infections with HAV and HEV are mainly self-limiting, infections with type B, C and D often lead to chronic liver diseases, which increases the risk of infected patients to develop hepatocellular carcinoma (HCC) [2]. Acute infections with HCV remain most often unrecognized due to the lack of specific symptoms. Persistency is established in the majority (50-80%) of infected patients, which progressively develop hepatosteatosis and liver fibrosis, which is followed by liver cirrhosis and can then ultimately lead (in 3-5% of all chronically infected patients) to HCC [3]. Disease progression is suggested to be influenced by factors, such as age at time point of infection, gender, heavy alcohol consumption as well as co-infections such as with the Human Immunodeficiency virus (HIV) [4].

1.1.2 Discovery and classification of HCV

The **discovery** made in the 1970ies, that the disease of many patients suffering of transfusion associated hepatitis, was neither linked to an infection with HBV nor with HAV led to the search for the identification of the non-A non-B infectious agent [5]. It was only in 1989 that the HCV RNA genome was identified and isolated from non-A non-B positive patient serum [6].

HCV has been grouped to the genus of *Hepaciviruses* within the family of *Flaviviridae*, which comprises members of two more genera such as the pestiviruses (i.e. Border-Disease virus (BDV)) and the flaviviruses (i.e. Dengue virus). All members of this family are enveloped viruses of 40-60 nm in diameter that exhibit a positive-sense single-stranded RNA genome [7]. The high mutation rate of the RNA-dependent RNA polymerase of HCV and the lack of proof-reading both account for the high heterogeneity of the viral genome. Accordingly, HCV circulates as a highly heterogenic population, named quasispecies, in the

blood of infected patients [8]. Conversely, the diversity is constrained by the intimate dependency of the virus on the cellular machinery [9]. On the basis of sequence analysis, HCV variants are classified into 7 groups, designated as genotype 1-7, that differ by 31-33% in their nucleotide sequence. Each group comprises further variants, designated as subtypes (labeled by letter a, b, etc.) that vary from each other by 20-25 % in their nucleotide sequence [8-10]. Despite the substantial genetic divergence between the genotypes, all variants share phenotypic features, such as a common virion structure, similarities in the viral life cycle, and the ability to cause persistence. In contrast some viral counteractions that aim to protect the virus from clearance through the immune system, appear to be genotype-specific [9]. This becomes most clear when comparing the genotype specific susceptibility towards the standard-of-care (SOF) therapy, which allows the clearance of about 85% of all genotype 2 and 3 but only 45% of all genotype 1 infections. The mechanisms underlying these differences are still elusive [11].

1.1.3 Epidemiology and treatment

Since its discovery almost 30 years ago and having been recognized as major cause of liver cancer, HCV has been focus of intense research [12]. Currently 3% of the world's population is thought to be infected, 160 million people of which are chronically infected [13]. About 350000-500000 deaths per year are attributed to HCV infections, deaths mainly caused by liver cirrhosis or HCC [12, 14]. Globally, approximately 27% of all liver cirrhosis and 25% of HCCs are attributed to HCV, indicating the massive health burden caused by the viral infection [15]. HCV infections are found worldwide, however the prevalence differs between countries. In some cases a high prevalence in a given country could be traced back to the use of contaminated medical equipment. Indeed Egypt is suggested to have the highest prevalence in the world (estimated at >10%) likely caused by the reuse of contaminated syringes and needles during a large schistosomiasis eradication program in the 1980s [16]. Furthermore, countries located in Africa, Latin America, Eastern Europe and Asia have been reported to have prevalence rates of about 3%, while the infection rates in countries of North America and Western Europe are lower (< 2%) [14]. In developing countries, new infections are mainly caused by the use of unscreened blood or blood products or unsterile medical equipment, while in developed countries the major transmission route is through unsafe injection drug use. Sexual transmission or the direct spread from mother to her baby have been reported but occur rather seldom [12, 13]. Interestingly genotypes are differently distributed throughout the world, with genotype 1 being the most common type accounting for 46.2% of all HCV infections. While genotype 1 is widely spread and accounts for the majority of infections in Europe, the Americas, Australia, and Asia, the second most common

4 | Introduction

genotype, genotype 3, is mainly restricted to South Asia and some Scandinavian countries. Genotypes 2, 4, and 6 are responsible for the majority of the remaining cases. Genotype 4 is mainly found in Africa and the Middle East, including Egypt. Genotype 6 is most common in South East Asia and genotype 2 is mainly in west and central Africa. Genotype 5 is only present in South Africa while the recently discovered genotype 7 was isolated in Canada from a patient from Central Africa (Figure 1.1) [17, 18]. As indicated above, the strong heterogeneity of HCV poses a great challenge in the development of pan-genotypic treatments or vaccines [12, 18].

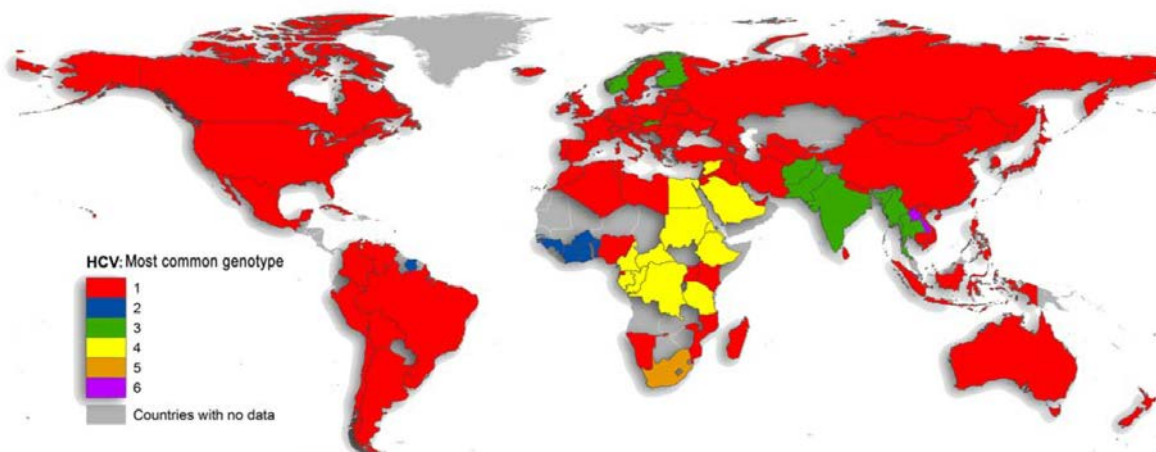


Figure 1.1 Countries according to their most prevalent HCV genotypes. Data includes 1217 studies of 117 countries, which represents 90% of the world's population. Genotype 1 (indicated in red) is the most prevalent worldwide and accounts for 46.2% of all infections. This is followed by genotype 3, giving rise to 30.1% of all infections, especially found in South Asia and parts of Scandinavia. The rest of all infections is caused by genotype 2, 4, and 6. Infections with genotype 5 are rather rare (1%). Adapted from [18].

The ultimate goal of **antiviral therapy** is the cure from viral infection, which is indicated by a sustained virological response (SVR), defined as the absence of detectable HCV RNA in the patient's serum 24 weeks after the end of treatment [19]. The standard-of-care (SOC) therapy comprises the combination of PEGylated interferon-alpha and the nucleoside analogue Ribavirin [20]. As indicated earlier, the success of SOC largely depends on the viral genotype. The fact that infections with genotype 1, the worldwide most prevalent genotype, are cleared with a success rate lower than 50% highlights the need of more efficient anti-viral therapeutics [21]. 2011 two direct-acting antiviral agents (DAA) targeting the NS3/4A protease, namely boceprevir and telaprevir, were approved and implemented in triple combination with the SOC for genotype 1 infections, thereby drastically increasing the SVR rate to around 75% [20]. However, the low barrier to resistance for these drugs, in addition to the severe side effects of triple therapy raises the need for improvement. Novel DAAs are currently being developed that aim at pan-genotypic activity with limited side effects [22]. Vaccine development has been challenging due to the large genomic heterogeneity of the

virus and the lack of immuno-competent small animal models that would allow the evaluation of the efficacy of vaccine candidates [23].

1.2 Molecular biology of HCV

1.2.1 HCV genome organization and viral proteins

The **HCV RNA genome** consists of a single-stranded RNA molecule of positive polarity. A single open reading frame (ORF) comprises approximately 3000 amino acids that encode for 10 viral proteins [11]. At its 5' and 3' end the ORF is flanked by non-translated regions (NTRs) which form particular secondary RNA structures. Those structures are essential for viral genome replication and cannot be complemented in *trans*, thus called *cis*-acting RNA elements. Importantly the 5' NTR encodes an internal ribosomal entry site (IRES) that directs cap-independent translation of the viral genome. Given the genome's positive polarity, the viral RNA is directly translated by cellular ribosomes, giving rise to a viral polyprotein precursor [24, 25]. The N-terminus of the polyprotein comprises the structural proteins core and envelope glycoproteins, E1 and E2 that are constituents of the HCV particle. Together with the viroporin p7 and NS2, they are mediating particle assembly and release and thus are designated as the assembly module. The remaining non-structural (NS) proteins are involved in steps of RNA replication, thus summarized as the replication module (Figure 1.2) [11].

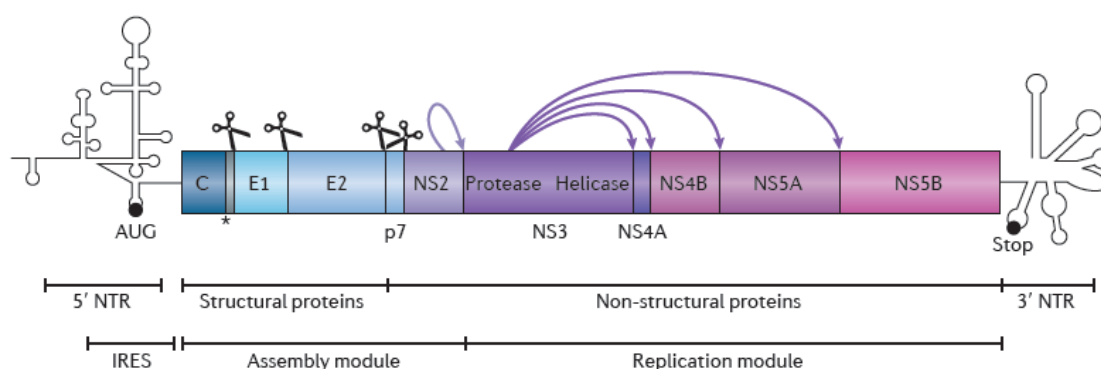


Figure 1.2 Hepatitis C virus genome organization. The viral genome encodes for a single open reading frame (ORF) flanked at its 5' and 3' end by non-translated regions (NTR) important for RNA replication. Simplified RNA secondary structure of both NTRs as well as the start (AUG) and stop codon are indicated. An internal ribosomal entry site (IRES) is present in the 5' NTR which induces ribosome-mediated translation of viral RNA giving rise to a single polyprotein precursor which is cleaved by viral proteases NS2-3 and NS3-4A (light and dark purple arrows) and cellular signal peptidases (scissors). The viral genome can be divided into the structural proteins comprising core and the two envelope glycoproteins E1 and E2 and the non-structural (NS) proteins 2, 3, 4A, 4B, 5A, 5B. The viral core protein, E1, E2, p7 and NS2 are required for virus assembly, thus designated as the assembly module, while the remaining proteins are involved in genome replication and thus called the replication module. The asterisk indicates the cleavage of the core protein at its carboxy-terminal region, necessary for its translocation to lipid droplets. Adapted from [11].

Interestingly all of the NS proteins have further been implicated in HCV assembly, although the precise mechanism is far from being understood [26]. Co- and post-translational processing of the viral polyprotein by cellular and viral proteases yields in mature structural and non-structural (NS) proteins. Endoplasmic reticulum (ER) signal peptidases catalyze the cleavage at the envelope glycoprotein E1/E2, E2/p7, p7/NS2 and core/E1 junction [11]. The latter cleavage yields in a core protein that remains bound to the ER through its association with the E1 signal peptide. Subsequent processing through a signal peptide peptidase then allows the liberation of the core protein from the ER and its association with lipid droplets [27]. Processing of the non-structural proteins is mediated by the viral proteases NS2-3, and NS3-4A [11, 21]. A general feature shared by all viral proteins is their association with host cell membranes. E1, E2, NS2, p7 as well as NS4B exhibit transmembrane domains, while hydrophobic domains such as amphipathic helices allow the tethering of the viral core protein, NS3, NS5A, NS5B and NS4A to membranes. The latter also acts as adaptor for NS3 [11, 28]. The membrane topology of the viral proteins is schematically depicted in Figure 1.3.

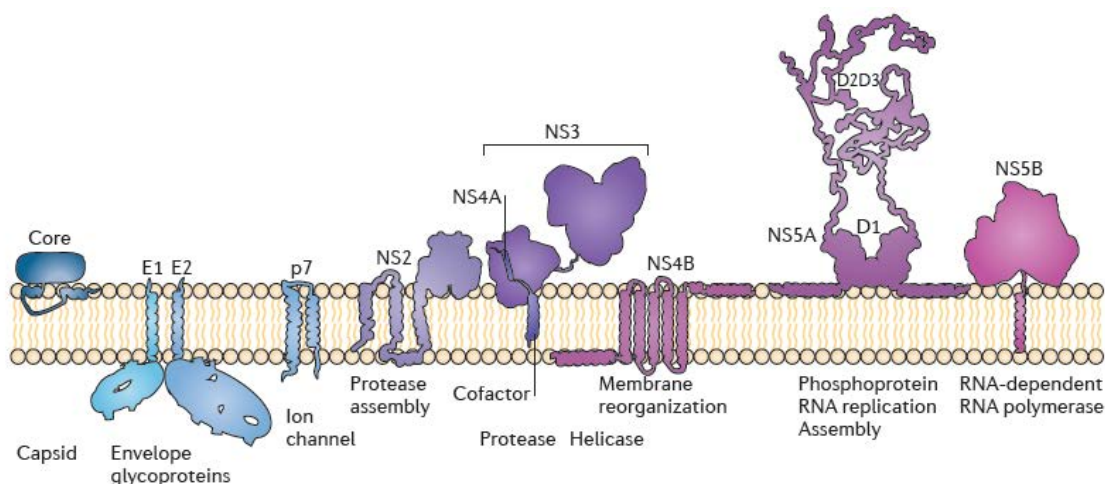


Figure 1.3 Schematic representation of the membrane topology of cleaved HCV proteins. The viral proteins are tethered either through transmembrane domains (E1, E2, p7, NS4B) or hydrophobic segments such as amphipathic helices (core, NS3, NS4A, NS5A, NS5B) to host cell membranes. NS3 is associated with membranes through its cofactor NS4A but also through a small alpha-helix. Note that most of the viral proteins form higher oligomeric complexes or homo-/ heterodimers, but only a NS5A dimer is depicted. For instance the transmembrane domains of E1 and E2 are involved in their heterodimerization. Predicted functions of the proteins are indicated. Adapted from [11, 28].

Unraveling **HCV protein function** has been the focus of intense research and a brief overview of the current general concepts is presented in the next section.

The **HCV core protein (21-23 kDa)** is the first protein being synthesized from the incoming viral RNA and thought to constitute the viral nucleocapsid [29]. The premature core protein is composed of three domains, of which large parts of the C-terminal domain 3 are involved in regulating the premature protein's recruitment to the ER [30]. As indicated earlier, proteolytic

cleavage of the C-terminal 20 amino acids allows the release of the mature core protein and its subsequent association with lipid droplets [27]. The mature protein is divided by its amino acid composition into two domains. The N-terminal domain 1 (approximately 117 amino acids) is largely hydrophilic being enriched in positively charged amino acids, that most likely contribute to the RNA binding capacity of the protein [31, 32]. Domain 1 further catalyzes the homo-oligomerization of the core protein but also its interaction with the glycoprotein E1 which might substantially contribute to nucleocapsid formation [33, 34]. The hydrophobic domain 2 at the C-terminus mediates membrane association, for example to lipid droplets, which is suggested to be important for core protein folding and stability [35]. An alternative reading frame resulting from a ribosomal frameshift near codon 11 in the HCV core sequence gives rise to a protein of up to 160 amino acids, designated alternative reading frame protein (ARFP). Although this protein was found to be expressed in HCV infected patients, its function in viral infection remains elusive [28, 36]. Interestingly the HCV core protein, in addition to NS4B (of genotype 3a), was reported to contribute to HCV-associated steatosis, most likely through the induction of the expression of lipogenic genes, thereby enhancing *de novo* lipid synthesis and uptake [37, 38]

The **envelope glycoproteins E1 (35 kDa) and E2 (70 kDa)** are heavily glycosylated type 1 transmembrane proteins with a large N-terminal ectodomain facing the ER lumen, and a small C-terminal transmembrane domain that contains an ER retention signal [39]. E1 and E2 are suggested to heterodimerize through their transmembrane domain [40]. Being constituents of the virion, they are suggested to be involved in early stages of viral entry such as receptor binding and membrane fusion [41, 42].

P7 (7 kDa) is a small hydrophobic ER resident protein, with two transmembrane passages linked through a short hydrophilic segment [43]. Given its ability to form pores in artificial membranes and its ion channel activity the protein is suggested to belong to the family of viroporins [28, 44-46]. P7 was shown to be dispensable for HCV RNA replication and this is most likely the case for virus entry too. However, it appears to be of significant importance for infectious particle production, which might require its ion channel activity but also direct interactions with other viral proteins, such as the non-structural protein 2 [44, 47, 48].

Similar to p7, **NS2 (23 kDa)** is not directly required for RNA replication but essential for infectious virion assembly [28, 49]. NS2 is a cysteine protease localized to the ER membrane through three N-terminal transmembrane domains [50]. Together with the N-terminal one third of NS3 it catalyzes its autoproteolytic cleavage from the N-terminus of NS3, which is important to allow the formation of an active replicase [51]. NS2 is believed to act as scaffold

for virion assembly by bringing together constituents of the replicase machinery (NS3, NS5A) and the envelope glycoproteins. Indeed NS2 was shown to interact with NS3, NS5A, p7 and the envelope glycoprotein E2. Mutations that abrogate this interaction were also reported to impair HCV particle production, while pseudoreversions that restored these interactions also restored particle production to various extents [52, 53].

Besides being a cofactor for the NS2 protease, **NS3 (72 kDa)** exhibits multiple enzymatic activities. The N-terminal part of NS3 forms together with its cofactor **NS4A (16 kDa)** a protease that mediates the downstream processing of the polyprotein [54]. Two-thirds of the NS3 C-terminus harbors a RNA helicase/NTPase function, which mediates the ATP hydrolysis coupled unwinding of RNA duplexes or single-stranded RNA regions with extensive secondary structures [55, 56]. While the precise function of NS3 RNA helicase activity in the viral replication cycle remains elusive the protein has been shown to be involved in HCV RNA replication and particle assembly [57, 58]. NS3-4A is localized to the ER and can be found in ER–mitochondrial membrane contact sites, which likely promotes its ability to interfere with the cellular innate immune induction. In fact NS3-4A is able to cleave the RIG-I (retinoic acid inducible gene) adaptor MAVS (mitochondrial antiviral signaling protein) and the Toll-like receptor 3 adaptor protein TRIF [59] that mediate the type I interferon induction in response to upstream viral RNA recognition [60].

While the N-terminus of **NS4A (16 kDa)** is involved in tethering NS3 to cellular membranes, and the protein's central core serves as cofactor to form the functional NS3-4A protease, little is known about the function of the C-terminal part of NS4A [61]. Alanine scanning mutagenesis studies on the protein's C-terminus suggested an involvement of NS4A in RNA replication as well as particle production, possibly by interacting with other viral NS proteins [62, 63].

NS4B (27 kDa) is an integral membrane protein that contains a central core of four predicted transmembrane domains, while its C- and N-terminus are suggested to face the cytoplasm [64]. Only little is known about the function of NS4B binding to viral RNA and its NTPase activity [65]. In contrast the best described characteristic of NS4B is its ability to deform membranes. Upon overexpression, NS4B was found to localize to cytoplasmic spots [64]. Immunoelectron microscopy studies further suggested that these spots might correspond to a collection of highly curved membranes that were designated as the membranous web (MW) [64-66]. The latter was shown to harbor components of the replicase as well as subgenomic RNA and thought to represent the viral replication factories [67]. How NS4B can deform intracellular membranes remains elusive, however, its oligomerization appears to be

of importance. NS4B is thought to be a key driver of the virally induced membranous web, and therefore plays a crucial role in HCV RNA replication [68]. The recent observation that a particular mutation within the NS4B gene enhanced virion biogenesis, while not affecting RNA replication, points to a novel function in HCV particle production [69].

The present literature on **NS5A (56-58 kDa)** is enormous indicating the strongest interest in this still enigmatic protein. Although no enzymatic activity has been described for NS5A it is involved in HCV RNA replication, particle production and the modulation of the cellular environment [70]. Two differentially phosphorylated forms of NS5A, designated according to their molecular mass namely the basal p56 and hyperphosphorylated p58, have been described. The relevance of the NS5A phosphorylation status is unknown, however it was reported that changes in the p56/p58 ratio alter RNA replication efficiency [71]. NS5A is tethered through its N-terminal alpha helix to the cytosolic leaflet of the ER membrane, which is crucial for RNA replication [72]. Furthermore, the protein is divided into one highly structured domain (DI) and two unstructured domains (DII and DIII), which are separated by so-called low-complexity sequences (LCS). While large parts of DII and DIII can be deleted without affecting RNA replication, DI seems to be essential. Although it is widely accepted that domain I mediates NS5A dimerization, the mode of dimerization and the thus resulting structure of the dimer remains under debate [11]. Extensive mutagenesis studies on DII and DIII revealed that only the very C-terminal part of DII is necessary for RNA replication, while the remainder appears to be dispensable. Similarly complete or large deletions within DIII do not alter RNA replication efficiency, which allowed the generation of fluorescent fusion proteins of NS5A in the context of a RNA replication competent replicon [73]. Nevertheless these mutants are substantially impaired in particle production, most likely due to the loss of NS5A interaction with the viral core protein [74, 75]. The highly unstructured character of DII and DIII is thought to promote the numerous interactions of NS5A with viral and cellular proteins. Indeed the list of NS5A interaction partners is extensive and believed to allow the virus to interfere with various cellular pathways [76]. One of the most prominent interaction partners is the Phosphatidylinositol-4-Kinase III alpha (PI4KIII α), an enzyme with lipid and protein kinase activity. The PI4KIII α kinase activity is thought to be stimulated through its interaction with NS5A, catalyzing the phosphorylation of the viral protein as well as of phosphatidylinositol (PtdInsP) leading to the massive accumulation of Phosphatidylinositol-4-phosphate (PtdIns4P) [77, 78]. Furthermore, NS5A was found to interact, depending on its phosphorylation status, with the vesicle-associated membrane protein A (VAP-A), which could possibly be important for the recruitment of downstream effectors such as the oxysterol-binding protein (OSBP) capable of binding VAP proteins [77, 79, 80]. A very recent study of two NS5A DIII mutants revealed distinct functions of the respective mutants in the

coordination of RNA encapsidation. In fact the mutation of a basic cluster disrupts NS5A-RNA binding, while the protein correctly localizes to core covered LDs. The presence of a functional serine cluster is important to recruit NS5A to LD-associated core, while the protein's RNA binding capacity remains unaltered [81]. It is proposed that NS5A, possibly in conjunction with NS2 [52], mediates the delivery of the viral genome from sites of RNA replication to the viral core protein (at LDs) for genome encapsidation [81].

Last but not least, **NS5B (65 kDa)** is the RNA-dependent RNA polymerase (RdRp) that catalyzes the propagation of the viral genome. The protein comprises a C-terminal catalytic domain that is linked to a hydrophobic transmembrane domain [57, 82, 83]. The viral RdRp uses the genomic RNA as template for the generation of a negative-strand RNA, from which then progeny RNA of positive polarity is generated [28].

1.2.2 Tools to study the HCV replication cycle

Despite the discovery of HCV in 1989, it took another ten years until the development of a first cell culture system that allowed to study viral RNA replication [84].

The establishment of the **subgenomic replicon** system was a major breakthrough that allowed to study the intracellular steps related to viral RNA replication and thus opened new doors for the search of antiviral drugs [84]. The subgenomic replicon is defined as the minimal viral genome capable of autonomous replication in cell culture. The first bicistronic replicon was established based on the full-length genome of gt1b, in which core to NS2 were replaced by a selection marker (neomycin phosphotransferase) under the control of the HCV IRES followed by the EMCV IRES regulating the expression of the non-structural proteins. Importantly the construct was flanked by the 3' and 5' NTR of HCV [85]. Further advances were made with the discovery of cell culture adaptive mutations present in the viral genome that were found to strongly enhance RNA replication [86, 87]. Additionally it appeared that throughout the selection process of replicon cells, only those that were most permissive were recovered, thus representing a small proportion of the whole cell population. This led to the observation that cell clones (Huh7.5 and Huh7/Lunet) that were "cured" from RNA replication through IFN-alpha treatment were more permissive to HCV RNA replication as compared to their parental cell line [88, 89]. These discoveries set the ground for the establishment of subgenomic replicons of different genotypes such as of 1a, 2a, 3a 4a, and 5a of which only genotype 2a does not require adaptive mutations for efficient RNA replication [87, 90-93]. The development of reporter (i.e. *Firefly* luciferase) replicons substantially facilitated measurement of subgenomic RNA replication [84]. However attempts to broaden this system

to the replication of full-length virus failed, most likely due to the fact that adaptive mutations that enhance replication are detrimental for infectious particle production [94, 95].

The development of **HCV pseudoparticles** (HCV_{pp}) allowed studying basic steps in virus entry. These particles consist of a retroviral core governing a retroviral genome that encodes a reporter or fluorescent protein to ease detection of viral entry. Importantly the lipid envelope comprises the authentic HCV envelope glycoproteins E1 and E2. Thus by the use of the pseudoparticles the role of both glycoproteins in early events of viral entry can be studied. Given that the HCV_{pp} does not reflect an authentic HCV particle, that in fact is heavily lipidated through its association with lipoproteins and neutral lipids, it may not recapitulate the authentic virus entry [96, 97].

The establishment of **HCV *trans*-complemented particles** (HCV_{TCP}) is based on the ability of efficient *trans*-encapsidation of HCV subgenomic RNA into infectious particles. These particles are obtained by the *in trans* expression of the core-NS2 cassette in cells that replicate the subgenomic replicon. The thereby formed particles contain the subgenomic replicon RNA and thus are only able of a single round of infection and do not spread. This contributes to the beauty of the TCP system that allows to study the entire viral replication cycle under improved biosafety levels (BSL2) [98].

A major breakthrough that finally allowed the recapitulation of the complete HCV replication cycle in cell culture (the **HCVcc system**) was the isolation of a full-length HCV genome (genotype 2a) from a patient suffering from fulminant hepatitis, thus designated as JFH1 (Japanese fulminant hepatitis 1). This unique isolate was found to efficiently replicate and produce infectious particles without the need of adaptive mutations in cell culture [99]. Subsequent generation of an intragenotypic chimera led to the establishment of the frequently used Jc1 chimera, that exhibits the core-NS2 moiety of the 2a isolate J6CF fused to NS3-5B and flanked by the 3' and 5' NTR of JFH1 [100]. This chimera showed exceptional high virion assembly efficiency and was basis for the establishment of several full-length reporter viruses such as the *Renilla* luciferase reporter virus JcR2A [77, 100].

1.2.3 The viral replication cycle

When studying the **viral replication cycle** it becomes apparent that HCV propagation is tightly linked to hepatocyte function. Some details showing the link between cellular lipid metabolism and the viral replication cycle are discussed under 1.2.4. In the following section

a brief overview of the distinct steps of the viral replication cycle are presented, which is illustrated in Figure 1.4.

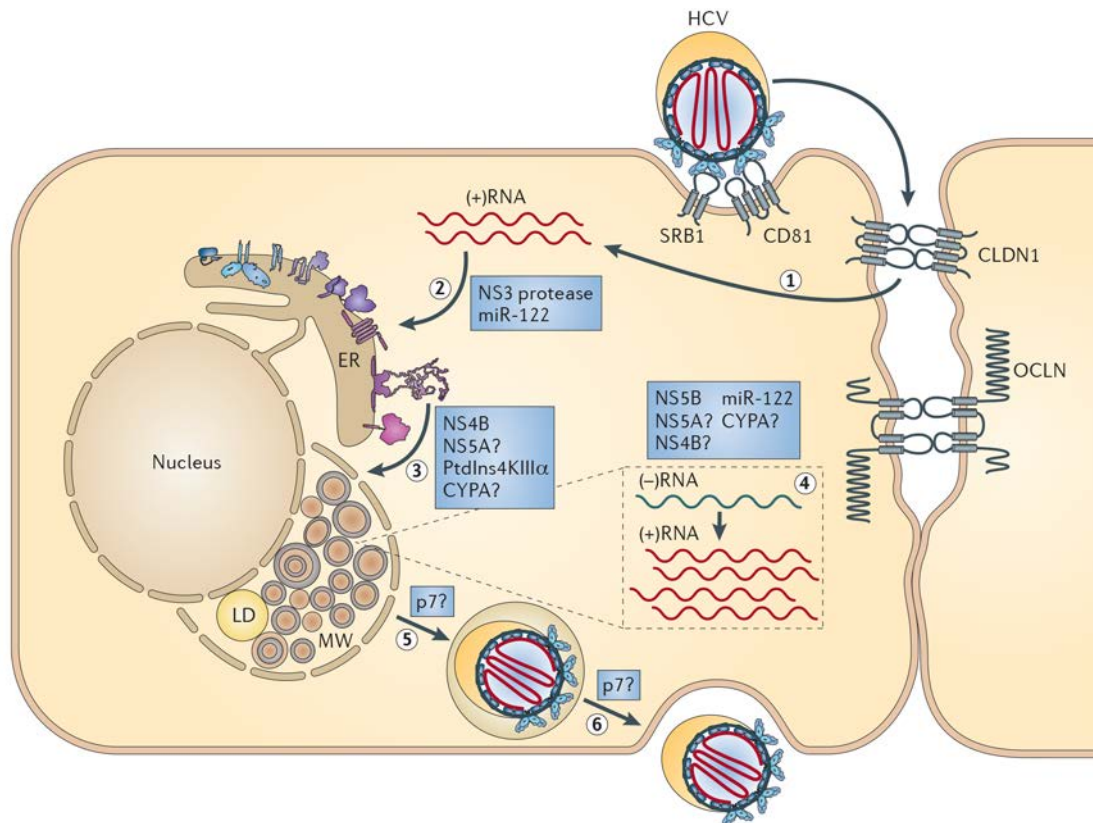


Figure 1.4 Schematic representation of the HCV replication cycle. Step 1: The engagement of the virion with several cell surface receptors triggers its uptake through clathrin-mediated endocytosis. Step 2: Upon release of the viral RNA into the cytosol it becomes translated through ribosomes at the rough ER giving rise to the viral polyprotein. The latter is processed through cellular and viral proteases giving rise to the mature proteins that build up the replicase. Step 3: Genome replication is suggested to occur at remodeled intracellular membranes, induced by a concerted action of viral and host proteins. The so-called membranous web (MW) harbors single, double and multi-membrane vesicles. Step 4: The viral RNA-dependent RNA polymerase NS5B catalyzes the generation of a negative-sense RNA, which is then used as template for the synthesis of multiple progeny RNA copies of positive polarity. Step 5: Lipid droplets (LD) can be found in close proximity of the MW and are most likely involved in the assembly process of infectious virions. The viral nucleocapsid it suggested to bud into the ER, thereby acquiring the glycoprotein E1 and E2 containing lipid envelope. Step 6: Secretion of the virion might follow the conventional secretory pathway. Adapted from [11].

A series of events mediate the **entry of HCV** into target cells. Viral particles circulate in blood in association with very-/ low-density lipoproteins (VLDL/ LDL) and this feature might substantially dictate receptor binding and membrane fusion during viral entry [101]. Initial attachment of the viral particle to the cell surface is mediated most likely by the interaction of envelope glycoproteins or virion associated lipoproteins with cell surface glycosaminoglycans or the LDL receptor (LDLR) [39, 102, 103]. This is followed by specific interactions of the envelope protein E2 with the tetraspanin Cluster of Differentiation 81 (CD81) [104] and the scavenger receptor class B type I (SR-BI) [105], followed by subsequent binding to the tight junction protein claudin-1 (CLDN1) [106] and occluding (OCLN) [107], the latter of which is involved in post attachment steps (Figure 1.4, step1). The involvement of two more

receptors, namely the LDLR and NPC1L1 will be presented in more detail in 1.2.4. The virus enters through clathrin-mediated endocytosis [108] and fusion requires low pH in endosomes [109] possibly involving the action of the envelope proteins E1 and E2 [110, 111]. Low pH in endosomes but also other triggers might contribute to the fusion of the viral envelope with endosomal membranes [109]. Upon uncoating the viral single-strand RNA genome is released into the cytosol, where it can directly be translated by ribosomes of the rough ER driven by the IRES at the 5'NTR of the genome [28]. One prominent host factor known to modulate viral RNA translation is the microRNA 122 (mir122) that binds the HCV RNA at three different positions. Mir122 is highly expressed in (and specific to) liver cells and is thought to stimulate RNA translation through enhancing the interaction with ribosomes, but also to increase RNA stability and RNA replication (Figure 1.4, step2) [11, 112]. Upon viral RNA translation the polyprotein precursor is processed by the action of host and viral proteases giving rise to the mature viral proteins (Fig 1.4, step2) [28].

Viral genome replication is suggested to occur in association with ER-derived membranes. Indeed, similar to other positive-strand RNA viruses, HCV has been shown to remodel intracellular membranes in conjunction with several host factors, such as the PI4KIII α . The thereby generated membranous web harbors the presumed sites of RNA replication (Figure 1.4, step3) [66, 77, 113, 114]. Details on the structure and biogenesis of these replication factories will be summarized in 1.2.4. The fact that in HCV replicating cells there is about a 5- to 10-fold excess of positive-sense RNA as compared to the negative-strand template, indicates that the latter can be used by the NS5B RdRp to generate multiple progeny RNAs [85].

The LDL/ VLDL-like nature of HCV virions found in patient serum suggests an involvement of the VLDL pathway in **HCV particle assembly** [115], which is presented in more detail in 1.2.4. In a first step viral RNA needs to be transported from the replication sites to sites of particle assembly. The latter are presumably at close proximity to LDs covered by the HCV core protein (Figure 1.4, step4) [116]. How this transfer is orchestrated is still elusive. It may involve NS2 that could bring assembly and replication compartments together through multiple interactions with other viral proteins such as NS3, NS5A and the envelope protein E2 [52, 53]. Additionally NS5A was suggested to deliver viral RNA from potential sites of replication to core to promote nucleocapsid formation [81]. Through subsequent budding of the nucleocapsid into the ER the virion most likely acquires its lipid shell containing the viral glycoproteins E1 and E2. The motors that could drive the budding event are not deciphered yet. HCV particles are finally secreted through their export along the conventional secretory pathway (Figure 1.4, step5, 6) [11, 117].

1.2.4 HCV and cellular lipid metabolism

Many steps of the HCV replication cycle are linked to the cellular lipid metabolism. In the following section only a few highlights are presented, demonstrating the intimate connection of the virus and lipid metabolic pathways.

A key characteristic of **infectious HCV particles** is their heterogeneous but low buoyant density with particles of lowest density being most infectious [115, 118]. Numerous studies on the biochemical composition of HCVcc and serum-derived HCV revealed common features with serum LDL and VLDL, thus called lipoviriparticle (LVP), implicating a tight link of host lipid metabolism with virus entry and particle production. In fact, several classes of Apo-lipoproteins were found to be associated with serum-derived as well as HCVcc particles [115, 119-121]. Furthermore mass-spectrometry analysis of purified HCVcc particles revealed striking similarities in the lipid composition with LDL and VLDL with the virion being especially enriched in cholesterol esters [115, 120]. The viral mimicry of LDL/ VLDL might confer several advantages for instance by providing ligands for receptor-mediated endocytosis into hepatocytes [122].

As indicated before HCV entry is a multi-step process that involves the interaction of the virion with various cellular receptors (Figure 1.4, step 1). It is interesting to note that the physiological role of three of them, namely SR-B1, LDLR and NPC1-L1 lies in the uptake of low density particles and cholesterol. SR-B1 and LDLR are present at the basolateral site of hepatocytes, the site of virus entry [122, 123]. The assumption of LDLR being a pivotal entry factor has recently been challenged, favoring, given the physiological function of the receptor in cholesterol metabolism, its involvement in post entry steps such as replication [122, 124]. SR-B1 is a crucial factor for HCV entry into hepatocytes and an authentic receptor for the uptake of HDL [105, 122]. Gene silencing or chemical inhibition of NPC1-L1 was reported to impair HCVcc infection [125]. With the receptor present at the apical site of hepatocytes, NPC1L1 is most likely indirectly involved in HCV entry through regulation of the cellular cholesterol uptake [122]. While the mimicry of LDL or VLDL might facilitate the attachment to entry receptors, the lipid composition of the virion as well as of the target membrane is crucial for membrane fusion events [111, 126]. Cholesterol depleted or sphingomyelin-hydrolyzed viral particles exhibited markedly reduced infectivity [126]. Interestingly the fusogenicity of HCVcc with liposomes was enhanced by the presence of cholesterol or cholesterol and sphingomyelin in target membranes [111]. Thus, the lipid and protein composition of both host and viral membranes is crucial for receptor recognition and cell entry.

A hallmark of **HCV replication** is the tremendous rearrangement of intracellular membranes, characterized by the accumulation of vesicles and designated as **membranous web (MW)**. Extensive studies have aimed at elucidating the function as well as lipid and protein composition of the MW. Early studies showed that the HCV induced MW contained replicase components such as non-structural proteins and viral RNA of positive polarity [67]. Subsequent electron microscopy studies on the course of MW morphology throughout HCV infection revealed that while single and double membrane vesicles (DMVs) were the main constituents of the MW, the appearance of DMVs correlated well with the viral RNA replication kinetics. Furthermore, they represented the predominant type of vesicles. Later in the course of viral infection multi-membrane vesicles were observed, which could possibly result from ER stress [113]. Biochemical analysis of purified DMVs from HCV stable replicon cells showed their enrichment in replicase components, as well as active replicase capable of *de novo* HCV RNA synthesis, indicating that DMVs might represent sites of viral RNA replication [114]. Although NS4B and NS5A alone can efficiently perturb membranes, authentic MW formation requires the expression of the NS proteins 3 to 5B, while HCV RNA replication is dispensable [113]. The **origin and lipid components of the membranous web** and DMVs are far from being deciphered. DMVs were shown to remain associated with their outer membrane to the ER and form primarily closed structures (90%), which raises the question of how important components of RNA replication can be exchanged [113]. Several findings point to a specific lipid environment of the viral replication sites: i) The membrane-protected nature of viral RNA against RNase digestion is overcome under treatment conditions that disrupt detergent resistant membranes (DRMs) [127]. ii) The association of non-structural proteins with detergent resistant membranes is sensitive to cholesterol removal [127, 128]. iii) Depletion of cholesterol from purified DMVs alters their size, suggesting the lipid being of importance for vesicle structure [114]. iv) The most prominent evidence is the massive generation of PtdIns4P at HCV replication sites through NS5A-mediated PI4KIII α induction, reported to be critical to retain the structure of DMVs [77]. It has been reported that the locally elevated PtdIns4P levels could serve to facilitate host membrane reorganization through the recruitment of PtdIns4P binding effectors, such as the lipid transfer proteins OSBP and FAPP2/PLEKHA8 (Oxysterol-binding protein and four-phosphate adaptor protein 2/plekstrin homology domain containing A8 protein) to HCV replication sites. The virus might then exploit the proteins physiological function for the recruitment of specific lipid species [79, 129].

HCV benefits from multiple **functions of DMVs**. The formation of membrane enclosed compartments allows to increase the local concentration of factors needed for RNA replication and could serve as physical tether for the RNA replication complex. Being surrounded by membranes, recognition or degradation of the viral RNA through innate RNA

sensors or cellular RNase respectively, might become limited. Additionally compartmentalization could promote the effective coordination of different steps of the viral replication cycle such as RNA translation, replication and encapsidation by spatially separating the involved factors (i.e. ribosomes, core proteins). Thus it is not surprising that the formation of specialized membranous compartments is shared by diverse positive-strand RNA viruses (reviewed in [130]).

Additional to the tremendous membrane rearrangement observed in HCV infected cells, the virus causes less 'obvious' alterations in the cellular lipid metabolism. Indeed, transcriptomic and proteomic analysis of infected cells revealed changes of factors involved in **lipid biosynthesis** [131, 132]. In fact, HCV infection was reported to induce the activation and expression of SREBPs in hepatic cells, which are transcription factors stimulating cellular lipogenesis [37]. In agreement with this, the levels of lipogenic transcripts such as of the fatty acid synthase (FASN) and of the HMGCoA (3-hydrox-3-methylglutaryl coenzyme-A) reductase (HMGCoAR), the rate limiting enzyme of the mevalonate cholesterol synthesis pathway, are elevated in infected cells [57, 132]. Over the past years, the contribution of cholesterol to genomic RNA replication has gained increasing attention. First insights were obtained by the use of statins, being potent inhibitors of the cholesterol mevalonate pathway targeting the HMGCoA reductase and impairing viral replication [133]. However it has to be taken into consideration that statins do not only interfere with cholesterol but also non-sterol isoprenoid synthesis [134]. Indeed, it was reported that the addition of isoprenoid geranylgeraniol restored viral replication upon statin treatment, arguing for an involvement of geranylgeranylation in HCV replication [135]. Nevertheless, in line with the notion of cholesterol being an important structural component of the viral replication sites, depletion of cholesterol has been reported to impair viral replication [79].

HCV particle production is suggested to involve **lipid droplets**, although their precise contribution is not well understood [116]. The notion of LDs to occupy a central role in infectious particle production, is supported by an increasing amount of experimental evidence: i) Throughout HCV infection, the viral structural core protein coats cytosolic lipid droplets (cLDs) which is followed by the recruitment of the viral replicase machinery [136, 137]. ii) HCV particle production is hampered when the recruitment of core or NS5A to cLDs is stalled [136, 138]. iii) DGAT1 and DGAT2 are catalyzing the last step in triacylglycerol synthesis, thus being crucial for LD biogenesis. Inhibition of DGAT1 mediated recruitment of the HCV core protein to LDs was reported to impair assembly of infectious particles [139]. iv) Electron-microscopy studies revealed a close proximity of LDs to DMVs and to virus-like particles [113, 136].

The fact that HCV circulates in the blood as particles of low buoyant density similar to LDL and VLDL suggests a tight connection of lipid droplet homeostasis and the **VLDL pathway** with the **assembly and release of infectious particles** [115]. The microsomal triglyceride transfer protein (MTP) catalyzes early steps in VLDL assembly comprising the lipidation of ApoB [140]. While some studies reported a dependency of HCV particle production on MTP function, others found that the expression of core results in the host protein's inactivation [141, 142]. Details on how different lipid and protein components are brought together for VLDL formation, and how and when it converges with HCV particles assembly, are not fully elucidated yet. One possibility is that the nascent virions acquire neutral lipids and lipoproteins such as ApoE during the budding process, forming a hybrid particle. On the other hand the virion might encounter VLDL at a later stage during particle egress [57, 143].

1.3 Dengue virus – lipid droplets and the membranous web

While the herein presented study focuses mainly on investigating the connection of HCV and the cellular lipid homeostasis, Dengue virus was included as a phylogenetically related but in its molecular biology partially distinct virus. Being another member of the family of *Flaviviridae* (genus *Flavivirus*) DENV shares similarities but also substantial differences with HCV in its genome organization and replication cycle, which are not focus of this work. The dedicated reader is referred to [144, 145]. However the next section aims to illustrate a **selection of differences** and **similarities** between **DENV** and **HCV** and their intimate link to **cellular lipid metabolism**. To this point the current knowledge on the role of lipid droplets in the DENV replication cycle will be presented. Moreover general features of the DENV induced membranous web will be highlighted.

The role of **lipid droplets (LDs)** in the DENV replication cycle is far from being understood. The present knowledge on the function of LDs in DENV replication is scarce and partially contradicting. In fact some studies report an increase in LD number upon DENV infection [146] others describe a DENV-induced autophagy dependent consumption of LDs, potentially for the generation of ATP through fatty acid beta-oxidation [147]. In contrast to HCV the DENV capsid protein is the only viral protein found at LDs [136, 146]. A DENV capsid mutant, carrying a mutation that abrogates membrane, thus LD association, was shown to be impaired in particle production. However it cannot be excluded that the impaired virion production was caused by a general defect of the cytosolic capsid mutant *per se*. Intriguingly the in *trans* expression of the aforementioned mutant was shown to impair RNA replication [146]. This could suggest that capsid localization to LDs is important for the coordination of distinct steps of the viral replication cycle and might serve to prevent untimely encapsidation of viral RNA at early stages of replication [148]. While in case of HCV the recruitment of the

viral replicase to LDs [136] as well as the presence of LDs at close proximity to the viral replication sites and to virus like particles points to a role of LDs in particle assembly [113], no such evidence is present for DENV. In fact, in case of DENV, virions were frequently observed at sites directly opposing the viral replication organelles, indicating that virion assembly might occur in their direct proximity and not involve LDs [149].

Similar to other RNA viruses, DENV has been reported to substantially remodel intracellular membranes inducing various membrane morphologies, including convoluted membranes and vesicular invaginations of the rough ER [130, 149]. This stands in contrast to HCV that primarily induces the formation of DMVs [113]. Immuno-electron microscopy analysis indicated the presence of viral dsRNA, a marker for replicating RNA, as well as of NS proteins in the DENV induced ER invaginations. These vesicles were further shown to exhibit pores that connect the interior of the vesicle with the cytosol that could allow the exchange of constituents needed for RNA replication and RNA *per se* [149]. As mentioned earlier, the HCV mediated induction of the MW and RNA replication was reported to substantially depend on the lipid kinase activity of PI4KIII α . In contrast DENV RNA replication does not require PI4KIII α /beta [77, 130]. Interestingly DENV NS3 was shown to recruit the FASN and to stimulate FASN activity [147].

1.4 The DEAD box RNA helicase 3, X-linked, (DDX3X, DDX3)

DDX3 belongs to the family of **DEAD box RNA helicases**, characterized by nine conserved motifs, one of which is eponymous. These conserved motifs are required for helicase activity and shared by all members of the family, while flanking sequences possibly confer helicase specificity mediating the interaction with other factors [150]. The family members, including DDX3, have been implicated in several cellular RNA related processes, such as RNA splicing, RNA export, transcriptional and translational control. DDX3 has further been implicated in tumorigenesis, acting either as oncogene or tumorsupressor [151]. The discovery that Vaccinia V7 protein can interfere with virus induced IFN β induction possibly through its interaction with DDX3, shed light on a novel role of DDX3 in antiviral signaling [152]. By now several reports suggest an involvement of DDX3 in the type I IFN induction pathway, either at the level of RNA sensing, at the level of intermediate signaling or at the level of transcriptional control of IFN β promotor activation [151]. Besides the described antiviral function in case of Vaccinia virus infection, DDX3 was reported to be an important host dependency factor for HIV, DENV or HCV replication [76, 151, 153, 154]. A yeast two-hybrid screen that aimed to identify host proteins of human liver cells interacting with the HCV core protein identified DDX3 as a putative interaction partner. This interaction was further mapped to a N-terminal region of the HCV core and a C-terminal arginine and serine

rich sequence of the DEAD box RNA helicase [155, 156]. It still remains to be elucidated whether this interaction is of any benefit to the virus. Until now several reports indicated a proviral role of DDX3 in early events of the HCV replication cycle. However given the wide spectra of possible functions exerted by the protein its precise role has not been unraveled [76, 154, 157]. Very recently DDX3 was suggested to act as sensor of HCV RNA, inducing a signaling cascade that leads to the induction of lipogenesis and increases the cellular neutral lipid content, thereby possibly promoting viral assembly [158]. Several other members of the DEAD box RNA helicase family have further been implicated to support HCV genomic RNA replication, such as DDX1 and DDX6 [159].

1.5 Cellular membrane homeostasis

1.5.1 Cellular membrane compartmentalization

The ability to form **spatially and functionally different compartments** is essential for the cell to create appropriate microenvironments for the simultaneous execution of distinct cellular processes. These compartments are substantially dependent on the lipid composition of their limiting membrane, which not only gives rise to a physical border but defines the identity of the cellular organelle [160]. The intrinsic biophysical properties of each lipid have a major influence on membrane curvature, thickness, fluidity and charge, which affects the partitioning of proteins. Indeed the phospholipids phosphatidylserine (PtdSer) and phosphatidylinositol (PtdIns) are key determinants giving rise to a negative surface charge that favors the interaction with positively charged domains of peripheral and membrane proteins [161]. The unique distribution of different phosphoinositides (PtdInsP) species, the phosphorylated forms of phosphatidylinositol, substantially contributes to the function of the corresponding organelle by regulating the recruitment of specific effector proteins. Just to mention a few, the Phosphatidylinositol-4,5-bisphosphate is mainly found at the PM and serves as an adaptor for the endocytic machinery thus initializing clathrin-mediated endocytosis. Phosphatidylinositol-3-phosphate (PtdIns3P) is present in the limiting membrane of endosomes and participates in essentially most of endosomal functions by recruiting of PtdIns(3)P binding proteins. Golgi function is dependent on the presence of Phosphatidylinositol-4-phosphate and its effectors, regulating the transport of Golgi vesicle formation [162, 163]. A hallmark of the plasma membrane (PM) is its enrichment in lipid rafts composed of sphingolipids and 65% of the cellular free cholesterol. This substantially contributes to the PM membrane properties, being more rigid and thicker as compared to the rather loosely organized ER membrane that is, despite being the site of cholesterol synthesis, low of cholesterol and mainly composed of neutral unsaturated phospholipids

[161, 162, 164]. The lipid composition of the endosome system varies from early endosome (EE) to late endosome (LE). According to this the content of cholesterol gradually decreases with the maturation of EE to LE [162]. Given that the lipid composition substantially contributes to the membrane's signature and thus organelle function [163], it is of major importance for the cell to maintain distinct lipid territories while providing dynamic exchange between organelles for biosynthetic and endocytic traffic [161].

1.6 Intracellular lipid traffic

In order to **maintain a non-random lipid distribution**, the cell employs different strategies. The PtdInsP signature of intracellular membranes is under control of a cohort of phosphoinositide kinases and phosphatases that catalyze the lipids inter-conversion directly at the target membrane [163, 165]. While such local synthesis accounts for the regulation of PtdInsP pools, this does not hold true for sterols and sphingolipids [166]. In fact, the ER represents the cell's main lipid factory generating phospholipids and sterols destined for various intracellular membranes. On the contrary sphingolipid synthesis is restricted to the Golgi compartment [161, 166]. According to this, lipids need to be efficiently transported along the biosynthetic but also the endocytic pathway [167]. In principle different motilities contribute to the lipids' unique cellular distribution. Although to a different extent, they may move laterally, which enables lipid transfer between connected membranes. Furthermore energy dependent or independent exchange of lipids between the membrane leaflets allows the generation of an asymmetric lipid distribution. However, transport of large amounts of lipids to distant organelles mainly depends on vesicular traffic [166, 168]. How lipid sorting occurs and how vesicles choose their specific lipid cargo for a particular compartment is not fully elucidated yet. Nevertheless it has been demonstrated that depending on the intrinsic properties of the lipid they preferentially sort into high ordered or disordered phases [169]. This feature contributes to lipid sorting, especially since the distinct lipid domains were reported to differ in their flexibility and ability to be modulated and shaped into tubular or vesicular structures [169-171]. Indeed COPI vesicles mediating the retrograde transport of cargo from the Golgi to the ER were found to exhibit a lower sphingomyelin content as compared to the parental Golgi membrane [171]. Thus exclusion of sphingomyelin from the retrograde transport might favor its anterograde traffic along the secretory pathway [166]. The concept of specific lipid species becoming excluded from the retrograde transport might at least, in part, account for the traffic of cholesterol, which preferentially associates with sphingolipids forming lipid rafts [172]. Although bulk transport of lipids is to a large extent mediated by an energy-dependent vesicular transport, increasing evidence points to alternative **non-vesicular transport** mechanisms for specific lipid species, particularly

essential for organelles not connected to the vesicular transport machinery such as mitochondria and lipid droplets [166, 168]. The generation of membrane contact sites, where two membranes are brought to close proximity of about 10 nm, might favor spontaneous monomeric lipid transport [166]. In fact, the ER generates MCS with several endomembranes, such as lysosomes, lipid droplets, mitochondria, the Golgi apparatus and the plasma membrane and for each of them lipid transfer activity has been reported [166, 173-175]. Given the slow and inefficient spontaneous diffusion of lipids from donor to target membranes, monomeric lipid transport is often assisted by lipid transfer proteins (LTPs) [168].

1.6.1 Lipid transfer protein (LTP)-assisted lipid transport

1.6.1.1 The concept of Lipid transfer protein (LTP)-assisted lipid transport

LTPs are suggested to **facilitate lipid transfer at MCS** by increasing the rate of lipid desorption from the donor membrane [168].

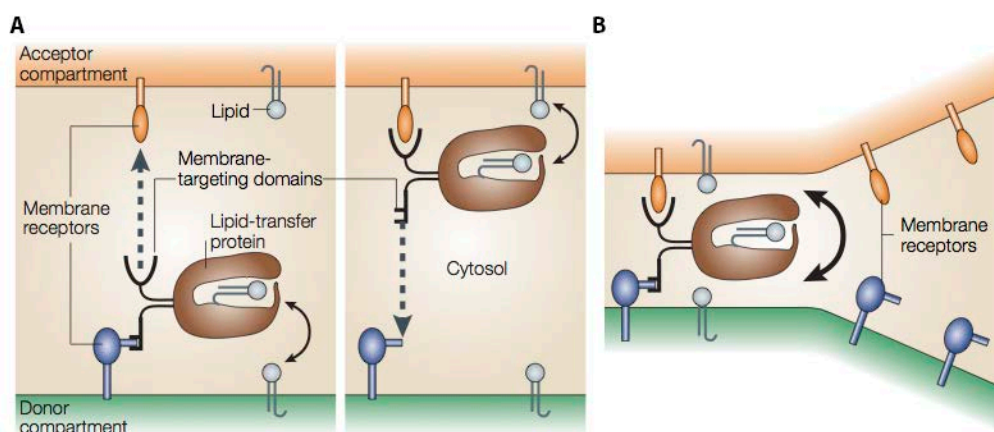


Figure 1.5 Scheme of Lipid transfer protein (LTP)-assisted lipid traffic at membrane contact sites (MCS). (A) Through a specific targeting motif, a LTP can associate with the donor membrane which leads to the opening of the hydrophobic lipid binding pocket. Upon desorption of the target lipid from the donor membrane and its binding through the LTP, the LTP engages a closed conformation (shown in graph) which then allows the transport of the lipid through the aqueous phase (indicated by dashed line). At the target membrane the lipid is released into the membrane leaflet. As indicated recognition of both cellular compartments is mediated by specific membrane targeting domains of the LTPs, that recognize particular lipid species or proteins, designated as 'membrane receptors' in the graph. (B) LTPs can interact with both membrane receptors simultaneously thus stabilizing the MCS and increasing the efficiency of lipid transfer. Adapted from [166].

In principle LTPs may engage two major conformations: an 'open' conformation, that reflects the membrane bound form of the protein ready for the uptake of the target lipid and a 'closed' conformation representing the transport-competent form, with a lid covering the lipid containing binding pocket [166, 176]. The association of LTPs to the donor membrane possibly induces a conformational change, which leads to the opening of the hydrophobic

lipid-binding cavity. Upon absorption of the target lipid, the LTP dissociates from the donor membrane and shuttles to its destination, where the lipid is introduced into the target membrane (Figure 1.5) [166, 168]. Although the directionality of LTP-mediated transport is defined by the lipid's concentration gradient, specific sequence motifs drive their membrane association, thus restricting LTP activity to certain cellular locations [168, 177-180]. For this reason, monomeric lipid transport through LTPs might represent a transfer mechanism that allows the extraction or delivery of specific lipid species at a certain membrane domain [168].

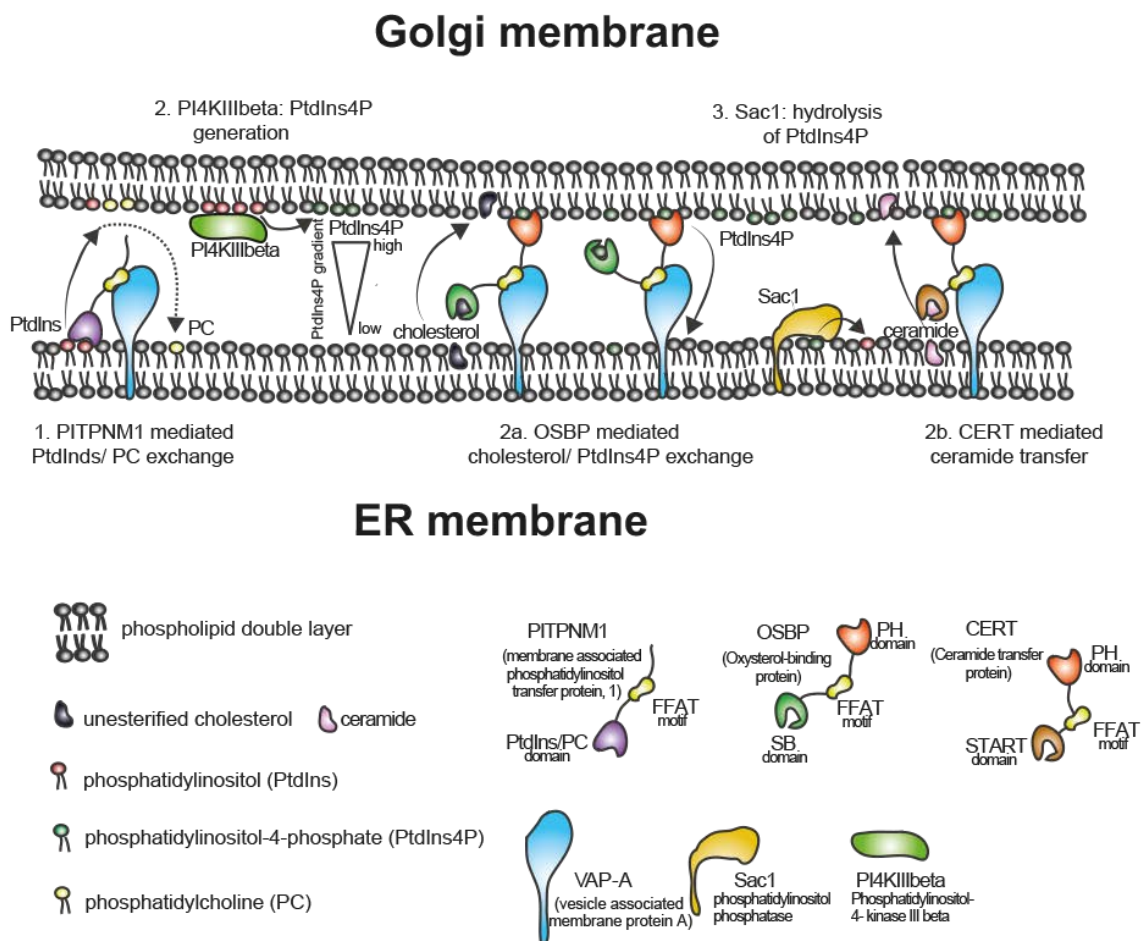


Figure 1.6 Model of lipid transfer at the Golgi/ER interface mediated by the membrane associated phosphatidylinositol transfer protein 1 (PITPNM1), the oxysterol-binding protein (OSBP) and the ceramide transfer protein (CERT). PITPNM1 can bind to VAP proteins present at the ER and mediates the bidirectional transfer of phosphatidylinositol (PtdIns, from ER to Golgi) and phosphatidylcholine (PC, from Golgi to ER). PtdIns at the golgi is substrate of the Phosphatidylinositol-4-kinase III beta (PI4KIIIbeta) for the generation of phosphatidylinositol-4-phosphate (PtdIns4P). OSBP and CERT can become recruited to the ER through their interaction with VAP proteins. Additionally they bind PtdIns4P present at the Golgi. CERT drives the transfer of ceramide from the ER to Golgi membranes, while OSBP might catalyse the bidirectional traffic of cholesterol and PtdIns4P. The ER resident phosphatidylinositol phosphatase Sac1 hydrolyzes PtdIns4P to PtdIns. Importantly, a concerted action of PITPNM1, PI4KIIIbeta and Sac1 allows the maintenance of a PtdIns4P gradient, which determines the directionality of lipid transport mediated through OSBP or CERT. Note, only lipids directly involved in the lipid transfer are depicted [181, 182]. Adapted from [181].

According to their lipid binding specificity, LTPs are grouped into three major classes: Phospholipid transfer proteins, sterol transfer proteins and sphingolipid transfer proteins [168]. Prominent members of these classes are the membrane associated

phosphatidylinositol transfer protein 1 (PITPNM1/ Nir2), the oxysterol-binding protein OSBP and the ceramide transfer protein (CERT) suggested to drive in a concerted fashion monomeric lipid transport between ER and Golgi. For details see Figure 1.6 [180, 181, 183].

1.6.2 Lipid transfer proteins involved in sterol transport

Sterol transfer proteins of several protein families are implicated in non-vesicular sterol transfer [184]. The LTPs studied in this work are presented in more detail in the following section.

The oxysterol binding protein (OSBP)-related/ like protein (ORP/OSBPL) family consists of at least 12 members, which share a highly conserved sterol binding domain at the C-terminus and in most cases a pleckstrin homology domain (PH) and/ or a VAP (vesicle associated membrane protein (VAMP)- associated protein) binding motif, denoted FFAT (two phenylalanine (FF) in acidic stretch) important for their cellular targeting [185, 186]. The most prominent and also founding member of this family is OSBP that has so far obtained most attention. OSBP is a multifunctional protein involved in lipid transport, cell signaling and regulation of cholesterol homeostasis [79, 186]. Recent *in vitro* studies propose a four step model of OSBP-mediated cholesterol (dehydrogesterol (DHE)) transfer between PtdIns4P rich and VAP-A containing membranes, supposedly the Golgi and ER compartments [182]. By interacting with VAP-A (ER) and PtdIns4P (Golgi), through its FFAT or PH domain respectively, OSBP allows the tethering of two opposing membranes. Subsequently the protein acts as a sterol/ PtdIns4P exchanger, catalyzing the bidirectional transport of cholesterol and PtdIns4P. PtdIns4P is then hydrolyzed by the ER resident Sac1 phosphatase, which might provide the metabolic energy driving the lipid transport (Figure 1.7) [182].

As indicated in Fig 1.6, OSBP function at ER Golgi MCS is tightly linked to the action of other LTPs. Interestingly several viruses have been reported to exploit the sterol transfer activity of OSBP. Indeed, some enteroviruses and HCV were recently shown to recruit OSBP to PtdIns4P rich replication organelles, likely for the delivery of cholesterol that may support the formation of the tremendous membrane rearrangements induced by both viruses [79, 187].

Golgi membrane

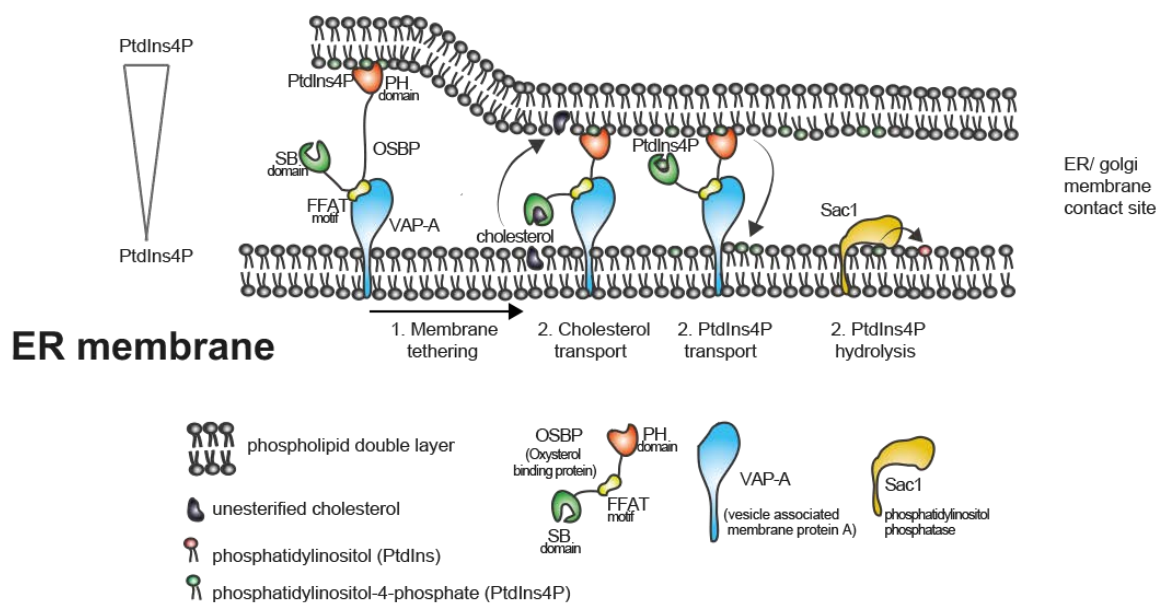


Figure 1.7 Scheme of Oxysterol-binding protein (OSBP) mediated cholesterol and phosphatidylinositol-4-phosphate (PtdIns4P) exchange at ER/ Golgi membrane contact sites. Step 1: Membrane tethering: OSBP can promote the formation of ER/ Golgi membrane contact sites through binding VAP-A at the ER and PtdIns4P at the Golgi through its FFAT motif or the plekstrin homology (PH) domain, respectively. Step 2: Cholesterol is then bound by the sterol binding (SB) domain and transported from the ER to the Golgi. Step 3: In exchange, PtdIns4P is trafficked from the Golgi membrane to the ER. Step 4: The ER resident phosphatidylinositol-4-phosphate phosphatase Sac1 hydrolyses PtdIns4P, which leads to the formation of phosphatidylinositol (PtdIns). The concentration gradient of PtdIns4P from Golgi to ER determines the directionality of the lipid transport. Note, the lipid composition of the ER and Golgi membranes is not adequately depicted. Only lipids directly involved in the OSBP cycle are shown. Adapted from [182].

Another member of the OSBPL family, OSBPL1A was shown to regulate the association of LE with the microtubule transport machinery depending on the organelles cholesterol content. Thus OSBPL1A acts as sterol sensor that links the LE sterol levels to their cellular positioning [188, 189]. Interestingly RNAi-mediated gene silencing of another OSBPL, namely OSBPL5 has been reported to induce the accumulation of cholesterol in late endosomes, indicating its potential role as cytosolic lipid acceptor [190]. The functions of the other ORP/OSBPL family members and their true involvement in cholesterol transport, is far less understood [191].

The second main family involved in sterol transfer comprises members of the **steroidogenic acute regulatory protein (StAR)-related lipid transfer (START) domain protein family**, characterized by a conserved 210 AS sequence that folds into a hydrophobic lipid binding pocket. The 15 members of this family are further grouped into six subfamilies depending on their sequence similarity and ligand binding affinity, which varies from binding to cholesterol, oxysterol, phospholipids or sphingolipids to possibly fatty acids [184, 192, 193]. 5 of them have been reported to bind cholesterol: StAR (STARD1) and STARD3 are both tethered to the mitochondria or LE membrane respectively, with the former protein being essential for the cholesterol transport from the outer mitochondrial membrane (MM) to the inner MM, thus

catalyzing the rate limiting step in steroid synthesis [184]. Mutagenesis studies on STARD3 revealed its importance in the mobilization of cholesterol from LE and transfer to either mitochondrial membranes or possibly other acceptors [184, 194]. STARD4, 5 and 6 are cytosolic proteins that share an affinity for cholesterol or hydroxycholesterol. STARD4 has been reported to regulate the transport of cholesterol to the endocytic recycling compartment (ERC) and the ER and therefore altering cholesterol esterification and cholesterol mediated regulation of cellular lipid homeostasis [192, 195]. The involvement of STARD5 and STARD6 in cellular cholesterol traffic has not been elucidated yet [192].

The **Niemann-Pick Type C (NPC)** disease is a lipid storage disorder caused by mutations in the NPC1 or NPC2 gene that cause an accumulation of LDL derived unesterified cholesterol in lysosomal compartments [196, 197]. The role of NPC1 and NPC2 in cholesterol mobility from lysosomes is described in more detail in the following section.

1.6.3 Lipid transfer proteins – Niemann-Pick Disease Type C (NPC) 1 (NPC1) protein

Pioneer work of Albert Niemann and Ludwig Pick in the 1920s led to the identification of a neurodegenerative lysosomal lipid storage disorder, autosomal recessively inherited, and designated as “**Niemann-Pick disease**” [196, 198]. To date two different groups are defined: Niemann-Pick Disease Type A and B are caused by defects in sphingomyelinase, resulting in intracellular accumulation of sphingolipids, thus designated as sphingolipidosis. Niemann-Pick disease type C is caused in 95% of the cases by roughly 300 distinct single point mutations in the NPC1 gene and in rare cases by mutations in the NPC2 gene [198, 199]. With the discovery of defective esterification of exogenous LDL and abnormal intracellular cholesterol traffic in NPC, the disorder was considered to be primarily a cholesterol lipidosis [198, 200]. NPC disease phenotype is very heterogeneous regarding the onset and severity of disease progression but ultimately lethal. Symptoms are neurologic, manifesting besides others in progressive ataxia (failure of muscular coordination), dystonia (abnormal muscle contraction) and dementia (loss of cognitive abilities) [201-203]. Treatment is currently mainly restricted to treatment of symptoms [202].

NPC1 is a **transmembrane protein**, localized to the limiting membrane of late endosomal and lysosomal compartments [204, 205]. As mutations in NPC1 were reported to be linked to a cholesterol trafficking defect characterized by the lipid's accumulation in lysosomal structures, NPC1 was suggested to function in the mobilization of free cholesterol from LE/LY [206]. Recent reports propose a handoff mechanism that involves both NPC1 and NPC2 in endosomal cholesterol transport, the latter protein being a small glycoprotein resident in

the lysosomal lumen. According to this NPC2 might catalyze the transfer of free cholesterol resident in the internal membranes to the limiting membrane of LEs, where it could be subsequently accessed by NPC1 [207]. How cholesterol is next transported to the PM, the ER or the Golgi network remains unclear. Nevertheless it is likely that post-lysosomal cholesterol traffic involves the vesicular transport machinery, possibly under the control of NPC1 function [206, 208, 209]. In fact, it has been reported that the motility of NPC1 positive vesicles is almost abolished in presence of an inactive form of the protein [210]. It remains to be elucidated whether the trafficking defect of endosomal structures in NPC1 deficient cells is a consequence of cholesterol accumulation that in turn has been reported to alter the association of endosomes with the cellular transport machinery [211]. Although cholesterol accumulation has been described as the hallmark of NPC1 disease pathogenesis it is not surprising that other lipids passing through the LE/LY system such as sphingolipids and gangliosides are also affected [196, 212].

1.6.4 Sterol transport and sterol homeostasis

The cell depends on the **maintenance of specific local cholesterol concentrations**, characterized by a gradual increase of the membranes' cholesterol content from the ER to the Golgi and to the PM. Similarly, vesicles of the early endocytic pathway, such as the recycling endosomes contain high cholesterol levels, which decrease along compartments of the later endocytic route, such as LE and LY [162, 167]. On the one hand the uneven distribution of cholesterol is modulated by a concerted action of vesicular and non-vesicular mechanisms, on the other hand, overall cellular cholesterol content is tightly regulated in order to prevent detrimental effects of excess free cholesterol [213, 214]. Three major pathways allow the cell to adapt to changing cholesterol needs. Through the regulation of **de novo synthesis of cholesterol**, its **uptake** from the plasma membrane or lipoproteins or through altering **cholesterol efflux** and lipid **conversion**, fine-tuning of cellular cholesterol levels is achieved. The abundance of proteins involved in these pathways is regulated either at the transcriptional level, or in need of acute modulations by ubiquitin dependent degradation [215]. Two major transcription factors, the liver X receptors (LXRs) and the sterol regulatory element binding proteins (SREBPs) control the expression of proteins involved in cholesterol homeostasis depending on the cellular sterol levels [215].

Proteins involved in **de novo synthesis of cholesterol** are expressed as a function of the cellular sterol content [216]. The ER appears to be the major organelle when it comes to cellular cholesterol turnover, as it is place of cholesterol synthesis and esterification. Additionally sensing of the cellular free cholesterol content involves SREBPs and the

accessory proteins SCAP (SREBP cleavage activating protein) and Insig present in a protein complex at the ER [217, 218]. In detail, low cholesterol levels induce a conformational change in SCAP which allows the dissociation of SREBP-SCAP from the ER retention protein Insig. Once SREBP-SCAP reaches the Golgi, proteolytic cleavage allows the release of SREBP and its transport to the nucleus in order to induce transcription of the respective target genes [217, 219, 220]. At present, three different isoforms of SREBPs are known, with SREBP1c and SREBP2 regulating the expression of genes of fatty acid synthesis or of cholesterol metabolism, respectively, while SREBP1a is suggested to target both pathways. Important target genes of SREBP2 encode for the HMGCoAR and the LDL receptor [215, 221].

The uptake of LDL is catalyzed by clathrin dependent LDL receptor (LDLR)-mediated endocytosis [215]. Cholesterol is then liberated from cholesteryl esters of LDL through the activity of acid lipase present in early compartments. So far it is unresolved at which stage cholesterol leaves the endocytic pathway to be further trafficked to the PM and the ER [217, 222]. Hepatocytes can further obtain cholesterol through the SR-B1 mediated uptake and processing of HDL [223].

The **efflux or conversion of cholesterol** to cholesterol derivatives allows the cell to prevent the accumulation of excessive free cholesterol. Members of the ATP-binding cassette transporter (ABC) protein family, in particular ABCA1, have been reported to catalyze the transfer of cholesterol to apolipoproteins for the secretion of HDL particles [215, 224, 225]. Interestingly the expression of ABCA1 and others is under the control of the LXR transcription factor, which itself is activated by oxidized cholesterol derivatives (oxysterols) [226, 227]. Cholesterol can further be converted into precursors of bile acids, which are subsequently secreted. Most importantly excessive cholesterol at the ER is readily esterified and transferred for the reversible storage in **lipid droplets** [217].

1.6.5 Lipid droplets

Lipid droplets are spherical structures, which consist of a neutral lipid core, mainly composed of triacylglycerides and cholesterol esters, surrounded by a phospholipid monolayer associated with proteins [228, 229]. Different models are suggested for the biogenesis of LDs, each of them involving the ER membrane, which is the site of neutral lipid synthesis [230]. Most likely, the accumulation of neutral lipids between ER leaflets leads to the formation of a lipid lens, which subsequently grows and buds from the ER giving rise to a nascent cytosolic LD. The nascent droplet may also remain connected to the ER. Alternative

models describe instead of a budding process an excision of LDs from both ER leaflets, leaving a pore behind. According to the vesicular budding model the accumulation of neutral lipids at the luminal site of the ER drives the formation of a vesicle giving rise to LDs [229, 231]. LDs have for a long time been underappreciated as simple storage vessels of neutral lipids. Indeed excess fatty acids and cholesterol are converted into neutral lipids and deposited in LDs, thus protecting the cells from toxic effects of exceeding lipid accumulation [232]. This storage is transient and can be reversed when cells are in need of lipids for membrane synthesis or the generation of energy [233]. Increasing evidence suggest a dynamic involvement of LDs in lipid homeostasis, but also in signal transduction by providing precursors for the synthesis of messengers compounds [230].

The **particular function of a LD** is mainly determined by its protein coat composition [230]. Members of the PAT (perilipin, adipose differentiation related protein (ADRP), tail anchoring protein 47 (Tip47)) protein family are so far the best characterized LD associated proteins that substantially alter neutral lipid storage. Perilipin is of particular interest, as upon phosphorylation, the protein switches from its role in neutral lipid storage to lipid mobilization by the recruitment of the hormone sensitive lipase (HSL). ADRP is suggested to function similarly and regulates the accessibility of the LD core through the Adipose triglyceride lipase (ATGL). Importantly both PAT (perilipin and ADRP) proteins are constitutively associated with LD [234]. Tip47 potentially function in the biogenesis of LDs [235]. With the aim to identify novel proteins regulating LD homeostasis, two different siRNA screens were performed in drosophila cells, monitoring the effect of gene knockdown on different LD features such as LD size and distribution. This led to the identification of the COPI system, that appears to substantially regulate lipolysis. Pharmacological inhibition or gene knockdown of COPI subunits induced neutral lipid storage, manifested in larger LDs [236, 237]. Interestingly, interference with COPI function led to an accumulation of the two PAT proteins ADRP and Tip47 at LDs, while the levels of ATGL were reduced [237].

Hepatocytes have the ability to store neutral lipids not only in cytosolic LDs but also in ER luminal LDs, possibly providing essential lipids for the synthesis of very low density lipoproteins [140]. As indicated in section 1.2.4 and 1.3, LDs play a central role in the replication cycle of HCV and DENV respectively. The observation that a pathogen exploits LDs function is not only restricted to HCV or DENV, but a common feature of multiple pathogens. There is a substantial list of bacteria which usurp LDs most often for nutritional purpose [230].

1.7 Aim of study

In the herein presented work I aimed at obtaining a better insight into the link between HCV and host cell lipid homeostasis. Being an obligate intracellular virus, HCV depends on and hijacks cellular pathways in order to reshape cellular functions for its own benefit. Indeed, similar to other plus-strand RNA viruses HCV remodels endomembranes for the generation of its replication factories and usurps cellular organelles, such as LDs, the latter being involved in cellular lipid metabolism.

In the first part of my PhD thesis I focused on investigating the role of LDs in the replication cycle of the two LD-dependent viruses HCV and DENV. To this end, I used as starting point a RNAi screen that was performed by Dr. G. Alvisi in our laboratory. This screen targeted host genes implicated in LD homeostasis and aimed at identifying novel candidates regulating the HCV/ DENV replication cycle as well as LD-dependent pathways. Top hits were several components of the COPI machinery as well as DDX3. By using additional knock-down approaches as well as biochemical methods and reverse genetics I wanted to decipher the role of these host cell factors and their contribution to efficient replication of HCV and DENV.

The second part of my PhD thesis aimed at unraveling the molecular details of whether and how HCV impacts the cellular cholesterol homeostasis, as earlier studies had shown that cholesterol is a critical component of the membranous HCV replication factory. By the use of several cholesterol-specific dyes I first sought to visualize the dynamic distribution of endogenous or exogenously added unesterified cholesterol in HCV replicating cells. To unravel the molecular details how HCV might remodel cholesterol homeostasis I performed a small scale RNAi screen targeting a selection of LTPs implicated in direct lipid transfer. The results of this screen should set the basis for subsequent studies that aimed at understanding the role of LTP-mediated endosomal cholesterol traffic in the viral replication cycle. Using several HCV model systems and shRNA-mediated gene knockdown, I sought to define the viral steps dependent on LTP function. These studies should be complemented by pharmacological perturbation of the LTP-mediated endosomal lipid transport and by evaluation of these perturbations on the different steps of the HCV replication cycle as well as lipid distribution. Finally, I planned to use electron microscopy in order to determine whether endosomal cholesterol traffic contributes to the integrity of the HCV replication factory.

2 Materials and Methods

2.1 Materials

2.1.1 Antibodies and dyes

Table 2.1 Primary antibodies and dyes used in this study

antibody/ fluorescent dye	specificity	type	WB	IF	reference
ApoE	Apolipoprotein E (human)	goat polyclonal	1:5000	n.t.	Millipore (Schwalbach, Germany)
beta actin (A5441)	beta actin (human)	mouse monoclonal	1:10000	n.t.	Sigma-Aldrich (St. Louis, USA)
calnexin (ADI-SPA 865)	Calnexin (human)	rabbit polyclonal	1:500	1:50	Enzo Life Science (Farmingdale, USA)
capsid core (C750) (sc-57800)	Virus capsid (Dengue) Core protein, aa 21-40 (HCV)	mouse monoclonal	n.t.	1:2	Dr. John Aaskov (Queensland University of Thechnology, Australia)
core (C830)	Core protein, aa 2-167 (HCV)	mouse monoclonal	1:1000	1:400	Prof. Dr. D. Moradpour (CHUV Lausanne, Switzerland)
DDX3X (A300-474A)	X-linked DEAD box RNA helicase 3 (human)	rabbit polyclonal	1:3000	1:200	home-made
Flag (M2) (F1804)	Flag tag	mouse monoclonal	1:1000		Bethyl Laboratories (San Joase, USA)
LAMP-1 (ab24170)	Lysosomal associated membrane protein 1 (human)	rabbit polyclonal	1:1000	1:500	Abcam (Cambridge, USA)
LAMP-2 (555803)	Lysosomal associated membrane protein 2 (human)	mouse monoclonal	n.t.	1:100	Abcam (Cambridge, USA)
MLN46 (STARD3) (ab3478)	StAR-related lipid transfer (START) domain containing 3 (human)	rabbit polyclonal	1:500	1:50	BD Pharmingen (San Jose, USA)
NS3 (2E3)	NS3 (HCV)	mouse monoclonal	1:1000	n.t.	BioFront Technologies (Tallahassee, USA)
NS4B (86)	NS4B (HCV)	rabbit polyclonal	1:2000	n.t.	home-made
NS5A (9E10)	NS5A (HCV)	mouse monoclonal	1:1000	1:1000	Prof. Dr. C. M. Rice (Rockefeller University, USA)
NS5A (4952)	NS5A (HCV)	rabbit polyclonal	1:200	n.t.	home-made
NPC1 (NB400-148)	Niemann-Pick disease type C1 (human)	rabbit polyclonal	n.w.	1:100	Novus Biologicals
OSBPL1A (ab131165)	Oxysterol binding protein-like 1A protein (human)	rabbit monoclonal	n.w.	n.w.	Abcam (Cambridge, USA)
PITPNM1/ Nir2	Membrane associated phosphatidylinositol-transfer protein 1 (human)	rabbit polyclonal	1:250	1:50	Biorbyt (Berkley, USA)
Bodipy 493/503 ((4,4-Difluoro-1,3,5,7,8-Pentamethyl-4-Bora-3a,4a-Diaza-s-Indacene) (D3992)	neutral lipid stain, Lipid droplets			20 ug/ml	Thermo Fisher Scientific (Waltham, USA)
HSC LipidTox™					
Deep Red neutral lipid stain (H34477)	neutral lipid stain, Lipid droplets			1:1000	Thermo Fisher Scientific (Waltham, USA)
Hoechst (33342)	DNA			1 ug/ml	Thermo Fisher Scientific (Waltham, USA)
Filipin complex (F9765)	free cholesterol			250 ug/ml	Sigma-Aldrich (St. Louis, USA)
Filipin III (F4767)	free cholesterol			250 ug/ml	Sigma-Aldrich (St. Louis, USA)
DAPI ((4',6-Diamidino-2-Phenylindole, Dihydrochloride) (D1306)	DNA			1:3000	Thermo Fisher Scientific (Waltham, USA)
Topfluor cholesterol (TFC)	unesterified cholesterol			1 uM	Avanti Polar Lipids (Alabama, USA)

Table 2.2 Secondary antibodies used in this study

antibody	specificity	type	IF/WB	reference
Alexa Fluor® 647 (A31573)	Anti-Rabbit IgG (H+L)	donkey polyclonal	1:1000	Thermo Fisher Scientific (Waltham, USA)
Alexa Fluor® 488 (A21206)	Anti-Rabbit IgG (H+L)	donkey polyclonal	1:1000	Thermo Fisher Scientific (Waltham, USA)
Alexa Fluor® 568 (A10037)	Anti-Mouse IgG	donkey polyclonal	1:1000	Thermo Fisher Scientific (Waltham, USA)
Alexa Fluor® 488 (A21202)	Anti-Mouse IgG (H+L)	donkey polyclonal	1:1000	Thermo Fisher Scientific (Waltham, USA)
Alexa Fluor® 488 (A11029)	Anti-Mouse IgG (H+L)	goat polyclonal	1:1000	Thermo Fisher Scientific (Waltham, USA)
Alexa Fluor® 568 (A10037)	Anti-Mouse IgG (H+L)	goat polyclonal	1:1000	Thermo Fisher Scientific (Waltham, USA)
Alexa Fluor® 647 (A31571)	Anti-Mouse IgG (H+L)	goat polyclonal	1:1000	Thermo Fisher Scientific (Waltham, USA)
Alexa Fluor® 488 (A11034)	Anti-Rabbit IgG (H+L)	goat polyclonal	1:1000	Thermo Fisher Scientific (Waltham, USA)
Alexa Fluor® 568 (A11036)	Anti-Rabbit IgG (H+L)	goat polyclonal	1:1000	Thermo Fisher Scientific (Waltham, USA)
anti-mouse HRP	Anti-Mouse IgG	goat polyclonal	0 1:2500	Sigma Aldrich (St. Louis, USA)
anti-rabbit HRP	Anti-Rabbit IgG	goat polyclonal	0 1:2000	Sigma Aldrich (St. Louis, USA)
anti-goat HRP	Anti-Goat IgG	goat polyclonal	0	Sigma Aldrich (St. Louis, USA)

2.1.2 Buffers and solutions

Table 2.3 Buffers and solutions used for protein work

buffer/ solution	composition
Bradford Reagent	100 mg Coomassie Brilliant Blue G250 dissolved in 50 ml Ethanol p.A., added to 100 ml 85% RIPA Buffer
RIPA Buffer	50 mM Tris-HCL (ph 7.4), 150 mM NaCl, 1% (v/v) Triton-X-100, 1% (w/v) Sodium Deoxicholate, 0.1% 10x TGS running buffer
Protein loading buffer (2x)	150 mM Tris, 1.92 M Glycine, 1% (w/v) SDS
Protein loading buffer (6x)	375 mM Tris-HCl (ph 6.8), 0.1% (w/v) Bromophenol Blue, 20% Glycerol, 3% (w/v) SDS, 2% (v/v) beta-mercaptoethanol
Resolving gel buffer	375 mM Tris-HCl (ph 6.8), 0.1% (w/v) Bromophenol Blue, 60% Glycerol, 6% (w/v) SDS, 9% (v/v) beta-mercaptoethanol
Semi-dry blotting buffer	1.5M Tris-HCl (ph 8.8), 0.4% (w/v) SDS
Stacking gel buffer	25 mM Tris Base (ph 8.3), 10% (v/v) Methanol, 150 mM Glycine
Western Blot blocking buffer	1 M Tris-HCl (ph 6.8), 0.8% (w/v) SDS
Western Blot washing buffer	0.5% (v/v) Tween-20, 5% Skim Milk Powder in 1x PBS
Western Blot antibody incubation buffer	0.5% (v/v) Tween-20
	0.5% (v/v) Tween-20, 2.5% Skim Milk Powder in 1x PBS

Table 2.4 Buffers and solutions used for nucleic acid work

buffer/ solution	composition
DNA loading dye (6x)	375 mM Tris-HCl, 60% Glycerol, 6% (w/v) SDS, 0.1% (w/v) Bromophenol Blue, 10% beta-mercaptoethanol (ph 6.8, -20°C)
NEB Buffer 1	10 mM Bis Tris Propane-HCl, 10 mM MgCl ₂ , 1 mM DTT (ph 7.0 at RT)
NEB Buffer 2	10 mM Tris-HCl, 10 mM MgCl ₂ , 50 mM NaCl, 1mM DTT (ph 7.9 at RT)
NEB Buffer 3	50 mM Tris-HCl, 10 mM MgCl ₂ , 100 mM NaCl, 1 mM DTT (ph 7.9 at RT)
NEB Buffer 4	20 mM Tris-acetate, 10 mM magnesium acetate, 50 mM potassium acetate, 1 mM DTT (ph 7.9 at RT)
PCR Buffer 10x	100 mM Tris-HCl (ph8.3), 500 mM KCl, 15 mM MgCl ₂ , 0.01% (w/v) gelatine
Sodium Acetate	2 M Sodium Acetate, ph adjusted to 6.8 with glacial acetic acid
TAE (50x)	2 M Tris-HCl, 2M Acetic acid, 50 mM EDTA, ph 8.3
Transcription buffer RRL (5x)	400 mM HEPES (ph 7.5), 60 mM MgCl ₂ , 10 mM spermidine, 200 mM DTT

Table 2.5 General buffers and solutions

buffer/ solution	composition
Cytomix	120 mM KCl, 1 mM Potassium phosphate buffer (ph 7.6), 25 mM HEPES (ph 7.6), 0.15 mM CaCl ₂ , 5 mM MgCl ₂ , 2 mM EGTA, adjusted to ph7.6 with KOH, before use: addition of 2 mM ATP, 5 mM Glutathione
Cacodylade buffer	50 mM Sodium Cacodylate (ph 7.2)
EM fixative	25% Gluteraldehyde, 50 mM KCl, 2 mM MgCl ₂ , 2 mM CaCl ₂ , 2% Sucrose in 50 mM Cacodyladebuffer
Immunofluorescence blocking buffer	5% (w/v) fatty acid free BSA in 1x PBS
Immunofluorescence antibody incubation buffer	1% (w/v) fatty acid free BSA in 1x PBS
Phosphate buffered saline (PBS, 10x)	80 mM Na ₂ HPO ₄ , 20 mM NaH ₂ HPO ₄ , 1.4 M NaCl, 2.7 mM KCl, 1.76 mM KH ₂ PO ₄
TCID50 detection substrate (Carbazol)	0.4 g 3-amino-9ethyl carbazol dissolved in 125 ml N,N-dimethyl-formamide, storage at 4°C in the dark
TCID50 Acetate solution	75 ml 0.5 M NaAcetate, 30 ml 0.5 M acetic acid, 945 ml dH ₂ O
TCID50 detection solution	5 ml Acetate solution, 1.5 ml Carbazol, 20 ul Peroxide, filtered through 0.45 uM filter
4% Paraformaldehyde (PFA)	4 g paraformaldehyde dissolved in 100 ml PBS, heat to 60°C
PHEM buffer (ph 6.9)	60 mM PIPEs, 25 mM HEPES, 10 mM EGTA, 2 mM MgCl ₂

Table 2.6 Buffers and solutions for luciferase activity assays

buffer/ solution	composition
Coelenterazine stock solution	5 mg dissolved in 11.6 ml methanol, aliquots stored at -80°C
Luciferin stock solution	1 mM luciferine, 25 mM Glycyl-glycin, storage at -80°C
Luciferase assay buffer	15 mM Potassium phosphate (ph 7.8), 15 mM MgSO ₄ , 4 mM EGTA, 25 mM Glycyl-Glycin (ph 7.8), before use: addition of 1 mM DTT and 2 mM ATP in case of <i>Firefly</i> luciferase measurements
Luciferase lysis buffer	1% (v/v) Triton-X-100, 10% Glycerol, 15 mM MgSO ₄ , 4 mM EGTA, 25 mM Glycyl-Glycin (ph7.8), before use: addition 1 mM DTT , storage at 4°C

2.1.3 Plasmid constructs

Table 2.7 pTM-based expression constructs

#	name	designated as	description	reference
1	pTM_NS3-3'_JFH1	pTM_NS3-3'_JFH1	HCV replicase protein NS3-5B of genotype 2a	C. Berger
2	pTM_NS3-3'_Con1ET	pTM-NS3-3'_Con1_ET	HCV replicase protein NS3-5B of genotype 1b	D. Paul
3	pTM_empty	pTM_empty	empty vectors, used as control.	C. Berger
4	pTM_Flag_J6core	Flag_J6 core	Encodes for the Flag tagged J6 core	M. Zayas
5	pTM_Flag_JFH1core	Flag_JFH1 core	Flag tagged JFH1 core	M. Zayas
6	pTM_Flag_H77core	Flag_H77 core	Flag tagged H77 core	self made
7	pTM_Flag_Con1core	Flag_Con1 core	Flag tagged Con1 core	self made

The F24A point mutation was introduced into plasmid 4-8. Mutants are designated with their original name followed by "F24A", i.e. pTM-Flag-J6coreF24A, pTM-Flag-JFH1coreF24A

pTM is a high copy plasmid, containing the T7 promoter followed by the EMCV IRES. pTM-based constructs were transfected into T7 bacteriophage RNA polymerase containing cells to allow cytosolic expression of the gene of interest.

Table 2.8 pFK based viral vectors used in this study

#	name	designated as	description
1	pFK_Jc1_dg	Jc1	Full-length HCV chimera consisting of the core-NS2 (1-648) of the genotype 2a isolate J6CF and the remaining sequence of NS2 (starting between first and second putative transmembrane domain) till the 3'UTR of JFH1 [100].
2	pFK_Jc1_ΔE1E2dg	Jc1ΔE1E2	Full-length HCV chimera consisting of the core-NS2 (1-648) of the genotype 2a isolate J6CF and the remaining sequence of NS2 (starting between first and second putative transmembrane domain) till the 3'UTR of JFH1. A deletion of most of the E1-E2 coding region impairs infectious particle production [74].
3	pFK-i389RLuc2A-Core-3'Jc1	JcR2A	Monocistronic full-length <i>Renilla</i> luciferase reporter virus of Jc1 containing a duplication of the first 16 aa of core, followed by <i>Renilla</i> luciferase and the foot and mouth disease virus (FMDV) 2a peptide to allow proteolytic cleavage of the reporter luciferase [77].
4	pFK_JFH1_wt_dg	JFH1	Full-length HCV genome isolate JFH1 [99]
5	pFK-i389-RLuc2a-core3' JFH1	JFH1R2A	Monocistronic full-length <i>Renilla</i> luciferase reporter virus of JFH1 containing a duplication of the first 16 aa of core, followed by <i>Renilla</i> luciferase and the foot and mouth disease virus (FMDV) 2a peptide to allow proteolytic cleavage of the reporter luciferase (Dr. M. Zayas)
6	pFK H77c-842/JHF1_Y835H_K1402Q_V2 440L_dg	H77/JFH1	Full-length virus chimera consisting of 5' UTR of JFH1, core to the first putative transmembrane domain of NS2 of H77, followed by the remaining sequence of JFH1. Three adaptive mutations Y835H, K1402Q, V2440L enhance the release of infectious particles as compared to the <i>wt</i> construct [261].
7	pFK_JFH1R2aH77C-842_Y835H_K1402Q_V2440L_dg	H77R2A/JFH1	Full-length <i>Renilla</i> luciferase reporter virus chimera consisting of 5' UTR of JFH1, containing a duplication of the first 16 aa of core, the <i>Renilla</i> luciferase and subsequently the region from core to the first putative transmembrane domain of NS2 of H77 followed by the remaining sequence of JFH1 [261].
8	pFK_JFH1/Con1C-842_Y835C_V2440L_dg	Con1/JFH1	Full-length virus chimera consisting of 5' UTR of JFH1, containing the region from core to the first putative transmembrane domain of NS2 of Con1 followed by the remaining sequence of JFH1. Two adaptive mutations Y835C and V2440L enhance the release of infectious particles as compared to the <i>wt</i> construct [261].
9	pFK_JFH1R2A/Con1C-842_Y835C_V2440L_dg	Con1R2A/JFH1	Full-length <i>Renilla</i> luciferase reporter virus chimera consisting of 5' UTR of JFH1, containing a duplication of the first 16 aa of core, the <i>Renilla</i> luciferase and subsequently the region from core to the first putative transmembrane domain of NS2 of Con1 followed by the remaining sequence of JFH1 [261].
10	pFK_i389LucNS3-3'_Con1ET_dg	subgCon1ET	Bicistronic subgenomic reporter replicon with 5' and 3' UTR as well as NS3-5B coding sequence of Con1 (genotype 1b). The first JFH1 IRES drives the expression of the <i>Firefly</i> luciferase (N-terminally fused to first 16 aa of core protein), the second cistron (NS3-5B) is under the control of the encephalomyocarditis virus (EMCV) IRES. Adaptive mutations E1202G, T1280I in NS3 and K1846T in NS4B enhance replication [85].
11	pFK_i389LucNS3-3'_JFH1_dg	subgJFH1	Bicistronic subgenomic reporter replicon of JFH1 (genotype 2a) with 5' and 3' UTR as well as NS3-5B coding sequence. The first HCV IRES drives the expression of the <i>Firefly</i> luciferase (N-terminally fused to first 16 aa of core protein), the second cistron (NS3-5B) is under the control of the EMCV IRES.
12	pFK_i389LucNS3-3'_Con1ET_GND_dg	subgCon1ET_GND	Replication deficient subgenomic reporter replicon of Con1 (genotype 1b)
13	pFK_i389LucNS3-3'_JFH1_ΔGDD_dg	subCon1ET_ΔGDD	Replication deficient subgenomic reporter replicon of JFH1 (genotype 2a)
14	pFK_DVs_R2A	DENVR2A	Monocistronic full length <i>Renilla</i> reporter virus of Dengue virus serotype 2 (Dr. W. Fischl)
15	pFKi_341_PiLuc_NS3-3' H77S	subgH77S	subgenomic gt1a replicon with 5A adaptive mutations [82]
16	pSGR S52/SG-Feo SHI	subg3a	subgenomic gt3a replicon with adaptive mutations P1226S+ D1437H+ S2210I, <i>Firefly</i> luciferase [90]
17	pSGR ED43/SG-Feo VYG	subg4a	subgenomic gt4a replicon with adaptive mutations M1205V+ D1421Y+R2882G, <i>Firefly</i> luciferase [90]
18	pSGR/SG-Feo-SKIP	subg5a	subgenomic gt5a replicon with adaptive mutations, E1203K+K1406S+S2205I+S2366, <i>Firefly</i> luciferase [91]

The Y35A single point mutation was introduced into the core protein of plasmid N°1,4,6 and 8. These mutants are designated with their original name followed by "Y35A", i.e. Jc1Y35A. The F24A single point mutation was introduced into the core protein of plasmid N°1,3, 4, 5, 6, 7, 8 and 9. These mutants are designated with their original name followed by "F24A", i.e. Jc1F24A. pFK based vectors are low copy plasmids. This vector backbone encoding genomic or subgenomic HCV sequences was used to generate viral RNA transcripts.

Table 2.9 NPC1 expression constructs

#	name	resistance	description	reference
1	pCMV6-XL4-NPC1 (human cDNA)	Ampicillin	human NPC1 gene	Amsbio (SC120010)
2	pWPI_NPC1 (human cDNA)	Ampicillin	human NPC1 gene	self made, based on pCMV6-XL4-NPC1
3	pWPI_NPC1 (human cDNA)-shNPC1(2) res	Ampicillin	human NPC1 gene with silent mutations in the shNPC1 (2) target sequence	self made

Table 2.10 Retroviral vectors

#	name	resistance	description
1	pWPI-blx	Ampicillin, Blasticidin	Lentiviral vector for mammalian expression of untagged proteins driven by the E2a promotor. Selection of transduced cells with blasticidin.
2	pCMV-dR8.91	Ampicillin	Gag-pol encoding packaging plasmid for pWPI and pLKO vector system
3	pMD.G		VSV envelope protein for pWPI and pLKO vector system
4	pLKO	Ampicillin, Puromycin	All Mission shRNAs are in pLKO Lentiviral vectors

2.1.4 Chemicals and compounds

Table 2.11 Chemicals and reagents

name	supplier
Acrylamide: Bisacrylamide Mix (29:1) 40%	Sigma Aldrich (St. Louis USA)
Agarose	Thermo Fisher Scientific (Waltham, USA)
Albumin, from bovine serum (BSA), fatty acid free	Sigma Aldrich (St. Louis USA)
Amersham Hyperfilm ECL	GE Healthcare Life Sciences (Uppsala, Sweden)
Coomassie Brilliant Blue G250	Serva Electrophoresis GmbH (Heidelberg, Germany)
Coelenterazine	PJK (Kleinblittersdorf, Germany)
Digitonin	Sigma Aldrich (St. Louis USA)
D-Luciferin	PJK (Kleinblittersdorf, Germany)
DMSO	Roth (Karlsruhe, Germany)
Dithiothreitol (DTT)	Sigma Aldrich (St. Louis USA)
dNTPs	Peqlab Biotechnologies (Bruchsall, Germany)
ECL Plus Western Blot Detection System	Amersham/Perkin-Elmer
EDTA	Merck (Darmstadt, Germany)
Ethanol p.A.	Sigma Aldrich (St. Louis USA)
HEPES	Thermo Fisher Scientific (Waltham, USA)
Hydrogen Peroxide	Roth (Karlsruhe, Germany)
Fluoromount G	Southern Biotechnology Associates (Birmingham, USA)
Fetal Calf Serum	PAA Laboratories (USA)
GeneRuler™ 100 bp DNA Ladder	Fermentas (St. Leon-Rot, Germany)
Green dye master mix 2x	PJK (Kleinblittersdorf, Germany)
Glutathione	Sigma Aldrich (St. Louis USA)
Glycerol	Roth (Karlsruhe, Germany)
Glycyl-glycine	Sigma Aldrich (St. Louis USA)
Isopropanol p.A.	Sigma Aldrich (St. Louis USA)
Lambda DNA/Eco1301 (Styl) Marker	Fermentas (St. Leon-Rot, Germany)
L-Glutamine for cell culture	Thermo Fisher Scientific (Waltham, USA)
Methanol p.A.	Sigma Aldrich (St. Louis USA)
beta-Mercaptoethanol	Roth (Karlsruhe, Germany)
Prestained protein marker	New England Biolabs (Frankfurt, Germany)
Polyethylen Glycol (PEG) -8000	Applichem (Darmstadt, Germany)
PVDF Western Blot membrane	Perkin Elmer (Waltham, USA)
rNTPs	Roche (Mannheim, Germany)
Skim Milk	Roth (Karlsruhe, Germany)
Sucrose	Sigma Aldrich (St. Louis USA)
Sodium dodecylsulfate	Applichem (Darmstadt, Germany)
Spermidine	Sigma Aldrich (St. Louis USA)
TEMED	Applichem (Darmstadt, Germany)
Triton-X-100	Merck (Darmstadt, Germany)
Tween-20	Roth (Karlsruhe, Germany)
Vectashield	Vector Laboratories Inc (Burlingame, USA)

Table 2.12 Compounds used in this study

chemical compounds	solvent	supplier
Clomiphene citrate (LKT-C44559.1)	DMSO	Biomol (Hamburg, Deutschland)
Mevastatin (M2537)	DMSO	Sigma Aldrich (St. Louis, USA)
Oleic acid (O10008)	isopropanol	Sigma Aldrich (St. Louis, USA)
U16888A (U3633)	water	Sigma Aldrich (St. Louis, USA)
Ro 48-8071 (EI342-0010)	water	Enzo (Lörrach, Germany)
Triacsin C (BML-EI218)	DMSO	Enzo (Lörrach, Germany)

2.1.5 Media and antibiotics

Table 2.13 Media

media/ media supplements	composition
Ampicillin stock solution	100 mg/ml Ampicilin in dH ₂ O, filter sterilized, storage at -20°C
Blasticidin stock solution	5 mg/ml in ddH ₂ O, filter sterilized, storage at -20°C
DMEM complete (cpl)	Dulbecco's modified minimal essential medium (DMEM) (GIBCO) supplemented with 2 mM L-glutamine (GIBCO), 1x nonessential amino acids (GIBCO), 100 ug/ml streptomycin (GIBCO), 10% fetal calf serum (heat inactivated) (PAA), 100 U/ml penicillin (GIBCO), storage at 4°C
Geneticin G418 stock solution	100 mg/ml in ddH ₂ O, filtered through 0.22 uM filter, storage at -20°C
Imaging media	Phenol Red-free DMEM complete, storage at 4°C, freshly prepared before imaging
Kanamycin stock solution	30 mg/ml in dH ₂ O, filter sterilized, storage at -20°C, working concentration 1:1000 dilution
Lysogeny broth (LB)	10 g Bacto-Trypton, 2.5 g NaCl, 5 g Yeast extract, total volume of 1L
LB-Agar	10 g Bacto-Trypton, 2.5 g NaCl, 5 g Yeast extract, 20 g Agar, total volume of 1L
Optimem	0.05% trypsin, 0.02% EDTA in 1x PBS (GIBCO), autoclaved, storage at 4°C
Trypsin solution	100 mM Tris-HCl (pH 8.3), 500 mM KCl, 15 mM MgCl ₂ , 0.01% (w/v) gelatine
Imaging media	Phenol Red-free DMEM complete, storage at 4°C, freshly prepared before imaging
Lysogeny broth (LB)	10 g Bacto-Trypton, 2.5 g NaCl, 5 g Yeast extract, total volume of 1L
LB-Agar	10 g Bacto-Trypton, 2.5 g NaCl, 5 g Yeast extract, 20 g Agar, total volume of 1L

Table 2.14 Antibiotics

antibiotics	supplier
Ampicillin	Roche (Mannheim, Germany)
Blasticidin	Thermo Fisher Scientific (Waltham, USA)
Geneticin sulfate (G418)	Invitrogen (Karlsruhe, Germany)
Kanamycin sulfate	Serva (Heildeberg, Germany)
Penicillin	Invitrogen (Karlsruhe, Germany)
Puromycin	Sigma Aldrich (St. Louis, USA)
Zeocin	Invitrogen (Karlsruhe, Germany)

2.1.6 Enzymes and kits

Table 2.15 Enzymes

name	supplier
Accu Prime Pfx DNA Polymerase	Thermo Fisher Scientific (Waltham, USA)
BP Clonase™	Thermo Fisher Scientific (Waltham, USA)
Calf Intestinal Phosphatase (CIP)	New England Biolabs (Frankfurt, Germany)
DNaseI	Promega (Mannheim, Germany)
FideliTaq® Polymerase	Affymetrix (Santa Clara, USA)
LR clonase™	Thermo Fisher Scientific (Waltham, USA)
NEB DNA restriction enzymes	New England Biolabs (Frankfurt, Germany)
Rnasin® Plus Rnase Inhibitor	Promega (Mannheim, Germany)
cOmplete™, EDTA-free protease inhibitor cocktail	Sigma Aldrich (St. Louis, USA)
Proteinase K	Thermo Fisher Scientific (Waltham, USA)
Superscript® III Reverse transcriptase	Thermo Fisher Scientific (Waltham, USA)
T4 DNA Ligase	Fermentas (St. Leon-Rot, Germany)
T7 RNA polymerase	Promega (Mannheim, Germany)

Table 2.16 Kits

kits	supplier
High Capacity cDNA Reverse Transcription	Thermo Fisher Scientific (Waltham, USA)
iTaq Universal SYBR® green	Bio-Rad (München, Germany)
One Step RT-PCR Kit	Quiagen (Hilden, Germany)
Nucleobond® PC100	Machery-Nagel (Düren, Germany)
Nucleospin® Extract II	Machery-Nagel (Düren, Germany)
Nucleospin® Plasmid	Machery-Nagel (Düren, Germany)
Nucleospin® RNA II	Machery-Nagel (Düren, Germany)
QIAGEN™ Plasmid Maxi Kit	Quiagen (Hilden, Germany)

2.1.7 DNA and RNA oligonucleotides

Table 2.17 DNA oligonucleotides (oligos) used for cloning

name of DNA oligos used for cloning	sequence 3-5'
AgeI_fwd	CCCGGGAGAGCCATAGTGG
BamHI_Flag_fwd	AAAAGCGGATCCACGAATCCTAAACCTCAAAGAAAAACCAAACG
BamHI_rev	CGACTTAATTAATTAGGGATCCACTAGT
BglIII_rev	CTG TAC TGT CTC GTG CCG GCG
BsABI_fwd	CCTGCGATGCAGATCCGGAA
BsiWI_rev	CCGAACATGACGCCCAATG
Con1F24A/JFH1_fwd	GACGTCAAGGCACCGGGCGG
Con1F24A/JFH1_rev	CCGCCCGGTGCCTTGACGTC
Con1Y35A/JFH1_fwd	GTCAGATCGTCGCTGGAGTTGCACTGTTGCCGCGCAGGGGCCCC
Con1Y35A/JFH1_rev	GGGGCCCCCTGCGCGGCAACAGTGCAACTCCACCGACGAACTCCAC CGACGATCTGAC
H77F24A/JFH1_fwd	GGACGTTCAAGGCACCGGGTGG
H77F24A/JFH1_rev	CCACCCGGTGCCTTGACGTC
H77Y35A/JFH1_fwd	GGTCAGATCCGTTGGTGGAGTTGCATTGTTGCCGCGCAGGGGCCCC
H77Y35A/JFH1_rev	GGGGCCCCCTGCGCGGCAACAATGCAACTCCACCAACGATCTGAC
JFH1F24A_fwd	GACGTCAAGGCACCGGGCGG
JFH1F24A_rev	CCGCCCGGTGCCTTAACGTC
Jc1F24A_fwd	CAAGACGTTAAGGCACCGGGCGG
Jc1F24A_rev	CCG CCC GG T GC C TTAACG TCT TG
NcoI_fwd	ATAATACCATGGCCATGAGCG
NruI_rev	GCCACCCAACACCTCGAGGC
Psil_fwd	CATGGCCTCGTGAATCCCG
5'NTR_fwd	ACCTGCCCTAATAGGGGG

oligos were ordered from Sigma Aldrich (St. Louis, USA)

Table 2.18 DNA oligonucleotides (oligos) used for qPCR

names of DNA oligos used for qPCR	sequence 3-5'
PI4KIIA_fwd	CAGCTCTGACCAAGTGGAGAT
PI4KIIA_rev	GCGGATGGTTGCATTGGAA
ABCA1_fwd	ACCCACCCTATGAACAACATGA
ABCA1_rev	GAGTCGGGTAACGGAAACAGG
HMGCoA reductase_fwd	GGGAATGCAGAGAAAGGTGCAA
HMGCoA Reductase_rev	TGCCACTCCAACAGGGATGG
LDLR_fwd	CCCATCGTGCTCCTCGTCTT
LDLR_rev	GCCACGTCATCCTCCAGACT
GAPDH_fwd	GAAGGTGAAGGTCCGAGTC
GAPDH_rev	GAAGATGGTGATGGGATTTC

oligos were ordered from Sigma Aldrich (St. Louis, USA)

Table 2.19 shRNA oligonucleotides used in this study

shRNA name	target	oligo sequence (3-5')
shApoE (1)	Apolipoprotein E (ApoE)	CCGGGACAATCACTGAACGCCGAAGCTCGAGCTTCGGCGTTTCAGTG ATTGTCCTTTTTG
shApoE (2)		CCGGACGAGACCATGAAGGAGTTGACTCGAGTCAACTCCTTCATGG TCTCGTTTTTTG
shApoE (3)		CCGGGAAGGAGTTGAAGGCCTACAACCTCGAGTTGTAGGCCCTCAAC TCCTCTTTTTT
shApoE (4)		CCGGGCAGACACTGTCTGAGCAGGTCTCGAGACCTGCTCAGACAGT GTCTGCTTTTTT
shApoE (5)		CCGGCCGCCTCAAGAGCTGGTTCGACTCGAGTCGAACCAGCTCTTG AGGCGGTTTTT
shNPC1 (1)	Niemann-Pick Disease Type C1 protein (NPC1)	CCGGCCACAAGTTCTATACCATATTCTCGAGAATATGGTATAGAACTTG TGTTTTT
shNPC1 (2)		CCGGCCTGTTACAAACCAGACGAAACTCGAGTTTCGTCTGGTTTGTA ACAGGTTTTT
shNPC1 (3)		CCGGCCTGTCTTACTCAGTTACATACTCGAGTATGTAAGTGAAGA CAGGTTTTT
shNPC1 (4)		CCGGAGAGGTACAATTGCGAATATTCTCGAGAATATTCGCAATTGTAC CTCTTTTTTTG
shNPC1 (5)		CCGGACTCCTACATGGTGGATTATTCTCGAGAATAATCCACCATGTAG GAGTTTTTTTTG
shOSBL1A (1)	Oxysterol binding protein- like 1A protein	CCGGGCAAAGTACCTGTGTACTTAACTCGAGTTAAGTACACAGGTAC TTTGCTTTTTTTG
shOSBL1A (2)		CCGGGCATCAAGAAACACAGAACAACCTCGAGTTGTTCTGTGTTTTCTT GATGCTTTTTTTG
shOSBL1A (3)		CCGGGCCGGATTCTGAAAGTGATTCTCGAGAATACACTTTCAGAATC CGGCTTTTTTTG
shOSBL1A (4)		CCGGGATGTAACCTTTGACATATTTCTCGAGAAATATGTCAAAGGTTA CATCTTTTTT
shOSBL1A (5)		CCGGATTTCATGCTGAAGGATTAACCTCGAGTTAATCCTTCAGCATG AAATTTTTTTG
shPITPNM1 (1)	Phosphatidylinositol transfer protein, membrane associated 1 (PITPNM1)	CCGGGCCTATAAGCTGTGCAAGGTTCTCGAGAACCTTGACAGCTTA TAGGCTTTTTT
shPITPNM1 (2)		CCGGGCCGGTTATGGGTCTCCCAAACCTCGAGTTTGGGAGACCCATA ACCGGCTTTTTT
shPITPNM1 (3)		CCGGAGTGGCGCATGCAGAACATTGCTCGAGCAATGTTCTGCATGC GCCACTTTTTTTG
shPITPNM1 (4)		CCGGTCCGGCTACCTGATCGTGTATCTCGAGATACACGATCAGGTAG CCGGATTTTTTTG
shPITPNM1 (5)		CCGGCGTCACGCTCACTGGAGAGAACTCGAGTTCTCTCCAGTGAGC GTGACGTTTTT
shSTARD3 (1)	StAR related lipid transfer domain containing 3 protein	CCGGCGCAAGACGTTTATCCTGAACTCGAGTTCAGGATAAACGCTCT TGCCGTTTTTTG
shSTARD3 (2)		CCGGCCAGTGCATTCCCTCATTGCTCACTCGAGTGACAATGAGGAATGC ACTGGTTTTTTG
shSTARD3 (3)		CCGGGACCTGGTTCCTTGACTTCAACTCGAGTTGAAGTCAAGGAAC CAGGCTTTTTTTG
shSTARD3 (4)		CCGGGAGATCATCCAGTACAACCTTCTCGAGAAAGTTGACTGGATG ATCTCTTTTTTTG
shSTARD3 (5)		CCGGCAGGAAGAGAACTGGAAGTTTCTCGAGAAACTCCAGTTCTCT TCCTGTTTTTTG
shNT (1)	non-targeting control generation 1	CCGGCAACAAGATGAAGAGCACCAACTCGAGTTGGTGCTCTTCATCT TGTTGTTTTT
shNT (2)	non-targeting control generation 2	CCGGCAACAAGATGAAGAGCACCAACTCGAGTTGGTGCTCTTCATCT TGTTGTTTTT

Mission shRNA was ordered from Sigma Aldrich (St. Louis, USA)

Table 2.20 siRNA oligonucleotides used in this study

siRNA name	solvent	sequence (sense)
siApoE	Apolipoprotein E	CUAGUUUAAUAAAGAUUCA
siCOPA(1)	Coat protein complex subunit alpha	UCGGAUGUGAGAGGAAUAA
siCOPA(2)	Coat protein complex subunit alpha	UGAUGGUGGUUAUGAUUGUG
siCOPgamma1(1)	Coat protein complex subunit gamma isoform 1	ACAAGCCAUUGUGAACAAG
siCOPgamma1(2)	Coat protein complex subunit gamma isoform 1	GGAGAUGUCUUGCAUUGCA
siCOPgamma2(1)	Coat protein complex subunit gamma isoform 2	GCUGCAUCAAGUGAAUUA
siCOPgamma2(2)	Coat protein complex subunit gamma isoform 2	UUAGUGCUCUCUGUCAGAA
siDDX3(1)	X-linked DEAD box RNA helicase 3	CAGAUUUAGUGGAGGGUUU
siDDX3(2)	X-linked DEAD box RNA helicase 3	GAUGCUGGCUCGUGAUUUC
siPI4KIIIA	Phosphatidylinositol-4-kinase III alpha	CAGUGGAAGGACAACGUGA
siRluc	<i>Renilla</i> luciferase	GUAGCGCGGUGUAUUUAC
siNS1	DENV nonstructural protein 1	ACACCAGAAUUGAAUCACA
non-targeting	negative control, non-targeting (NT) control	UGGUUUACAUGUCGACUAA

siRNAs were ordered from MWG (Ebersberg, Germany)

2.1.8 Instruments

Table 2.21 Instruments relevant for this study

name	supplier
ABI PRISM™ 7000 Sequence Detector System	Applied Biosystems (Foster city, USA)
Branson Sonifier 450	Branson (Danbury, USA)
Confocal laser scanning microscope sp2	Leica (Heidelberg, Germany)
Curix 60 Developer Machine	AGFA (Köln, Germany)
Gene pulser II	Bio-Rad Laboratories, Inc. (Hercules, USA)
Intas Science imager	Intas Science Imaging Instruments GmbH (Göttingen, Germany)
Luminometer Lumat LB 9507	Berthold Technologies (Bad Wildbad, Germany)
Luminometer Mithras LB940	Berthold Technologies (Bad Wildbad, Germany)
Spinningdisc confocal microscope ERS-6	PerkinElmer (Baesweiler, Germany)
Tecan Fluor4	Tecan (Wiesbaden, Germany)

2.1.9 Transfection reagents

Table 2.22 Transfection reagents

transfection reagent	supplier
INTERFERin	Polyplus transfection (Illkirch, France)
jetPEI	Polyplus transfection (Illkirch, France)
Lipofectamin 2000	Thermo Fisher Scientific (Waltham, USA)
Mirus TransIT Transfection Reagent	Mirus Bio (Madison, USA)
Optimem	Thermo Fisher Scientific (Waltham, USA)
Lipofectamine® RNAimax	Thermo Fisher Scientific (Waltham, USA)

2.1.10 Cell culture

Eukaryotic cell lines

HEK-293T: highly transfectable derivative of the human embryonic kidney 293 cells that contains the SV40 T antigen [238].

Huh7.5: highly permissive cell line for genomic and subgenomic HCV RNA replication derived from a human hepatoma cell line that was cured from subgenomic HCV RNA replication by IFN-alpha treatment [88].

Huh7.5FLuc: Huh7.5 cells that constitutively express the *Firefly* luciferase that can be used as an estimate for cell number [77].

Huh7/Lunet: highly permissive for HCV genomic and subgenomic HCV RNA replication, but not for infection due to low CD81 expression levels. Cell line derived from Huh7 human hepatoma cells that were cured from subgenomic HCV RNA replication by treatment with an inhibitor for NS5B [239]. Compared to naive Huh7 cells, Huh7/Lunet exhibit a higher potency of HCV RNA replication.

Huh7/LunetCD81H: derived from the parental cell line Huh7/Lunet by stable transfection of a CD81 expression construct [240].

Huh7/Lunet_Lucubineo_JFH1 (here designated as LucUbiNeo_JFH1): Huh7/Lunet cells stably replicating the subgenomic HCV RNA of genotype 2a and the Firefly Reporter under the selection of G418 (1mg/ ml) [241].

Huh7/Lunet_Lucubineo_Con1ET (here designated as LucUbiNeo_Con1ET): Huh7/Lunet cells stably replicating the subgenomic HCV RNA of genotype 1b and the *Firefly* reporter under the selection of G418 (0.5 mg/ ml). Replication enhancing mutations are: E1202G, T1280I and K1845T [86].

Huh7/Lunet-T7 (Zeocin/ Blastidicin): Huh7/Lunet cells constitutively expressing the T7 RNA polymerase of the T7 bacteriophage that allows the cytosolic expression of T7 driven expression constructs under Zeocin or Blastidicin selection [242].

Huh7/LunetCD81H-RFP: Huh7/LunetCD81H cells stably expressing the Tag-RFP-T that allows the visualization of the cell boundary, generated by Dr. G. Alvisi [243].

Huh7/LunetCD81H_core-NS2: Huh7/LunetCD81H cells stably expressing the core-NS2 proteins of JFH1 (gt2a), kindly provided by Dr. JY. Lee.

VeroE6 cells: African green monkey kidney cells [244].

Bacteria

For classical cloning the chemically competent E-ColiDH5 α (F⁻, ϕ 80dlacZ Δ M15, Δ (lacZYA-argF)U169, deoR, recA1, endA1, hsdR17(rK⁻, mK⁺), phoA, suE44, λ ⁻, thi-1, gyrA96, relA1) were used (homemade).

2.2 Methods

2.2.1 Cell culture

Long-term storage and thawing of cells

Cells were kept at -80°C or in liquid nitrogen for long-term storage. Therefore cells of a confluent 15 cm dish were detached by trypsinization and resuspended in DMEMcplt. Cells were spun for 5 min at 700 g and the pellet was resuspended in 11 ml of ice-cold cryo solution. The cell suspension was immediately aliquoted in re-chilled cryotubes. Cells were first frozen at -80°C before transfer to liquid nitrogen.

For thawing of the cells, the cryotubes were heated in a 37°C water bath before resuspending in 10 ml preheated DMEMcplt. Cells were spun for 5 min at 700 g, the pellet was resuspended in fresh DMEMcplt and cells were seeded in the respective cell culture dish. If necessary, 24 h post seeding the media was replaced by antibiotic containing media for selection.

2.2.2 Nucleic acid standard methods

DNA restriction digest

Restriction digest of plasmid DNA or PCR products was performed using NEB enzymes. The amount of enzyme added to the reaction was adjusted depending on the amount of DNA, on the number of restriction sites, as well as on the unit definition given by the manufacturer. Digest was either performed in a total volume of 100 μl (for preparative digestions) or 20 μl (for analytic digestions).

Dephosphorylation of DNA

In order to prevent ligation of linearized dsDNA without the integration of the desired insert during ligation, the 5' phosphates were dephosphorylated using calf intestine alkaline phosphatase (CIP). Subsequently the DNA was purified by agarose gel electrophoresis.

Ligation of DNA

Ligation of the insert DNA fragment and the respective DNA backbone was carried out using the T4 DNA Ligase. The reaction mixture contained 1x Ligase Buffer, 1U T4 DNA Ligase and the respective amounts of DNA in a 1:3 ratio of backbone to insert. Ligation was performed at RT for 2 h. An empty control lacking the insert was included in order to estimate true integrations of the insert into the backbone.

Agarose gel electrophoresis and gel extraction

DNA fragments can be separated according to their size in an agarose gel matrix by applying an electric field. Depending on the size of the respective DNA fragments 0.8-2% agarose gels in ionic 1x TAE buffer were prepared. For visualization of the DNA under ultraviolet light ethidium bromide (0.1% final concentration) was added to the agarose gel. The DNA was mixed with 1/6 volume of 6x protein loading buffer before loading onto the gel. The addition of a DNA molecular weight marker (Lambda-DNA/Eco130I/Styl) allowed the determination of the length in base pairs of the respective DNA fragment. After electrophoresis the desired DNA fragment was cut out of the gel and purified using the Nucleospin Extract II kit according to the manufacturer's protocol.

Transformation of competent E.Coli DH5 α

50 μ l of competent E.Coli DH5 α were incubated with the desired DNA or ligation reaction for 10 min on ice. Heat shock was performed for 45 sec at 42°C allowing the uptake of DNA, followed by a 5 min incubation of the bacterial suspension on ice. Next, 250 μ l of plain LB-medium were added and the bacteria were incubated for 1 h at 37°C while shaking. Finally they were plated on the respective antibiotic-containing LB agar plate and incubated over night at 37°C to allow colonies to form.

Plasmid DNA isolation and purification from bacteria

Depending on the desired amount of DNA, small scale (6 ml), medium scale (100 ml) or large scale (200 ml) bacterial E.Coli culture were grown over night. Extraction and purification of the desired DNA from the bacterial culture was performed according to the manufacturer's protocol.

Quantification of nucleic acid concentration

Determination of nucleic acid concentration was performed using the NanodropLite Spectrophotometer (Thermo Fisher Scientific, Waltham USA) measuring the absorbance at 260 nm. The ratio of absorbance at 260 and 280 nm $A_{260}/280$ was used as an indicator of nucleic acid purity, with proteins exhibiting an absorbance peak at 280 nm. Therefore $A_{260}/280$ between 1.8 and 2 was considered to represent pure DNA, and when larger than 2 pure RNA.

DNA transfection by lipofection

Target cells were seeded 1 day prior to transfection. Transfection of plasmid DNA was performed according to the manufacturer's protocol (Mirus Biol, Madison, USA).

RNAi transfection by lipofection

Target cells were seeded either one day prior to transfection or transfected while being seeded according to the manufacturer's protocol using the Lipofectamine[®] RNAimax transfection reagent (Thermo Fisher Scientific, Waltham, USA).

RNAi transfection by electroporation

Cells were detached from the cell culture dishes, thoroughly resuspended and counted. The required amount of cells was spun down, resuspended and washed in PBS and again spun down. The pellet was finally resuspended in cytomix to a final concentration of 1.5×10^7 cells/ml in case of Huh7.5 or 1×10^7 cells/ml in case of bigger cells such as Huh7/Lunet cells. For big electroporations 400 μ l of the cell suspension were added to either 5 μ g of subgenomic viral RNA or 10 μ g of full-length viral RNA and electroporated at the following settings: High Capacity 975 μ F, voltage 270 V, expected time constant approx. 18/20 ms. In case of small epos 100 μ l of the cell suspension were mixed with either 2.5 μ g of viral RNA or 2.5 μ l of 100 μ M siRNA at the following settings: High Capacity 0.5 μ F, voltage 166 V, expected time constant approximate 12/14 ms. In case of co-electroporation equal volumes of siRNA and vRNA were used in a total volume of 2.5 μ l. Electroporated cells were immediately resuspended in fresh DMEMcpl. The electroporations were performed using the gene pulser II (Bio-Rad Laboratories Inc., Hercules, USA) and GenePulser[®]/MicroPulser[™] Electroporation cuvettes with 0.2 or 0.4 cm gap respectively (Bio-Rad).

***In vitro* transcription and RNA transfection**

For the generation of *in vitro* transcripts 10 µg of the respective plasmid DNA were linearized by enzymatic digest (i.e. MluI in case of JFH1 based constructs) and subsequently purified using the Nucleospin® RNAII kit (Machery-Nagel, Düren, Germany). Next the *in vitro* transcription reaction mixture consisting of 80 mM HEPES (ph 7.5), 12 mM MgCL₂, 2 mM spermidine, 40 mM dithiothreitol (DTT), 3.125 mM of each nucleoside triphosphate, 1U/µl of RNasin (Promega), 0.6 U/µl of T7 RNA polymerase (homemade), 1U/µl RNasin (Promega) and the purified DNA in a total volume of 100 µl was incubated for 2 h at 37°C. Subsequently 0.3 U/µl of T7 polymerase was added for another 4 h of incubation. Transcription was terminated by the incubation with 2U of RNase free DNase (Promega) per µg DNA for 1 h at 37°C. RNA was purified by acidic phenol/chloroform extraction at 4°C followed by precipitation with isopropanol at room temperature. RNA pellets were dissolved in RNase free water. The quality of the obtained *in vitro* transcript was checked by agarose gel electrophoresis.

Total cellular RNA isolation

Isolation of total cellular RNA was carried out using the Nucleospin® RNAII kit (Machery-Nagel, Düren, Germany). Typically 350 µl of buffer A1 supplemented with 1% beta-Mercaptoethanol were added to a confluent 24 well and RNA isolation was performed as described in the manufacturer's protocol.

Quantification of cellular RNA by reverse transcription (RT) and quantitative PCR (qPCR)

In order to generate cDNA from isolated RNA the High Capacity cDNA Reverse Transcription Kit (Thermo Scientific, Waltham, USA) was used. First a 2x reaction master mix (5ul/sample) was prepared containing 2x RT Buffer, 4 mM dNTP Mix, 2x RT Random Primer, 25 U Reverse transcriptase and RNase inhibitor. This was then added to 5 µl of the isolated RNA, mixed well and centrifuged to eliminate air bubbles. The reaction mixture was placed into a Thermocycler (Eppendorf, Hamburg, Germany) using the following program: 10 min at 25°C, 120 min at 37°C, 5 min at 85°C, storage at 4°C. The cDNA was diluted 1:10 in RNase free water and directly used for qPCR using the iTaq Universal SYBR Green Kit (Bio-Rad, München, Germany). A master mix (12 µl/ sample) consisting of 2x iTaq Universal Bio Rad and 0.5 µM of the corresponding sense and antisense primer was prepared, to which 3 µl of pre-diluted cDNA was added. Each reaction was conducted in triplicates. Additionally the RNA levels of the housekeeping gene GAPDH were determined in parallel for each condition.

2.2.3 Standard cloning methods

Polymerase chain reaction (PCR)

The PCR allows the specific amplification of a desired DNA fragment from a given DNA template. The PCR reaction mixture contained 0.2 mM of each dNTP, 2 µM of sense and antisense primer, 0.5 µg template DNA, 1x PCR Buffer in addition to 0.02 U/µl FidelityTaq for amplicon sizes smaller than 1.5 kb. Amplification was carried out using a thermocycler following the program: i) 2 min at 95°C, ii) 30 sec at 95°C for denaturation, iii) 30 sec at 55°C for annealing of the primers, iv) 1 min per 1kb for elongation, v) 4 min at 68°C followed by termination at 4°C. Steps ii)-iv) were repeated 15-20 times. For amplification of DNA fragments bigger than 1.5 kb the AccuPrime (Thermo Scientific, Waltham, USA) was used

according to the manufacturer's protocol. In short the reaction mixture of a total volume of 25 μ l contained 1x PCR reaction buffer, 0.5 μ g of template DNA, 2 μ M of sense and antisense primer and 0.25 μ l AccuPrime. The above-described PCR cycling program was used with an extended elongation time allowing the amplification of long DNA fragments.

Site-directed mutagenesis using overlap PCR

By performing overlap PCR, point mutations were introduced into the respective target DNA. In principle PCR in combination with the use of partially complementary oligodeoxyribonucleotide primers containing nucleotide alterations allow the introduction of mutations into the target sequence. In addition to the mutagenesis primers two primers flanking the target sequence upstream and downstream are needed. In a first PCR either the upstream primer (sense) and the mutagenesis primer (antisense) or the downstream primer (antisense) and the mutagenesis primer (sense) were combined leading to the generation of DNA fragments that contained the desired nucleotide alteration either at the 3' or 5' end. These fragments were separated by agarose gel electrophoresis and subsequently purified using the Nucleospin Extract II Kit (Machery Nagel). In a last PCR 1 μ l of each purified PCR product was used as template in combination with the upstream primer (sense) and the downstream primer (antisense). This overlap PCR allowed the generation of amplified DNA fragments that carried the desired mutations.

Cloning of Y35A or F24A mutants

These mutations were separately introduced by site directed mutagenesis into the respective backbones (Table 2.8).

Table 2.23 Constructs generated in this study with the respective restriction enzymes used for cloning

name of mutant construct	name of primers	restriction enzymes	original constructs
Con1Y35A/JFH1	BsABI_fwd, Con1Y35A/JFH1_rev, Con1Y35A/JFH1_fwd, BgIII_rev	BsABI, BgIII	pFK_JFH1/Con1C-842_Y835C_V2440L_dg
Con1F24A/JFH1	BsABI_fwd, Con1F24A/JFH1_rev, Con1F24A/JFH1_fwd, BgIII_rev	BsABI, BgIII	pFK_JFH1/Con1C-842_Y835C_V2440L_dg
Con1F24AR2A/JFH1	Psil_fwd, Con1F24A/JFH1_rev, Con1F24A/JFH1_fwd, BgIII_rev	Psil, BgIII	pFK_JFH1R2A/Con1C-842_Y835C_V2440L_dg
H77Y35A/JFH1	H77Y35A/JFH1_fwd, H77Y35A/JFH1_rev Agel_fwd, H77F24A/JFH1_rev,	Agel, AvrII	842/JHF1_Y835H_K1402Q_V2440L_dg
H77F24A/JFH1	H77F24A/JFH1_fwd, Nrul_rev Psil_fwd, H77F24A/JFH1_rev,	Agel, Nrul	842/JHF1_Y835H_K1402Q_V2440L_dg
H77F24AR2A/JFH1	H77F24A/JFH1_fwd, Nrul_rev	Psil, Nrul	pFK_JFH1R2A/Con1C-842_Y835C_V2440L_dg
JcR2AF24A	Psil_fwd, Jc1F24A_rev, Jc1F24A_fwd,	Psil, BsiWI	pFK-i389RLuc2A-Core-3'Jc1
JFH1Y35A	5'NTR, Y35A_fwd, Y35A_rev, A2A/1394	Psil, SexAI	pFK_JFH1_wt_dg
JFH1F24A	5'NTR, JFH1F24A_fwd, JFH1F24A_rev, A2A/1394, BsiWI_rev	Agel, BsiWI	pFK_JFH1_wt_dg
JFH1F24AR2A	Psil_fwd, JFH1/F24A_rev, JFH1F24A_fwd, BsiWI_rev	Psil, BsiWI	pFK-i389-Rluc2a-core3' JFH1
FlagCon1core	BamHI-Flag_fwd, BamHI-Con1_rev	BamHI	pFK_JFH1/Con1C-842_Y835C_V2440L_dg
Flag-Con1coreF24A	NcoI_fwd, Con1F24A/JFH1_rev, Con1F24A/JFH1_fwd, BamHI_rev	NcoI, BamHI	pTM_Flag_Con1core
Flag-H77core	NcoI_fwd, H77F24A/JFH1_rev, H77F24A/JFH1_fwd, BamHI_rev	NcoI, BamHI	pTM_Flag_H77core
Flag-H77coreF24A	BamHI-Flag_fwd, BamHI-H77_rev	BamHI	pFK H77c-842/JHF1_Y835H_K1402Q_V2440L_dg
Flag-J6-coreF24A	NcoI_fwd, Jc1F24A/JFH1_rev, Jc1F24A/JFH1_fwd, BamHI_rev	NcoI, BamHI	pTM_Flag_J6core
Flag-JFH1coreF24A	NcoI_fwd, JFH1F24A/JFH1_rev, JFH1F24A/JFH1_fwd, BamHI_rev	NcoI, BamHI	pTM_Flag_JFH1core

Jc1Y35A, Jc1F24A were generated by S. Kallis and I. Aydin respectively.

A summary of the primer pairs used for site directed mutagenesis as well as the enzymes used for the digest of the backbone and insert are listed in Table 2.23.

Cloning of NPC1 expression and shRNA rescue construct

A plasmid encoding the human NPC1 cDNA was ordered from Amsbio and used as template for cloning a shRNA resistant construct into the retroviral pWPI vector. To this end 5 single silent point mutations were introduced into the target sequence of the shRNA of interest. The respective primer and enzymes used for cloning are depicted in the table below.

Table 2.24 NPC1 expression plasmids used in this study

name of construct	name of primers	restriction enzymes	original constructs
pWPI_NPC1	NPC1-BamHI_fwd, NPC1-MluI_rev	BamHI, MluI	pCMV6-XL4-NPC1
pWPI_NPC1_shNPC 1(2) res	NPC1-BamHI_fwd, NC1sh9res_rev, NPC1sh9res_fwd, NPC1-BIPL-rev	BamHI, BlnI	pWPI_NPC1

Sequence analysis

DNA was sequenced using the sequencing services by GATC Biotech (Konstanz, Germany).

2.2.4 Protein analysis standard methods

Protein concentration determination by Bradford assay

Protein concentration determination by Bradford is based on the absorbance of the dye Coomassie Brilliant Blue G-250, which binds under acidic conditions to cationic and apolar side chains of proteins. The unbound form exhibits an absorbance maximum at 470 nm, which shifts to 595 nm upon protein binding. The increase of absorbance at 595 nm is proportional to the bound form and a good measure of the amount of present protein. First Bradford assay solution was allowed to reach room temperature. A protein standard curve was prepared by making serial dilutions of BSA in HPLC water starting from 20 µg/ml to 0 µg/ml in a final volume of 20 µl. To each dilution 5 µl of the respective lysis buffer were added. For the determination of the protein concentration in the sample of interest 5 µl of the cell lysate were added to 20 µl of HPLC water. 1 ml of Bradford solution was added to each cuvette mixed well and incubated for 10 min at room temperature. Absorbance was measured at 595 nm. With the help of a standard curve, based on different BSA concentrations, the protein concentrations were determined in the samples of interest.

Preparation of samples for protein standard analysis methods

Cells were typically lysed in an appropriate amount of RIPA Buffer supplemented with 1x Protease Inhibitor cocktail. Lysates were incubated for 45 min on ice and cleared by centrifugation at maximum speed for 45-60 min at 4°C. The perinuclear supernatant was then transferred into a fresh tube and used for subsequent analysis. In case that lysis was not carried out with RIPA buffer, cells were directly lysed in 2x Protein Loading buffer and sonicated (2x15 pulses).

Sodium Dodecyl Sulfate polyacrylamide gel electrophoresis (SDS PAGE)

Similar to the agarose gel electrophoresis the SDS page allows the separation of macromolecules according to their mobility in an electric field. For proteins, a sodium dodecyl sulfate containing buffer is added to the sample followed by cooking at 95°C that leads to complete denaturation and linearization of the protein of interest. The binding of the anionic

SDS imparts a negative charge to the denatured protein and the amount of bound SDS depends on the mass of the protein. This allows the separation of the denatured protein dependent on its length and mass to charge ratio in an acrylamide matrix. Depending on the molecular weight of the protein of interest samples were loaded onto 6-12% acrylamide gels and run for 1.5 h at 100V. To estimate their molecular weights a prestained protein marker was added as a reference. Proteins separated through SDS page were further processed by Western Blot analysis for their visualization.

Western Blot analysis

After SDS page, proteins were electro-transferred onto a PVDF membrane (PerkinElmer Life Sciences) for 1-4 h either using the semidry or wet-transfer apparatus. Membranes were blocked by incubation with 5% Skim milk dissolved in PBS-Tween (0.5%) for 1 h at room temperature, followed by their incubation with primary antibody for 1 h at RT or overnight at 4°C. Primary antibody was removed by washing three times for 5 min with PBS-Tween. Next the membranes were incubated with the respective secondary antibody conjugated with horseradish-peroxidase for 1 h at RT. Membranes were washed again as before and developed by using the Western Lightning Plus-ECL reagent (Perkin Elmer) and visualized on Amersham Hyperfilm ECL (GE Healthcare) or by using the Intas science imager.

2.2.5 Virological methods

Preparation of Hepatitis C virus stocks and PEG precipitation

Huh7.5 cells were resuspended in cytomix to a final concentration of 1.5×10^7 cells/ml. 400 μ l of the cell suspension were mixed with 10 μ g of full-length viral RNA and electroporated as described earlier. Two electroporations were resuspended in 20 ml of fresh medium and seeded onto one 15 cm cell culture dish. The next day the supernatants were removed and fresh media (15-20 ml) was added. 48, 72 and 96 h post electroporation the supernatant was collected and spun down for 10 min at 1500 rpm or sterile filtered through 0.45 μ m sterile filters, (Merck Millipore, Darmstadt, Germany). The supernatant was either directly frozen at -70°C or further concentrated. For virus precipitation sterile polyethylene glycol (PEG)-8000 was added to the virus supernatants to a final concentration of 8% PEG-8000. The mixture was incubated over night at 4°C and then spun at 8000g for 90 min at 4°C. Pellets were resuspended carefully in fresh media. Aliquots of 100 μ l were stored at -70°C.

Preparation of Dengue Virus stocks

Dengue virus stocks (serotype 2a, DENVR2A and DENV-2 166681) were kindly provided by Dr. E. Acosta.

Lentivirus production

One day prior to transfection 4.7×10^6 293T cells were seeded per 10 cm cell culture dish. For each transfection reaction 400 μ l optiMEM and 30 μ l jetPEI (Polyplus transfection, Illkirch, France) were mixed as well as 400 μ l optiMEM with 4.3 μ g of packaging plasmid pCMV-dR8.91, 1.4 μ g of the envelope plasmid pMD.G and 4.3 μ g of the transfer plasmid encoding the desired shRNA or cDNA. Both mixtures were brought together, vortexed for 10 sec and incubated for 10 min at room temperature. Finally 800 μ l were transferred drop-wise while shaking the 10 cm dish to allow an even distribution of the transfection reagent. 6 h post transfection the supernatant was removed and fresh media (8 ml) was added. 48 and 72

h post transfection the supernatants were harvested and filtered through 0.45 µm filters in order to remove dead cells. Aliquots of 1.5 ml were stored at -70°C.

Determination of virus titers by limiting dilution assay (TCID₅₀/ ml, 50% tissue culture infective dose per ml)

1x10⁴ Huh7.5 cells/ 96 well were seeded in 160 µl of DMEMcplt. The following day 200 µl of the pure supernatant from a previous virus production or a respective dilution was added per well into the first 6 wells of the 96 well. For serial 1:5 dilutions 40 µl were then transferred to the next row, resuspended well by pipetting up and down and subsequently transferred to the following row. 72 h after titration cells were fixed with cold methanol for at least 20 min at -20°C. For visualization of infected cells, cells were washed 3 times with PBS followed by incubation for 1 h at room temperature with an antibody against NS3 or NS5A diluted 1:1000 or 1:10000 respectively. Next, cells were washed 3 times with PBS and subsequently incubated with the respective secondary antibody conjugated with horseradish-peroxidase for 1 h at room temperature. Prior to addition of the substrate (5 ml Acetate, 1.5 ml Carbazol, 20 µl Peroxide, filtered) cells were washed 3 times with PBS. The reaction was stopped by addition of water when a strong positive signal was detectable. The plates were counted considering a cell as infected when a strong cytosolic red staining was apparent. Virus titers were determined according to Spearman [245].

Determination of Lentivirus titers by colony forming assay

A frozen aliquot of the lentivirus of interest was thawed on ice. As lentiviral transduction of the cells was carried out while seeding the cells two dilutions (1:400 and 1:10000) were prepared beforehand. Therefor 94.5 µl of DMEMcplt and 2 µl of polybren were mixed. For an initial 1:40 dilution 92.3 µl of the premix were added to 2.5 µl of the virus stock and vortexed well. 4 µl of this dilution were then added to 95.8 µl of the premix resulting in a 1:100 predilution. 8 µl of each dilution were next added to 75 µl of cell suspension (8000 cells/ 75 µl) in a 96 well plate giving rise to a final 1:400 and 1:10000 dilution. Each dilution was carried out in duplicates. One day after transduction, cells were selected with the appropriate antibiotic (Puromycin 1 µg/ ml). Additionally cells that had not been transduced were either treated with media with or without any antibiotic as controls for the selection process. Selection was stopped when all the control cells had died and colonies of around 5-7 adjacent cells were apparent for the transduced conditions. Therefor cells were washed twice with PBS and incubated with 50 µl of 1% crystal violet solution for 15 min at RT. The remaining crystal violet was recycled followed by two more washings with water. Before counting the colonies the water was removed and the wells were allowed to dry. The mean of the counted duplicates was used for determination of the viral titers as follows: 1:400 dilution: 4800x number of colonies, 1:10000 dilution: 120500 number of colonies.

2.2.6 Experimental procedures

Full-length *wild-type* (wt) and *Renilla* luciferase reporter virus infection/ reinfection assays

Infection assays with *wt* or *Renilla* luciferase reporter virus (both HCV or DENV) were either carried out in 24 or 96 well plates. Typically Huh7.5, Huh7.5Fluc or LunetCD81H cells were used. Cells were infected with *Renilla* luciferase reporter virus at a MOI of 0.2 or *wt* virus at a MOI of approximately 5. Infection with *wt* virus was mostly used for immunofluorescence analysis. 6 h post infection the supernatant was changed into 500 µl/ 24 well or 100 µl/ 96

well respectively. If not otherwise stated the infection was allowed for 48 h. Cells were then harvested for luciferase reporter activity assay by addition of 100 μ l/ 24 well or 30 μ l/ 96 well of luciferase lysis Buffer. Cells were further harvested for i) extraction of total cellular RNA by the addition of 350 μ l of A1 + 1% beta-mercaptoethanol per 24 well ii) immunofluorescence analysis by fixation with 4% PFA in PBS at room temperature for 15 min or iii) Western Blot analysis by the addition of 50 μ l of either 2x SDS sample buffer or RIPA buffer. In case of reinfection of naive Huh7.5 cells, the supernatants were harvested and spun at full speed for 10 min to remove cell debris. Reinfection was performed in 24 wells and allowed for 48 h.

Determination of intracellular and extracellular viral titers

In short 400 μ l of cell-cytomix suspension of 1×10^7 Huh7/Lunet cells/ ml were electroporated with 10 μ g of full-length viral RNA. Electroporated cells were resuspended in 20 ml DMEMcplt. 3 ml were transferred into a 6 well. 24 h post electroporation the supernatant was replaced by 2 ml of fresh media. 48 and 72 h post electroporation the supernatants and cells were harvested for determination of intra- and extracellular viral titers. The supernatant was collected in 2 ml safe lock Eppendorf tubes and spun 10 min at maximum speed at 4°C in order to pellet present cells and cell debris. 200 μ l of the supernatant was then transferred into a fresh 2 ml tube for subsequent freeze and thawing cycles. Intracellular virus was harvested by first washing the cells with 1 ml PBS. Cells were gently scraped in 1ml PBS and transferred into a 2 ml tube. Cells were pelleted at 700 g for 5 min and resuspended in 200 μ l of fresh medium. For freeze and thaw cycles equivalent volumes (here 200 μ l) of intra and extracellular virus were transferred 3 times into liquid nitrogen followed by thawing at 37°C. Finally samples were spun down for 5 min at 700 g to remove broken cells and the supernatant was transferred into a fresh tube. Depending on the respective virus construct different initial dilutions were made and virus titers were determined by limiting dilution assay.

siRNA lipofection/ electroporation followed by infection with full-length virus

Cells were either presilenced by lipofection or electroporation as described earlier. 48 h post-silencing cells were infected with *Renilla* luciferase reporter virus at an approximate MOI of 0.2. Experiments were performed in duplicates.

siRNA electroporation of stable replicon cell lines

100 μ l of 1×10^7 cells/ ml of LucUbiNeo_JFH1 and LucUbiNeo_ConET were electroporated with 2.5 μ l of siRNA. Electroporated cells were resuspended in 6 ml fresh DMEMcplt. 350-400 μ l were seeded into a 24 well plate to be harvested 48, 72 and 96 h post electroporation for luciferase reporter activity assay. 100 μ l were seeded into a 96 well plate for the determination of the cell viability and 1 ml was seeded into a 12 well for harvesting for Western Blot analysis. Experiments were performed in duplicates.

Lentiviral transduction of target cells followed by infection with full-length virus

Typically 2-3 $\times 10^4$ cells (Huh7.5, Huh7.5FLuc, Huh7/LunetCD81H) were seeded per 24 well. In parallel 0.5 $\times 10^4$ cells were seeded per 96 well for cell viability assay. One day later cells were transduced with the corresponding lentivirus at an MOI of 1, 2 or 4. 24 h later the inoculum was removed and 500 μ l/ 24 well or 100 μ l/ 96 well of fresh media was added. 48 h post transduction cells were infected with full-length *Renilla* luciferase reporter virus of HCV and DENV at a MOI of 0.2. 6 h later the inoculum was replaced by 500 μ l/ 24 well or by 100 μ l/ 96 well of fresh media respectively. 48 h post infection and 96 h post transduction cells

were harvested for Luciferase reporter activity assays. In case of reinfection the supernatants were spun down at max speed for 10 min and transferred onto naive Huh7.5 cells for another incubation period of 48 h. Experiments were performed in duplicates.

Lentiviral transduction of target cells followed by transfection of pTM expression constructs for immunofluorescence analysis

For the expression of T7-promotor driven constructs as in case of pTM-based expression plasmids, Huh7-Lunet/T7 cells stably expressing the T7 polymerase were used [242]. 1×10^4 cells/ 24 well were seeded onto coverslips one day prior to transduction with lentivirus at a MOI of 4. 24 h post transduction the media was replaced by fresh DMEMcpl containing $1.5 \mu\text{g}/\mu\text{l}$ Puromycin for the selection of transduced cells. 54 h post transduction cells were transfected using the Mirus TransITL1 transfection reagent (Mirus Bio, Madison, USA) according to the manufacturer's protocol. 72 h post transduction and 14-16 h post transfection cells were fixed with 4% PFA in PBS for 15 min at RT and processed for immunofluorescence analysis.

Lentiviral transduction of stable replicon cell lines

0.5×10^4 LucUbiNeo_Con1ET and LucUbiNeo_JFH1 cells were seeded per 96 well. One day later cells were transduced with Lentivirus at a MOI of 1, 2 and 4. Cells were harvested for Luciferase reporter activity assay as well as cell viability assay 48, 72 and 96 h post transduction. Experiments were performed in triplicates.

Luciferase reporter activity assay

Depending on the format different amounts of Luciferase lysis buffer were added to the washed cells for lysis at -20°C ($250 \mu\text{l}/ 12$ well, $100 \mu\text{l}/ 24$ well, $30 \mu\text{l}/ 96$ well). Samples were analyzed either using the tube luminometer Lumat LB9507 or the plate Luminometer Mithras LB940 (Berthold Technologies, Bad Wildbad, Germany), the later one being less sensitive. For measuring *Renilla* luciferase activity by the tube luminometer, $20 \mu\text{l}$ of the lysate were transferred into a measurement tube and $100 \mu\text{l}$ of luciferase assay buffer containing $1.4 \mu\text{M}$ Coelenterazine (PJK Chemikalien, Kleinblittersdorf, Germany) were added and measured for 10 sec. For measuring the *Firefly* luciferase activity $10 \mu\text{l}$ lysate were mixed with $360 \mu\text{l}$ assay buffer containing ATP and DTT. To each measurement $200 \mu\text{l}$ of the 0.2 M Luciferin containing luciferase assay buffer were automatically added by the machine and measurements were carried out for 20 sec. Measurements were generally performed in duplicates. The plate reader is able to determine *Firefly* and *Renilla* luciferase activity within the same sample in parallel. First Luciferin containing assay buffer is added, followed by *Firefly* luciferase activity measurement. Next, Coelenterazine containing assay buffer is added to the same well and *Renilla* Luciferase activity is measured using the respective filter. By the addition of SDS the reaction is stopped.

HCV Core ELISA

Core ELISA analysis was carried out by the Analysen Zentrum Universitätsklinik Heidelberg. Samples were prepared by lysing cells in 0.5% Triton-X-100 in PBS or adding 10% Triton-X-100 to the respective supernatants to a final concentration of 1% Triton-X-100. An appropriate dilution of the sample of interest in a final volume of 0.5–1ml was transferred into a collection tube and stored at -20°C until measurement.

Dose response assays using JcR2A or DENVR2A reporter virus

For dose response assays using the HCV or DENV *Renilla* reporter virus 1×10^4 Huh7.5 cells were seeded per 96 well. The next day, cells were either i) pretreated for 24 h prior to

infection ii) treated while infection or iii) drug treatment started 6 h post infection. Either way, infection was allowed for 6 h followed by removal of the inoculum and the addition of drug containing media. Cells were then incubated in presence of the drug or the corresponding water/ DMSO control for 48 h followed by lysis of the cells. Effect of drug treatment on entry/ replication of the reporter virus was next assessed by luciferase activity assay as described earlier.

Dose response assays using stable replicon cell lines

For dose response assays using stable replicon cell lines, 1×10^4 LucUbiNeo_JFH1 and LucUbiNeo_Con1ET were seeded per 96 well. One day later medium was replaced by drug or the corresponding water/ DMSO control-containing medium at different concentrations of the compound. Cells were harvested 48, 72 and 96 h post treatment and effects on replication were assessed by luciferase assay as described earlier.

Dose response assays upon transfection of subgenomic replicon RNA

Lunet cells were electroporated with subgenomic *Firefly* luciferase reporter replicon RNA and seeded into 24 well plates. 4 h post electroporation the media was replaced by drug or water/ DMSO containing medium. Additionally cells were lysed to assess the input RNA levels for each condition. Next cells were harvested 24, 48 and 72 h post treatment and effects of drug treatment on replication were analyzed by luciferase assay as described earlier.

2.2.7 RNAi screens

Comparative Lipid droplet RNAi screen

The LD RNAi screen was designed and performed by Dr. G. Alvisi.

LD RNAi library – Due to the lack of a commercially available library of genes whose gene products are implicated in LD homeostasis in human liver cells, a custom made RNAi library was assembled. Thus, based on several studies that identified potential candidates regulating LD morphology a homemade RNAi library of 230 genes was generated [236, 237, 246-249]. Next, ON-TARGETplus® SMARTpool siRNAs were purchased from Dharmacon, that were pre-spotted onto 96 well plates. Several controls were included in case of the virus screen: Dharmacon ON-TARGETplus® Non-Targeting Control Pool, PI4KIII α (Phosphatidylinositol-4-kinase-III α), Apolipoprotein E. Additionally two different RNAi oligonucleotides targeting the *Renilla* luciferase were used. In case of the virus screens, 5 μ l of siRNAs (100 μ M) were spotted into white assay plates, while black plates were used for the LD morphology imaging screen. In case of the imaging screen a SMARTpool siRNA targeting the PLK-1 was added as control of the silencing efficiency.

Virus screen setup, performance and statistical analysis – Huh7.5FLuc cells were silenced by reverse transfection of SMARTpool siRNAs. To this point, the lipid free transfectant Interferin was diluted 1:40 in optimem and 40 μ l were then added per 96 well to the pre-spotted plates. Plates were spun for 5 sec at 700 rpm and subsequently incubated for 10 min at RT under shaking. Next 8×10^3 Huh7.5FLuc cells were added to each well in a volume of 155 μ l DMEM. They were subsequently spun down as before and transferred into cell culture incubators (37°C, 5% CO₂). 8 h later the supernatant was removed and replaced by 200 μ l of fresh DMEM. Infection with HCV or DENV *Renilla* luciferase reporter virus was performed 36 or 48 h later, respectively. To this point the supernatant was removed and cells were infected at a MOI of 0.2 (TCID₅₀/ cell) in a volume of either 150 μ l for HCV or 50 μ l for DENV. Cells were then incubated for 60 (HCV) or 48 h (DENV). Cell supernatant were next

transferred onto naïve Huh7.5 (HCV) or Vero (DENV) cells, which had been seeded 24 h earlier at a concentration of 5 or 10 x10³ cells/ 96 well respectively. 12 h later 100 µl of fresh medium was added. Furthermore silenced cells were lysed and plates were stored at -20°C. The reinfection was allowed for 24 (DENV) or 48 h (HCV) which was followed by lysis of the cells. The effect of gene knockdown on viral replication was assessed by measuring *Renilla* luciferase activity in whole cell lysates. In order to identify candidates important for early events of the viral replication cycle such as entry and replication the *Renilla* luciferase counts in the infection plates were normalized to the corresponding *Firefly* counts, representing cell number. To determine host factors involved in assembly and release of infectious virions the *Renilla* activity measured in the reinfection plates was normalized to the respective *Renilla* counts of the infection plates. Statistical and bioinformatical analysis of the screen data was performed Prof. Dr. Lars Kaderali and his group at the University of Dresden.

LD morphology screen setup, performance and statistical analysis – The SMARTpool siRNA transfection was performed as described above, with the exception that 2.45 x10³ Huh7/LunetCD81H-TRFP cells were seeded. The plates were again spun and 8 h later the transfection medium was replaced by 100 µl of fresh DMEM. 80 h post siRNA transfection 3 wells of the siRNA non-targeting control per plate were treated with either BSA-loaded oleic acid (100 nM) or Triacsin C (2.7 µM) to induce or inhibit LD biogenesis, respectively. 16 h post treatment cells were incubated for 30 min with DMEM containing 20 µg/ ml Bodipy 493/503 and 1 µg/ ml Hoechst 33342 at 37°C and 5% CO₂. Cells were then washed 3 times with 100 µl of 0.1 M PHEM, subsequently fixed with 4% PFA for 15 min at RT and again washed as before. The plates were then automatically imaged with an Olympus IX81 automated microscope using a 20x objective. For image analysis four different 12-bit images were taken. These four different images comprised the visualization of the cell boundary (RFP), of the cellular nuclei and two images of the Bodipy 493/503 labelled LDs. These two images were taken with different acquisition times in order to guarantee the recording of LDs of low intensity, as well as to circumvent saturation in case of strong signal intensities. For each candidate 9 different positions within the same well were imaged. The screen was performed in quadruples. The following features were extracted and analyzed: cell area, nucleus area, LD total area, LD mean area, LD cell area coverage, LD number, LD mean intensity, LD total intensity, LD mean distance to nucleus, cell mean intensity, nucleus mean intensity. Importantly genes were classified as hits when their knockdown lead to significant changes in either one of the LD related features. The z-score threshold was set to >2 and <-2.

Small scale LTP RNAi screen (designated as Lipid transfer protein /LTP screen)

The siRNA ON-TARGET plus SMART pools were reconstituted in RNase free water to a final concentration of 100 µM. 2.5 µl aliquots were prepared and stored at -20°C. siRNA was transfected by electroporation. To this end, cell monolayers of Huh7.5FLuc cells were detached by trypsinization, resuspended well in fresh preheated DMEMcpl+ and single cell suspensions were counted. The respective amount of cells were spun down at 700 g for 5 min, washed with PBS, spun again and resuspended in Cytomix. 100 µl of 1.5x10⁷ cells/ ml cytomix were used per electroporation. Therefor the cell suspension was added to the siRNA, resuspended well, transferred into the electroporation cuvette (0.2 cm gap) and electroporated with the following settings: 166V, 0.5 µF. Electroporated cells were immediately resuspended in 6 ml of preheated fresh DMEMcpl+. 100 µl of the cell suspension were seeded per 96 well plates (white bottom) in triplicates. In order to decrease edge effects, the outermost wells of the 96 well plates were omitted and filled with 200 µl of media.

36 or 48 h post electroporation cells were infected with HCV *Renilla* reporter virus (JcR2A, MOI 0.5) or DENV *Renilla* reporter virus (DENVR2A, MOI 0.5) respectively. 24 h post infection the inoculum was replaced by 100 μ l of fresh DMEMcplt. In case of DENV infection 10 mM Hepes was added to the media. Our pretests revealed that infection with JcR2A for 60 h or with DENVR2A for 48 h followed by reinfection of naïve cells for 48 h resulted in the best window between the non-targeting and the positive controls. The latter ones included siRNA ON-TARGET plus SMART pools targeting the cellular Phosphatidylinositol-4-kinase III alpha (PI4KIII α), the Apolipoprotein E, both known HCV dependency factors as well as the *Renilla* luciferase or the DENV non-structural protein NS1 [121, 250]. Infection was allowed for 60 h in case of JcR2A and 48 h in case of DENVR2A prior to lysis of the cells in 30 μ l *Renilla* luciferase lysis Buffer. For reinfection, the supernatant of the infected cells was transferred onto naive Huh7.5 or Vero cells, seeded 1 day prior to infection at a concentration of 1×10^4 cells/ 96 well. Reinfection was allowed for 48 h before lysis of the cells with 30 μ l Luciferase lysis buffer. Luciferase activity assays were conducted as described earlier.

To allow accurate statistical analysis 6 independent repetitions were carried out, each time using different plate layouts and freshly thawed cells of the same passage. Prof. Dr. L. Kaderali carried out statistical analysis of the RNAi screen raw data. To this end, effects of siRNA knockdown on viral entry/ replication were determined by dividing the *Renilla* (RLuc) counts measured in the infection plates by the respective *Firefly* (FLuc) counts of the same well. This allowed the normalization of detected viral replication to the respective amount of cells present per well. Effects of siRNA mediated knockdown on the viral reinfection efficiency were determined by dividing the RLuc counts measured in the reinfection plates by the RLuc counts determined in the corresponding infection plate. Outliers caused by technical difficulties were removed from the analysis. A z-score threshold of >2 and <-2 was used for hit definition, as well as a p-value < 0.05 .

2.2.8 Biochemical assays

Cell viability measurement by cell proliferation reagent WST-1 (Roche)

Cell viability measurements were typically conducted in a 96 well format and performed in triplicates. The WST-1 reagent contains a stable tetrazolium salt which is reduced to soluble formazan by a complex cellular mechanism. This reduction is largely dependent on the presence of Nicotinamide Adenine Dinucleotide (Phosphate) NAD(P)H, an energy rich metabolic intermediate that is generated throughout glycolysis and citric acid cycle for the production of ATP. Therefore the rate of conversion of tetrazolium salt (red) to formazan (dark red) correlates to the amount of present NAD(P)H and the metabolic activity/viability of the present cells. To this end, cells were incubated with 10 μ l/ 96 well of WST-1 reagent for approximately 30 - 45 min. Cell viability was determined by measuring the absorbance at 450 nm in the Tecan XFluor4 reader (Wiesbaden, Germany)

Cell titer glo® Luminescent Cell viability assay (Promega)

Cell viability measurements were typically conducted in a 96 well format and performed in triplicates. The cell titer glo cell viability assay is based on the determination of ATP present in the cell lysates as an indicator for cell viability/ metabolic activity. To this end an extensive amount of *Firefly* luciferase and substrate is added to the cells. As the *Firefly* luciferase activity is largely dependent on ATP, the measured luminescence correlates to the present ATP levels and is therefore an indicator for cell viability/ metabolic activity. Cells were

typically incubated with a 1:1 mixture of the cell titer glo reaction mixture and DMEMcpl1 for 10 min at RT before measurement was conducted. In case of infected cells, cells and supernatants were inactivated by the addition of Triton-X to a final concentration of 1% prior to measurement.

NS4B-HA affinity purification

One 80% confluent 15 cm dish of Huh7/Lunet-T7 (Blasticidin) was transfected with the pTM expression construct encoding the NS3-3' of genotype 2a (JFH1) that either contained *wild-type* NS4B or a Hemagglutinin affinity (HA)-tagged version. 6 h post transfection, the medium was replaced by media containing 1 μ M Topfluor-Cholesterol (TFC). Cells were harvested 18 h later and HA-specific affinity purification was performed by Dr. D. Paul as described elsewhere [114]. The presence of TFC in immunoprecipitates or the perinuclear supernatant of complete cell lysates was measured using the Luminometer Mithras LB940. Samples were further processed for detection of NS5A and NS4B by Western Blot.

2.2.9 Imaging

Indirect immunofluorescence

Cells were grown on coverslips, washed once with PBS and fixed with 4% PFA in PBS for 15 min at room temperature. Cells were typically permeabilized with digitonin (50 μ g/ml in PBS) for 10 min at RT and subsequently blocked with 3% fatty acid free BSA in PBS for 30 min at room temperature. Coverslips were then incubated with the primary antibody diluted in 1% BSA/PBS for 1h at room temperature. After washing three times for 5 min with PBS, coverslips were incubated in the dark with the corresponding secondary antibody diluted in 1% BSA/PBS. Next cells were incubated for 1 min with DAPI (DNA stain) for staining of the nucleus followed by three washes with PBS. Depending on the specimen, coverslips were mounted with glycerol based Fluoromount G (Southern Biotech) or Vectashield (Vector Laboratories Inc., Burlingame, USA). Samples were stored in the dark at 4°C.

Neutral lipid staining with Bodipy or LipidTOX™

Neutral lipids present in lipid droplets were visualized for light microscopy using the fluorescent dye Bodipy493/503 or HSC LipidTOX™ Neutral Lipid stain (Thermo Fisher Scientific, Waltham, USA). To this end after secondary antibody incubation and prior to the last washing steps coverslips were incubated for 10 min with 20 mg/ml Bodipy495/503 in PBS for 20 min at room temperature. In case of staining with more than 3 colors, HSC LipidTOX™ was used. LipidTOX™ was added to the secondary antibody and visualized by excitation at 647 nm and detection in the far red.

Microscopes and Image analysis programs

Samples were analyzed using the Leica Sp2 confocal laser scanning microscope or PerkinElmer ERS-6 spinning disc confocal microscope. Image analysis was performed using Fiji software package based on Image J (NIH) or Imaris 8 software (Bitplane, Zurich, Switzerland). Deconvolution was carried out using Autoquant X3 (Bitplane, Zurich, Switzerland).

Free cholesterol staining using filipin complex or filipin III

Free cholesterol staining was carried out using the filipin complex that contains 8 isomeric components with filipin III as the major component or filipin III (Sigma Aldrich, St. Louis, USA). Filipin complex or filipin III is a tool widely used for the visualization of free and unesterified cholesterol [251, 252]. As filipin III has been shown to perforate the membrane [253] permeabilization of the samples through detergent was omitted. Filipin binds to free cholesterol forming a filipin-cholesterol complex with a detection range similar to ultraviolet light (360/ 460nm).

Image analysis: Determination of LDs labeled with Bodipy493/503

For quantification of Bodipy493/503 labeling in cells the plugins „DogSpot Enhancer2D“ and „Double Threshold“ of the Fiji software were used. To this point background was equally subtracted for all pictures analyzed. By the use of the before mentioned plugins, the area, number and integrated density of the Bodipy493/503 signal per cell was determined.

Image analysis: Determination of volumes of filipin positive structures

Quantification of the volume of filipin III positive structure was carried out using the Imaris software. Therefor z-stacks were taken that captured the complete volume of a cell. Images were first deconvolved. Using the Imaris software, a surface was fitted filling the filipin III positive structures as good as possible. To this end the signal threshold was adapted as well as seed points were set, that allowed the program to distinguish between structures that were in close proximity. The settings were used to calculate and compare the volume of filipin III positive structures of different treatment conditions.

Image analysis: Colocalization analysis

Colocalization of two signals was determined using the „Intensity correlation Analysis“ Plugin of Fiji. To this end, background signal was equally subtracted for all samples analyzed. Pearson Correlation coefficient or Manders correlation coefficients were determined.

Life cell imaging and movie analysis

Huh7/LunetCD81H cells were electroporated with 5 µg of subgenomic viral RNA (sbNS3-3', NS5A-mCherry, JFH1) and plated into 8 well Lab-Tek[®] imaging chamber. Media was replaced by U18666A or control containing media 24 h prior to the start of imaging. Topfluor-Cholesterol (TFC) was added to the cells for 10 min before extensive but careful washing with fresh media. The chamber environment (in particular CO₂) was allowed to equilibrate for 30 min before the onset of imaging. Live cell imaging was performed in Phenol-Red free imaging media at 37°C and 5% CO₂. Images were taken every 15 min for approximately 16 h. Thereby the complete volume of each cell was imaged by taking three sequential z-stacks. Image analysis was performed using the Fiji software. To determine the TFC accumulation velocity of TFC in NS5A positive cells background was equally subtracted for all samples. Only a single plane was analyzed, thus the z-stack with the strongest TFC signal at the perinuclear region was chosen. The signal intensity of TFC at the perinuclear region was determined by measuring the Integrated Density. To determine the colocalization efficiency of TFC and NS5A stringent background subtractions was performed. Colocalization was determined as described before.

Sample preparation for Electron microscopy (EM)

3x10⁴ Huh7/Lunet-T7 (Zeocin) cells were seeded onto coverslips per 24 well. 24 h later, cells were treated with the respective concentrations of the cationic amphiphile. After another 24 h cells were transfected with the respective pTM expression construct encoding the NS3-

3' of genotype 2a (JFH1) or genotype 1b (Con1ET). 6 h later medium was changed into compound containing medium again. 24 h post transfection cells were washed three times with PBS and fixed with 2.5% Glutaraldehyde + 2% Sucrose for 30 min at RT. Cells were then washed five times with CaCo Buffer for 5 min and stored at 4°C until further processing. The subsequent steps were performed by Dr. I. Romero-Brey. Cells were treated with 2% OsO₄ in CaCo buffer for 40 min on ice, and rinsed with water. Cells were then treated with 0.5% uranyl acetate (dissolved in water) for 30 min, and rinsed again with water. Samples were dehydrated by treatment with an ethanol series (first 40% Ethanol followed by 50%, 60%, 70%, 80%, for 5 min each, and then 95% and 100% for 20 min each). Embedding, sectioning and staining was performed as described elsewhere [254]. DMV diameters were measured using the iTEM application software (version 5.2 Olympus).

2.2.10 Statistical analysis

Statistical analysis was performed using the GraphPad Prism or Microsoft Excel software. Statistical significances were calculated by using the two-tailed, unpaired Student's t-test or the one-way analysis of variance (ANOVA) and Dunnett's Multiple Comparison test when several conditions were compared to a single control (***, $p < 0.001$, **, $p < 0.01$, *, $p < 0.05$).

3 Results

3.1 Identification and characterization of novel factors involved in lipid droplet homeostasis and in the replication cycle of HCV and DENV

LDs are dynamic lipid storage organelles that play a central role in the cellular lipid homeostasis. Mobilization or storage of neutral lipids is mainly regulated by LD-associated proteins [232]. While two independent RNAi screens led to the identification of novel factors that regulate LD morphology in drosophila cells, cellular factors involved in LD homeostasis in human liver cells are only poorly characterized [236, 237]. Interestingly the replication cycles of the liver-tropic Hepatitis C virus, and the related Dengue virus, have been reported to depend on LDs, although the organelle's precise role is yet unclear [148, 255]. Thus, the identification and characterization of cellular factors regulating LD function might shed new insight into the connection between the viruses and the cellular organelle. This could lead to the identification of potential targets for therapeutic treatment of HCV and DENV infection.

3.1.1 Setup, performance and statistical analysis of the LD-RNAi screen

Setup of a bipartite comparative RNAi screen. With the aim to identify novel factors involved in LD homeostasis in liver cells and in the replication cycle of HCV and DENV, Dr. G. Alvisi from our laboratory performed a comparative RNAi screen targeting genes implicated in LD biology (unpublished data). Due to the lack of a commercially available siRNA library he assembled a home-made library based on present literature. The majority of the genes had earlier been identified by a RNAi screen as LD homeostasis regulators in drosophila cells, thus their human orthologues were added to the library, which finally comprised 230 genes (Figure 3.1A, Supplementary Table S 1) [236, 237, 246-249]. In a comparative screen, the effect of gene knockdown was assessed on i) the full replication cycle of HCV or DENV reporter viruses, engineered to express *Renilla* luciferase (Figure 3.1C) and on ii) LD morphology in a microscopy-based study (Figure 3.1B). Details of the screen setup can be found in Figure 3.1 and under section 2.2.7.

In order to identify host factors regulating LD homeostasis, Dr. Alvisi assessed the effect of gene knockdown on LD morphology in a microscopy-based approach (Figure 3.1B). To this end Huh7/LunetCD81H cells stably expressing Tag-RFP-T, enabling the visualization of the cell boundary [243] were silenced for 96 h. Control cells transfected with non-targeting siRNA were treated with BSA-loaded oleic acid or Triacsin C to promote or inhibit LD formation, respectively. Lipid droplets were labeled with the fluorescent neutral lipid stain Bodipy495/503 [256]. In an automated quantitative image analysis changes in the following LD features were measured: LD total area, LD mean area, LD cell area coverage, LD number, LD mean intensity, LD total intensity, LD mean distance to nucleus (Figure 3.1B).

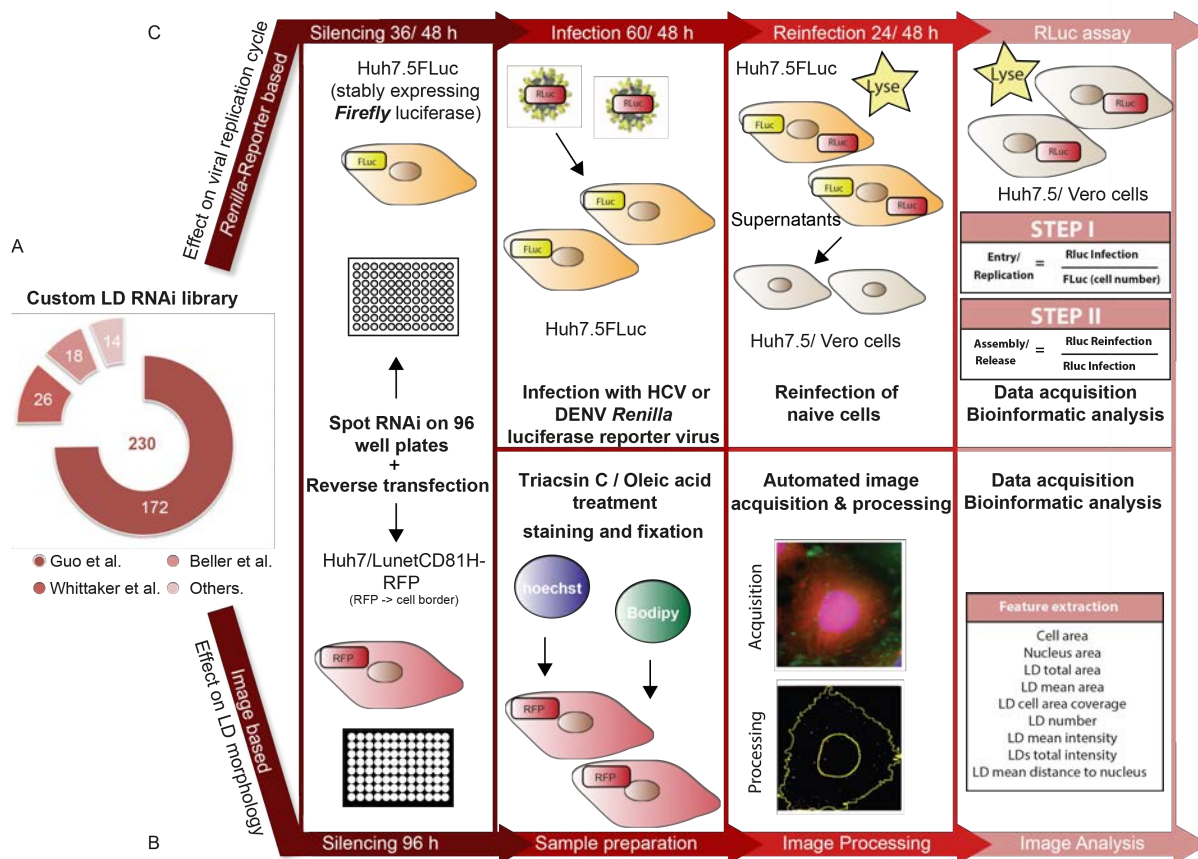


Figure 3.1 Primary screen setup (A) Composition of the LD RNAi library. The number of genes taken from the respective reference is indicated. **(B) LD morphology screen.** Huh7/LunetCD81H stably expressing Tag-RFP-T, a marker of the cell border, were reverse transfected with ON-TARGETplus® SMARTpool siRNA. 80 h later a fraction of the cells transfected with the non-targeting siRNA control were treated with either 100 nM BSA-loaded oleic acid or 2.7 μM Triacsin C to induce or inhibit LD formation, respectively [256]. The remaining fraction of the control cells was left untreated. 96 h post silencing, cell nuclei were stained with Hoechst and LDs were visualized by the use of Bodipy493/503. Cells were then fixed and plates were automatically imaged. Four different images were taken, including one for cell nuclei (Hoechst), one for the cell boundary (RFP) and two images with different acquisition times for Lipid droplets (Bodipy493/503). The latter aimed to allow the acquisition of low Bodipy signal intensity and to prevent saturation in case of strong signal intensities. Last, different features were extracted and data was bioinformatically analyzed. **(C) Virus screen.** Gene silencing in Huh7.5FLuc was conducted by reverse transfection of the above mentioned siRNA pools. 36 (HCV) or 48 h (DENV) later cells were infected with *Renilla* luciferase reporter HCV or DENV respectively. 60 (HCV) or 48 h (DENV) post infection i) supernatants were transferred onto naïve Huh7.5 (HCV) or Vero cells (DENV) and ii) cells were lysed. Reinfection of naïve cells was allowed for 24 or 48 h in case of DENV or HCV respectively, which was followed by cell lysis. In order to determine the viral replication efficiency, *Renilla* luciferase activity was measured in cell lysates. The results were analyzed as following: Effects on entry and replication were determined by normalizing the *Renilla* counts (replication) in the silenced cells to the respective *Firefly* counts, which represent the cell number (Step I). In order to determine potential changes in infectious particle production *Renilla* counts in the reinfection plates were normalized to those of the infection plates (Step II). The obtained data was bioinformatically analyzed. Adapted from Dr. G. Alvisi.

To address the importance of the selected candidates in the viral replication cycle of HCV or DENV, a primary screen was performed using the ON-TARGETplus® SMARTpool siRNA. Pre-silenced Huh7.5 cells stably expressing *Firefly* luciferase were infected with the respective *Renilla* luciferase reporter virus (Figure 3.1C). In silenced cells, measuring and normalizing the *Renilla* luciferase counts (viral replication) to the *Firefly* luciferase counts (cell number) allowed determining the effect of gene knockdown on early phases of viral replication, namely virus entry and RNA replication (Figure 3.1C, Step I). In a second step

the cell supernatants of silenced cells were transferred onto naive Huh7.5 (HCV) or Vero (DENV) cells for reinfection. Thus, by measuring the *Renilla* luciferase counts in the reinfection plates and subsequent normalization to the corresponding *Renilla* luciferase counts in the infection plates, changes in virus particle assembly and release were determined (Figure 3.1C, Step II). Hit candidates were then further analyzed in a deconvolution screen, which was performed under the same conditions using four individual siRNA oligos that were comprised in the original ON-TARGETplus® SMARTpools (Supplementary Table S 1). A deconvolution screen was not performed for the image-based LD morphology screen.

Statistical analysis and hit definition. For the analysis of the primary image-based LD morphology screen, genes were classified according to their knockdown phenotype. Genes whose knockdown altered at least one of the following features: LD total intensity, total LD area or LD area coverage were considered to alter cellular lipid storage. If their knockdown led to changes in LD count, LD mean intensity, LD distance to nucleus, or LD mean area they were considered to be important for regulating lipid distribution. A z-score threshold of $>2/<-2$ was used.

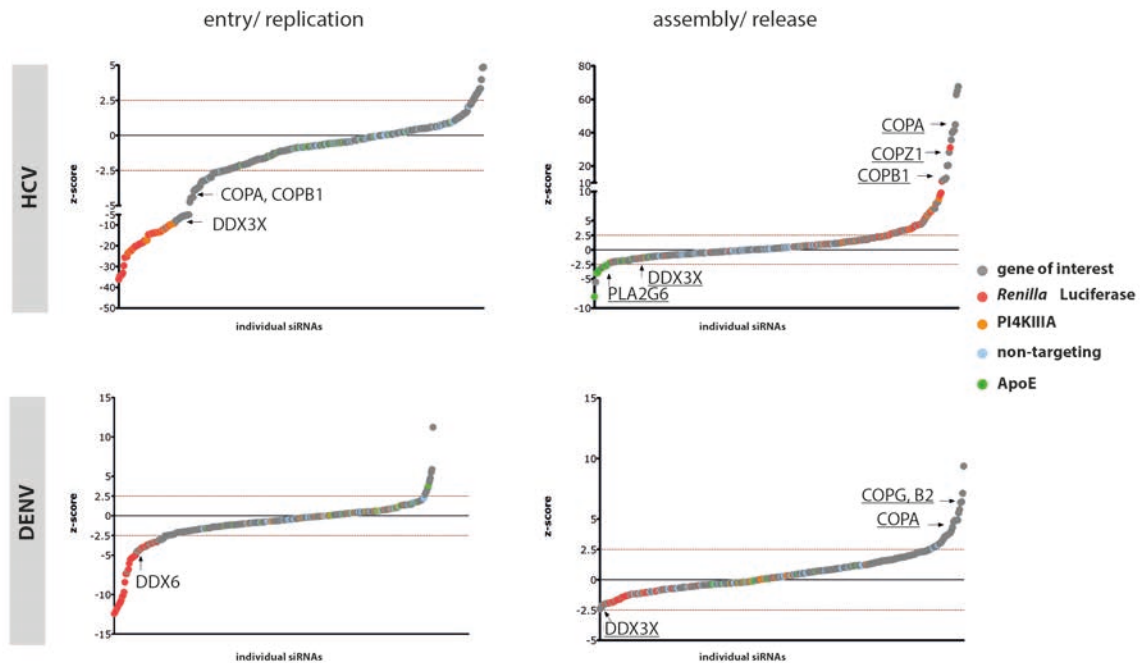
In case of the virus replication screens, hit candidate genes identified in the primary screen as being important for entry/ replication (step 1) or assembly/ release (step 2) of HCV or DENV were defined using a z-score threshold of $>2.5/<-2.5$. For hit classification of the deconvolution screen a less stringent z-score threshold of $>2/<-2$ was used. When two out of the four siRNAs were giving the same phenotype as determined in the primary screen, the gene was considered as a high confidence hit. Candidates were defined to act as restriction factors (RFs) if their knockdown enhanced viral fitness, conversely genes were classified as dependency factors (DFs) when their knockdown impaired viral replication. Hit candidates with opposing effect on early (step 1) and late (step 2) phases of viral replication were defined as life cycle regulators. The statistical analysis of the screen data was conducted by Dr. Lars Kaderali and his group at the University of Dresden.

3.1.2 Performance of control siRNAs and hit calling

Robust performance of the RNAi screen. A general marker of the quality of the screen performance is the distribution of z-scores of the individual control siRNAs in comparison to the z-scores of the target genes [257]. In the present screen a siRNA targeting the *Renilla* gene, present in the genome of both reporter viruses was used as positive control. Moreover, siRNAs targeting host factors known to be involved in HCV RNA replication (PI4KIII A, [250])

or assembly/ release of HCV infectious particles (Apolipoprotein E, [121]) served as additional controls for Step I and Step II of the screen, respectively.

A



B

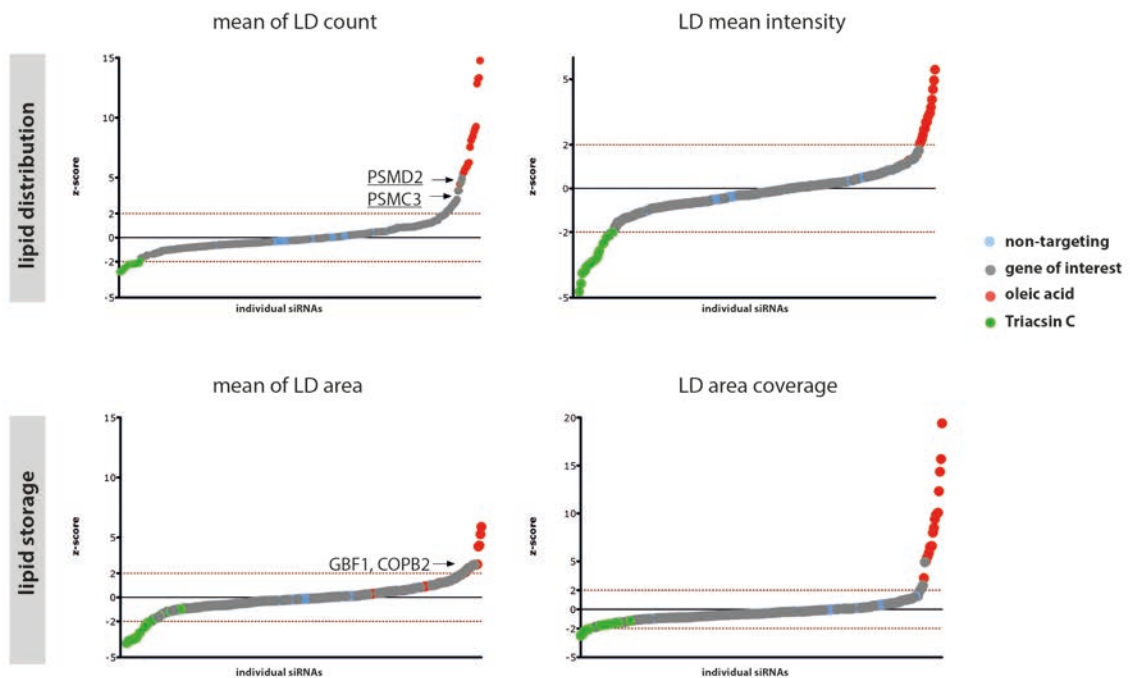


Figure 3.2 Performance of control siRNAs (A) Results of the primary virus screen. Individual siRNAs are listed according to their z-scores. The z-scores of individual genes are indicated in grey; a blue color marks the z-scores of the non-targeting siRNAs. The positive siRNA controls of viral entry and replication are indicated in either red (*Renilla luciferase*) or orange (*PI4KIIIA*, HCV specific). Z-scores of siRNAs targeting the Apolipoprotein E (ApoE), an important host factor for infectious particle production of HCV are indicated in green. Known host factors involved in HCV or DENV replication cycle are depicted. Selected host factors with a potential novel function are underlined. **(B) Results of the LD morphology screen.** The z-scores of individual siRNAs targeting the gene of interests are depicted in grey, while the non-targeting control is shown in blue. The z-scores upon Triacsin C or oleic acid treatment are illustrated in green or red respectively. Adapted from Dr. G. Alvisi.

As expected, silencing of the *Renilla* luciferase gene substantially impaired the early phase of HCV and DENV replication. In contrast the non-targeting controls did not cause major changes, indicated by a z-score that fluctuates around 0 (Figure 3.2A). Furthermore, gene knockdown of PI4KIII A impaired entry/ replication of HCV but not DENV, and silencing of the Apolipoprotein E specifically altered HCV particle assembly/ release. (Figure 3.2A A, Supplementary Table S 2). Thus all controls behaved as predicted indicating the high quality of the screen performance. The screen confirmed the involvement of several already described factors such as DDX3, COPA, COPB1 or DDX6 in the early events of HCV or DENV replication, respectively [76, 154, 258, 259]. In addition the results revealed host factors with potential novel function in the replication cycle of these viruses. (Figure 3.2A A, underlined factors are novel).

As indicated earlier, in case of the high content image-based LD morphology screen two control conditions were included that are known to inhibit or enhance LD formation, namely treatment with Triacsin C or BSA-loaded oleic acid respectively [256]. Indeed, Triacsin C substantially reduced neutral lipid storage as well as neutral lipid distribution, while treatment with oleic acid had the opposite effect. Additionally, transfection of the siRNA non-targeting control had no effect on any of the evaluated features, indicating that the introduction of the siRNAs did not affect LD morphology *per se* (Figure 3.2A B, Supplementary Table S2). Interestingly knockdown of subunits of the proteasome as well as of the Coat protein complex I vesicle machinery appeared to enhance the mean of LD counts or the LD mean area in human hepatoma cells, respectively (Figure 3.2B).

The bipartite primary screen led to the identification of 133 genes involved in the replication cycle of HCV and/or DENV and 59 genes that alter LD features. The results of the primary screen are summarized in Figure 3.3, the Supplementary Table S2, S3 and S4.

Of the 93 HCV hits, half of the hits appeared to be important for the early phase of the viral replication cycle, while only 26 affected later stages. 18 genes were classified as life cycle regulators. In case of the 82 DENV hits, 32 and 37 candidates were found to be important for early or late stages of the viral replication cycle, respectively. 13 life cycle regulators were identified (Figure 3.3A, B). Of these 133 viral hit genes, 51 were specific for HCV, 42 were common for both viruses and the remaining 40 were unique for DENV (Figure 3.3B). With the help of the deconvolution screen 61 high confidence hits were identified to be unique for HCV, while 16 DENV specific high confidence hits were found. Both viruses shared 13 common high confidence hits (Figure 3.3D, Supplementary Table S 5). Thus the deconvolution screen confirmed the importance of 67.6% of the primary hits for either virus. The best hit recovery rate was obtained for HCV, for which 78.8% of the primary hits were confirmed to be high confidence hits (Figure 3.3E).

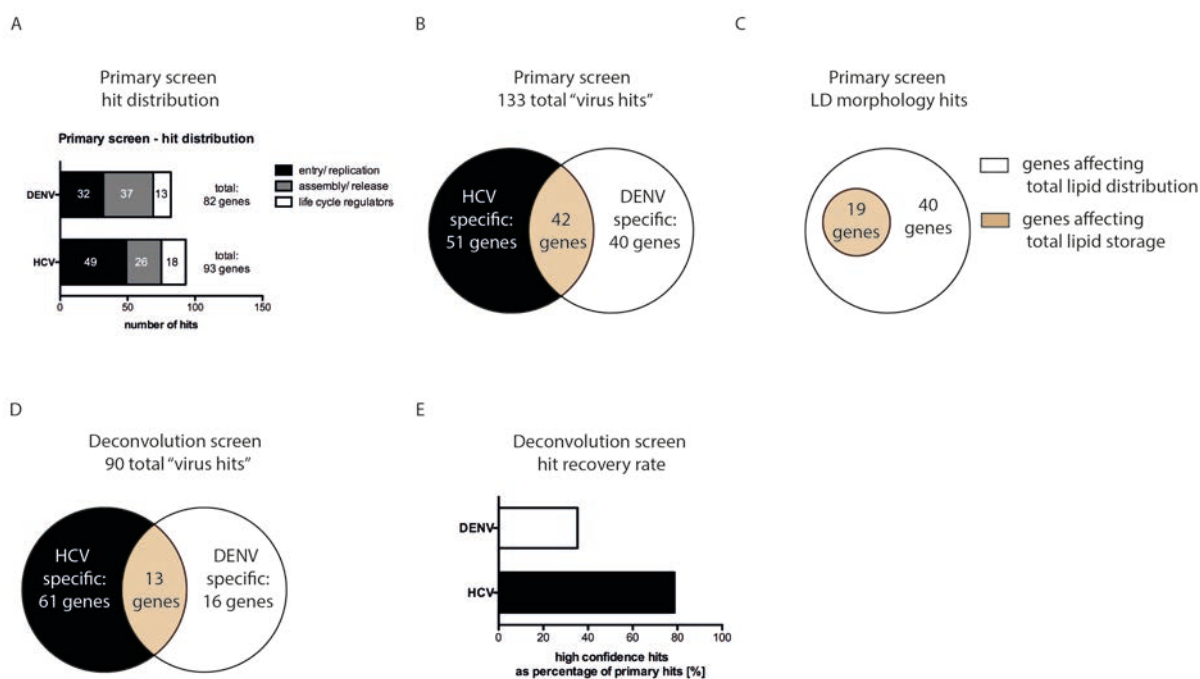


Figure 3.3 Primary and deconvolution screen results (A) Results of the primary screen. The number of genes either affecting entry/ replication (black bar) or assembly/ release (grey bar) or having an opposing effect on both steps (white bar) is depicted. (B) Diagram showing the number of HCV or DENV specific hit genes. The number of hit candidates common for both viruses is indicated in the overlapping section of both circles. (C) LD morphology hits. Genes shown to affect lipid storage and/ or lipid distribution are depicted. (D) High confidence hits identified by the deconvolution screen. The number of genes that are either specific for HCV or DENV or common for both viruses is shown. (E) Hit recovery rate of the deconvolution screen. The hit recovery rate is defined as the percentage of primary hits that were confirmed to be high confidence hits by the deconvolution screen.

The image-based LD morphology screen led to the identification of 59 hits, 40 of which showed an impact on lipid distribution, the remaining 19 candidates were additionally involved in lipid storage (Figure 3.3C). These hit candidates were members for several major cellular pathways, such as the COPI vesicular trafficking machinery (COPA, COPB1, COPB2, COPZ1), the proteasome degradation pathway (PSMC3, PSMC4, PSMC6, PSMD1, PSMD12, PSMD2, PDMD3) as well as translation initiation factors (EIF3C, EIF3E, EIF3F, EIF3G). The complete list of hit candidates is depicted in Supplementary Table S 4.

3.1.3 Analysis of the connection of LD-dependent viruses and the lipid storage organelle

Central role of LDs in the replication cycle of HCV and DENV. Given that the LDs play a pivotal role in the replication cycle of HCV and DENV, we argued that targeting genes that alter LD function would most likely also affect either virus. Indeed our screen had a relatively high hit rate of 57.8% (Figure 3.4A). Furthermore we were able to confirm that 25.7% of the analyzed genes were indeed affecting LD morphology in human hepatoma cells (Figure 3.4B). Interestingly almost 80% of those genes had an additional effect on either virus, and about 40% were common hits (Figure 3.4C). This suggests a strong relationship between the

replication cycle of HCV and DENV and LD homeostasis, and furthermore that HCV and DENV depend on similar LD-related pathways.

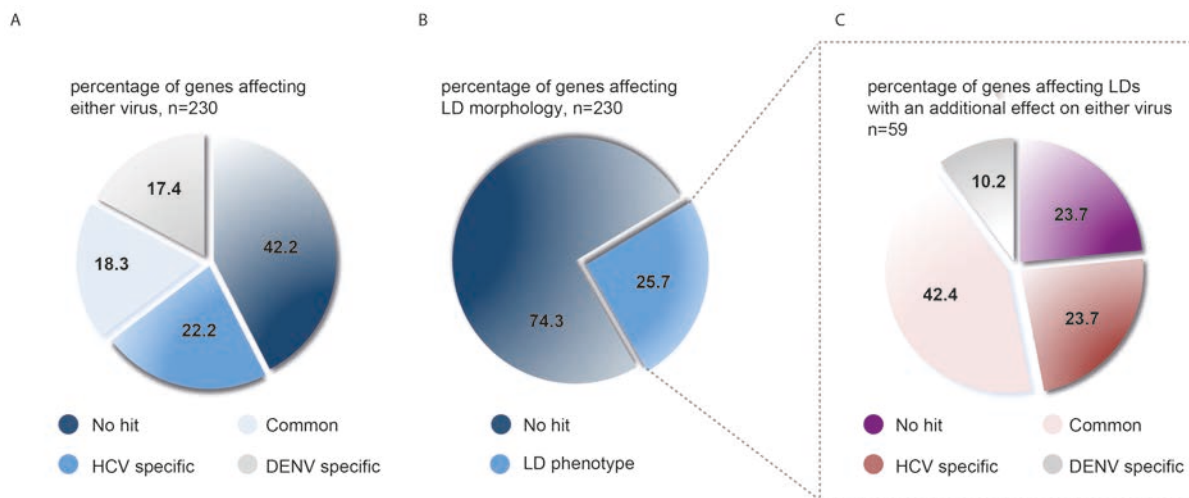


Figure 3.4 Analysis of the relationship of the viral replication cycle and LD biology based on the primary screen data. **(A)** Percentage of the 230 genes that alter HCV and/ or DENV replication cycle. **(B)** Percentage of the 230 genes with a given phenotype on LD morphology. **(C)** Percentage of the 59 LD hits that have an additional effect on the replication cycle of HCV and/or DENV. Adapted from Dr. G. Alvisi.

3.1.4 Bioinformatic analysis of LD RNAi screen

Enrichment of hit candidates involved in major cellular pathways. In order to gain a better insight into the cellular pathways that might be involved in the viral replication cycles as well as LD homeostasis a bioinformatic analysis was performed, in which the hits were grouped according to their most relevant function and to their cellular localization. This highlighted the importance of members of several biological processes involved in RNA metabolism, cell cycle control and protein degradation for both viruses. Most interestingly the vesicular coat protein complex I (COPI) transport machinery appeared to regulate LD biology as well as the viral replication cycles and thus might represent a central hub (Figure 3.5).

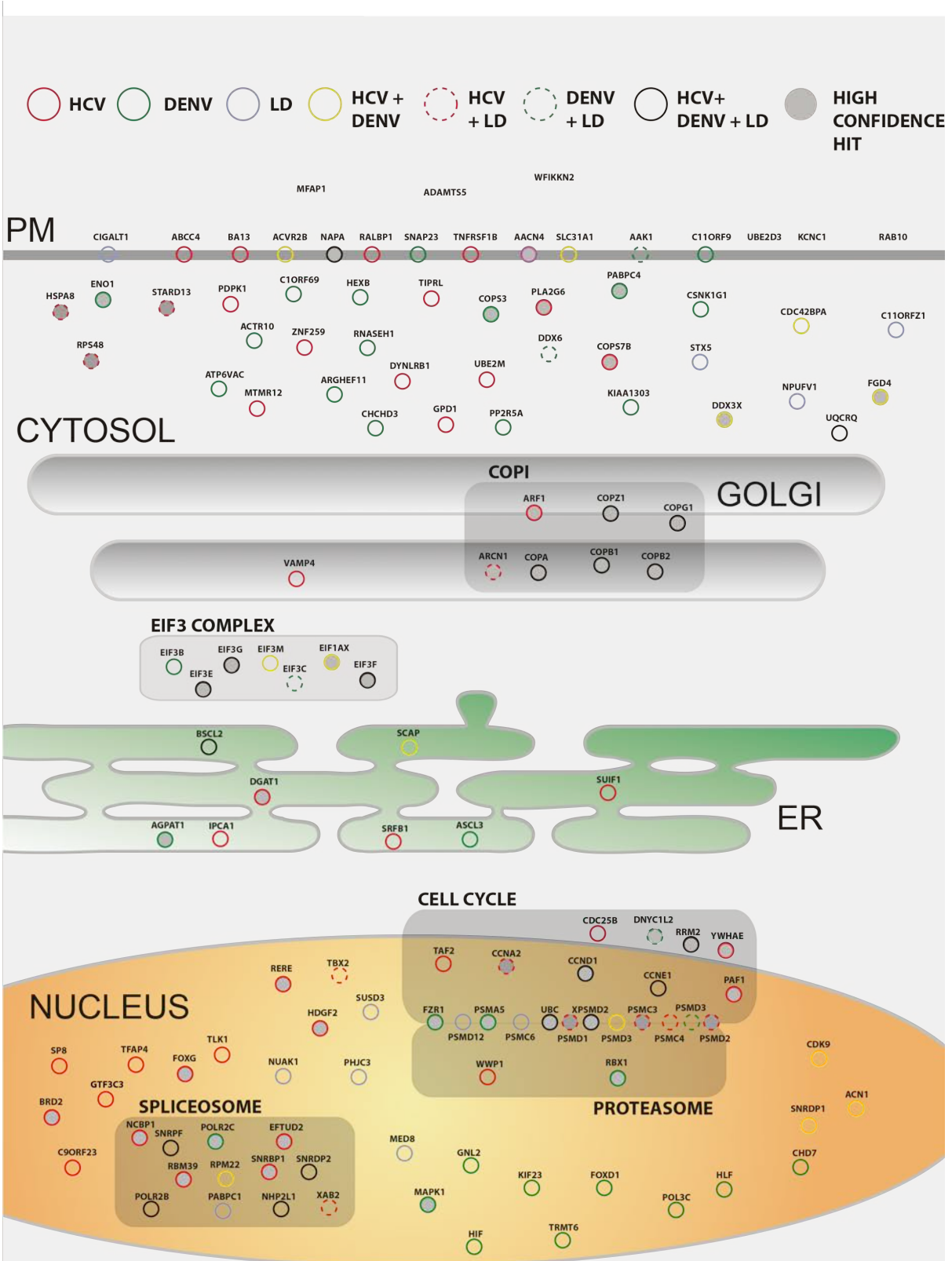


Figure 3.5 Schematic representation of the subcellular localization of hit candidates identified by the primary screen. The most relevant function of several candidates is presented and indicates the enrichment of distinct cellular pathways, i.e. Coat protein complex I (COPI) vesicle trafficking, eukaryotic translation initiation factor 3 complex eIF3. The following colour code for hit definition was used: HCV: red (solid line), DENV: green (solid line), LD: blue (solid line), HCV+DENV: yellow (solid line), HCV+LD: red (punctate line), DENV+LD: green (punctate line), HCV+DENV+LD: black. The grey filling indicates that the candidate gene was identified to be a high confidence hit for HCV and/ or DENV by the deconvolution screen. Scheme was adapted from Dr. G. Alvisi.

3.1.5 Follow-up studies of the LD RNAi screen

3.1.5.1 Selection of candidates for in depth characterization

Building on the screening results that had been obtained by Dr. Alvisi, I joined in for the subsequent follow-up studies, with the aim to elucidate in more detail the role of several candidates in the viral replication cycles and LD homeostasis. We therefore chose to focus on candidates that were either involved in all three processes, or specific for both viruses. The candidates and their respective phenotypes are depicted in Figure 3.6A and B.

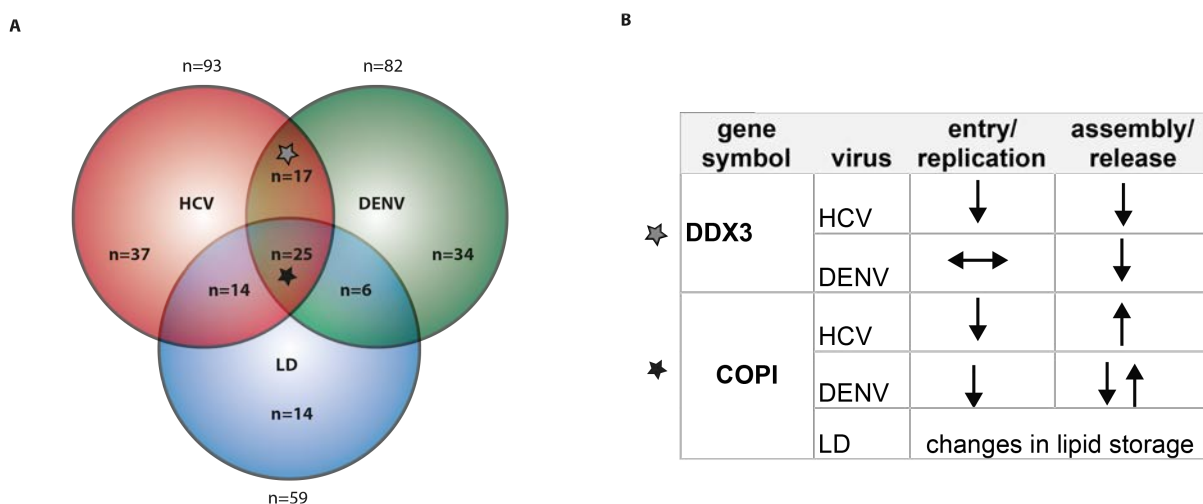


Figure 3.6 Candidates for follow-up studies. (A) Schematic representation of the hit distribution of the primary screen. (B) Knockdown phenotype of the respective candidate on entry/ replication or assembly/ release of HCV or DENV or LD morphology. The arrows pointing to the top or the bottom represent an enhancement or impairment of the respective step in the viral replication cycle upon gene knockdown. Arrows pointing to the left and right indicate that no effect was observed. Note that several subunits of the COPI coat are summarized, thus different outcomes are possible, depicted by several arrows. The stars indicate the association to different fields in (A).

Comparative bioinformatic analysis of the RNAi screen data suggested the COPI-mediated membrane trafficking machinery to act as a central node connecting all three processes. Our screen revealed, that knockdown of several members of the COPI coat efficiently reduced HCV entry and replication while increasing assembly and release of infectious particles. Dengue virus entry and replication was also impaired, while assembly and release of virions was either enhanced or reduced, depending on the COPI subunit. In agreement with earlier studies performed in drosophila cells, our screen identified the COPI system as a regulator of LD homeostasis, which was manifested by alterations in cellular lipid storage [236, 237] (Figure 3.2). In initial experiments transient siRNA-mediated knockdown of several COPI subunits did not cause a significant reduction in HCV RNA replication, while depending on the siRNA oligo used and on the siRNA gene target the viral reinfection efficiency was either

found to be enhanced or unaltered (Supplementary Figure S1). We found that only short periods of gene knockdown up to 48 h were well tolerated by our cellular system (Supplementary Figure S1D). Given that we were not able to reproduce the RNAi screen phenotype we set our major focus on another hit candidate, the DEAD box RNA helicase 3 (DDX3/DDX3X), which has a potential role in HCV and DENV life cycle (Figure 3.2A).

DDX3 is an established HCV entry/ replication dependency factor [76, 154], which was confirmed by our screen (Figure 3.2). Intriguingly the deconvolution screen revealed an additional role of the host factor in infectious particle production, which had not been described thus far. This is particularly interesting, as DDX3 was reported to be recruited to LDs by its interaction with the HCV core protein [260]. Furthermore our screen identified a novel function of DDX3 as an important dependency factor for DENV particle production (Figure 3.2, Figure 3.6).

3.1.5.2 The DEAD box RNA helicase 3, X-linked (DDX3X, DDX3)

In 2007 DDX3 was reported for the first time to be required for the replication of stable subgenomic HCV gt1b replicons [154]. Two years later, a RNAi screen targeting 62 host genes that interact either with HCV proteins or viral RNA confirmed the role of DDX3 in early events of the viral replication cycle (gt2a) [76]. So far the only hepatitis C virus protein that has been found to interact with DDX3 is the structural protein core [155, 156]. Until now, the function of this interaction remains unresolved. One study demonstrated that the interaction of both proteins is dispensable for the replication cycle of HCV (JFH1, gt2a), while another study indicated a possible function in RNA replication of genotype 1b replicons [260, 261].

3.1.5.2.1 Involvement of the DEAD box RNA helicase DDX3 in the replication cycle of HCV and DENV

The first set of experiments aimed to confirm the results of the RNAi screen that indicated a role of DDX3 in entry and replication of HCV. Additionally our screen implicated a novel function of the protein in infectious particle production of both HCV and DENV. Given that DDX3 has been implicated to interact with the HCV core protein at LDs we speculated that the protein could directly be involved in HCV virion biogenesis [260].

DDX3 is involved in early events of HCV reporter but not of DENV reporter virus replication cycle. In initial experiments DDX3 expression was silenced by transient electroporation of either one of two different siRNA oligos into target cells. In a similar setup

as compared to the RNAi screen, the effect of gene knockdown on the full infectious cycle of HCV or DENV was assessed (Figure 3.7A).

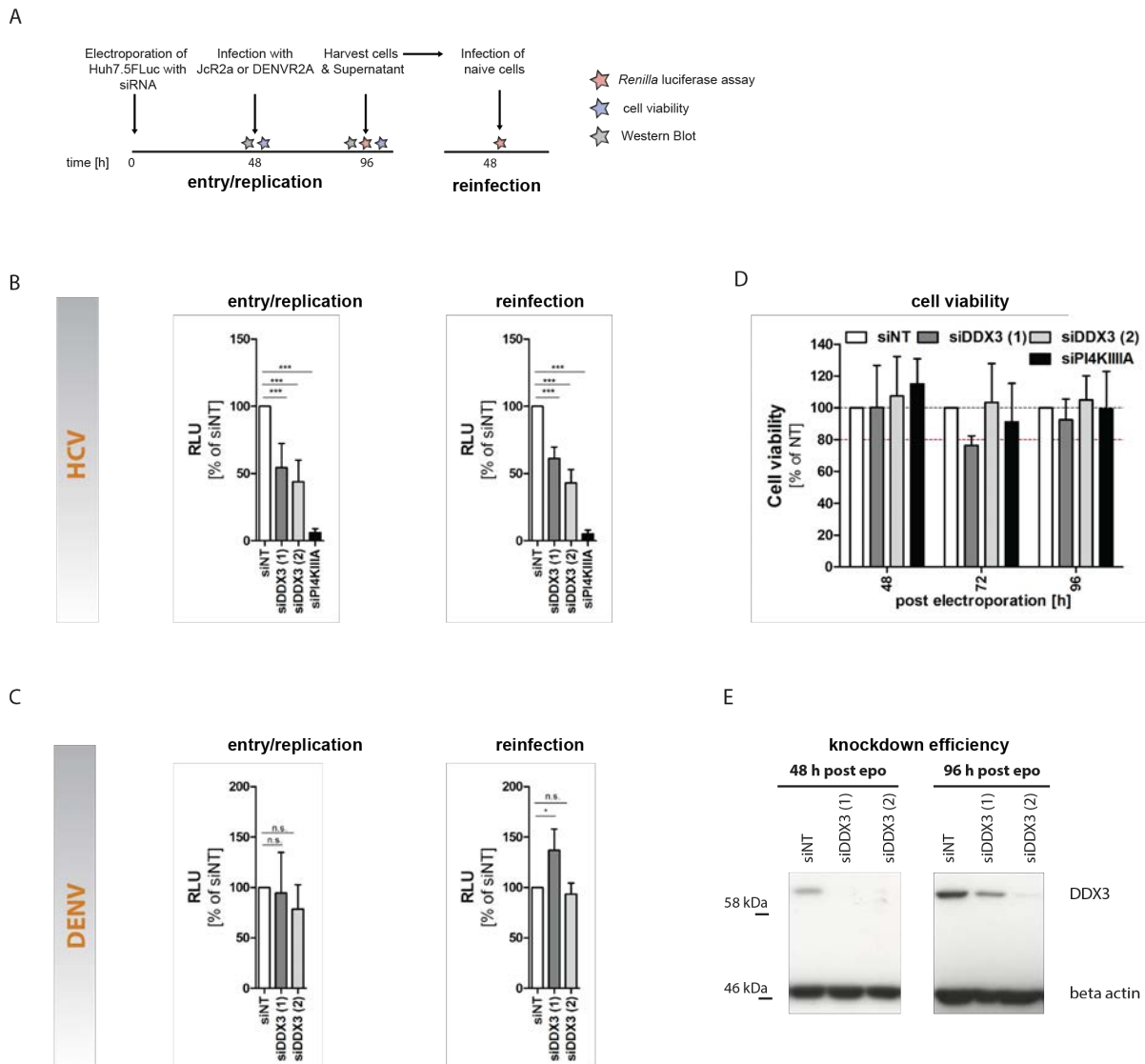


Figure 3.7 DDX3 knockdown affects HCV reporter but not DENV reporter virus replication cycle. (A) Description of the experimental setup. Huh7.5FLuc cells were electroporated with the respective siRNA. 48 h post silencing, cells were infected with HCV or DENV *Renilla* luciferase reporter virus at a MOI of 0.5. 48 h later cells were lysed and cell supernatants were transferred onto naïve cells for 48 h of reinfection. (B-C) Effect of gene knockdown of DDX3 on the entry/replication (left panel) and on the reinfection efficiency (right panel) of HCV or DENV *Renilla* luciferase reporter virus. Relative light units (RLU) are depicted as percentage of the non-targeting siRNA control. (D) Effect of gene knockdown on cell viability. Cell viability was assessed by measuring the metabolic activity of the cells using the WST-1 assay at different time points post siRNA electroporation. (E) Validation of knockdown efficiency. Cell lysates were harvested at the time-point of infection (48 h post siRNA epo) or reinfection (96 h post siRNA epo) and DDX3 protein levels were determined by Western Blot. Beta actin served as loading control. (A-D) The mean and standard deviation of at least 3 independent experiments are shown. (***, $p < 0.001$, **, $p < 0.01$, *, $p < 0.05$).

In agreement with the screen data, siRNA-mediated DDX3 gene knockdown efficiently impaired entry and replication of HCV *Renilla* luciferase reporter virus, while it caused no changes in the early events of DENV replication (Figure 3.6B, Figure 3.7B and C, left panels). Knockdown of the known HCV RNA replication dependency factor PI4KIII A, used as a positive control, dramatically reduced the *Renilla* luciferase reporter activity. We confirmed that the impact on virus replication was not a consequence of cell death, as DDX3 gene

silencing had only mild effects on cell viability (Figure 3.7D). However we were not able to validate the DDX3 knockdown phenotype of the screen on assembly and release of either virus under the given experimental conditions (Figure 3.6B, Figure 3.7B, C right panel). This could possibly be due to an inefficient gene knockdown. Indeed, we observed that DDX3 protein levels were severely reduced at the time point of infection (48 h post siRNA electroporation), while its expression appeared to partially recover at later stages, coincident with the time frame when most HCV particles are expected to be formed and released from the cell (Figure 3.7E).

DDX3 knockdown only mildly affects HCV RNA genome replication. The observed effect of DDX3 silencing on HCV replication suggests that this host factor might be involved in viral entry or post entry steps such as RNA translation and replication.

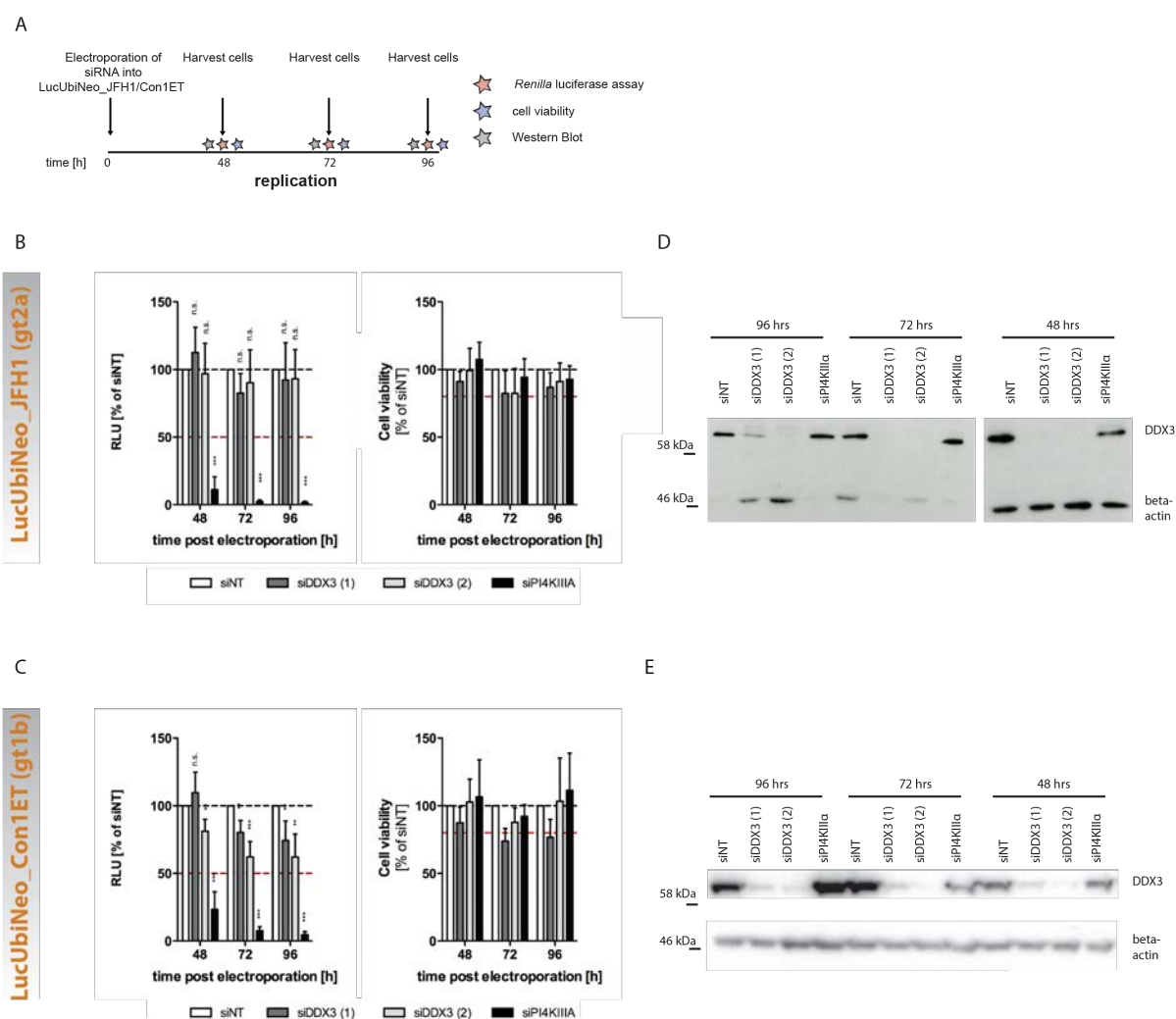


Figure 3.8 Effect of DDX3 gene knockdown on RNA replication of gt1b (LucUbiNeo_Con1ET) and gt2a (LucUbiNeo_JFH1) stable *Firefly* luciferase replicon cell lines. **(A)** Description of the experimental setup. Stable replicon cell lines of gt1b or 2a were electroporated with the respective siRNA and viral RNA replication efficiency was determined at different time points post silencing. **(B-C)** Left panels: The effect of DDX3 gene silencing on RNA replication of gt2a and gt1b stable *Firefly* luciferase reporter replicons was determined by measuring the *Firefly* luciferase activity in cell lysates at different time points post silencing. Relative light units

(RLU) are shown. Right panels: Effect of DDX3 gene knockdown on cell viability as determined by WST-1 assay. The mean and standard deviation of 6 independent experiments are shown (***, $p < 0.001$, **, $p < 0.01$, *, $p < 0.05$). (D-E) The DDX3 gene silencing efficiency was analyzed by Western Blot. DDX3 and beta actin protein levels at 48, 72 and 96 h post siRNA electroporation are shown for (D) LucUbiNeo_JFH1 or (E) LucUbiNeo_Con1ET.

In order to elucidate this in more detail we made use of gt2a (LucUbiNeo_JFH1) and gt1b (LucUbiNeo_Con1ET) stable *Firefly* luciferase reporter replicon cell lines (Figure 3.8).

DDX3 gene knockdown did not alter the viral RNA replication efficiency of gt2a replicons, while it mildly reduced gt1b RNA replication (Figure 3.8B, C). Importantly, DDX3 silencing did not significantly affect cell viability, especially in the case of siDDX3(2), the siRNA giving the best phenotype on virus replication (compare Figure 3.8C, E, left and right panels). Silencing of PI4KIII A however substantially impaired RNA replication of both viral genotypes (Figure 3.8B, C, left panels.) We further assessed the silencing efficiency by measuring DDX3 protein levels over time. We found that protein expression was reduced to different extent depending on the time point and siRNA used (Figure 3.8D, E). In general, we obtained an overall better silencing efficiency upon transfection of siDDX3(2) as compared to siDDX3(1), which correlated with a mildly stronger effect of siDDX3(2) transfection on early events of the HCV replication cycle (compare Figure 3.7B and E, Figure 3.8C and E). Taken together these results could indicate a specific role of DDX3 early in HCV replication.

DDX3 knockdown causes a slight reduction in infectious particle production of gt2a/2a and gt1b/2a intra-/ intergenotypic chimeras. In a last set of experiments we aimed to confirm the involvement of DDX3 in HCV particle production. To this end, we made use of two viral full-length *Renilla* luciferase reporter constructs, which share the same non-structural proteins of gt2a, but differ in the sequence of the structural proteins (and parts of NS2). The most efficiently replicating construct, is based on an intragenotypic chimera, designated Jc1, consisting of the core to NS2 sequence of the infectious isolate J6CF (gt2a) and the remaining sequence of JFH1 (gt2a) [100]. Similar to this virus construct, an intergenotypic chimera of gt1b and 2a, with two cell culture adaptive mutations that enhance viral particle production was used [262]. Both viral genomes had an integrated *Renilla* luciferase reporter gene that allowed a sensitive and efficient readout of viral RNA replication (Figure 3.9B).

In order to circumvent the negative effect of DDX3 gene silencing on early events of HCV replication, siRNA was transfected 48 h after the electroporation of *in vitro* transcripts of the respective full-length *Renilla* luciferase reporter virus. 48 h post silencing cell supernatants were transferred onto naïve cells for the determination of the viral reinfection efficiency (Figure 3.9A). Under these conditions gene knockdown of DDX3 did not affect viral replication (Figure 3.9C) but caused a mild, but significant, reduction of released infectivity. This effect was almost comparable to the ApoE knockdown condition, which resulted in the expected reduction in infectious particle production (Figure 3.9D). Importantly, DDX3 protein

levels were reduced upon DDX3 gene silencing, while the number of silenced cells remained unaffected (Figure 3.9E, F). This indicates that the observed effect of DDX3 silencing on the late stages of the viral replication cycle was not due to cell death.

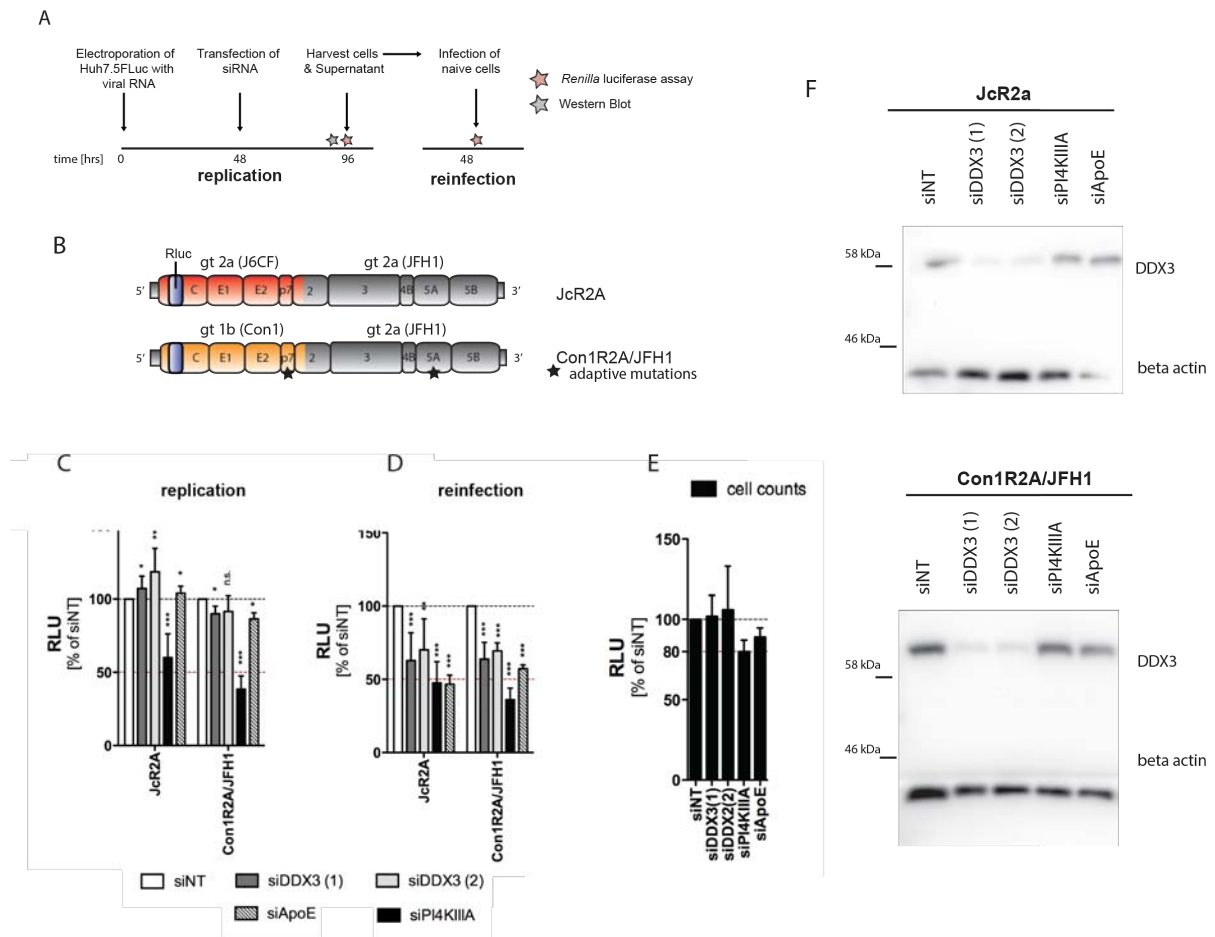


Figure 3.9 Effect of DDX3 gene knockdown on later stages of full-length *Renilla* luciferase reporter virus replication. (A) Description of the experimental setup. (B) Scheme of constructs used in this experiment. Two different intra-/ intergenotypic chimeras containing the *Renilla* luciferase reporter gene were used. Gt2a/2a: J6/JFH1, also designated JcR2A, gt1b/2a: Con1R2A/JFH1 [262]. (C) Effect of DDX3, PI4KIIIA or ApoE gene knockdown on viral replication. Replication was determined by measuring the *Renilla* luciferase activity in cell lysates. (D) Effect of DDX3, PI4KIIIA or ApoE gene silencing on the assembly and release of infectious particles. Reinfection efficiency was determined by measuring the *Renilla* luciferase activity in cell lysates of reinfected cells. (C-D) The mean relative light units (RLU) and standard deviation of at least 4 independent experiments are shown (***, $p < 0.001$, **, $p < 0.01$, *, $p < 0.05$). (E) Cell number as determined by measuring the *Firefly* luciferase counts. The effect of gene knockdown on the cell number, as an estimate for cell viability, was determined for cells electroporated with either viral construct in addition to siRNA and is summarized in the panel. (F) DDX3 gene knockdown efficiency as determined by Western Blot 48 h post silencing.

Taken together, DDX3 seems to be important for early events in the HCV replication cycle. Additionally DDX3 might further be involved in HCV particle production.

3.1.5.2.2 Analysis of the cellular distribution of DDX3 in HCV or DENV infected cells

DDX3 has been reported to interact with the HCV core protein resulting in the protein's relocalization to LDs in HCV infected cells [155, 156, 260]. This is of peculiar interest, given that DDX3 was found to promote late stages of the viral replication cycle (Figure 3.9), possibly infectious particle production, which in turn is suggested to involve LDs [136, 138].

DDX3 is relocalized to LDs in HCV but not in DENV infected cells. Indeed immunofluorescence analysis of HCV (Jc1, gt2a) infected as compared to uninfected cells revealed a striking relocalization of the cytosolic DDX3 protein pool to dot-like structures at close proximity of LDs (Figure 3.10A, C).

Although DDX3 and the HCV core protein were found to surround the same lipid droplets, they did not substantially colocalize. Instead the DEAD box RNA helicase was found at sites adjacent to the viral core protein (Figure 3.10A, white arrow). Similar to the HCV core protein, the DENV capsid protein localizes to LDs (Figure 3.10B, white arrow). Interestingly DDX3 was not found to change its cellular distribution in DENV infected cells and remained evenly distributed in the cytosol, similar to the protein's localization in mock cells (Figure 3.10B, C). This suggests that the recruitment of DDX3 to LDs might specifically depend on the presence of the HCV core protein at the lipid storage organelle.

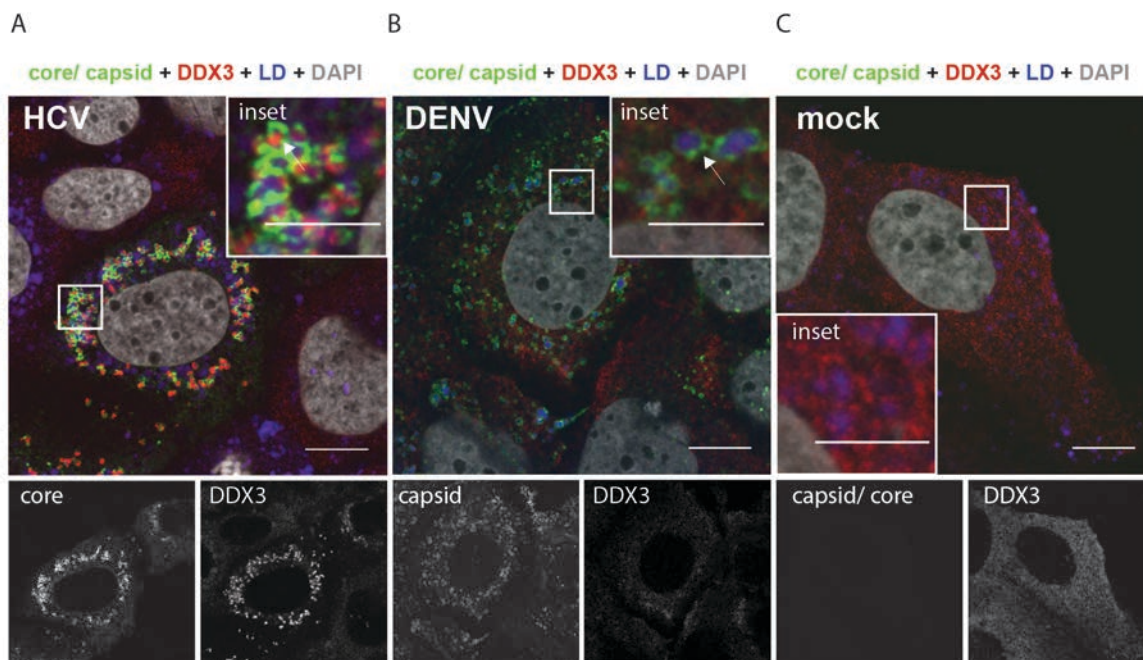


Figure 3.10 Cellular distribution of DDX3 in HCV or DENV infected cells. Huh7HP cells were infected with (A) HCV (Jc1), (B) DENV (DENV-2 16681) at a MOI of 5 or were (C) left uninfected. 48 h post infection cells were processed for indirect immunofluorescence. Cells were labelled for the nuclei with DAPI (grey), the viral capsid or core proteins (green), endogenous DDX3 (red) and lipid droplets (LDs, blue). Representative pictures of HCV or DENV infected cells as well as of an uninfected cell are shown. Note that the signal intensity of DDX3 was enhanced in order to visualize the cytosolic distribution of DDX3 in mock cells. The areas highlighted with a white box are shown in larger magnification in the insets. Scale bars indicate 10 μ m or 5 μ m in the insets.

The HCV core protein is sufficient for recruitment of DDX3 to LDs. The HCV core protein has been shown to recruit other viral replicase components such as the viral RNA and several non-structural proteins to LDs [136]. Although in a yeast two hybrid screen a direct protein-protein interaction of the viral core with DDX3 was observed [156], it is still possible that under authentic infection conditions, the recruitment of DDX3 to LDs is involving any of the other viral components. Another interesting possibility would be that DDX3, being an RNA binding protein, could be trafficked together with viral RNA molecules to LDs [263].

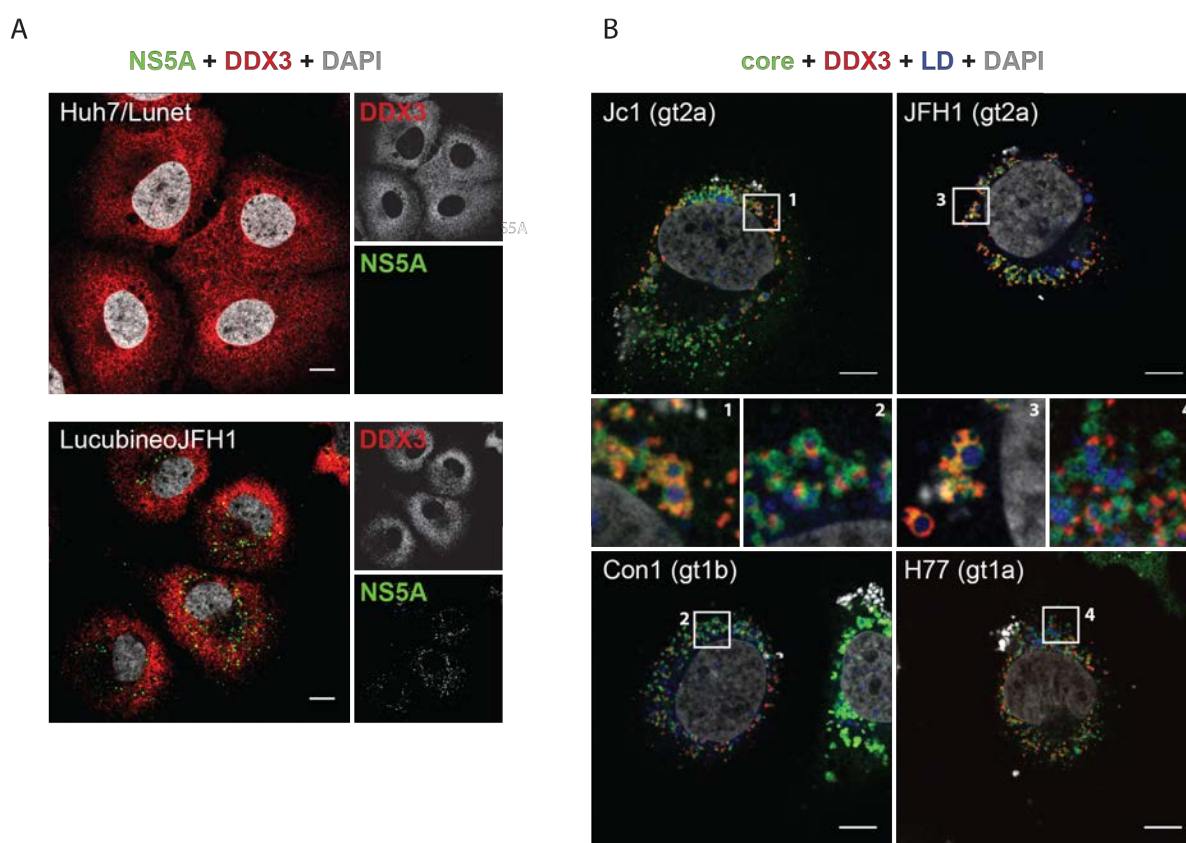


Figure 3.11 Localization of DDX3 to lipid droplets is dependent on the presence of the HCV core protein. (A) Distribution of DDX3 in Huh7/Lunet or gt2a stable replicon cells (LucUbiNeo_JFH1). DDX3 is shown in red, NS5A in green. Scale bars indicate 10 μ m. (B) Distribution of DDX3 in Huh7/Lunet-T7 cells expressing the core protein of different genotypes: Jc1 (gt2a), JFH1 (gt2a), Con1 (gt1b), H77 (gt1a). The core is shown in green, endogenous DDX3 in red, cell nuclei in grey and lipid droplets in blue. Magnifications of the area encircled by a white box are shown in the insets. Scale bars represent 10 μ m.

In order to examine in more detail the viral determinants that induce this tremendous redistribution of DDX3 we performed a set of immunofluorescence studies (Figure 3.11). In order to rule out the involvement of any of the non-structural proteins NS3-5B in the recruitment of DDX3 to LDs we analyzed the protein's localization in stable replicon cell lines of gt2a (LucUbiNeo_JFH1), which lack the viral proteins core to NS2. In this case, DDX3 was found evenly distributed in the cytosol, similar as compared to the protein's distribution in control Huh7/Lunet cells (Figure 3.11A). In contrast, the sole expression of the core protein

of different genotypes induced an efficient recruitment of DDX3 to dot-like structures at LDs, similar to that observed in infected cells (compare Figure 3.10A and Figure 3.11B).

In summary, the cytosolic DEAD box RNA helicase DDX3 is recruited to LDs in HCV infected cells in a core-dependent manner. The fact that DDX3 is recruited by the core protein of several genotypes supports the notion that this host factor has an important role in the HCV replication cycle.

3.1.5.2.3 Studying the effect of disrupting DDX3 relocalization to LDs on the viral replication cycle

Extensive comparative studies of two hepatitis C genomes, namely Jc1 and JFH1, led to the interesting finding that the J6 core moiety of Jc1 showed a fairly stable binding to LDs, while only few lipid droplets were covered by the viral core protein. The JFH1 core in contrast was shown to extensively localize around LDs where it was highly mobile and exchangeable. It was argued that the lower mobility of the J6 core at LDs might somehow facilitate particle assembly, which would contribute to the more efficient infectious virion production in case of Jc1 as compared to the low assembly competent JFH1 [264]. In addition the core protein of a Jc1 mutant, incapable of virus assembly, was found to heavily accumulate around LDs. This suggests that the rapid release of viral particles in case of J6 might prevent the accumulation of core protein around LDs [264]. These observations generally raise the question which viral or host determinants might contribute to differences in the efficiency of infectious particle production. Given the interaction of the HCV core protein with the cellular DEAD box RNA helicase DDX3, we hypothesized that the recruitment of this host factor to LDs might contribute to HCV particle production. We further wondered whether the infectious particle production of different viral genotypes was similarly dependent on DDX3 recruitment to LDs by the viral core protein.

LD core coverage determines DDX3 relocalization efficiency. In a first set of experiments we performed immunofluorescence analysis to compare the distribution of DDX3 and of the viral core protein in cells replicating the highly assembly competent Jc1, its assembly deficient mutant Jc1 Δ E1E2 or the low assembly competent JFH1. Almost all cellular LDs were observed to be covered by the HCV core protein of JFH1 and Jc1 Δ E1E2 (core in doughnut shaped structures), while the Jc1 core protein showed the expected less prominent association to LDs (core in dot-like structure) (Figure 3.12A) [264]. Quantification of the DDX3 relocalization efficiency, defined as percentage of NS5A positive cells with a DDX3 speckle-like phenotype, demonstrated a dot-like distribution of DDX3 in almost all cells

transfected with the low (JFH1) or assembly incompetent (Jc1 Δ E1E2) viral constructs. In marked contrast, DDX3 remained cytosolic in 80% of cells transfected with the highly assembly competent Jc1 (Figure 3.12B). In line with our previous observation of the HCV core protein being the sole determinant for DDX3 recruitment to LDs, these results indicate a correlation between LD-HCV core coverage and the efficiency of DDX3 recruitment.

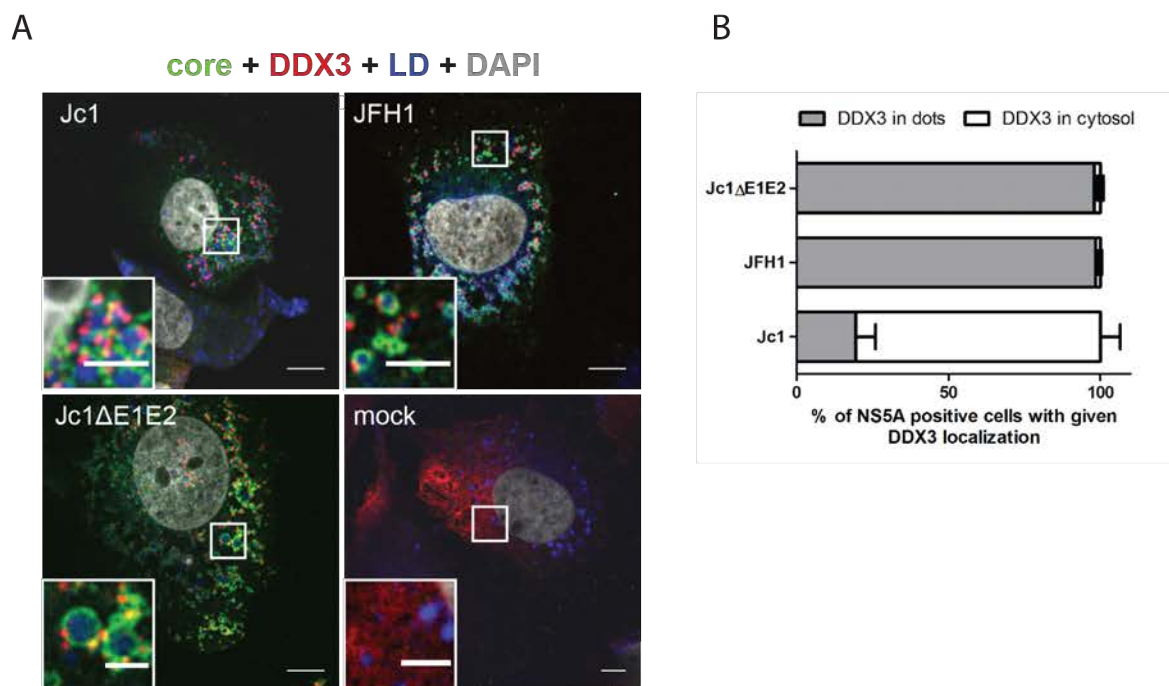


Figure 3.12 HCV isolate specific differences in DDX3 relocalization efficiency. (A) Localization of endogenous DDX3, lipid droplets and the viral core protein in HCV transfected cells. Huh7/Lunet cells were electroporated with the genomic transcripts of Jc1, JFH1 or Jc1 Δ E1E2 or a water control. 72 h post electroporation cells were fixed with 4% PFA and processed for indirect immunofluorescence. The HCV core protein (green), endogenous DDX3 (red), lipid droplets (blue) and the nuclei (DAPI, grey) are shown. Magnifications of the area highlighted with a white box are shown. Scale bars represent 10 μ m in the overview or 5 μ m in the insets respectively. (B) Percentage of NS5A positive cells with given DDX3 distribution 72 h post viral RNA transfection. Results of two independent experiments are shown; at least 70 cells were analyzed per experiment and per condition.

The Y35A core point mutation disrupts DDX3 relocalization to LDs. We next aimed at investigating the role of DDX3 recruitment to LDs during HCV infection. Given its interaction with the viral core protein, DDX3 might most likely be involved in steps of viral particle production. In addition we wondered whether distinct viral chimeras that differ in their infectious particle assembly competence [262] would depend equally on the recruitment of DDX3 to LDs. To this end we introduced either one of the two core point mutations, Y35A or F24A, into several different viral constructs (Figure 3.13). Both mutations have earlier been described to disrupt DDX3-core protein interaction, with Y35A having a higher efficiency as compared to the F24A mutation [260]. We choose to introduce these mutations into core

protein of several viral chimeras, that share the NS2 to 3' moiety of gt2a and but contained the remaining parts of either one of two different HCV genotypes and subtypes (gt1a, 1b, 2a). Note, the gt1b/2a (Con1/JFH1) and gt1a/2a (H77/JFH1) chimeras exhibit two to three cell culture adaptive point mutations that substantially enhance infectious particle production as compared to the corresponding *wild-type* constructs [262].

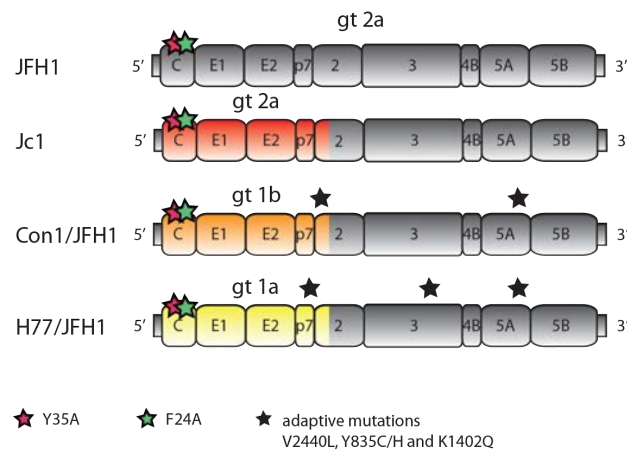


Figure 3.13 Schematic representation of viral constructs used in the subsequent experiments. Either one of the two point mutations Y35A or F24A that have been described to interfere with protein interaction of DDX3 and HCV core were introduced into the viral core proteins [260]. In case of two constructs additional adaptive mutations were introduced which have been reported to substantially enhance infectious particle production [262].

Immunofluorescence analysis of the cellular distribution of DDX3 showed that upon the introduction of the Y35A point mutation into the HCV core protein of either genotype, DDX3 was no longer found in dot-like structures at LDs, but remained evenly distributed in the cytosol (Figure 3.14A, B). Of note, the DDX3 protein levels were the same in cells replicating *wild-type* or mutant virus (Figure 3.14C). This suggests that the HCV core mediated recruitment of DDX3 to the LDs represents a relocalization of the cytosolic pool, while overall DDX3 protein levels and possibly protein stability remain unaltered. In addition, these results reinforce the notion that the HCV core protein is the sole viral factor mediating DDX3 recruitment to LDs.

Disrupting core-mediated relocalization of DDX3 to LDs through the Y35A core point mutation does not affect HCV RNA replication but reduces infectious particle production as well as HCV core protein levels. To elucidate the impact of the Y35A core mutation on the viral replication cycle, intracellular as well as extracellular viral titers were determined by limiting dilution assay. To this end, viral titers were determined 48 or 72 h after transfection of *in vitro*-transcribed viral RNAs of the Jc1, JFH1, Con1/JFH1 and H77/JFH1 constructs, carrying or not the point mutation in core. While differences in the extracellular titers would account for an impact of the mutation on the release of infectious particles,

differences in intra- and extracellular titers would be an indication of an impaired virus assembly process.

A

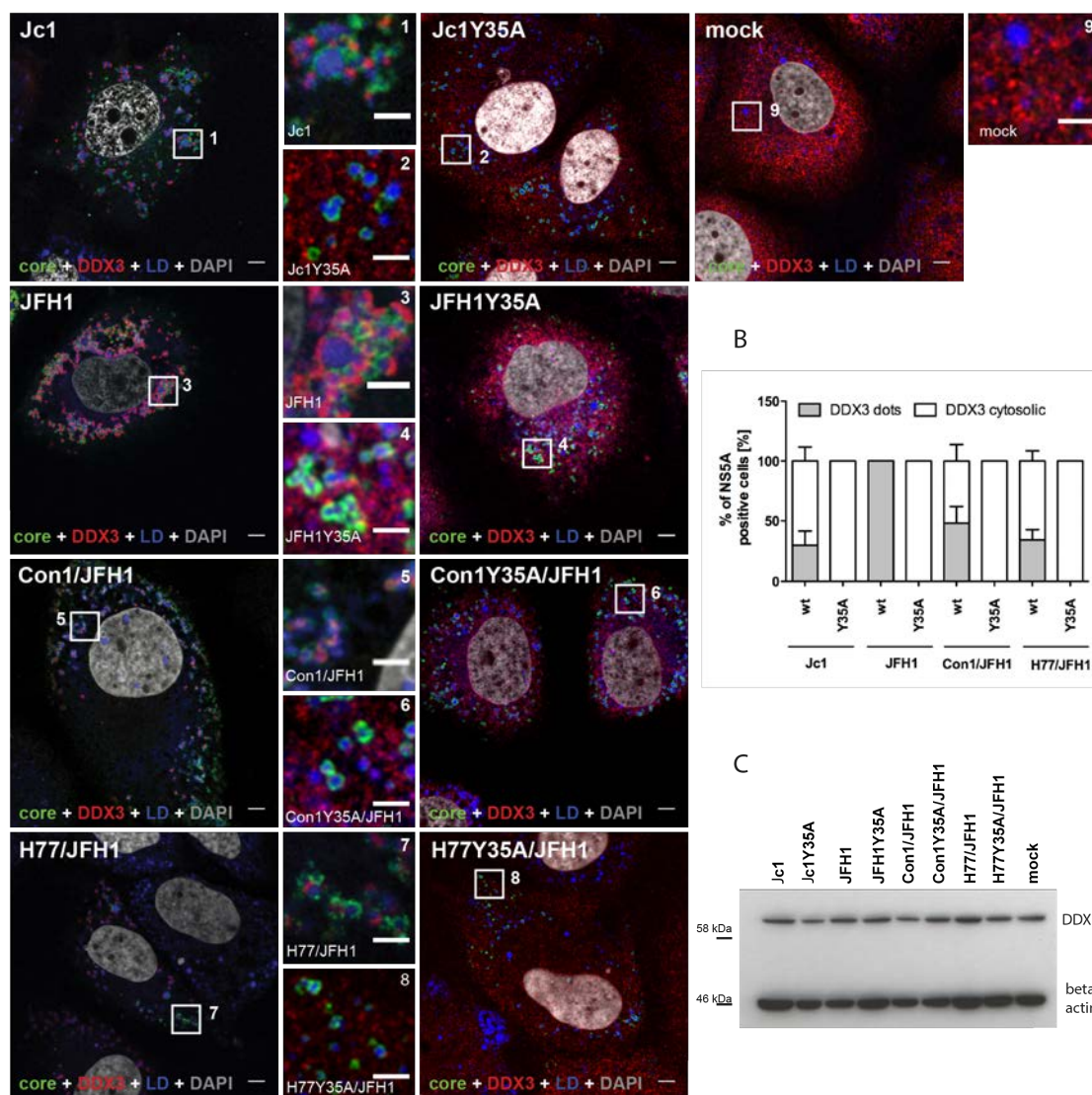


Figure 3.14 Effect of Y35A HCV core point mutation on DDX3 distribution. (A) Immunofluorescence analysis of DDX3 localization in Huh7/Lunet cells 72 h after transfection of the respective constructs depicted in Figure 3.13. Endogenous DDX3 is shown in red, the viral core protein in green, lipid droplets in blue and cell nuclei in grey. Magnifications of the area highlighted with a white rectangle are shown. Scale bars represent 10 μm in the overview or 5 μm in the respective magnification pictures. Note that in order to illustrate the cytosolic distribution of DDX3, the signal of DDX3 was enhanced in case of the Y35A mutants and the mock control (B) Percentage of NS5A positive cells with given DDX3 distribution. The results of a single experiment are shown. At least 100 cells per condition were analyzed. (C) Western Blot analysis of the protein levels of DDX3 and beta actin in cell lysates 72 h after transfection of the viral RNA.

We found no significant difference in intra- or extracellular virus titers after 48 h of viral RNA transfection (Figure 3.15A). However at a later time point (72 h post viral RNA electroporation), both intra and extracellular viral titers were reduced ~ 10 -fold in case of mutant Jc1, Con1/JFH1 as well as H77/JFH1. This result indicates a defect in infectious virus particle assembly when DDX3 is not properly recruited to LDs (Figure 3.15B, C). In contrast

the core point mutation did not alter viral titers of JFH1Y35A, which were similarly low as compared to the corresponding wild-type virus (Figure 3.15B).

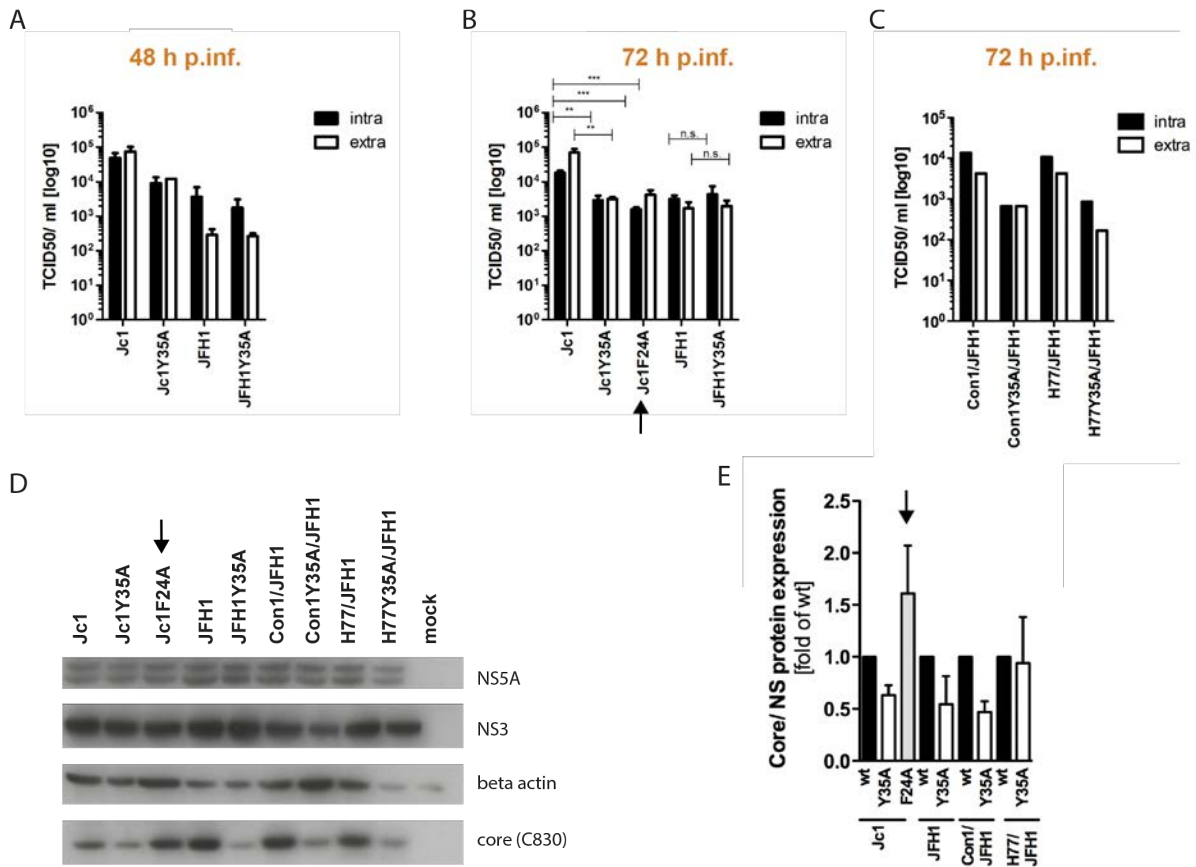


Figure 3.15 Effect of Y35A HCV core point mutation on the full replication cycle of HCV. (A-C) Intra and extracellular viral titers as determined by limiting dilution assay. Huh7/Lunet cells were electroporated with the viral RNA. 48 and 72 h post electroporation intra and extracellular viral titers were determined. (A) $n=2$, (B) $n=4$, (C) $n=1$ (***, $p < 0.001$, **, $p < 0.01$, *, $p < 0.05$). (D) Protein levels of NS5A, NS3, beta actin and the viral core protein in cell lysates 72 h post viral RNA transfection. A representative picture of a Western Blot is depicted. (E) Quantification of the Western Blot analysis of two to three independent experiments. HCV core signal was normalized to protein expression of a non-structural protein (NS). wt= wild-type

In order to exclude the possibility that the reduction in titers is simply a reflection of different replication capacities among the viral mutants, we measured NS5A and NS3 protein levels by Western Blot. All mutant viruses appeared to replicate to similar extent as no dramatic differences in the levels of the non-structural proteins were detected (Figure 3.15D). This result further suggests that the recruitment of DDX3 to LDs is dispensable for HCV RNA replication.

In the course of these experiments, when we analyzed the core protein expression it became apparent that mutant core protein levels of all genotypes tested were reduced by almost two-fold in comparison to the respective wild-type counterpart (Figure 3.15D, E). Although the levels of core protein reduction did not correlate to the corresponding reduction in viral titers, it cannot be ruled out that, at least in parts, the reduced core protein levels account for the lower viral titers. Interestingly, the introduction of the F24A point mutation into Jc1 led to a

substantial decrease of viral titers while the protein levels of core were not reduced but conversely, increased (Figure 3.15B, D, E, indicated by black arrow).

The F24A core point mutation abrogates DDX3 relocalization, impairs infectious particle production and partially reduces HCV core protein levels. As the F24A core mutation caused a drop in intracellular and extracellular viral titers while not substantially reducing the core protein levels of Jc1, we assessed the effect of this point mutation on the cellular distribution of DDX3.

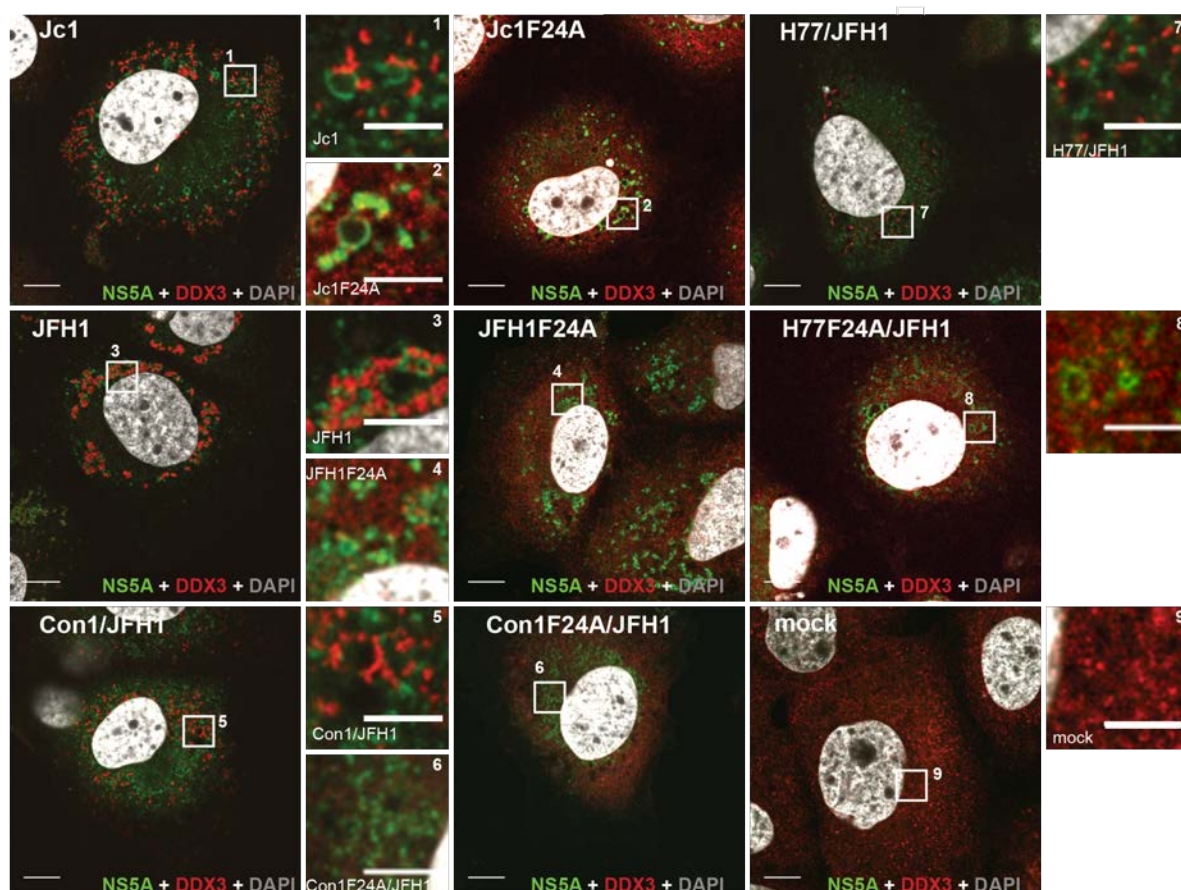


Figure 3.16 Effect of F24A HCV core point mutation on the cellular distribution of DDX3. Huh7/Lunet cells were electroporated with the *wild-type* or F24A mutant constructs depicted in Figure 3.13. 72 h post electroporation cells were fixed and processed for immunofluorescence staining of NS5A (green), DDX3 (red) and cell nuclei (grey). Scale bars represent 10 μ m or 5 μ m in the inset, respectively. Note that the DDX3 signal was increased in case of the F24A mutants and the mock control to visualize the protein's cytosolic localization.

As observed for the Y35A core mutant, DDX3 was found evenly distributed in the cytosol of cells transfected with the F24A core mutant virus (Figure 3.16). In the case of cells replicating the corresponding *wild-type* virus DDX3 was found in defined spots in close proximity to NS5A often present in doughnut shaped structures, suggesting the protein's accumulation around LDs (Figure 3.16).

To elucidate whether the F24A mutation differentially affects the replication cycle of the distinct virus chimeras of low or high assembly efficiency, intra- and extracellular viral titers of mutant and wild-type virus were assessed 72 h post viral RNA transfection. As observed

before in the case of the Y35A mutation, intracellular and extracellular titers of the F24A mutant viruses were reduced by almost 10-fold in case of Jc1, Con1/JFH1 and H77/JFH1. No difference was observed between *wild-type* JFH1 and its respective F24A core mutant version (Figure 3.17A). In addition we introduced the F24A mutations into full-length *Renilla* luciferase reporter genomes and assessed the replication and reinfection efficiency of *wild-type* and mutant virus. In agreement with our previous results replication was unaltered in presence of the F24A mutation, as determined by the *Renilla* luciferase activity in cell lysates 48 and 72 h post viral RNA transfection in addition to measurements of NS5A protein levels (Figure 3.17B, E). Interestingly the reinfection efficiency of all mutant viral constructs, including JFH1F24A, was significantly impaired as compared to their respective *wild-type* counterparts (Figure 3.17C).

The decrease of intra- and extracellular viral titers to similar extent (Figure 3.17A) suggests a defect in HCV particle assembly. Another possibility could be that the decrease in viral titers is caused by a reduced infectivity of assembled particles (specific infectivity). Thus we determined the intracellular and extracellular core protein levels by core ELISA, which can be used as an indication of the total amount of particles present in the sample, independent of their infectious potential (Figure 3.17D). To this end, intra- and extracellular core protein levels were determined 72 h post viral RNA transfection. In order to normalize for the differences in input RNA, the amount of intracellular core protein was determined 4 h post transfection. We observed that intra- and extracellular F24A mutant core protein levels were reduced 72 h post transfection, which would suggest that the recruitment of DDX3 to LDs does not alter specific infectivity of viral particles but instead affects the viral assembly efficiency (Figure 3.17D, numbers indicate fold reduction of mutant core protein levels as compared to wild-type). However we observed an additional reduction of mutant core protein levels early after viral RNA transfection (4 h post electroporation), which indicates that mutant core protein levels are generally lower as compared to the wild-type condition (Figure 3.17D). This could possibly be due to defects in viral RNA translation or an inefficient recognition of the mutant core protein by the antibody used. Indeed, earlier results indicated that a core antibody (C750) specific against the N-terminal epitope of core that comprises the region of the point mutation recognizes the mutant core proteins to lower efficiency as compared to the wild-type protein (data not shown). In contrast the core antibody C830, specifically targeting the core polyprotein and frequently used in our Western Blot analysis, was shown to recognize *wild-type* and mutant protein to similar extent (Supplementary Figure 2). Unfortunately we were not provided with any information regarding the epitope recognized by the antibody used in the core ELISA. Taken together, due to the present technical limitations the core ELISA results cannot easily be interpreted. In order to corroborate further whether the F24A mutation altered mutant core protein stability, the HCV

core protein levels were assessed by Western Blot using the C830 core specific antibody. The mutant core protein levels were found to be reduced in case of two out of the four mutant chimeras, namely, JFH1F24A and H77/JFH1F24A (Figure 3.17E, F). There was no obvious correlation between the extent of reduced core protein levels and the observed reduction in infectious particle assembly. In fact, although the F24A mutation in the context of JFH1 reduced the core protein levels by almost two-fold, this mutant showed the least reduction in the viral reinfection efficiency (compare Figure 3.17A, C, E, F).

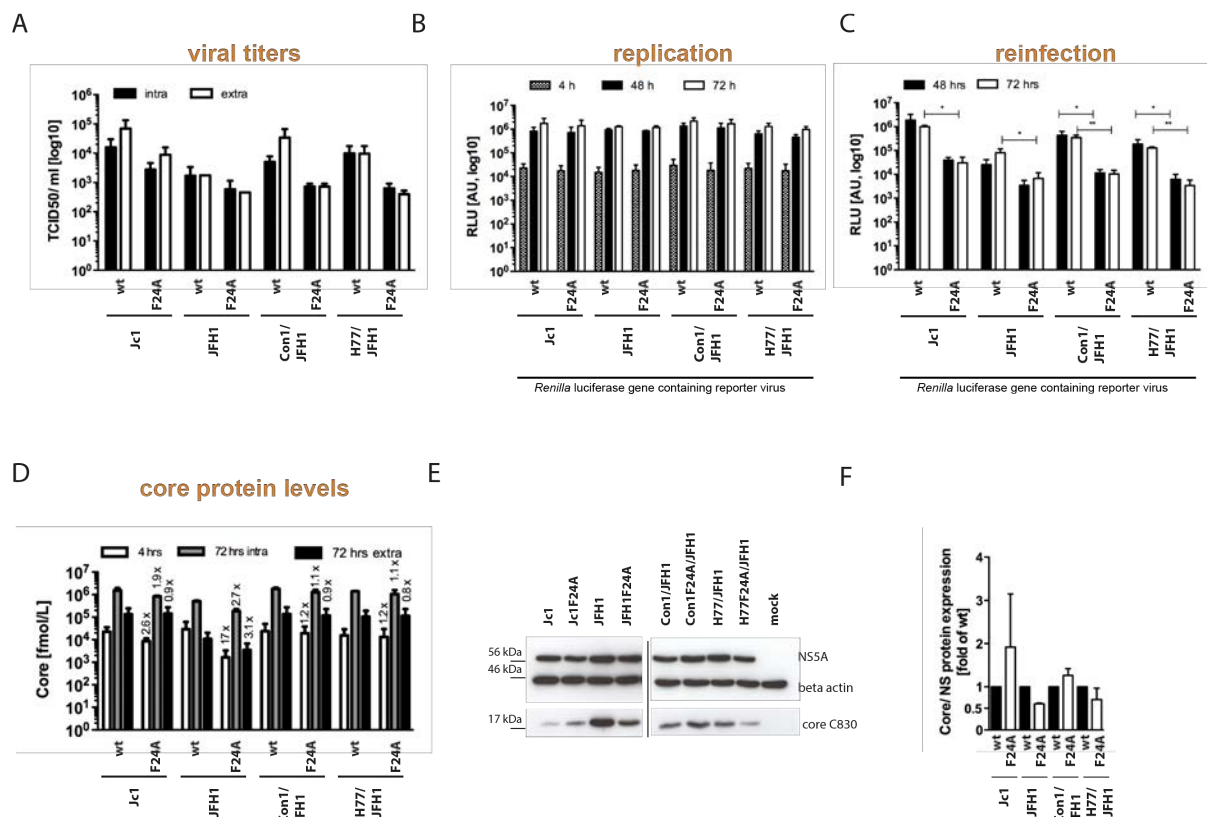


Figure 3.17 Effect of F24A HCV core point mutation on the full replication cycle of HCV. (A) Intra- and extracellular viral titers 72 h post viral RNA transfection as determined by limiting dilution assay. The mean and standard deviation of two independent experiments are shown; only 1 experimental result is presented in case of “JFH1 extra”. (B-C) Replication and reinfection efficiency of wild-type and F24A core mutant *Renilla luciferase reporter virus*. *Renilla luciferase* activity was measured in Lunet/Huh7 cells transfected with the respective construct. Cells were harvested 4, 48 and 72 h post viral RNA transfection. Supernatants collected 48 and 72 h post transfection were used for reinfection of naïve Huh7.5 cells. The results of three independent experiments are shown. Mean and standard deviation of relative light units (RLU) are depicted (***, $p < 0.001$, **, $p < 0.01$, *, $p < 0.05$). (D) Core ELISA analysis of the intra- and extracellular core protein levels of cells transfected with wild-type or F24A core mutant virus. The mean and standard deviation of two independent experiments are shown. The numbers indicate the fold reduction as compared to the respective wild-type condition. (E) Western Blot of NS5A, core and beta actin protein levels present in whole cell lysates of (A). A representative picture is shown. The NS5A, beta actin and core signals were detected on the same membrane. (F) Quantification of core protein levels as determined by Western Blot in two independent experiments. The core protein levels were normalized to the expression levels of a non-structural protein (NS). wt= wild-type

In summary our data indicates that the core-mediated relocalization of DDX3 to LDs is dispensable for HCV RNA replication, while it might play a role in infectious particle

production. Given that some of the core mutants showed decreased core protein levels, it cannot be excluded that the point mutation alters core protein stability and thus impairs infectious particle formation.

3.1.5.2.4 Studying the role of the DDX3 core interaction in the HCV replication cycle

There are several indications that DDX3 might be involved in the regulation of cellular lipid metabolism. In an image-based miRNA screen that assessed the role of 327 human miRNAs in LD morphology, several miRNAs were identified to reduce the cellular lipid content by more than 60%. Interestingly DDX3 was predicted to be targeted by one of the hit miRNAs. Follow-up studies that focused on the effect of siRNA-mediated knockdown of DDX3 on LDs revealed a slight reduction by 20% in the cellular LD content [246]. Additionally, while our study was in progress, DDX3 was described to recognize the 3' untranslated region of HCV RNA, which subsequently triggers a signaling cascade leading to the induction of lipogenic genes. This in turn enhances lipid droplet formation that could support HCV particle production [158]. Thus we wondered whether the core-dependent recruitment of DDX3 to LDs is important for the DDX3 mediated regulation of the cellular neutral lipid content.

Effect of F24A core mutation on cellular neutral lipid content. To address the question whether the localization of DDX3 to LDs is important for the induction of lipogenesis and thus the formation of lipid droplets, we studied the LD content of cells transfected with either *wild-type* or the F24A mutant of the high or low assembly competent Jc1 or JFH1 respectively. To this end cells were transfected with the respective full-length viral constructs and the cellular neutral lipid content of NS5A positive cells was determined by immunofluorescence using the neutral lipid stain Bodipy493/503 (Figure 3.18A). Several LD features were extracted. The overall neutral lipid content per cell was determined by measuring the overall Bodipy493/503 signal intensity (Integrated Density) (Figure 3.18 B). The LD coverage was defined as the percentage of the cell cytoplasm covered by Bodipy. Furthermore the LD area (size of an individual LD) as well as LD number/ cell area were determined for cells transfected with Jc1 and its corresponding F24A mutant (Figure 3.18 D, E). This analysis was not feasible for cells transfected with JFH1, as LDs were found to cluster and were not easily distinguishable (Figure 3.18 A, white arrows). The overall neutral lipid content and LD coverage was higher in Jc1- or JFH1- transfected cells as compared to mock cells, suggesting an induction of neutral lipid storage in HCV replicating cells (Figure 3.18 B, C). In general the results of the immunofluorescence analysis were not highly reproducible, indicating the high susceptibility of the read-out towards variations in the experimental procedure, such as the efficiency of the LD staining. Analyzing the overall neutral lipid content as well as the LD coverage, it appeared that the cellular neutral lipid content and distribution was slightly reduced in case of

cells transfected with the F24A mutant virus (Figure 3.18 B, C). This was reproducible in regard to JFH1 and its respective mutant, while in case of Jc1 the results were contradicting. Although there were statistical significant differences in LD area as well as LD number/ cell area between the different conditions, these differences were either subtle or not reproducible (Figure 3.18 D, E).

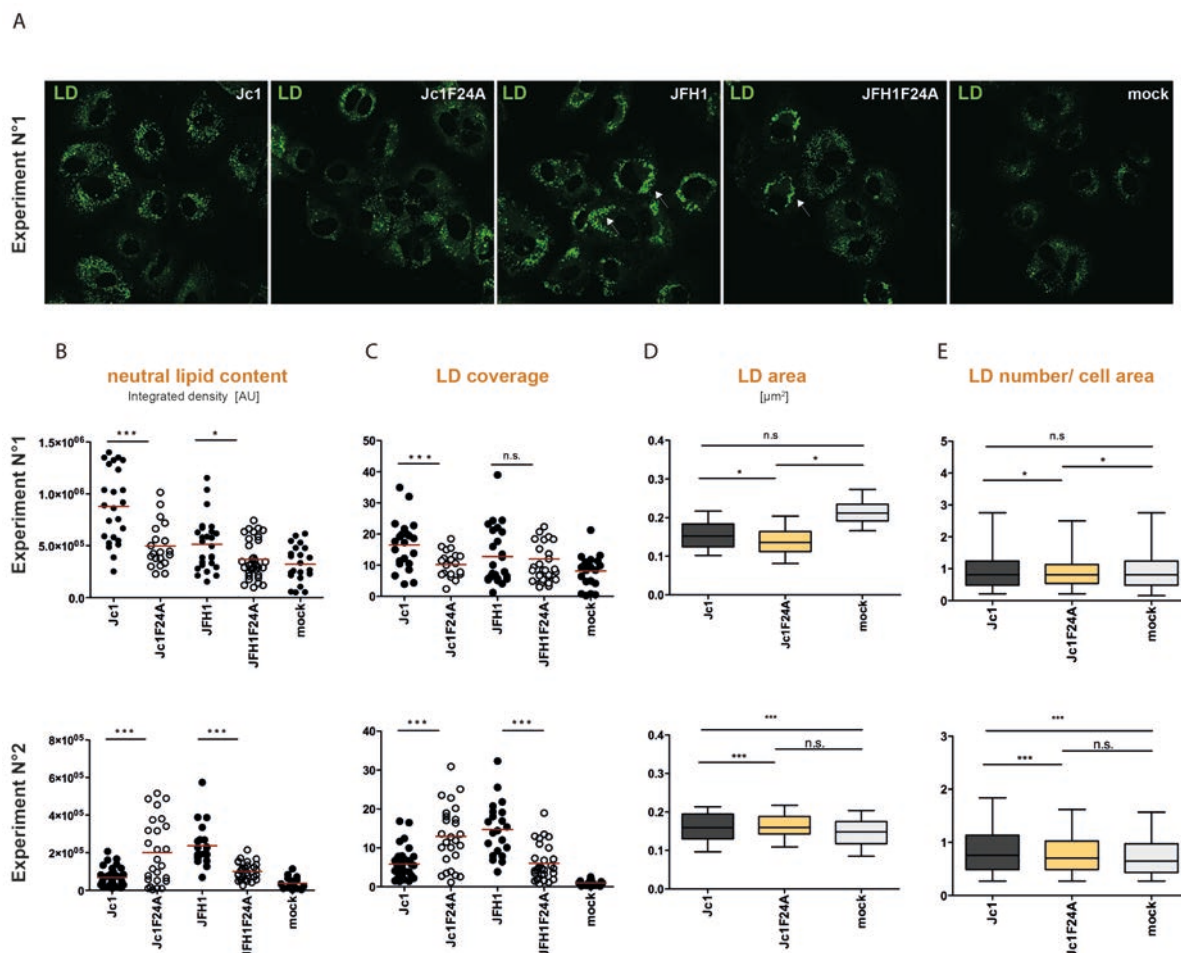


Figure 3.18 Effect of F24A core mutation on the cellular neutral lipid content. (A) Lipid droplet staining in Huh7/Lunet cells transfected with wild-type or F24A mutant virus. 72 h post viral RNA transfection cells were fixed and lipid droplets were stained with the neutral lipid stain Bodipy489/503 in addition to the labelling of the viral NS5A. Representative pictures of the lipid droplet (LD) staining are depicted. White arrows indicate LD cluster. (B-E) Quantitative analysis of LD features. Results of two independent experiments are shown. (B) The overall neutral lipid content was assessed by measuring the integrated density of the Bodipy489/503 signal intensity per NS5A positive cell. (Experiment N°1: n>20, experiment N°2 n>16, n= number of cells). (C) The LD coverage was defined as the percentage of the area of the cytoplasm covered by LDs. (experiment N°1: n>20, experiment N°2 n>16). (D) The LD area was measured per individual LD. LD area was not determined for wild-type and mutant JFH1, as in these cases the LDs were clustering and thus could not be separated efficiently. (E) The LD number was normalized to the cell area of the respective cell (experiment N°1: n>17, experiment N°2 n>16, n= number of cells). (D-E) Whisker box plot. Whiskers range from 10 to 90 percentile. (***, p< 0.001, **, p< 0.01, *, p< 0.05)

DDX3 recruitment is dispensable for its role in HCV particle production. The rather weak effect of DDX3 gene knockdown on the HCV reinfection efficiency (Figure 3.9B) and the inconsistent/ unsteady phenotype of the HCV core mutants concerning mutant core protein levels and HCV particle production (Figure 3.15 and Figure 3.17) raised the question

whether the HCV core dependent recruitment of DDX3 to LDs is of any importance to the virus, in particular to virion biogenesis.

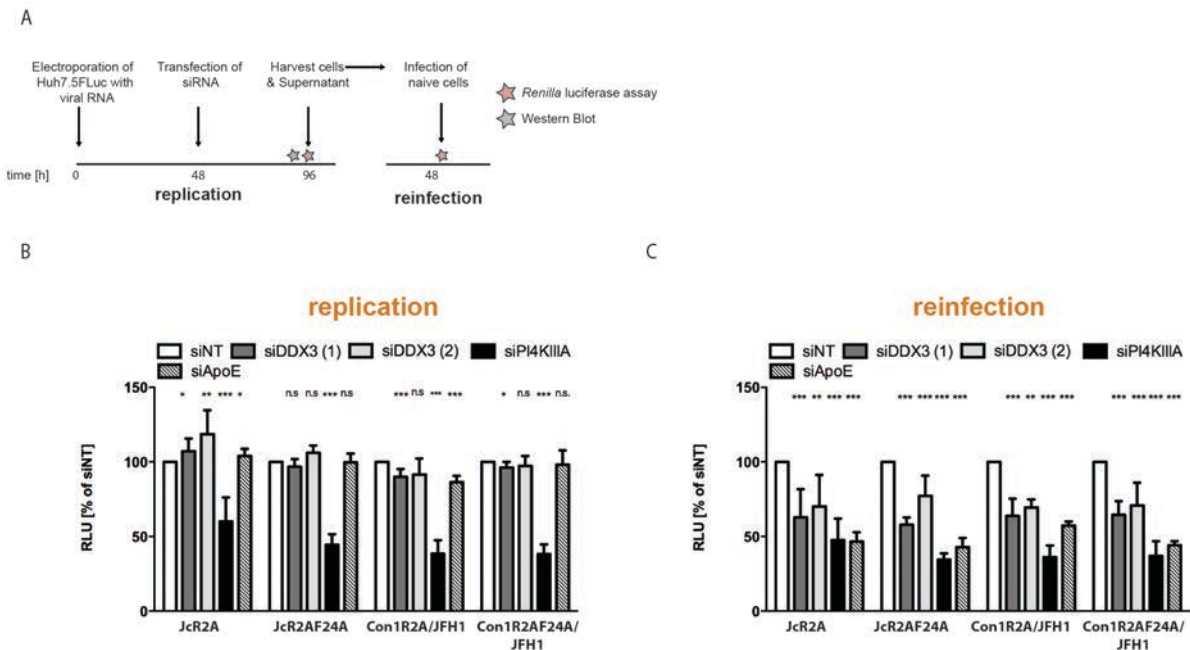


Figure 3.19 Sensitivity of *wild-type* and F24A core mutant virus towards DDX3 gene knockdown (A) Schematic representation of experimental setup. Huh7/Lunet cells were transfected with the respective viral RNA constructs. 48 h later cells were transfected with siRNA. 48 h post siRNA transfection supernatants were transferred onto naïve cells for reinfection. Viral replication efficiency was determined by measuring the *Renilla* luciferase activity in cell lysates. **(B) Viral replication efficiency of *wild-type* and F24A core mutant virus upon gene knockdown of DDX3, PI4KIII A or ApoE.** **(C) Viral reinfection efficiency of *wild-type* and F24A core mutant upon gene knockdown of DDX3, PI4KIII A or ApoE.** The mean relative light units (RLU) and standard deviation of 4 independent experiments are shown. The data is presented as percentage of the non-targeting siRNA control. (***, $p < 0.001$, **, $p < 0.01$, *, $p < 0.05$)

To tackle this question, we compared the sensitivity of mutant and wild-type virus particle production towards DDX3 gene knockdown. We argued that core mutant virus particle production should not be altered upon DDX3 silencing as compared to transfection with the non-targeting control siRNA, while wild-type virus should show an impairment of infectious particle production upon DDX3 gene knockdown. Given that in some cases the F24A mutation appeared to reduce HCV core protein levels, we focused on those mutants that exhibited protein levels comparable to the *wild-type* version, namely Jc1 and Jc1F24A as well as Con1/JFH1 and Con1F24A/JFH1. In order to circumvent potential effects of DDX3 knockdown on early events of virus entry, the viral constructs were electroporated into Huh7/Lunet cells, which were transfected with the respective siRNA 48 h later (Figure 3.19A). We observed that under these conditions the replication efficiency was reduced only upon silencing of the known HCV replication dependency factors PI4KIII A (Figure 3.19 B). Importantly, the infectious particle production of F24A mutant and *wild-type* virus was reduced to similar extent by DDX3 or ApoE knockdown (positive control) (Figure 3.19 C). This suggests that the recruitment of DDX3 to LDs by the HCV core protein is dispensable for its function in HCV particle production.

3.2 Studying the role of LTP-assisted cholesterol traffic in HCV replication

3.2.1 Distribution of unesterified cholesterol in HCV infected cells

Infection by positive-strand RNA viruses is characterized by massive rearrangements of the cellular endomembrane system, giving rise to the so-called replication organelles or replication factories [130]. HCV infection has been reported to induce ER-derived single, multi and double membrane vesicles (DMVs) [113, 265]. Appearance of the latter ones correlates with HCV RNA replication kinetics and purified DMVs were shown to be bona fide replication sites [113, 114, 266]. While the induction of DMVs is believed to be facilitated by a concerted action of viral and co-opted cellular proteins, the precise lipid composition of DMVs remains elusive. The fact that HCV RNA synthesis occurs at lipid raft-like membrane domains suggests an enrichment of specific lipid species [127, 128]. Indeed electron microscopy-based analysis of DMVs purified from HCV replicating cells indicated an important role of cholesterol as a structural component of the DMVs [114].

As part of this PhD project we aimed to unravel whether and how HCV might exploit cellular membrane homeostatic pathways in order to recruit specific lipids such as cholesterol, for the biogenesis and maintenance of viral replication organelles. Therefore we first sought to investigate whether HCV induces alterations in the distribution of cellular unesterified (free) cholesterol. To this end the distribution of unesterified cholesterol was monitored in HCV infected cells by using specific dyes and confocal microscopy analysis.

3.2.1.1 Time course analysis of the distribution of endogenous free cholesterol in HCV infected cells

Free cholesterol accumulates at the perinuclear region of HCV infected cells. The distribution of free cholesterol in HCV infected cells was visualized by using filipin III, designated as filipin, an antifungal polyene derived from streptomyces *filipinensis*. Filipin has been widely applied as a probe to study sterol partitioning in membranes as it selectively binds free, unesterified cholesterol, forming a fluorescent complex [251].

First we analyzed the cellular distribution of free cholesterol in HCV infected cells at different time points starting from 24 h post infection (Fig 3.20). Earlier time points were omitted as the low NS5A levels did not allow a specific discrimination of infected from uninfected cells. During the proceeding course of infection an accumulation of free cholesterol in the perinuclear region of the cytoplasm was observed, concomitant with a decrease of the lipid's plasma membrane localization. Importantly, the cholesterol distribution in uninfected cells

remained constant over time (Fig 3.20A). To quantify this phenomenon, we classified the HCV infected, NS5A positive cells according to the most prominent type of free cholesterol distribution either (i) being mainly at the plasma membrane (ii) being present as discrete cytoplasmic dots, presumably representing isolated vesicles or (iii) accumulating in a web-like structure at the nuclear periphery of the cytoplasm. Indeed, early in infection (24 h p.inf.) most of the free cholesterol was found at the plasma membrane or vesicular structures. Later (32 h p.inf.), the majority of the cells exhibited a prominent labeling of vesicular structures, which appeared to redistribute to a diffuse web at later times of infection (48 h. inf.). However, in uninfected cells free cholesterol was mainly found at the plasma membrane or in vesicular structures (Figure 3.20B).

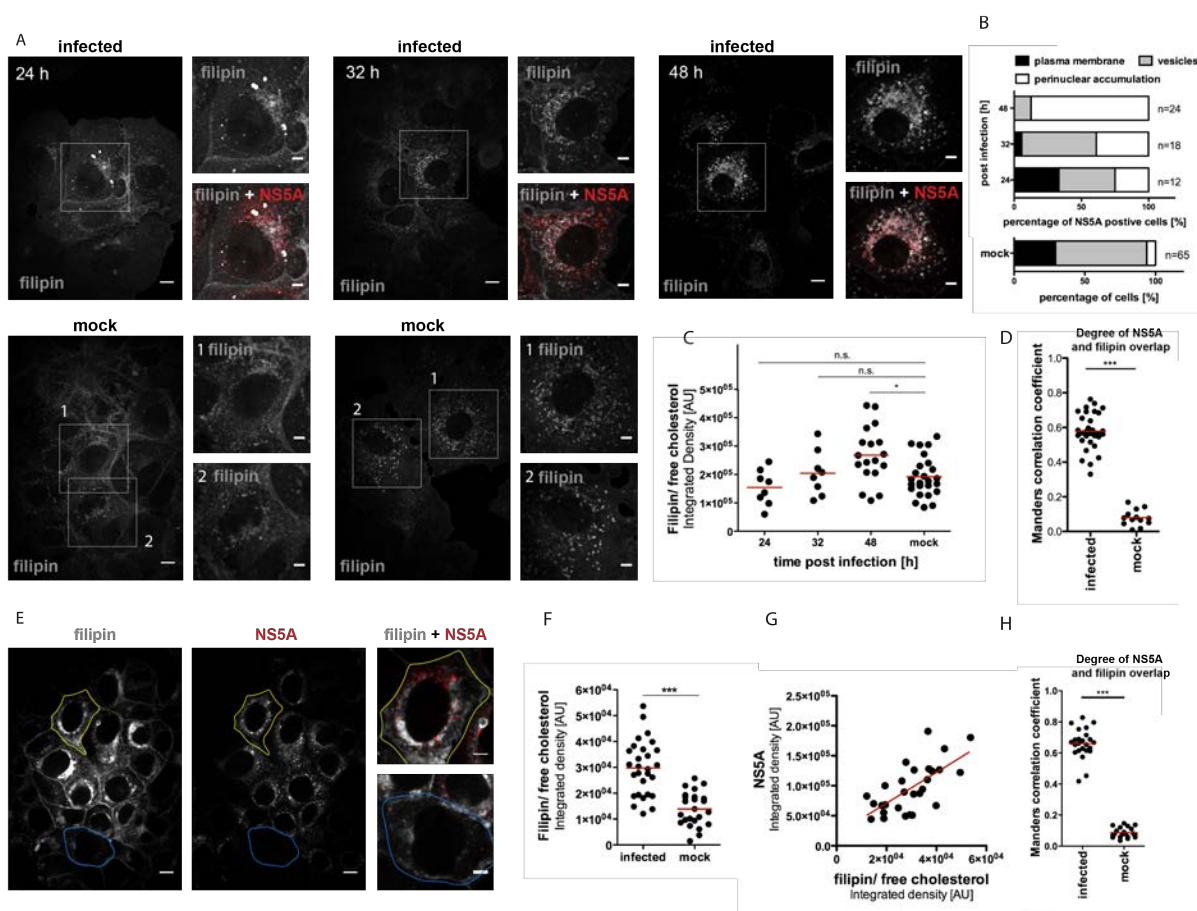


Figure 3.20 Distribution of free/ unesterified cholesterol in HCV infected and mock cells. (A) Distribution of unesterified cholesterol in HCV infected cells over time. Huh7/LunetCD81H cells were infected with Jc1 (MOI5) and fixed 24, 32 and 48 h post infection. The viral non-structural protein 5a (red) was visualized by indirect immunofluorescence. Unesterified cholesterol (grey) was labelled using the fluorescent free cholesterol marker filipin. Three representative images for each time point of infection are depicted. Two uninfected cells are shown depicting the most prominent cholesterol distribution in mock cells. The areas highlighted with white rectangles are shown as enlargement adjacent to the corresponding picture. For better visualization purposes the signal intensities were equally enhanced. Scale bars represent 10 μ m in the overview and 5 μ m in the inset pictures. (B) Classification of cells according to the most prominent cholesterol/ filipin distribution. Cells were classified according to three possible cholesterol/ filipin distributions: i) cholesterol mainly present at the PM ii) cholesterol mainly found in distinctive vesicles iii) cholesterol accumulating at the perinuclear region of the cytosol in a web-like and diffuse structure. The results of a single experiment are shown. (C) Quantification of the filipin signal 24, 32 and 48 h post infection. The integrated fluorescent density of the filipin signal in NS5A positive or negative cells was measured. 7-25 cells of a single experiment were analyzed. (D) Quantification of the degree of NS5A and filipin signal overlap 48 h post infection. The degree of colocalization of NS5A and filipin was determined by measuring the Manders correlation coefficient. At least 20 cells of a single experiment were analyzed. (E) Distribution of free cholesterol at late time points of infection. Huh7/LunetCD81H cells were infected with Jc1 (MOI5) for 72 h. Cells

were fixed and processed for fluorescence microscopy. The yellow border indicates a NS5A positive, whereas the blue border marks a NS5A negative cell. Both regions of interests are shown in the adjacent blow-up. Scale bars represent 10 μm in the overview and 5 μm in the inset pictures. **(F)** *Degree of intracellular filipin accumulation.* Integrated fluorescent density of filipin was measured in more than 20 NS5A positive or negative cells. **(G)** *Correlation of integrated fluorescent density of filipin and NS5A.* The NS5A signal intensity is plotted against the respective filipin signal intensity determined in individual cells. More than 20 cells of a single experiment were analyzed. The red line indicates a linear regression of all data points (R-square: 0.45). **(H)** *Quantification of the degree of NS5A and filipin signal overlap 72 h post infection.* The degree of signal overlap was determined by measuring the Manders correlation coefficient. Results of more than 20 cells of a single experiment are shown. (***, $p < 0.001$, **, $p < 0.01$, *, $p < 0.05$)

In order to judge the HCV-induced intracellular cholesterol accumulation, we further quantified the signal intensity of filipin at the perinuclear region of the cytoplasm over time. With progressing infection (48 h and 72 h p.inf.) the measured signal intensities were significantly increased in infected as compared to mock cells. (Figure 3.20C, E, F). Interestingly, we additionally observed a (although weak) positive correlation of NS5A and filipin signal intensities at the single cell level (i.e. the higher the abundance of NS5A the stronger the intensity of filipin) (Figure 3.20G). Furthermore to estimate the subcellular localization of free cholesterol with respect to NS5A, used as potential marker for viral replication sites [113, 114], we measured the degree of both signals 48 and 72 h post infection. This analysis showed that NS5A and filipin partially colocalized, as determined by the Manders correlation coefficient (Figure 3.20 D, H). Taken together HCV infection resulted in the recruitment of unesterified cholesterol to the perinuclear region of the cytoplasm where also the viral replicase protein NS5A localized. These results suggest a biological link between HCV replication and the distribution of free cholesterol in infected cells.

3.2.1.2 Studying the fate of plasma membrane derived free cholesterol at early and late stages of HCV replication by live cell imaging

Our and previous studies suggest that HCV induces changes in the cellular cholesterol distribution potentially aiding the establishment or maintenance of the DMVs, the putative sites of RNA replication [79, 114]. However, neither the source of the lipid nor the molecular mechanisms underlying the cellular cholesterol redistribution have been fully elucidated yet. Cholesterol could possibly be recruited from the plasma membrane (PM), the cellular site where the majority of unesterified cholesterol resides [162]. Indeed our previous results suggest a relocation of plasma membrane localized cholesterol to the perinuclear region (Fig 3.20). To further corroborate this, we next aimed at visualizing the dynamics of plasma membrane cholesterol in HCV replicating cells, using live cell imaging.

3.2.1.3 Setting up the conditions for live cell imaging of Topfluor-Cholesterol (TFC) dynamics

Plasma membrane (PM) derived TFC is redistributed in HCV replicating cells. In order to study the fate of PM derived cholesterol we made use of commercially available fluorescently tagged cholesterol, which exhibits a Bodipy moiety attached to its alkyl side chain, designated Topfluor-Cholesterol (TFC) (Figure 3.21A). While the introduction of fluorescent tags into proteins and into the even smaller lipids can greatly change their properties, TFC has been described to closely mimic the distribution and traffic of unesterified cholesterol [267, 268]. TFC has been reported to prominently label the plasma membrane early after TFC addition and being subsequently distributed to vesicular structures, suggested to be endosomes [267].

In a first set of experiments we determined the distribution pattern of TFC in fixed cells (Figure 3.21B). To this end Huh7.5 cells were pulsed with 4 μ M TFC for 10 min, followed by extensive washing with fresh media and fixed at different time points after TFC addition. In order to address the distribution of TFC we imaged the whole cell volume taking several z-stacks. 10 min after pulsing, TFC was readily found in dot-like structures and labeled the cytosol (Figure 3.21B, first panel). With proceeding time, TFC increasingly labeled distinct spots, presumably representing vesicular structures such as endosomes (Figure 3.21B, white arrows). After 1 h of incubation, TFC became apparent at the perinuclear region of the cytoplasm in a Golgi- or ER-like pattern and additionally detected as clear, bright round structures of 1- 1.2 μ m diameter, possibly being lipid droplets (Figure 3.21B, orange and yellow arrows respectively). In order to visualize the previously described integration of TFC into the PM shortly after its addition [267] we analyzed the TFC distribution at earlier time points. Indeed, 5 min post TFC addition, TFC was found at the plasma membrane but also labeled the perinuclear region of the cytoplasm (Figure 3.21C). In summary, in line with an earlier report we observed that TFC was integrated into the plasma membrane from which it was rapidly distributed into vesicular structures as well as to the perinuclear region of the cytoplasm and thus potentially to the ER/ Golgi. TFC might further become esterified and incorporated into lipid droplets [267]. This suggests that TFC mimics the distribution of endogenous (mostly unesterified) cholesterol and hence, represents a useful tool to monitor the dynamics of plasma membrane derived cholesterol in live cell imaging.

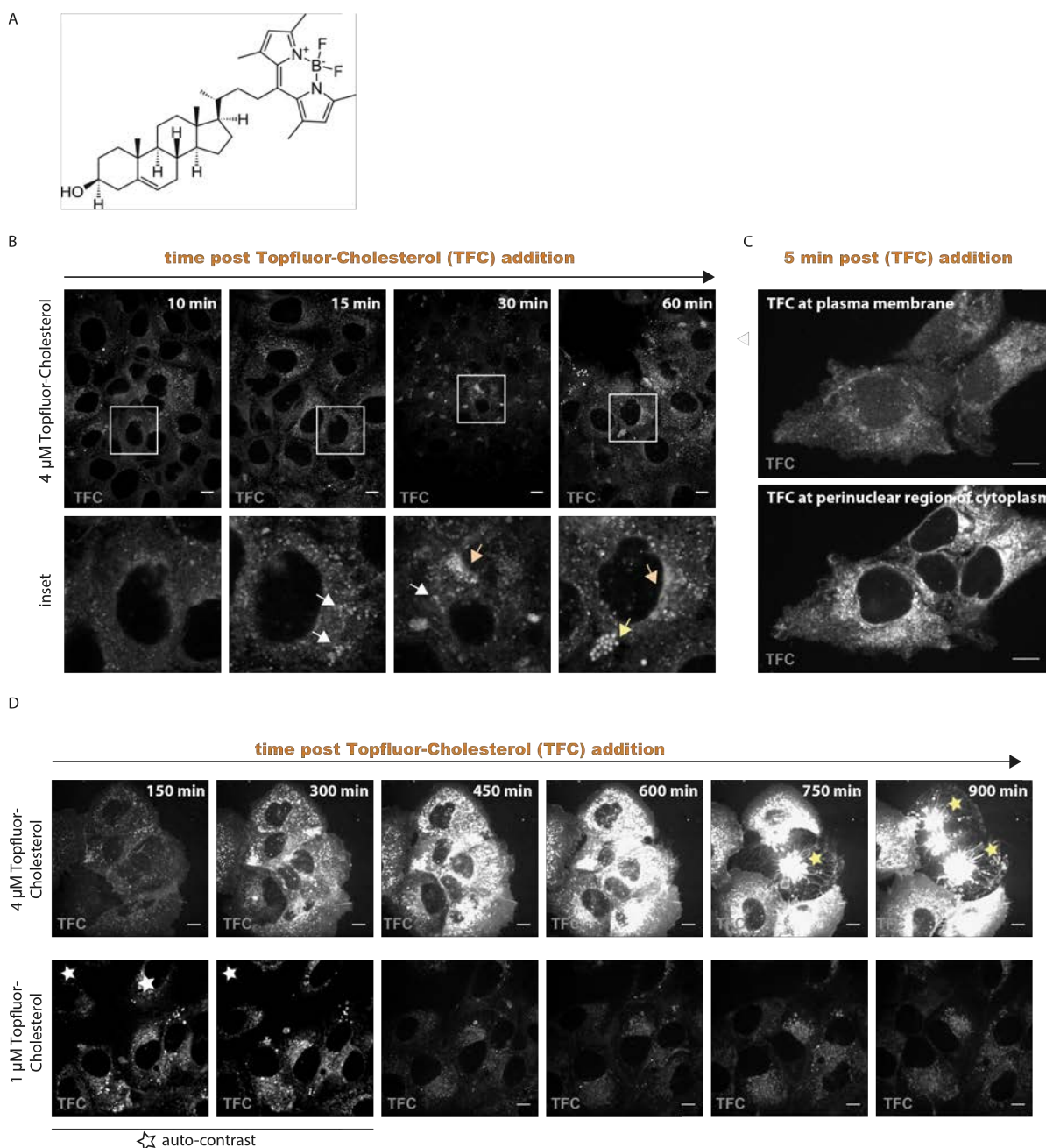


Figure 3.21 Pretests for Topfluor-Cholesterol (TFC) live cell imaging. **(A)** Chemical structure of Topfluor-Cholesterol (Avanti Polar lipids). **(B)** Naïve Huh7.5 cells were pulsed with 4 μM TFC for 10 min, followed by extensive washing with fresh media. Cells were fixed 10, 15, 30 or 60 min after TFC addition and the TFC localization was analyzed by confocal microscopy. Enlargements of the areas highlighted with a white rectangle are shown below. White arrows point to TFC in vesicular structures, the yellow arrow labels TFC in potential lipid droplets. Orange arrows indicate a juxtannuclear localization of TFC. Scale bars represent 10 μm . **(C)** Naïve Huh7.5 cells were pulsed for 5 min with 2.3 μM TFC and cells were fixed 5 min later. Two pictures of the same cell are shown. The upper panel depicts TFC at the plasma membrane, the lower panel the intracellular accumulation of TFC. Scale bars represent 10 μm . **(D)** LunetCD81H cells stably expressing core to NS2 transfected with the subgenomic replicon were pulsed for 10 min with either 1 or 4 μM TFC respectively, followed by extensive washouts with fresh imaging media. TFC dynamics was imaged live; thus every 15 min the cells were imaged taking 3 sequential z-stacks. Only a single stack is shown in the figure. The yellow asterisk indicates dead cells. Note that for the two pictures labeled with a white asterisk the signal was enhanced by auto-contrast. Scale bars represent 10 μm .

With the aim to visualize cholesterol dynamics throughout the full infection cycle of HCV, we took advantage of the trans-complementation system that is based on the ability to split the viral genome which allows the reconstitution of a full infectious cycle under biosafety level 2

conditions [98]. To this end Huh7/LunetCD81H helper cells expressing the viral proteins core to NS2 (core, E1, E2, p7, NS2) were transfected with the subgenomic replicon containing a fluorescent protein (mCherry) tagged NS5A. Providing the structural proteins *in trans* allows infectious virus-like particle production, which however, only support a single round infection and are incapable to spread [98].

We first performed long-term live cell imaging in HCV replicating Huh7/LunetCD81H_core-NS2 cells to monitor the distribution of exogenous cholesterol using TFC. Huh7/LunetCD81H_core-NS2 helper cells were incubated with either 1 or 4 μM of TFC for 10 min. The excessive TFC was removed by extensive washing with fresh imaging media. While using the higher concentration of 4 μM allowed an efficient detection of the weak TFC signal at early time points, the fluorescent signal was readily saturated after 300 min of imaging. Further high amounts of TFC seemed to be cytotoxic (Fig 3.21D, upper panel). In contrast pulsing cells for 10 min with 1 μM TFC, followed by extensive washing with fresh media, did not affect cell viability and allowed the detection of the fluorescently labeled lipid throughout the entire imaging period up to 15 h (Figure 3.21D, lower panel).

3.2.1.4 Studying Topfluor-Cholesterol dynamics early and late in HCV replication

With the aim to understand whether HCV infection alters the subcellular distribution of free cholesterol pools of the plasma membrane, we studied the time-dependent distribution of TFC in HCV replicating cells. LunetCD81H_core-NS2 cells, transfected with the subgenomic replicon, were pulsed with 1 μM of TFC for 10 min, followed by extensive washing. The distribution of fluorescently labeled cholesterol as well as of mCherry tagged NS5A was monitored over 17 h. Therefore images were acquired every 15 min with 3 sequential z-stacks to cover the entire cell volume. To further elucidate whether HCV utilizes cholesterol differently at early as compared to late stages of viral replication, cells were pulsed with TFC at either 30 h (“early” setup) or 53 h (“late” setup) post electroporation respectively (Figure 3.22A, B). Earlier time points were not studied since the low NS5A signal did neither allow adequate imaging nor the discrimination between transfected and mock cells. Upon measuring of the NS5A signal intensity over time we observed a time-dependent increase in NS5A fluorescence intensity reflecting the increase in HCV RNA replication in the “early” setup, while the NS5A signal remained constant at later time points suggesting a steady state of viral replication (Figure 3.22C).

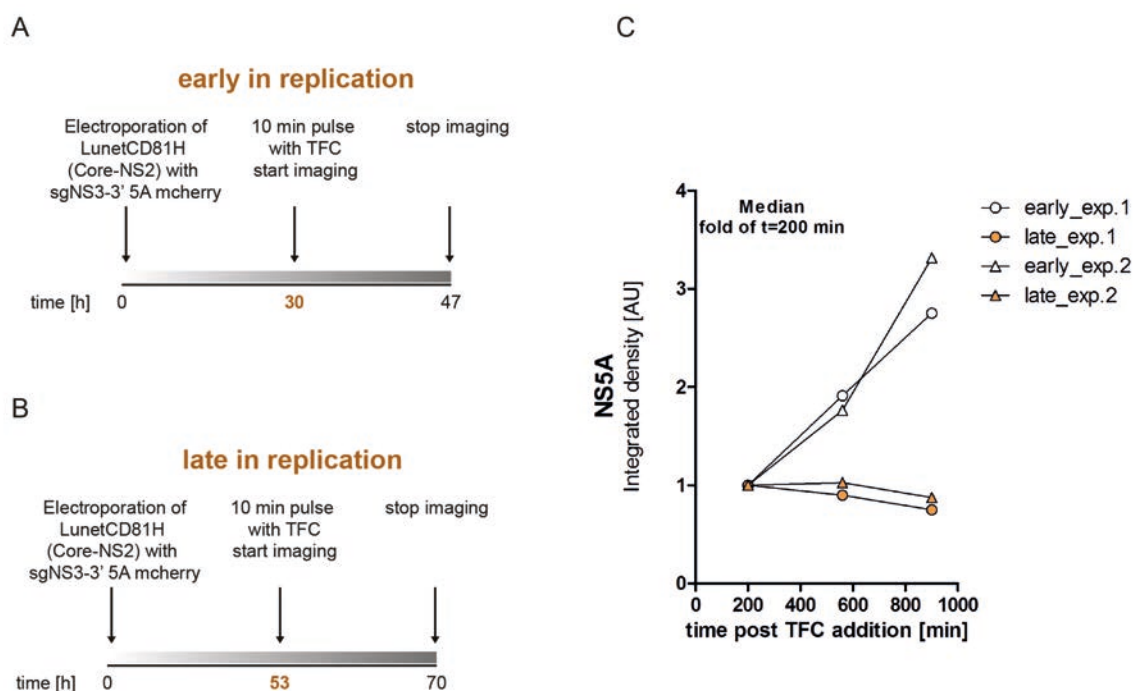


Figure 3.22 Experimental setup of live cell imaging of Topfluor-Cholesterol (TFC) added early or late in HCV replication. (A-B) Huh7/LunetCD81H cells expressing the viral proteins core to NS2 were transfected with *in vitro* transcripts of a subgenomic replicon containing mCherry tagged NS5A (sgNS3-3' 5Amcherry, gt2a). (A, early) 30 h or (B, late) 53 h later, cells were pulsed with 1 μ M TFC for 10 min, followed by extensive washing. TFC distribution was imaged every 15 min for 17 h. (C) NS5A signal intensity over time, early or late in replication. The results of two independent experiments are shown. The median of the analysis of at least 8 cells per experiment is shown and is presented as fold of the value of the earliest time point of measurement (t=200 min).

TFC accumulates in the perinuclear region of the cytoplasm of HCV replicating cells.

First we analyzed the overall dynamics of TFC within 17 h of imaging (Figure 3.23). To this point the TFC distribution in NS5A positive cells, designated as HCV positive, as well as NS5A negative cells, designated as HCV negative/ mock cells, was analyzed at three different time points. Note that these “mock” cells do stably express the viral proteins core to NS2. In agreement with our previous results, TFC accumulated in the perinuclear region of the cytoplasm of HCV positive cells when either added early or late in replication (Figure 3.23A, B). Comparing the fluorescent lipid’s distribution it appeared that upon its addition late in replication TFC was present in a more diffuse pattern around the nucleus, whereas early in replication it labeled more distinctive structures (Figure 3.23A, B, number 2 and 3). In mock cells TFC appeared to be more dispersed in vesicular structures throughout the cytosol (Figure 3.23A, B number 1).

We next aimed at determining whether there are differences in the extent of TFC accumulation at the perinuclear region when comparing “mock” to HCV replicating cells, similar to what was observed earlier for endogenous free cholesterol (Figure 3.20). To this end we measured the TFC recruitment velocity, which we defined as the TFC signal intensity at the perinuclear region of the cytoplasm in NS5A positive or mock cells over time.

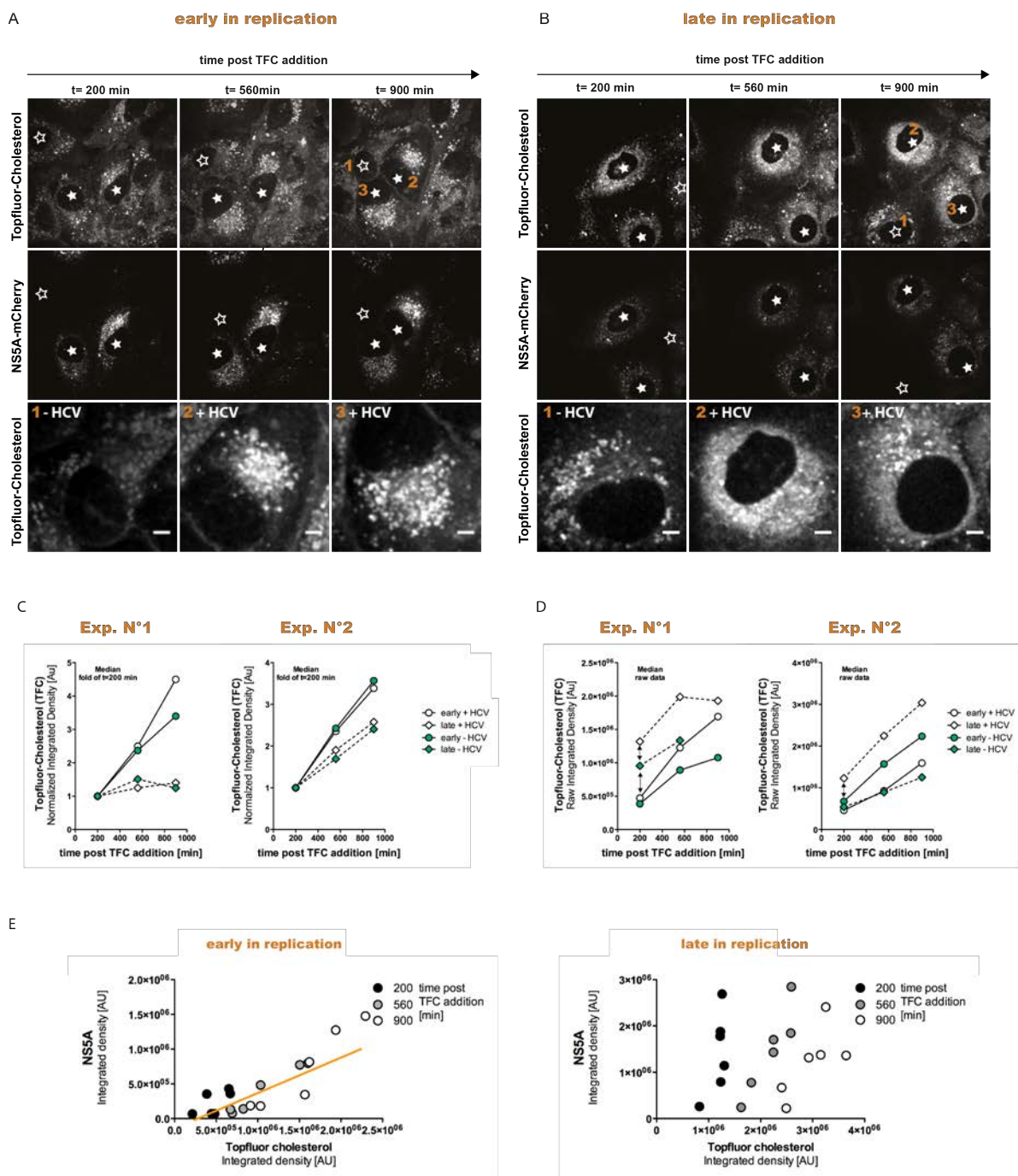


Figure 3.23 Topfluor-Cholesterol (TFC) dynamics at early and late stages of HCV replication. (A-B) TFC distribution over time in cells pulsed with TFC either (A) early or (B) late in replication. The TFC and NS5A distribution in Huh7/Lunet_Core-NS2 cells either transfected with (+HCV, filled stars) or without (-HCV, empty stars) the subgenomic replicon (containing mCherry tagged NS5A) is shown in the upper and middle panels. The distribution of NS5A and TFC is shown in representative pictures at three different time points post TFC addition. Enlargements of the cells indicated by the yellow number are presented in the lowest panel. Scale bars represent 5 μm . (C) TFC recruitment velocity of cells pulsed early (circle) or late (rectangle) in replication. TFC signal intensities at the perinuclear region were measured over time in HCV replicating or mock cells (white and green symbols respectively). Two independent experiments are shown. The median of at least 6 cells per experiment is shown. The presented values were normalized to the value measured at the earliest time point (t=200 min). (D) Raw TFC signal intensities. The median of at least 6 cells per experiment is depicted. The results of two independent experiments (presented in C) are shown. (E) Correlation of TFC and NS5A signal intensity at the perinuclear region as determined in individual cells pulsed with TFC early or late in replication. Each dot represents the intensity measurements of a single cell at a specific time. One representative result of three independent experiments is shown. R-square: 0.7792.

There was no apparent difference in the rate of TFC accumulation between mock and HCV replicating cells. Yet, TFC was accumulating faster in HCV replicating and mock cells, when added 30 h post electroporation as compared to later time points (Figure 3.23C). Given the equal TFC accumulation velocity of HCV replicating and of mock cells, the observed difference in TFC incorporation at early as compared to late time points of replication might be due to an altered behavior of the cells throughout the course of the experiment. We further analyzed the correlation of NS5A and TFC signal intensities. Indeed there was a slight time-dependent increase of TFC intensity, which further correlated positively with an increase in NS5A signal intensity when TFC was added early in replication (Figure 3.23E). Given our previous results indicating a fast uptake and redistribution of TFC within the first hour after TFC addition (Figure 3.21B, C), we wondered whether changes in TFC dynamics are controlled by fast feed-back regulation and thus of short duration. Hence potential differences in the uptake velocity between HCV replicating and mock cells might have been missed in our present analysis. Indeed when comparing the raw TFC signal intensities in HCV replicating cells it became apparent that they were slightly elevated as compared to mock cells. In particular when TFC was added late in replication the TFC signal was enhanced already at the earliest time point of measurement as compared to the mock control as well as compared to cells in the early phase of replication (Figure 3.23D). Therefore we analyzed the time-dependent lipid uptake starting from the earliest time point possible. Given the used experimental limitations the detection of TFC was possible starting from 75 min post pulse. Hence the TFC accumulation velocity was determined by measuring the lipids intracellular fluorescence intensity over time starting from 75 min post addition (Figure 3.24). In agreement with our previous analysis, TFC accumulated in either vesicular structures (Figure 3.24A, 2+HCV) or a more diffuse pattern (Figure 3.24B, 2+HCV) around the nucleus in HCV replicating cells. Again, TFC was of lower intensity and appeared more evenly distributed in vesicular structures throughout the cytosol in mock cells (Figure 3.24A, B 1-HCV). When we analyzed the rate of intracellular TFC accumulation no reproducible difference between mock and HCV replicating cells was observed (Figure 3.24C). However similar to our previous analysis, we observed that the TFC raw signal intensities were elevated (already 75 min post TFC addition) when cells were pulsed late in HCV replication, as compared to the respective control condition (Figure 3.25D). This could indicate that even earlier time points need to be analyzed.

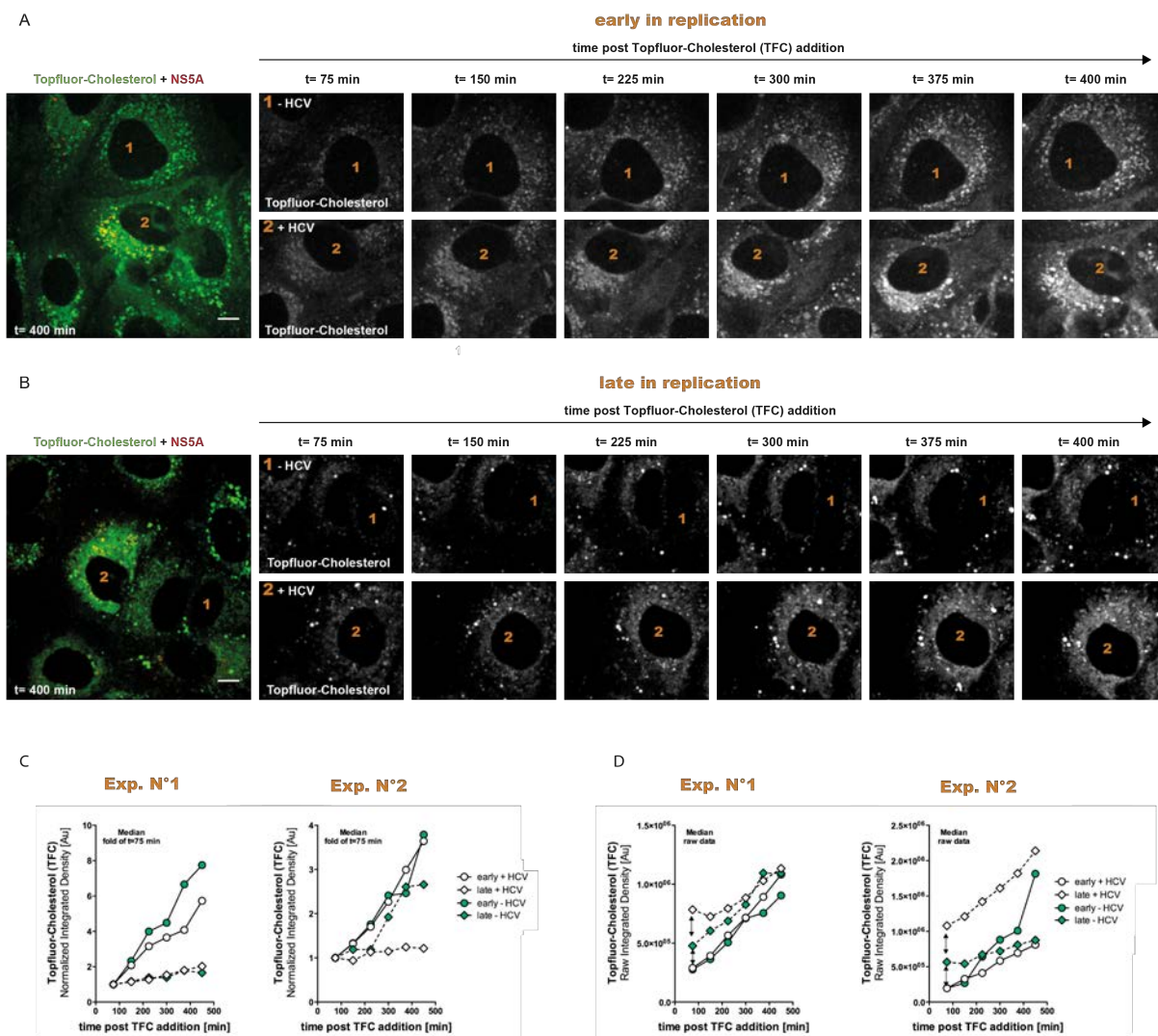


Figure 3.24 Topfluor-Cholesterol (TFC) dynamics in the early phase upon TFC addition at early or late stages of HCV replication. (A-B) TFC distribution over time in cells pulsed with TFC either (A) early or (B) late in replication. The TFC and NS5A distribution in Huh7/Lunet_Core-NS2 cells either transfected with (+HCV, lower panels) or without (-HCV, upper panels) the subgenomic replicon (containing mCherry tagged NS5A) is shown. Scale bars represent 10 μ m. (C) TFC recruitment velocity of cells pulsed early (circle) or late (rectangle) in replication. TFC signal intensities at the perinuclear region were measured over time in HCV replicating or mock cells (white and green circles respectively). Two independent experiments are shown. The median of at least 6 cells per experiment is shown. The median is presented as fold of the value at the earliest time point of measurement (t= 75 min). (D) Raw values of TFC signal intensities. The results of two independent experiments (presented in C) are shown. The median of at least 6 cells per experiment is shown.

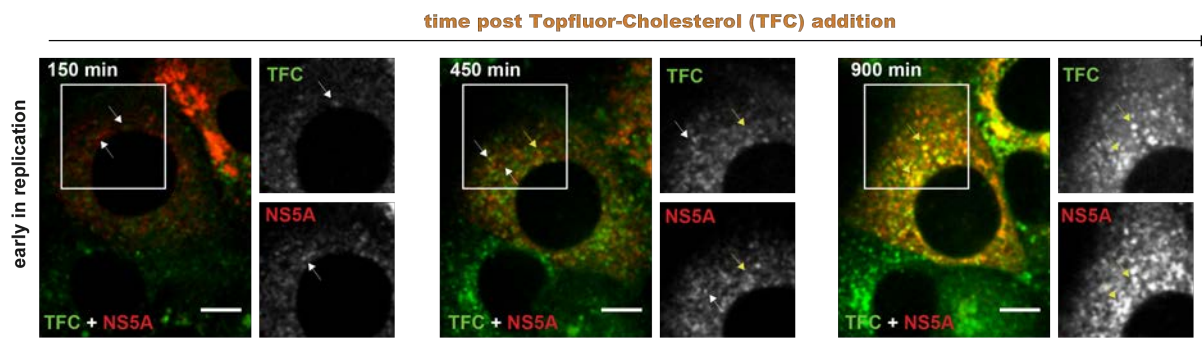
Taken together, exogenously added cholesterol as determined here for TFC is efficiently trafficked to the nuclear periphery of the cytoplasm in HCV replicating cells. While under the given experimental setup, the overall accumulation velocity was found to be similar in presence or absence of viral replication, the fluorescent lipid's distribution pattern appeared different, with TFC clustering at the perinuclear region of the cytoplasm in HCV replicating cells as compared to a more dispersed vesicular TFC pattern in mock cells. In addition, when TFC was added late in HCV replication, intracellular TFC levels were higher in HCV replicating cells as compared to mock cells.

3.2.1.5 Analysis of TFC recruitment to HCV replication sites

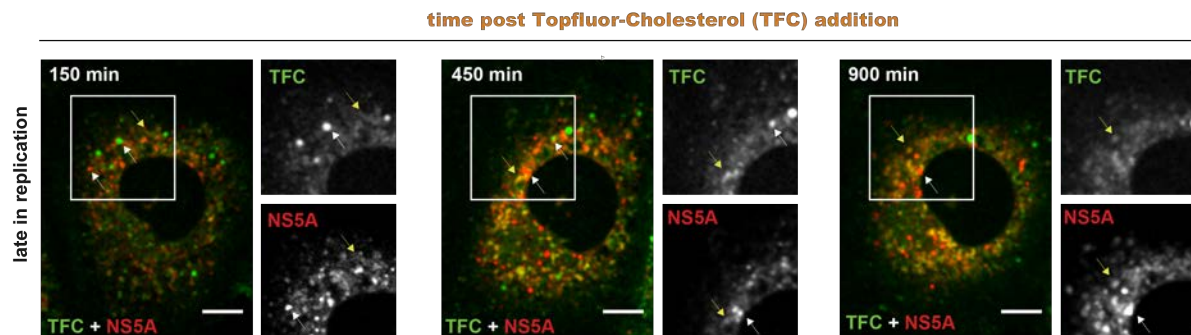
TFC is trafficked to NS5A positive sites. Given the fact that HCV replication appears to trigger the accumulation of plasma membrane derived cholesterol at the perinuclear region, we examined whether TFC could be found at sites of viral replication. For this purpose we analyzed the co-traffic of TFC with NS5A, a multifunctional viral protein involved in RNA replication and particle production [74, 77, 81]. NS5A has so far been the only non-structural protein that tolerates the insertion of a fluorescent tag while retaining replication competence of subgenomic replicons [73]. In Live-cells, NS5A has been described to form large immobile structures with a diameter up to several microns, preferentially found at the perinuclear region of the cytoplasm, which might represent the viral replication complexes. Besides, small vesicular structures scattered throughout the cytosol that exhibit fast saltatory movement were observed [73, 269]. Indeed NS5A was found in puncta but also exhibited a diffuse web-like distribution at the perinuclear region of the cytoplasm (Figure 3.25A, B, NS5A insets, white arrows). Shortly upon addition of TFC early in replication, the fluorescent lipid was present in small puncta with no apparent colocalization with NS5A (Figure 3.25A, first panel “150 min”, TFC inset, white arrows). With proceeding time, TFC accumulated in a diffuse structure and also distinct spots at the perinuclear region, where it partially colocalized with NS5A. (Figure 3.25A, yellow arrows). When cells were incubated with TFC at late time points of infection, the fluorescent lipid was mainly recovered in a diffuse web, where it partially colocalized with NS5A (Figure 3.25B, yellow arrows). Additionally TFC was found in clear round structures, possibly lipid droplets (Figure 3.25B, white arrows). We further quantified the degree of overlap of both signals over time. In line with our previous observations that indicate a recruitment of endogenous cholesterol to NS5A positive sites at the perinuclear region upon HCV infection, the colocalization of NS5A and exogenously added TFC was increasing over time (Figure 3.25C). The degree of signal overlap was generally higher at late stages of replication (Figure 3.25D).

Taken together, our results point to a recruitment of plasma membrane derived cholesterol to the perinuclear region of the cytoplasm in HCV-infected cells, where in a time-dependent manner TFC recruitment to NS5A positive structures is observed.

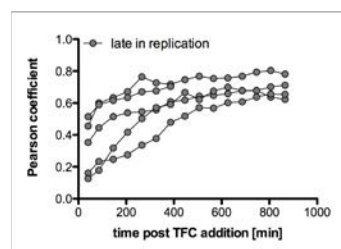
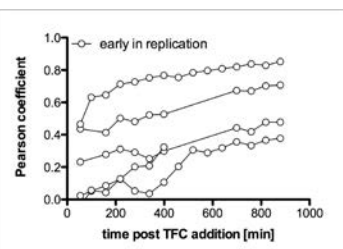
A



B



C



D

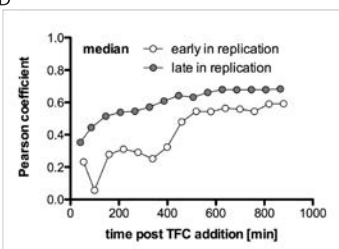


Figure 3.25 Topfluor-Cholesterol (TFC) and NS5Amcherry trafficking over time. (A-B) TFC and NS5A distribution in HCV replicating cells after TFC addition (A) early or (B) late in replication. Huh7/LunetCD81H cells expressing the viral core to NS2 proteins were electroporated with the subgenomic replicon harboring mCherry tagged NS5A. The localization of NS5AmCherry and TFC upon TFC addition either (A) early or (B) late in replication was imaged over time. Representative pictures of three different time points are shown. The white rectangle marks the area for which insets of NS5A or TFC are depicted adjacently. White arrows point to either TFC or NS5A structures that do not overlap, whereas yellow arrows indicate structures that are TFC and NS5A positive. Scale bars represent 10 μ m. For visualization purposes the intensity of the signals was adjusted. (C) Degree of NS5A and TFC signal overlap. The Pearson correlation coefficient (PCC) of NS5A and filipin was determined as a measure of the degree of signal overlap over time. 4-5 cells of a single experiment were analyzed. (D) Median of the PCCs presented in C.

3.2.1.6 Recovery of Topfluor-Cholesterol from HCV replication organelles

TFC is recovered from NS4B-HA purified membrane fractions. Given the colocalization of endogenous but also exogenous Topfluor-Cholesterol with the HCV non-structural protein 5A we wondered, whether PM derived cholesterol would be targeted to DMVs, the presumed sites of RNA replication. In order to investigate this further, we made use of a method which is based on the Hemagglutinin (HA)-specific affinity purification of NS4B containing membranes from cells stably replicating a (gt2a) replicon that harbours a HA-affinity tagged

NS4B. These purified membranes have been shown to be predominantly DMVs, to contain viral proteins such as NS3 and NS5A and to harbor enzymatically active viral replicase. Taken together this method represents a powerful tool to isolate and study the biochemical composition of HCV induced DMVs [114].

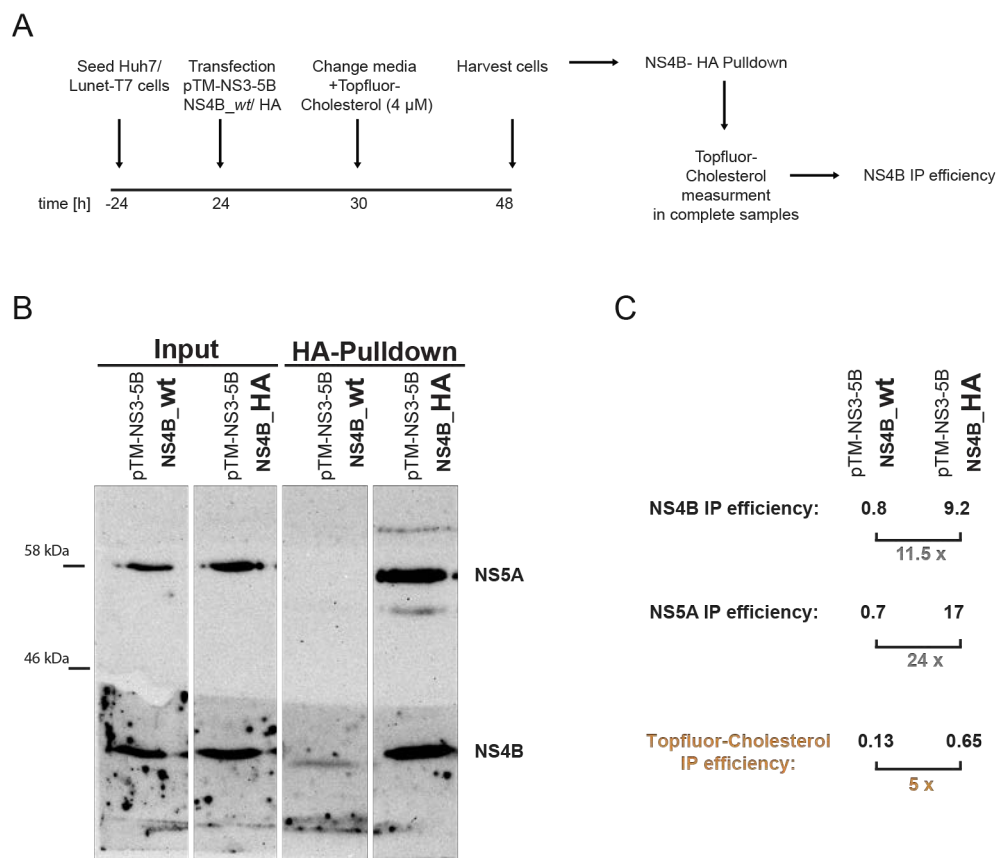


Figure 3.26 Topfluor-Cholesterol (TFC) recovery from NS4B-HA mediated DMV purification. (A) Schematic representation of the experimental setup. Huh7/Lunet-T7 cells were transfected with pTM-NS3-5B expression constructs containing the *wild-type* or HA tagged NS4B. 6 h later, the medium was replaced by fresh media containing 4 μ M TFC, followed by 18 h of incubation. Cells were lysed and subjected to NS4B-HA Immunoprecipitation [114]. (B) Western Blot showing the NS5A and NS4B protein levels in the input as well as the HA-IP samples of the respective transfection condition (pTM-NS3-5B NS4B *wt*/ HA). 2.5% of the input and half of the IP samples were loaded for subsequent protein detection. (C) The NS4B, NS5A as well as TFC IP efficiencies are shown. TFC was measured in each sample using the Mithras Plate Luminometer (Berthold Technologies). Next, samples were subjected for Western Blot shown in (B). The NS4B pulldown efficiency was determined by calculating the fraction of the immunoprecipitated NS4B protein of the protein's input levels. The TFC pulldown efficiency was determined accordingly. The grey or orange numbers present the enrichment of NS4B, NS5A or TFC in the HA-NS4B as compared to the NS4B-*wt* sample respectively. One single experiment is shown.

In a pilot experiment Huh7/Lunet-T7 cells were transfected with the pTM-NS3-5B expression constructs that do or do not contain a HA tagged version of NS4B (Figure 3.26A). It is important to note that expression of the non-structural proteins NS3-5B has been shown to induce DMV formation in a similar fashion as compared to the DMVs found in HCV infected cells [113]. Cells were then incubated for 18 h with TFC, followed by HA-specific pulldown under native, membrane-preserving conditions. In cells transfected with the HA-NS4B containing expression construct, the HA-specific pulldown led to a 24- or 11.5- fold enrichment of NS5A or NS4B protein levels respectively, as compared to the technical

negative control (NS4B *wild-type*) (Figure 3.26B, C, grey numbers). Concomitantly, a 5-fold enrichment was observed for TFC, demonstrating the recruitment of exogenously supplied cholesterol to NS4B-containing membrane fractions (Figure 3.26C, orange number).

Hence our data suggests that the cholesterol found in HCV-induced DMVs [114] is recruited both via mobilization of cholesterol from the PM and by incorporation of extracellular cholesterol. In either case, intracellular trafficking of cholesterol is required.

3.2.2 Identification of important Lipid transfer proteins (LTPs) required for the HCV and DENV replication cycle

Our results indicate that HCV alters the cellular distribution of cholesterol and moreover causes an enrichment of this lipid at the juxtannuclear region of the cytoplasm and at NS5A positive sites, likely representing viral replication sites. Due to the hydrophobic nature of cholesterol its spontaneous exchange between membranes through the aqueous cytoplasm is slow and inefficient [168]. Thus, in cells, transport of cholesterol is conducted by a combined action of vesicular and non-vesicular mechanisms. The latter ones involve the action of cytosolic lipid transfer proteins (LTPs) harboring structurally encoded targeting information, such as pleckstrin homology domains, that drive their localization to distinct intracellular membranes [168, 217] (see 1.6).

We next aimed at identifying cellular proteins including LTPs that could allow the virus to specifically recruit cholesterol to sites of RNA replication. To investigate this further we focused on a selection of members of several protein families implicated in direct non-vesicular lipid transfer between intracellular membranes. These comprise the members of the oxysterol-binding protein (OSBP)-like protein (ORP/OSBPL) family and of the steroidogenic acute regulatory protein-related lipid transfer (START) domain family, both implicated in non-vesicular sterol and/or phospholipid transport [185, 186]. Further, the Niemann-Pick Disease Type C1 and C2 protein (NPC1, NPC2) were targeted, because they facilitate the egress of LDL-derived free cholesterol from late endosomal compartments [207]. Additional candidates comprised the ATP-binding cassette subfamily A member 1 (ABCA1), a protein involved in cellular cholesterol efflux [224], the membrane associated phosphatidylinositol transfer protein 1 (PITPNM1) acting at the Golgi/ ER interface [183], as well as the four-phosphate adapter protein 2 (FAPP2/PLEKHA8) [270]. More detailed information on the cellular targets is presented in Table 3.1.

Table 3.1 LTPs targeted in the RNAi screen

Gene ID	Gene product	Suggested cellular function regarding cellular lipid metabolism	Cellular localization
19	ABCA1 - ATP- binding cassette, subfamily A (ABCA) member 1	involved in cellular sterol mobilization from LY, regulates egress of cholesterol through lipoproteins [224]	PM, LE, LY
10087	COL4A3BP - collagen, type IV, alpha binding protein	transcript variant CERT is involved in ceramide transfer between ER and golgi [180]	golgi, ER
4864	NPC1- Niemann - Pick disease, type C1	catalyzes in a concerted action with NPC2 the egress of unesterified cholesterol from LE/LY [207]	LE, LY
10577	NPC2- Niemann - Pick disease, type C2	catalyzes in a concerted action with NPC1 the egress of unesterified cholesterol from LE/LY [207]	LE, LY
5007	OSBP - oxsterol binding protein	potentially involved in transfer of sterol and PI4P between ER and golgi [182]	golgi, ER
114876	OSBPL1A - oxysterol binding protein-like 1A/1B	OSBPL1A is cytosolic, OSBPL1B present at late endosomes where it regulates their intracellular positioning depending on their cholesterol content [188]	LE, cytosolic
9885	OSBPL2 - oxysterol binding protein-like 2	involved in the transport of cholesterol from the PM to the ER and LD, regulator of neutral lipid metabolism [272, 273]	golgi LD
26031	OSBPL3 - oxysterol binding protein-like 3	involved in the communication between PM and ER [274]	PM, ER
114879	OSBPL5 - oxysterol binding protein-like 5	involved in the exit of unesterified cholesterol from late endosomes/ lysosomes [190]	ER
114880	OSBPL6 - oxysterol binding protein-like 6	potentially involved in sterol transfer between PM and ER [278]	PM, ER
114883	OSBPL9 - oxysterol binding protein-like 9	potentially involved in the sterol transfer between ER and golgi [179, 275]	ER, golgi, LE
114884	OSBPL10 - oxysterol binding protein-like 10	regulates lipoprotein secretion [277]	cytosolic, microtubules
114885	OSBPL11 - oxysterol binding protein-like 11	involved in lipid traffic [275]	LE, golgi
9600	PITPNM1 -membrane associated phosphatidylinositol transfer protein 1	involved in the transport of phosphatidylinositol and phosphatidylcholine between ER and golgi [181, 183]	golgi , ER
84725	PLEKHA8 - pleckstrin homology domain containing family A	involved in transfer of glycosceramide from the ER to the golgi [270]	golgi, ER
10948	STARD3 - StAR related lipid transfer (START) domain containing 3	involved in the egress of cholesterol from the LE [192, 193, 194]	LE
134429	STARD4 - StAR-related lipid transfer (START) domain containing 4	potentially involved in the transport of cholesterol to the ER and mitochondria [192, 193, 194]	ER, PM, mitochondria

EE= early endosome, LE= late endosome, ER= endoplasmic reticulum, PM= plasma membrane

3.2.2.1 Setup of a RNAi screen for the identification of LTPs important for the HCV and/or DENV replication cycle.

In search of LTPs important for HCV replication, a small scale siRNA screen was performed monitoring the effect of LTP gene knockdown comprising the full infection cycle of HCV in comparison to the related Dengue virus. A detailed description of the screen setup can be

found in 2.2.7. In short, Huh7.5FLuc cells were electroporated with siRNA ON-TARGETplus® SMARTpools, omitting commonly used lipid-based transfection reagents that could, through the addition of exogenous lipids, affect the experimental outcome. Silencing was allowed for 36 to 48 h followed by infection with either *Renilla* luciferase reporter HCV or DENV at a MOI of 0.5. 36 (DENV) or 60 h (HCV) post infection, cells were lysed and cell supernatants were transferred onto naive cells. Reinfection was allowed for 48 h (Figure 3.27A). Effect of gene knockdown on the early events of the viral replication cycle (part I) of both reporter viruses was assessed by measuring *Renilla* luciferase activity in cell lysates of the silenced cells, which were normalized to the cell number, as estimated by the measurement of the respective *Firefly* luciferase counts. Changes in the infectious virion assembly and release efficiency (part II) were determined by normalizing the *Renilla* counts of the reinfection plates to the respective *Renilla* counts in the infection plates. The screen was repeated 6 times, each time using a different plate layout. Importantly several siRNA controls were included, either exhibiting no known target, designated non-targeting (NT), or targeting the cellular PI4KIII A or ApoE, both well-known dependency factors of HCV [77, 78, 121, 143]. As such cellular factors were not well established in case of DENV, the only controls at hands were a siRNA ON-TARGETplus® SMARTpool directed against the *Renilla* luciferase itself as well as one against the DENV non-structural protein 1 (NS1). Several independent electroporations per biological replicate (run) were performed in case of the controls (Figure 3.27B).

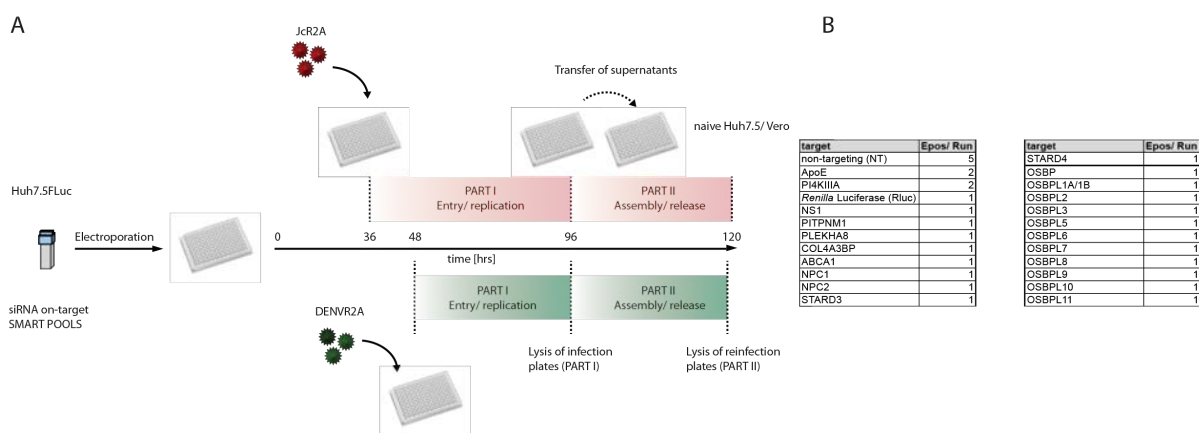


Figure 3.27 Lipid transfer protein (LTP) RNAi screen setup. (A) Huh7.5FLuc cells were electroporated with siRNA ON-TARGETplus® SMARTpools and seeded in triplicates into 96 well plates. 36 or 48 h post silencing cells were infected with *Renilla* luciferase HCV or DENV (JcR2A, DENVR2A) respectively at a MOI of 0.5. Infection was allowed for either 48 or 60 h. Then cells were lysed and cell supernatants were transferred onto naive Huh7.5 or Vero cells for reinfection. Effect of gene knockdown on viral entry and replication (part I) was assessed by determining the *Renilla* luciferase activity in cell lysates of the infection plates, normalized to the cell number, as determined by measurements of *Firefly* luciferase activity. Effects of gene knockdown on the reinfection efficiency of the virus (part II) was determined by measuring and normalizing the *Renilla* counts in the reinfection plates to the respective *Renilla* counts in the infection plates. The screen was repeated 6 times, each time using a different plate layout. (B) Table showing how many independent electroporations of siRNA per gene were performed per run. Several independent electroporations of the control siRNAs (non-targeting, ApoE, PI4KIII A, *Renilla* luciferase, DENV NS1) were conducted, whereas siRNAs against a specific target gene were electroporated into the cells only once per biological replicate/ run.

3.2.2.2 LTP RNAi screen results

Targeting LTPs alters the HCV but barely the DENV replication cycle. While definition of hit criteria can be ambiguous, in this study candidate genes were classified as hits when the *Renilla* luciferase signal was increased or decreased by at least 2 standard deviations from the mean of the non-targeting control, designated as z-score, and when the p-value was smaller than 0.05.

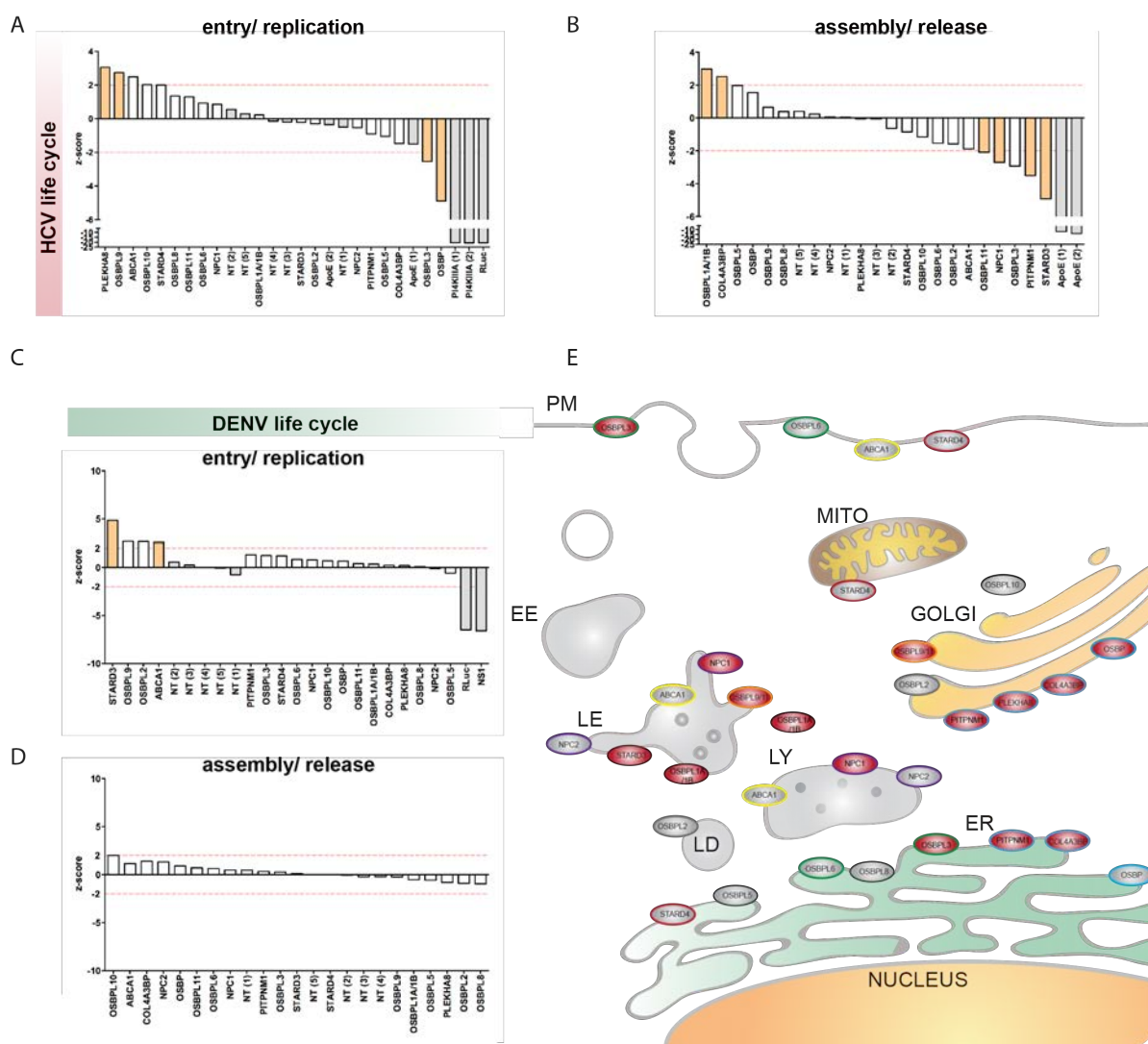


Figure 3.28 Screen results. (A-B) Representation of the screen results for either HCV or DENV. The z-score is shown for each gene. The z-score was defined as the number of standard deviations from the mean of the negative controls. Genes with a z-score bigger than 2 or smaller than -2 were considered to be hit candidates. The controls are indicated in grey, whereas hits with a significant z-score but also a p-value smaller than 0.05 are indicated in orange. (C) Subcellular distribution of all candidates analyzed in the screen. Hits are indicated in red. Some proteins can be found at several sites within the cell, which is highlighted by the respective color of the boundary of the symbols. PM= plasma membrane, MITO= mitochondria, EE= early endosome, LE= late endosome, LY= lysosome, LD= lipid droplet, ER= endoplasmic reticulum. [179, 180, 188, 190, 192, 193, 207, 270-278]

All controls gave the expected results, indicating a robust performance of the screen. In detail, knockdown of the known HCV dependency factors, such as PI4KIII A or ApoE efficiently impaired early or late events in the HCV replication cycle, respectively (Figure

3.28A, B). Targeting the *Renilla* luciferase similarly affected the HCV and DENV replication cycle, whereas the non-targeting control did not exert any impact on viral replication (Figure 3.28A-D). Gene knockdown of NS1 also efficiently reduced early events in the DENV replication cycle (Figure 3.28C).

The small-scale siRNA screen led to the identification of 10 LTPs potentially involved in the replication cycle of HCV (Figure 3.28A, B). In particular, we were able to identify six HCV dependency factors and four HCV restriction factors (Figure 3.28A, B). OSBP has recently been described as important dependency factor of HCV genome replication [79] and indeed we obtained similar results. Additionally two more members of the OSBPL family, namely OSBPL3 and OSBPL9, as well as PLEKHA8/FAPP2, a glycolipid transfer protein were identified by our screen to regulate early events in the HCV replication cycle (Figure 3.28A). Gene knockdown of the (START) domain containing 3 protein (STARD3, MLN46), of OSBPL11, of PITPNM1 or of NPC1 significantly impaired late stages of the viral replication cycle. In contrast gene silencing of OSBPL1A/1B as well as of the Collagen, type IV, alpha (Goodpasture antigen) binding protein (COL4A3BP) enhanced HCV particle production (Figure 3.28B). Only two of the proteins studied, namely STARD3 and ABCA1 seemed to be of importance for the related Dengue virus (Figure 3.28C, D).

The subcellular localization of all candidates is schematically depicted in Figure 3.28E. COL4A3BP, PITPNM1, OSBP and PLEKHA8/FAPP2 are Golgi associated proteins suggested to mediate lipid traffic between the ER and Golgi (Figure 3.28E) [180, 181, 183, 270, 276]. The results of our screen indicate that all these proteins are of relevance for the HCV replication cycle (Figure 3.28A, B). OSBPL9 and OSBPL11 can both be found at contact sites of the Golgi apparatus and late endosomes. OSBPL3 is present at the ER and plasma membrane [179, 185, 275]. All of them were found to affect HCV replication or particle production (Figure 3.28A, B). NPC1, STARD3 and OSBPL1A are present at late endosomal and lysosomal compartments of the cell [188, 196, 279]. All three proteins were identified to be crucial regulators of the replication cycle of HCV (Figure 3.28A, B, E).

3.2.2.3 Validation of selected candidates by shRNA-mediated knockdown

The primary screen results suggest an important role of LTPs residing at the ER/Golgi interface in the replication cycle of HCV. Indeed, while this study was in progress, numerous reports demonstrated that several LTPs involved in lipid transfer between ER and Golgi, namely OSBP, COL4A3BP and PLEKHA8/FAPP2 were hijacked by the virus for efficient replication [79, 129, 280]. Therefore, we decided to focus mainly on members involved in lipid traffic through the late endosomal/ lysosomal pathway, involving NPC1, STARD3,

OSBPL1A/1B but also PITPNM1, for which our screen results suggested a so far undescribed role in HCV replication. In a first step we aimed to confirm the results of the siRNA screen. For this purpose we made use of the MISSION™ TRC shRNA library commercially available from Sigma Aldrich. The gene knockdown efficiency of five different shRNAs per gene was validated and the ones causing the best gene knockdown were used for the following studies (Supplementary Figure 3).

3.2.2.4 Validation of selected candidates

shRNA-mediated knockdown of NPC1, STARD3, OSBPL1A and PITPNM1 indicates their involvement in early events of the HCV replication cycle. The LTP RNAi screen suggested a novel role of NPC1, STARD3, PITPNM1 and OSBPL1A/B in late stages of the HCV replication cycle. Nevertheless, there are many sources of errors that can affect the outcome of RNAi screens such as cell death or cell clumping, different infection efficiencies, siRNA off-target effects, different silencing efficiencies, etc. [257]. Therefore a first set of experiments focused on the validation of the screen phenotype. To this end the impact of shRNA-mediated gene knockdown on the early phase of the viral replication cycle was assessed by measuring HCV *Renilla* reporter luciferase activity in silenced cells. Additionally the reinfection efficiency of virus released from silenced cells was quantified (Figure 3.29B). Lentiviral transduction of shRNA was applied in order to achieve an efficient long lasting knockdown and for each biological replicate, naive cells were freshly transduced with shRNA encoding lentivirus. A shRNA targeting the PI4KIII A and a shRNA targeting ApoE served as positive controls for HCV RNA replication and particle production, respectively. Additionally the results of two different non-targeting controls were combined and are designated as shNT (Figure 3.29). Surprisingly, gene knockdown of NPC1, STARD3, OSBPL1A/1B and PITPNM1 in the two highly permissive human hepatoma cell lines (Huh7.5Fluc, Huh7/LunetCD81H) efficiently reduced entry and replication of the hepatitis C *Renilla* luciferase reporter virus (Figure 3.29C, D, upper panels), which stands in contrast to the primary siRNA screen data where they were identified as being required for late stages of the viral replication cycle. Amongst the candidates present in the late endosomal/ lysosomal pathway the most prominent phenotype was observed by shRNA-mediated silencing of NPC1, which impaired early phase replication to a similar extent as silencing of the PI4KIII A positive control (Figure 3.29C, upper panel). No additional effect on the release of infectious virus was observed, while gene knockdown of ApoE caused a two-fold reduction in progeny virus production (Fig. 3.30C, middle panel). Upon gene silencing of STARD3 or OSBPL1A/1B, virus entry and replication was reduced by at least two-fold. Furthermore the release of

infectious virus from STARD3 or OSBPL1A silenced cells seemed to be either unaffected or slightly increased, depending on the shRNA used (Figure 3.29C).

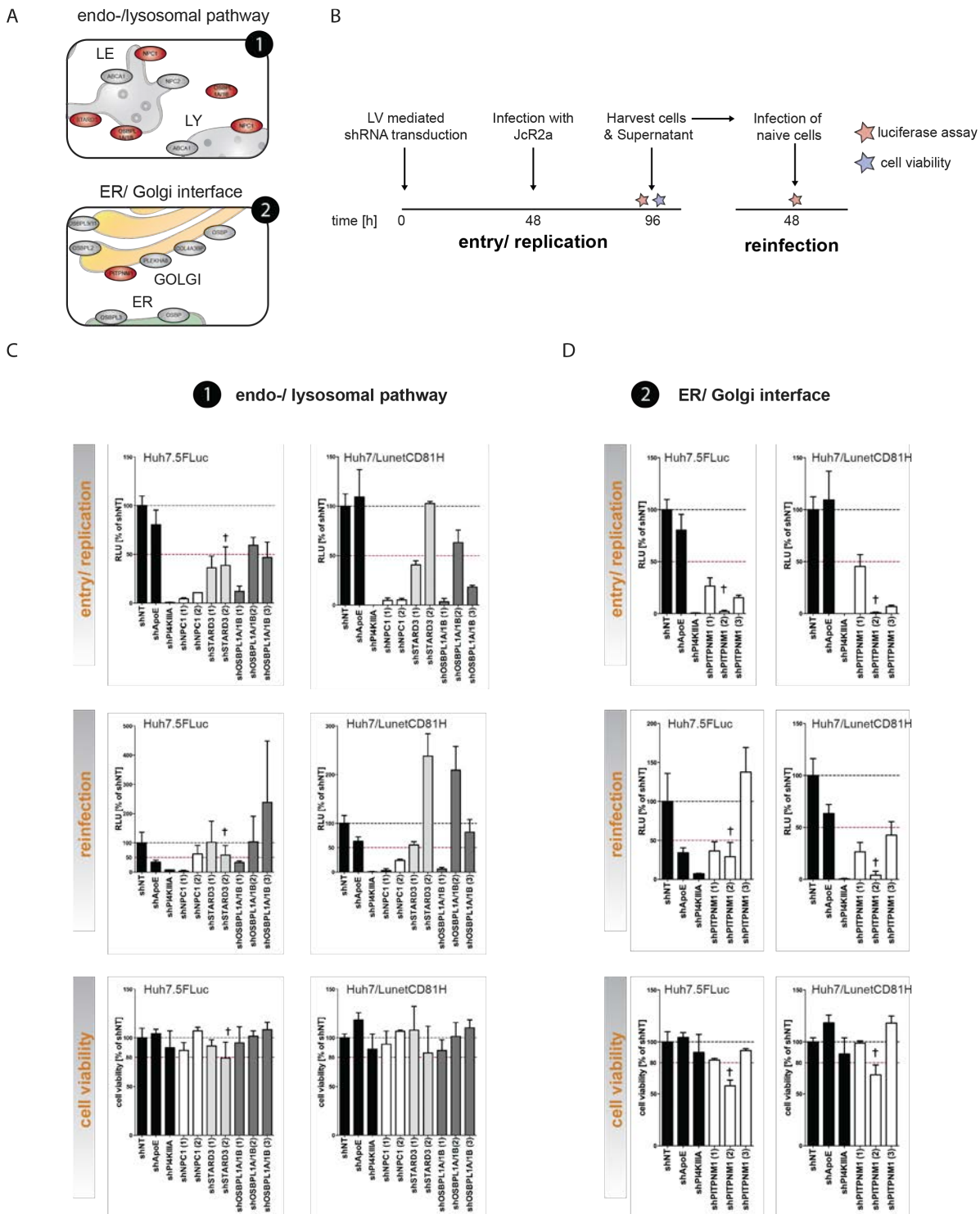


Figure 3.29 Validation of selected candidates by shRNA-mediated knockdown. (A) Schematic representation of the cellular localization of selected candidates. Hits are shown in red and were either (1) associated with the endo-/lysosomal pathway or (2) present at the ER/ Golgi interface. (B) Scheme of experimental setup. Huh7.5FLuc cells or Huh7/LunetCD81H were transduced with shRNA containing lentiviruses (MOI 1). 48 h post transduction, cells were infected with *Renilla* luciferase reporter HCV. 48 h post infection, (i) cells were lysed and (ii) cell supernatants were transferred onto naive Huh7.5 cells. Reinfection was allowed for 48 h followed by lysis of the cells. Effect of gene knockdown on viral replication or reinfection was assessed by measuring *Renilla* luciferase activity in the respective cell lysates. (C-D) Effect of gene knockdown of host factors involved in the endo-/lysosomal pathway or present at the ER/Golgi interface on the viral replication cycle. At least two different shRNAs were used per candidate gene. The results of two different non-targeting controls were

combined and are designated as shNT. Only the best working shRNAs targeting either the PI4KIII A or ApoE were used as positive controls. Changes in viral replication were analyzed by measuring the *Renilla* luciferase activity and the given relative light units (RLU) are presented as percent of the non-targeting control. Simultaneously cell viability was determined using the cell titer glo assay. Cytotoxic effects of shRNA treatment are indicated with a cross. Mean of duplicates and standard deviations of two independent experiments are shown.

Importantly, cell viability measurements revealed that shRNA-mediated gene silencing of most of the target genes was well tolerated, except of depletion of STARD3, which caused cytotoxic effects (Figure 3.29C, lower panel). Gene knockdown of the Golgi associated PITPNM1 by 3 different shRNAs led to a profound reduction of entry and replication of the hepatitis C *Renilla* luciferase reporter virus (Figure 3.29D, upper panel). Concomitantly, the release of infectious particles was reduced in a similar range with one shRNA inducing an increase in infectious particle production. (Figure 3.29D, middle panel). Additionally the shRNA (1) and (3) did not affect cell viability, while shRNA (2), causing the most prominent phenotype, was observed to substantially reduce cell viability (Figure 3.29D, lower panel.)

Altogether, shRNA-mediated gene knockdown of proteins implicated in the lipid traffic through the endo-/lysosomal pathway and of the Golgi-localized PITPNM1 impaired the early phase of the viral replication cycle, including steps in virus entry and replication. When analyzing the effect of gene silencing on the release of infectious particle production no additional or no consistent phenotype was observed. Given that the most prominent and reproducible phenotype was obtained for NPC1 gene knockdown, we decided to focus on this cellular factor for further in depth characterization.

3.2.3 Evaluating the role of the Niemann-Pick Disease Type C1 protein in the HCV replication cycle

In the following we focused on the Niemann-Pick Disease Type C1 protein (NPC1), mutations in which have been linked to an eventually fatal lysosomal storage disorder the Niemann-Pick Disease Type C (NPC) [201]. This disease is characterized by an impaired egress of cholesterol, but likely also of other lipids, from late endosomal/ lysosomal compartments resulting in their intracellular accumulation in the endo-/ lysosomal vesicles [198]. Given our previous results of a HCV-induced perinuclear accumulation of (endogenous and exogenously supplied) free cholesterol (Figure 3.20, Figure 3.23, Figure 3.24) and assuming that cholesterol is an important structural component of the DMVs [114] we wondered whether an altered intracellular lipid traffic caused by the loss of NPC1 function would cause a defect in HCV RNA replication.

3.2.3.1 Dissecting the role of NPC1 in early events of the HCV replication cycle

NPC1 is important for steps in HCV RNA replication. Being localized to the endosomal/lysosomal compartment NPC1 has been described to be required for the escape of incoming Ebola virus particles from lysosomal vesicles [281]. Thus, given our previous results we wondered whether NPC1 was indeed involved in HCV RNA replication or rather important for earlier events such as virus entry. To this point we determined the relevance of NPC1 for RNA replication of subgenomic reporter replicons, thereby bypassing the viral entry step (Figure 3.30C, D). In order to produce most consistent results, we simultaneously determined the effect of NPC1 gene knockdown on the full replication cycle of HCV and DENV *Renilla* luciferase reporter virus as well as on subgenomic reporter replicons and in parallel harvested samples for cell viability assay, Western Blot and for determination of the knockdown efficiency by RT-qPCR. (Figure 3.30A, B). As observed before, shRNA-mediated gene knockdown of NPC1 efficiently impaired the early phase of the HCV replication cycle, while not exerting an additional effect on virus particle production. In agreement with the results of the screen, DENV entry and replication was only mildly altered upon gene knockdown, however one shRNA significantly increased the release of infectious particles. Importantly cell viability was not substantially impaired (Figure 3.30B, three upper rows). Evaluation of the knockdown efficiency by RT-qPCR revealed a correlation of the extent of the reduction in NPC1 transcript levels with the observed effect on HCV genome replication, indicating that the effect of NPC1 gene knockdown on viral replication is specific (Figure 3.30B, 4th row). We further determined NS5A protein levels in cell lysates of silenced cells at the end of the experiment. While the effect of NPC1 or PI4KIII A gene knockdown on *Renilla* luciferase activity were comparable, the protein levels of NS5A were much more reduced upon knockdown of PI4KIII A as compared to NPC1 (compare Figure 3.30B HCV panel 'entry/ replication' with Figure 3.30E,F). Nevertheless NPC1 gene silencing reduced NS5A protein levels by almost two-fold when compared to the non-targeting control (Figure 3.30E, F). In parallel Huh7/Lunet cells containing a persistent, selectable subgenomic *Firefly* luciferase reporter replicon of genotype 2a (LucUbiNeo_JFH1) or of genotype 1b (LucUbiNeo_Con1ET) were transduced with shRNA containing lentivirus (Figure 3.30C). Silencing of NPC1 gene expression significantly reduced replication of subgenomic RNA of either genotype. Of note, RNA replication of the genotype 1b replicon was impaired to a larger extent as compared to the genotype 2a replicon (Figure 3.30D, two upper panels). Indeed, in case of genotype 1b, lentivirus-mediated knockdown at the highest MOI (MOI4) reduced, the *Firefly* luciferase reporter activity to almost similar extent as compared to the positive control (PI4KIII A). In contrast, genotype 2a RNA replication was on average decreased maximally two-fold upon NPC1 gene knockdown, whereas the silencing of the

PI4KIII A gave similar results as observed for the genotype 1b replicon (Compare Figure 3.30D, left and right panel). Importantly gene silencing of NPC1 did not impair the cell viability of both stable replicon cell lines (Figure 3.30D lower panels).

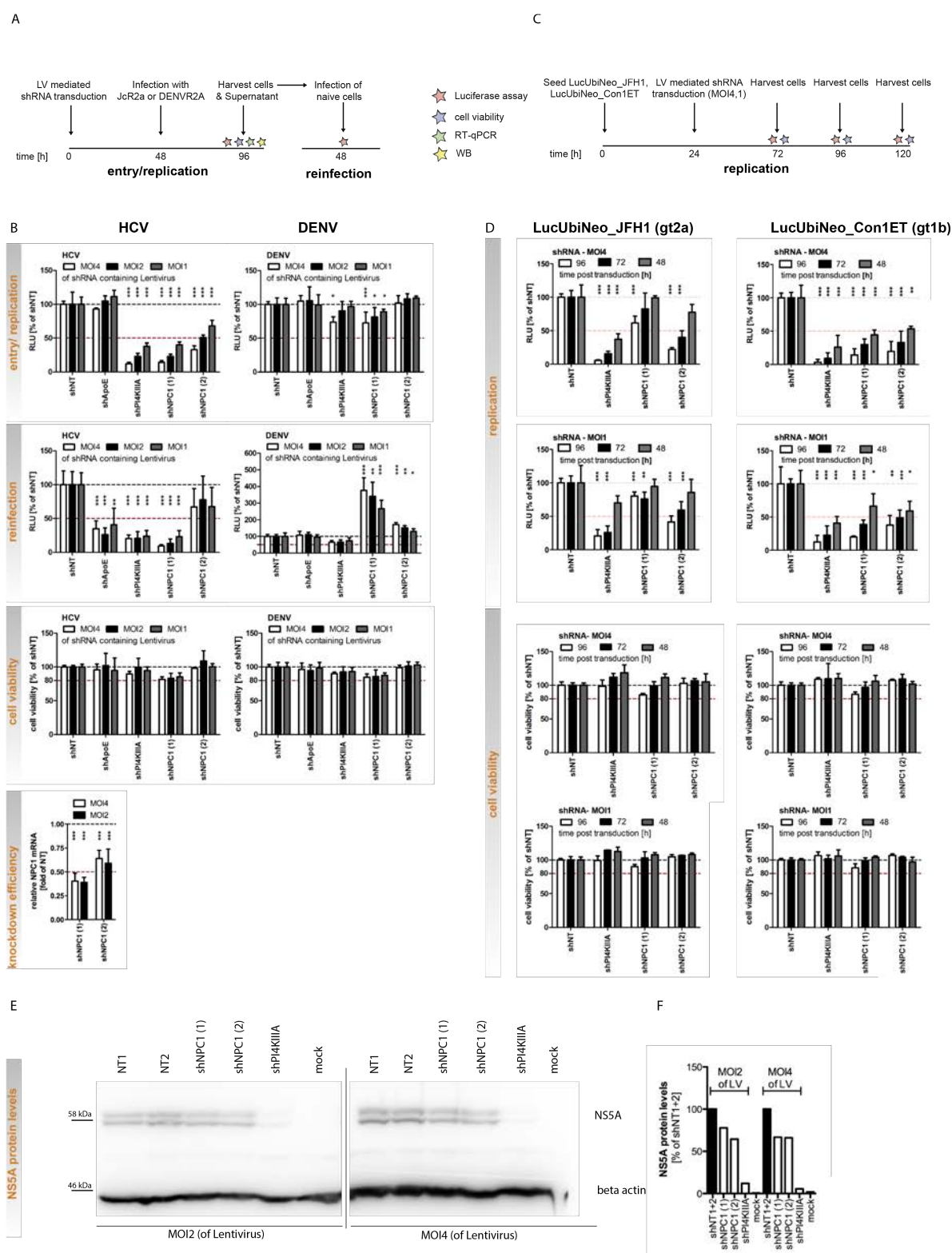


Figure 3.30 NPC1 gene knockdown reduces HCV RNA replication. The effect of gene knockdown of NPC1 on the full infection cycle of *Renilla* luciferase reporter HCV or DENV (A-B) as well as on replication of stable *Firefly* luciferase reporter replicons (C-D) was assessed. (A) Schematic representation of experimental setup. Huh7.5 cells were transduced with shRNA containing lentivirus at different MOIs (1, 2, 4). 48 h post transduction cells were infected with *Renilla* luciferase reporter HCV or DENV respectively at a MOI of 0.5. 48 h post infection (i) cells were lysed, (ii) supernatants were transferred onto naive Huh7.5 or Vero cells for reinfection, (iii) total

cellular RNA was collected to determine the knockdown efficiency and (iv) the cell viability was assessed by cell titer glo assay. **(B) Effects of gene knockdown on early and late events of the HCV and DENV replication cycle.** Effect of gene knockdown on entry/ replication was determined by measuring *Renilla* luciferase activity in cell lysates harvested 48 h post infection. As positive control a shRNA targeting the PI4KIII α was included. Determining *Renilla* luciferase activity in cell lysates of the reinfection plates allowed to assess alterations in particle production. shRNA-mediated knockdown of ApoE served as positive control. Relative light units (RLU) are presented. Cell viability was analyzed simultaneously by performing the cell titer glo assay. Knockdown efficiency was measured by determining the amount of NPC1 transcripts levels relative to the one of GAPDH within the same sample. Results are shown either as percent or fold of the mean of two non-targeting controls (shNT). The mean of duplicates and standard deviation of two independent experiments are shown. **(C) Schematic representation of experimental setup.** Stable replicon cell lines of genotype 1b (LucUbiNeo_Con1ET) and genotype 2a (LucUbiNeo_JFH1) were transduced with shRNA containing Lentivirus at a MOI of 1 or 4. The effect of gene knockdown on established replication was assessed 48, 72 and 96 h post transduction. **(D) Effect of gene knockdown on replication of *gt1b* and *gt2a* stable replicons.** The replication efficiency of *gt1b* and 2a stable replicons was assessed by measuring the *Firefly* luciferase activity in cell lysates harvested 48, 72 and 96 h post transduction and relative light units (RLU) are depicted. Cell viability upon gene knockdown was measured using the cell titer glo assay. The mean and standard deviation of at least 3 independent experiments are shown (***, $p < 0.001$, **, $p < 0.01$, *, $p < 0.05$). **(E) NS5A protein levels in NPC1 or PI4KIII α silenced cells.** NS5A protein levels were determined by Western Blot in cell lysates at the end of the experiment presented in (A). Beta actin served as loading control. **(F) Quantification of Western Blot shown in (E).** NS5A protein levels were normalized to the respective beta actin control and are presented as fold of the non-targeting controls. Data of a single experiment is shown.

In order to prove that indeed NPC1 was involved in HCV replication and that the observed phenotype was not due to any off-target effects of the shRNAs, we sought to rescue NPC1 knockdown by introducing a shRNA resistant NPC1 expression construct. First attempts of a functional rescue were unsuccessful, which could be due to an inefficient rescue of NPC1 protein levels (Supplementary Figure 4). This remains elusive due to the lack of an efficient antibody that would allow the determination of NPC1 protein levels by Western Blot.

Taken together NPC1 knockdown impaired early steps in HCV replication, but did not substantially alter the DENV replication cycle. Given the observed decline in *Firefly* luciferase activity of stable reporter replicons of genotype 1b and 2a upon gene silencing, NPC1 appears to be involved in HCV RNA replication.

3.2.3.2 Subcellular localization of NPC1 in HCV infected cells

HCV does not change the subcellular localization of NPC1. NPC1 is a multi-pass transmembrane protein localized to the limiting membrane of late endosomes/ lysosomes [204]. We next analyzed the distribution of NPC1 in HCV infected and naïve cells (Figure 3.31). In uninfected cells NPC1 labeled vesicular structures that were evenly distributed throughout the cytosol. A fraction of NPC1 was found in lysosomal LAMP2 positive compartments. Nevertheless a substantial part of the protein was present in distinct vesicular structures (Figure 3.31A). HCV infection did not induce any obvious alteration in the partitioning of the protein as NPC1 positive structures seemed similarly distributed in infected as compared to mock cells. Furthermore NPC1 did not colocalize with the HCV non-structural protein 5A. Yet NS5A was found in close proximity to NPC1 positive vesicular structures (Figure 3.31B).

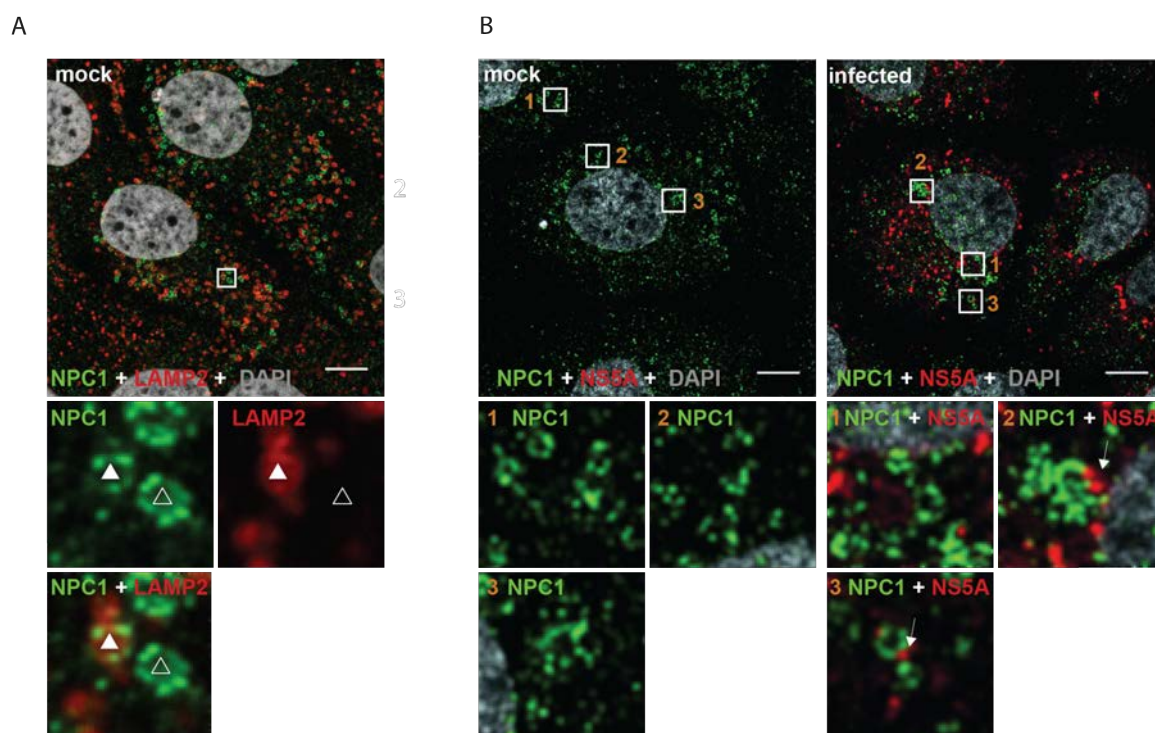


Figure 3.31 Subcellular localization of NPC1 in HCV infected cells. (A) Distribution of NPC1 and the lysosomal marker LAMP2 in naive cells. Naive Huh7/LunetCD81H cells were seeded and fixed 48 h later with 4% PFA. Staining of endogenous NPC1 (green), the lysosomal marker LAMP2 (red) and the nucleus (grey) is shown. An enlargement of the area highlighted with the white box is shown below. The white filled or open triangles indicate NPC1 structures that are either LAMP2 positive or not, respectively. (B) Distribution of NPC1 in a HCV infected cell. Huh7/LunetCD81H cells were infected with the full-length virus Jc1 (MOI5). 48 h post infection, cells were fixed and endogenous NPC1 (green) as well as the viral non-structural protein 5a (NS5A, red) were detected by indirect immunofluorescence. The nucleus was stained with DAPI (grey). Enlargements of the areas highlighted with the white rectangles are shown below. Scale bars represent 10 μ m. For better visualization signal intensities were equally enhanced.

3.2.3.3 Studying the involvement of NPC1 in cellular free cholesterol distribution

The distribution of free cholesterol is altered upon NPC1 gene knockdown. Loss of NPC1 function has been described to result in an impaired export of free cholesterol from late endosomal and lysosomal compartments, thus causing a lipid trafficking disorder [198]. To investigate this further in the context of viral replication we analyzed the distribution of free cholesterol upon gene knockdown of NPC1 or of PI4KIII A in HCV transfected cells (Figure 3.32A). In cells transduced with the non-targeting shRNA control, filipin was found in a diffuse, web-like pattern at the perinuclear region of the cytoplasm. NPC1 gene knockdown moderately but significantly increased the filipin signal intensity at the perinuclear region, while it was significantly reduced upon PI4KIII A gene silencing. In case of the latter, filipin was mainly found at the plasma membrane as well as at some intracellular vesicles (Figure 3.32A). As NPC1 knockdown appeared to induce a clustering of filipin in large vesicles, we determined the vesicle volume of filipin positive structures. Indeed, silencing of NPC1

resulted in a slight, but significant enlargement of filipin containing vesicles as compared to the control condition, indicating an accumulation of unesterified cholesterol in vesicular structures (Figure 3.32C).

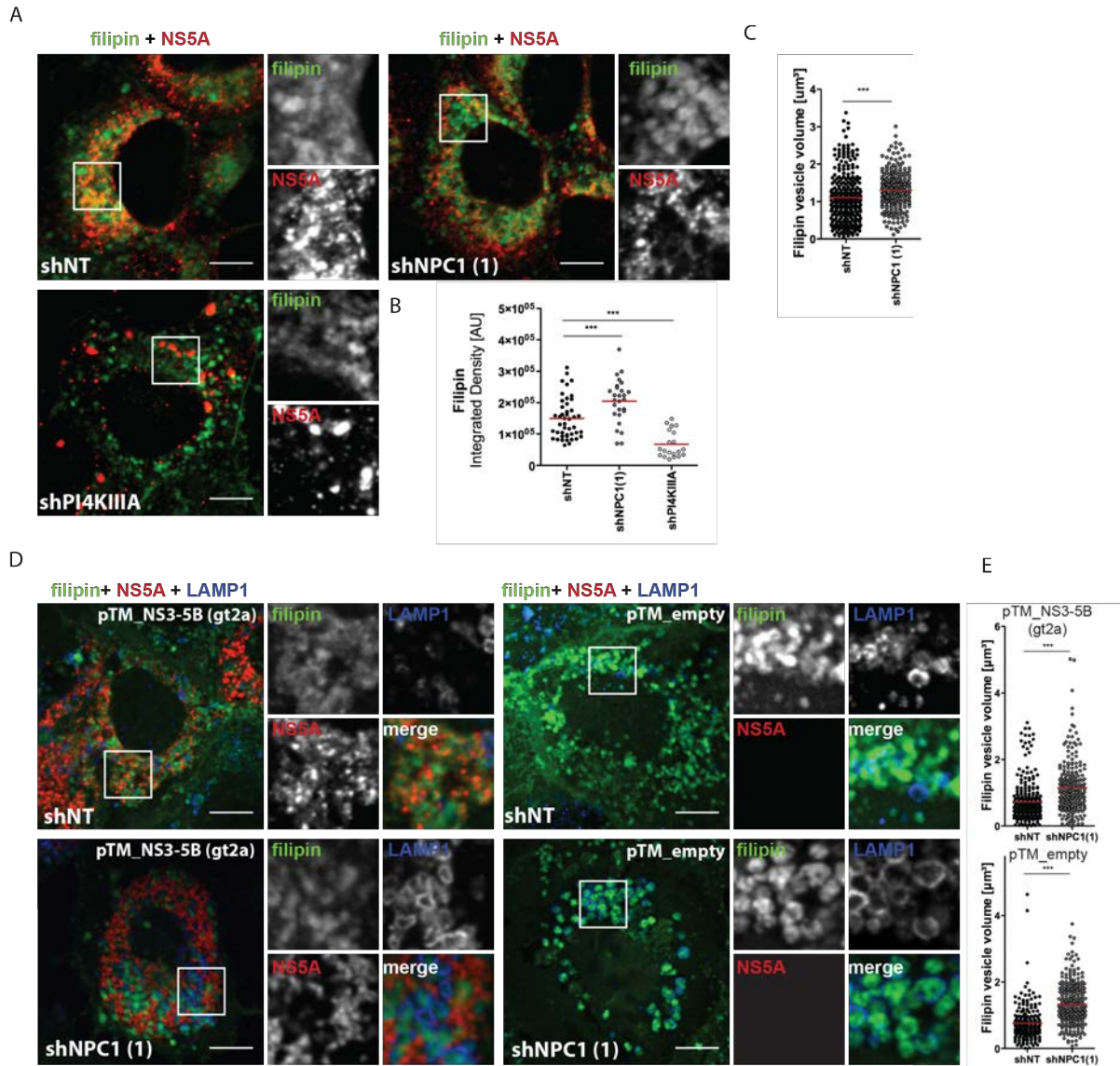


Figure 3.32 Effect of NPC1 gene knockdown on the cellular distribution of free cholesterol (A) Distribution of free cholesterol (filipin staining) and NS5A in NPC1 or PI4KIII A silenced or control cells. Huh7/Lunet cells were transfected with the HCV full-length genome Jc1. 4 h post transfection cells were transduced with shRNA containing Lentiviruses at a MOI of 4. 68 h later cells were fixed and free cholesterol (filipin, green) and the viral non-structural protein 5a (NS5A, red) were detected by indirect immunofluorescence. (B) Determination of the signal intensity of filipin at the perinuclear region of the cytoplasm. 20 cells of a single experiment were analyzed. Mean values are indicated by the red bar. (C) Quantification of the volume of filipin positive structures. The volumes of at least 253 structures determined in $n=10-13$ cells are depicted. Mean values are indicated by the red bar. (D) Effect of NPC1 gene knockdown on filipin distribution in Huh7Lunet/T7 cells expressing or not the non-structural proteins (NS3-5B, gt2a). Huh7Lunet/T7 cells were transduced with shRNA containing Lentivirus at a MOI of 4. 48 h post transduction cells were transfected with a pTM-based expression construct encoding the non-structural proteins of genotype 2a or with the empty vector control. 24 h post transfection cells were fixed and free cholesterol (green), lysosomes (LAMP1, blue) and NS5A (red) were stained by indirect immunofluorescence. The areas highlighted by white rectangles are shown as enlargements. Scale bars represent 10 μm . (E) Quantification of the volume of filipin positive structures. At least 200 structures of 10 cells of a single experiment were measured. Mean values are indicated by the red bar. For better visualization pictures were auto-contrasted. (***, $p < 0.001$, **, $p < 0.01$, *, $p < 0.05$)

In parallel, the effect of NPC1 gene knockdown on the cellular cholesterol distribution was tested in a HCV RNA replication independent system to circumvent a potential impact of reduced viral protein levels upon NPC1 gene knockdown on cellular cholesterol levels. In presence or absence of the non-structural proteins NS3-5B, gene knockdown of NPC1 led to an intracellular accumulation of filipin positive structures. These structures were found to be LAMP1 positive indicating their lysosomal origin (Figure 3.32D). In agreement with our previous observation the volume of the filipin containing structures was increased upon NPC1 silencing, in fact to a similar extent in either presence or absence of the non-structural proteins (Figure 3.32E).

Hence our results indicate that NPC1 function regulates the distribution of free cholesterol. In addition NPC1 is involved in early events of the HCV replication cycle such as RNA replication. In line with our previous results that indicated a recruitment of plasma membrane derived cholesterol to NS5A positive sites (see 3.2.1) this points to a potential involvement of NPC1 mediated cholesterol traffic in HCV replication.

3.2.4 Studying the effect of U18666A on HCV replication

Our previous results suggested that HCV replication depends on NPC1 mediated cholesterol transport through the endo-/ lysosomal pathway. Nevertheless, HCV replication could also be regulated by any other function of NPC1, independent of the protein's role in lipid transport. To further elucidate the role of endosomal lipid traffic in HCV replication, we made use of a drug known to mimic NPC1 loss-of-function. The compound U18666A (3bta-(2-(diethylamino)ethoxy)androst-5-en-17-one) has been described to inhibit the egress of cholesterol from late endosomes and lysosomes and thus provides a useful tool in addressing questions on molecular trafficking through the endo-/lysosomal pathway [282].

3.2.4.1 Effect of U18666A treatment on the cellular distribution of free cholesterol

Treatment with U18666A alters the distribution of free cholesterol and reduces the lipid's colocalization with NS5A. We first studied the effect of U18666A treatment on the distribution of unesterified cholesterol and determined the lowest effective concentration (Figure 3.33). To this point cells transfected with full-length wild-type virus (Jc1) were treated for 48 h with different concentrations of U18666A. In agreement with our previous results, filipin was found in a diffuse web-like structure in presence of the virus in untreated cells. Treatment with concentrations equal to or higher as 0.625 μ M U18666A induced a significant accumulation of filipin in dilated vesicles clustering around the nucleus, which resembled the

NPC1 knockdown phenotype (compare Figure 3.32A and Figure 3.33A). Interestingly the increase in filipin vesicle volume coincided with a decrease in the degree of NS5A and filipin colocalization (Figure 3.33B, C). Indeed, comparing the localization of NS5A with respect to filipin in untreated and treated cells, it seemed that upon addition of the drug filipin became excluded from NS5A positive sites (Figure 3.33A, white arrows = filipin exclusion, yellow arrows = colocalization).

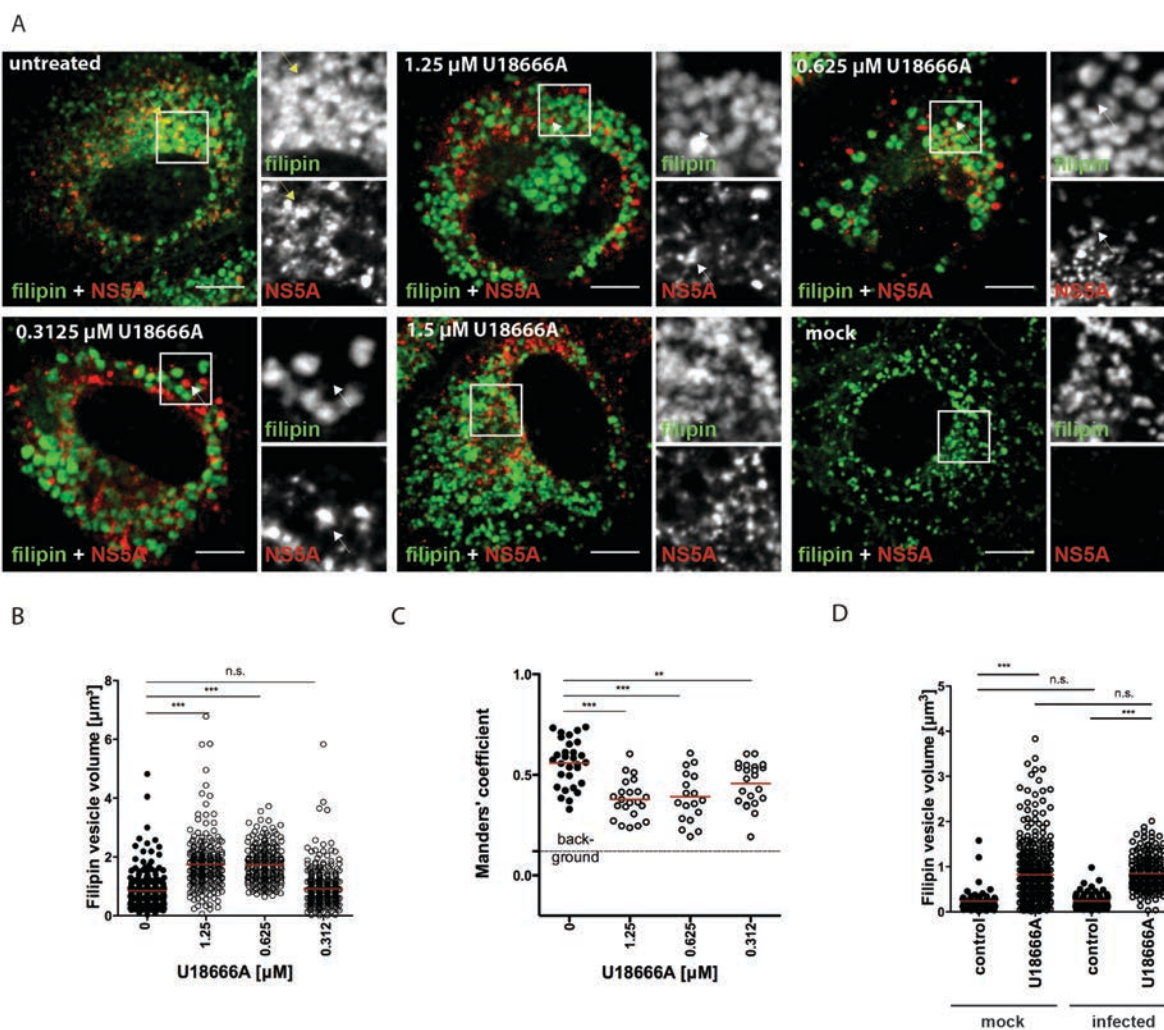


Figure 3.33 Effect of U18666A treatment on cellular localization of free cholesterol. **(A)** Distribution of free cholesterol (filipin) and NS5A in HCV (Jc1) transfected cells treated with various concentrations of U18666A. Huh7/Lunet cells were transfected with full-length Jc1 followed by treatment with different concentrations of U18666A for 48 h. Free cholesterol (filipin, grey) and the non-structural protein 5A (NS5A, red) were labelled by indirect immunofluorescence. The insets show magnifications of the areas highlighted by the white rectangle. Scale bars represent 10 µm or 5 µm (inset) respectively. Yellow arrows indicate filipin and NS5A signal overlap, white arrows point to exclusion of TFC from NS5A positive sites. **(B)** Quantification of the volume of filipin positive structures in infected cells treated with U18666A. The volumes of more than 60 structures of at least 6 cells from a single experiment were analyzed per condition. Mean values are indicated by the red bar. **(C)** Quantification of the degree of NS5A and filipin signal overlap. The Manders' correlation coefficient was quantified for at least 20 cells per condition of a single experiment. The background represents the Manders' coefficient measured in NS5A negative cells. **(D)** Quantification of the volume of filipin positive structures in HCV (Jc1, MOI 5) infected Huh7.5 cells treated for 48 h with 1.25 µM of U18666A. The mean values of a single experiment are shown. 250 structures of at least 7 cells were analyzed. (***, $p < 0.001$, **, $p < 0.01$, *, $p < 0.05$)

We next asked whether something similar could be observed in infected cells treated with 1.25 μ M U18666A, the highest dose previously tested. Upon addition of U18666A, filipin was found in enlarged structures, irrespective of the presence or absence of the virus (Figure 3.33D).

3.2.4.2 Impact of U18666A treatment on early phases of HCV and DENV replication cycle

U18666A impairs early events in the HCV replication cycle. As we were able to recapitulate the effect of NPC1 knockdown on free cholesterol distribution by U18666A treatment we next investigated the drug's potential to interfere with HCV or DENV replication (Figure 3.34). To this point different treatment conditions were tested in the highly permissive Huh7.5 cell line. Cells were either pre-treated 24 h prior to infection (Figure 3.34A) or treatment was started at time point of infection (Figure 3.34B), or right after the removal of the viral inoculum (Figure 3.34C). Since the effects of U18666A have been described to be reversible, cells were kept in presence of the drug for 48 h [283]. Either treatment condition led to a maximally two-fold reduction in the entry and replication of *Renilla* luciferase reporter HCV (Figure 3.34 upper panels). The longer the treatment period the stronger the impact of the drug on the early phase of HCV replication. In contrast Dengue *Renilla* luciferase reporter virus replication was mainly unaffected and only altered by incubation with the highest, non-cytotoxic, concentrations possible (Figure 3.34, middle panels). For each treatment condition cell viability was assessed simultaneously which demonstrated that treating cells for 48 h with 0.625 μ M and 1.25 μ M U18666A did not exhibit cytotoxic effects but significantly impaired viral replication by almost two-fold.

Given the fact that the experiments were conducted in presence of the drug, the observed reduction in *Renilla* luciferase activity may have been caused by the impairment of virus spread or by a direct virucidal effect of the drug. In order to determine the drug's true impact on viral replication, we first tested its inhibitory potential on replication of *Firefly* luciferase reporter replicon cell lines of genotype 2a and genotype 1b. Indeed treatment with 1.25 or 0.625 μ M U18666A impaired genotype 2a and genotype 1b replication, with the latter one being more sensitive towards drug treatment (Figure 3.34D). To corroborate this further, we determined the drug's effect on viral replication in Huh7/Lunet cells transfected with full-length *wild-type* virus (Jc1), therefore omitting the virus entry step. Moreover as these cells exhibit low cell surface expression of the HCV entry factor CD81, virus spread is largely restricted [240]. Interestingly NS5A protein levels, here used as a marker for viral RNA replication, were markedly reduced when U18666A was added 4 h post viral RNA transfection, while they were only little altered when the drug was added at later time points.

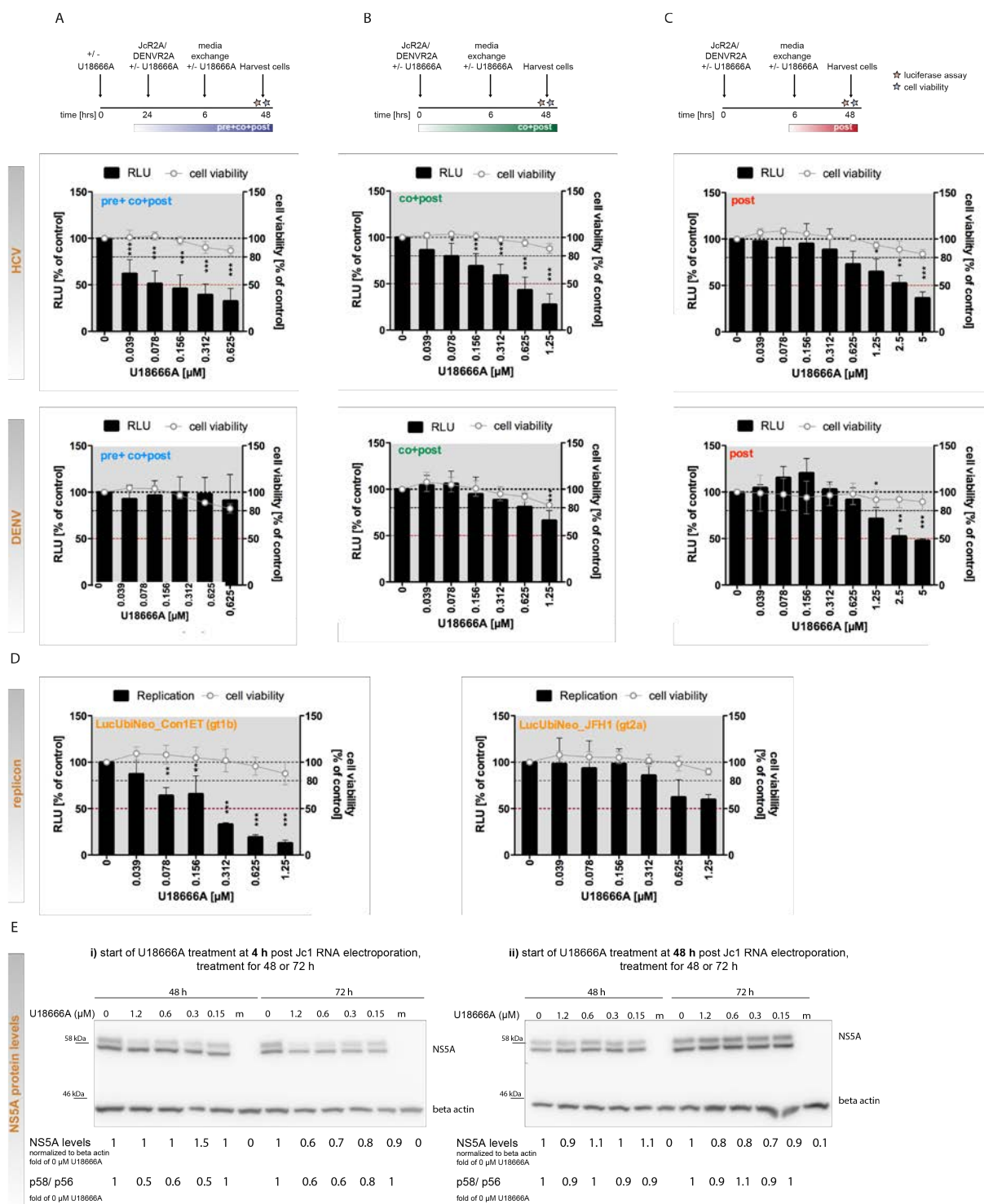


Figure 3.34 Effect of U18666A treatment on the early phase of HCV replication **(A)** Schematic representation of the experimental setup. **(A)** *Pre+co+post* treatment. Huh7.5 cells were pre-treated with U18666A, followed by infection with Renilla luciferase HCV or DENV (JcR2A, DENVR2A, MOI 0.5) in presence of the drug. 6 h post infection the inoculum was removed and fresh drug containing media was added. **(B)** *Co+ post* treatment. Huh7.5 cells were infected with JcR2A or DENVR2A in presence of the drug. 6 h post infection the inoculum was replaced by fresh drug containing media. **(C)** *Post* treatment. Huh7.5 cells were infected with viral Renilla luciferase reporter HCV or DENV. 6 h post infection the viral inoculum was replaced with fresh media supplemented with U18666A. **(A-C)** Effect of different drug treatment conditions on the early phase of Renilla luciferase reporter HCV or DENV replication. The effect of drug treatment on viral replication was assessed by measuring Renilla luciferase activity in the cell lysates; relative light units (RLU) are shown. Additionally cell viability was measured by cell titer glo assay. Of all drug concentrations tested, only those that were not cytotoxic are shown. **(D)** Effect of 48 h treatment with U18666A on stable Firefly luciferase reporter replicon cell lines of

gt2a (LucUbiNeo_JFH1) and gt1b (LucUbiNeo_Con1ET). Effect of drug treatment was determined by measuring the *Firefly* luciferase activity in cell lysates. Cell viability was determined by cell titer glo assay. Relative light units (RLU) are depicted. (A-D) Results are shown as percentage of the untreated control. The mean and standard deviation of at least three independent experiments, measured in triplicates, are shown (**, $p < 0.001$, *, $p < 0.01$, *, $p < 0.05$). (E) *Effect of U18666A treatment on replication of full-length HCV (Jc1) as determined by measurement of NS5A protein levels*. Huh7/Lunet cells were transfected with full-length Jc1. (i) 4 or (ii) 48 h post electroporation cells were treated with different concentrations of U18666A for either 48 or 72 h. The protein levels of NS5A were determined by Western Blot. Beta actin served as loading control. The numbers indicate changes in NS5A protein levels or in the ratio of the hyperphosphorylated (p58, upper band) to the basal phosphorylated (p56, lower band) form of NS5A. Data is represented as fold of the untreated control.

Moreover, drug treatment caused a reduction in the hyperphosphorylated form of NS5A (p58) as compared to its basal phosphorylated version (p56) (Figure 3.34E). Altogether, this suggests that U18666A affects early stages in viral replication, such as RNA replication.

The molecular mechanisms of how U18666A induces alterations in the cellular cholesterol distribution have not been elucidated yet. Given its structure being similar to unesterified cholesterol, which is targeted by NPC1 [284], it is possible that the drug mediates its inhibitory function by directly binding to NPC1 (Supplementary Figure 5A). While our preliminary results suggested that NPC1 function is not targeted by U18666A, others have reported a loss in sensitivity towards U18666A treatment upon NPC1 overexpression (Supplementary Figure 5C, D) [285].

Taken together, U18666A treatment mimicked NPC1 knockdown causing a reduction in viral RNA replication and an altered intracellular free cholesterol distribution.

3.2.5 Studying the impact of sterol synthesis inhibitors on sterol homeostasis and HCV replication

Our previous results suggest that alterations in the free cholesterol distribution following NPC1 knockdown or U18666A treatment might hamper the early phase of viral replication of HCV. These results encouraged us to study in more detail the potential role of endosomal cholesterol traffic in HCV RNA replication. In order to corroborate this hypothesis we made use of several cationic amphiphiles (Ro 48-8071, clomiphene citrate), which are, similar to U18666A, suggested to interfere with endo-/lysosomal lipid traffic. In addition they are known inhibitors of the sterol synthesis pathway [285]. To control for any sterol synthesis-related effects, we included a specific inhibitor of the sterol synthesis pathway, namely Mevastatin. This compound is known to target the rate-limiting enzyme of the sterol synthesis pathway, the HMGCoA Reductase [286], but an additional impact of Mevastatin on lipid traffic has not been described so far.

In a first set of experiments we addressed the drugs' potential to alter the subcellular distribution of lipids within the cell as well as their impact on viral RNA replication.

3.2.5.1 Studying the effect of sterol traffic and synthesis inhibitors on cellular lipid distribution

Cationic amphiphiles cause an accumulation of free cholesterol and the ganglioside GM1 in lysosomal structures. So far, this study had only focused on visualizing unesterified free cholesterol by the use of filipin. Given the likelihood, that not only cholesterol but also other lipids are affected by targeting the endo-/lysosomal lipid trafficking machinery, we aimed to visualize further lipid species. As HCV replication occurs at detergent resistant membranes, we focused on components of detergent resistant lipid rafts, which are cholesterol and sphingolipid rich microdomains [127, 287]. To this end, we attempted to visualize two raft lipids: the ganglioside GM1 and the sphingolipid sphingomyelin. The cholera toxin subunit b, produced by *vibrio cholerae* binds GM1 with high affinity and has therefore been frequently used as a probe for this ganglioside [288]. The presence of sphingomyelin in membranes can be visualized by the use of two toxins, lysenin and equinatoxin II [289]. In contrast to the effective visualization of GM1 with fluorescently tagged cholera toxin subunit B, our efforts to label sphingomyelin with lysenin were unsuccessful (data not shown). Thus we tested the impact of the cationic amphiphiles as well as of Mevastatin on the cellular distribution of GM1 and of unesterified cholesterol (Figure 3.35, Figure 3.36). Treatment with the amphiphiles U18666A, Ro 48-8071 and Clomiphene citrate caused an accumulation of free cholesterol but also of the ganglioside GM1 in dilated lysosomal structures (Figure 3.35A, Figure 3.36A, white arrows in inset pictures). Quantification of their volume revealed a slight but significant enlargement as compared to the untreated control (Figure 3.35B, Figure 3.36B). Furthermore these structures were found in clusters at the perinuclear region (Figure 3.35A, Figure 3.33A, upper panel). Treatment with Mevastatin barely altered the lipids' cellular distribution. In fact GM1 or free cholesterol positive structures were of similar size or even smaller as compared to the untreated control and were evenly spread throughout the cytoplasm (Figure 3.35A, Figure 3.36A, upper panel). This was further reflected by the presence of less dilated lysosomal membranes (Figure 3.35A, Figure 3.36A, grey arrows in inset pictures). We further compared the NS5A pattern of control cells with NS5A localization in cells treated with either Mevastatin or the cationic amphiphiles (U18666A, Ro 48-8071, Clomiphene citrate). In case of Mevastatin treated or control cells, NS5A was evenly distributed in an ER-like pattern at the perinuclear region. However in presence of the cationic amphiphiles, NS5A was more frequently observed in a patchy distribution and partially accumulating in large clusters (Figure 3.35A, Figure 3.36A, yellow arrows).

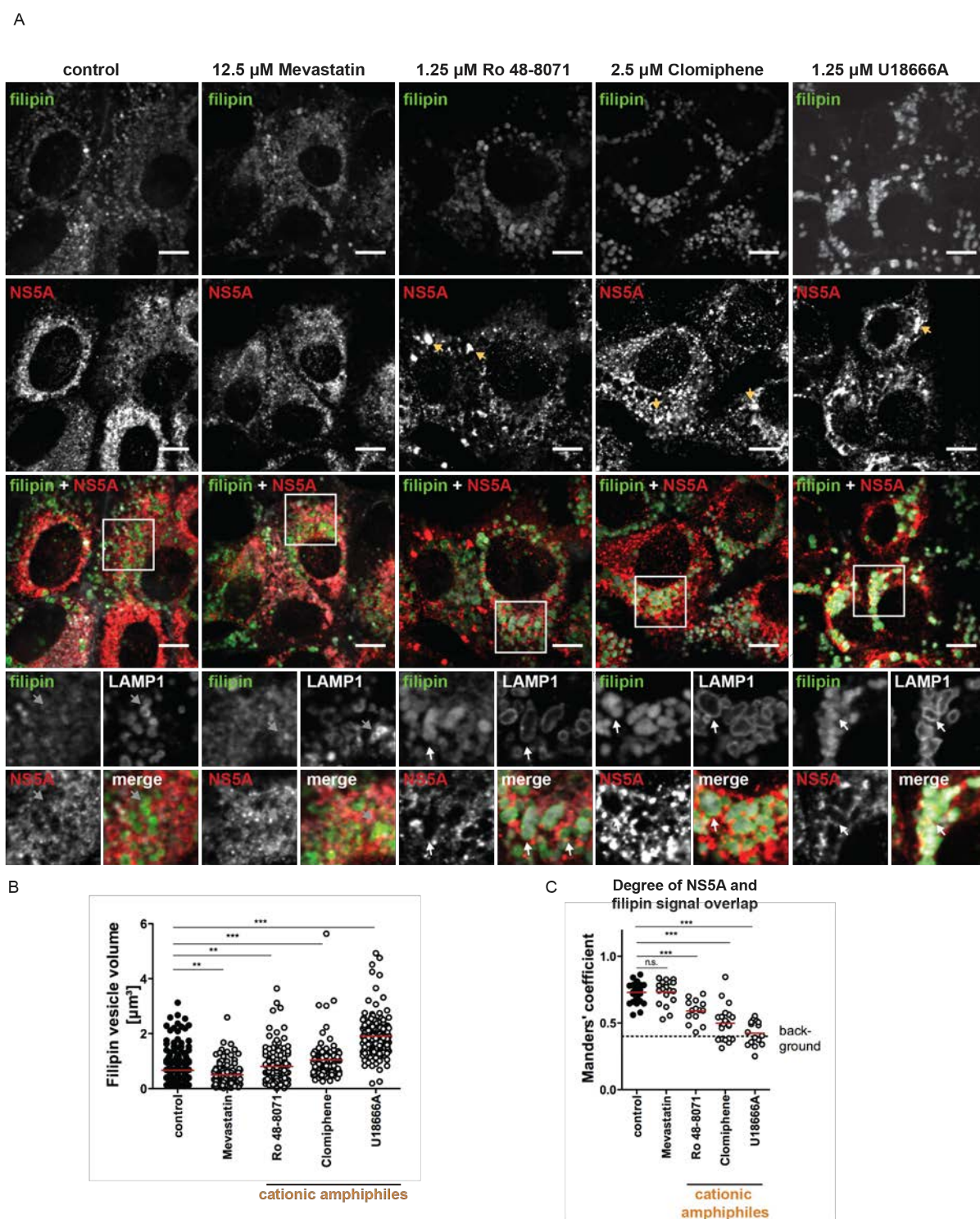
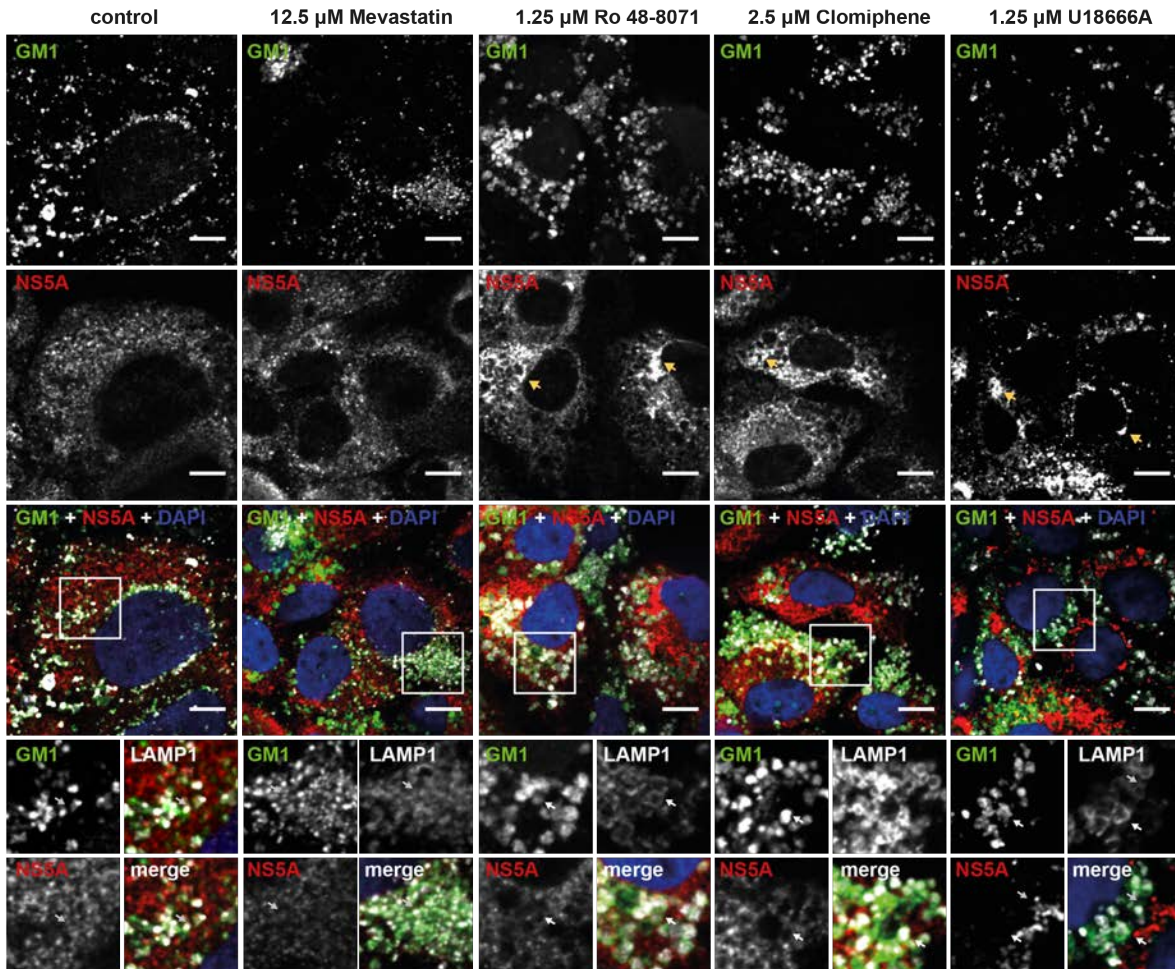


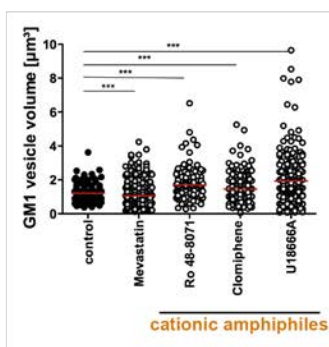
Figure 3.35 Effect of inhibitors of the sterol synthesis and trafficking pathway on the subcellular distribution of unesterified cholesterol. **(A)** Distribution of NS5A, free cholesterol (filipin staining) and the lysosomal marker LAMP1 in infected cells treated with Mevastatin, Ro 48-8071, Clomiphene citrate, U18666A or the respective control. Cells were infected with full-length virus Jc1 (MOI 3). 48 h post infection cells were treated with the indicated drugs. 48 h post treatment cells were fixed and the distribution of unesterified cholesterol (grey), of the lysosomal marker LAMP1 (green) and of the non-structural protein 5A (red, NS5A) was assessed by indirect immunofluorescence. Representative images are shown. The insets show magnifications of the area highlighted with a white rectangle. White or grey arrows label dilated or smaller LAMP1 positive structures, respectively. NS5A clusters are indicated with a yellow arrow. Scale bars represent 10 μm . **(B)** Quantification of the volume of filipin positive structures as determined for each treatment condition. A minimum of 10 cells of a single experiment was analyzed, within which at least 98 individual structures were measured. The red bar indicates the mean of all measurements. **(C)** Degree of filipin and NS5A signal overlap as determined for each treatment condition. The Manders correlation coefficient of NS5A and filipin was determined for at least 15 cells of

a single experiment. The background represents the Manders' coefficient measured in NS5A negative cells. (***, $p < 0.001$, **, $p < 0.01$, *, $p < 0.05$)

A



B



C

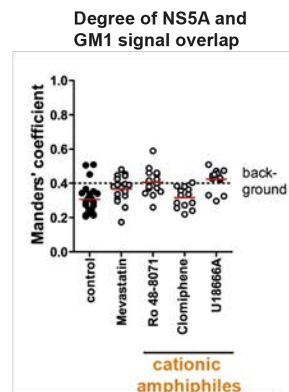


Figure 3.36 Effect of inhibitors of the sterol synthesis and trafficking pathway on the subcellular distribution of the ganglioside GM1. (A) Distribution of NS5A, ganglioside GM1 (as determined by the use of cholera toxin subunit B) and the lysosomal marker LAMP1 in infected cells treated with Mevastatin, Ro 48-8071, Clomiphene citrate, U18666A or the respective control. Cells were infected with full-length virus Jc1 (MOI 3). 48 h post infection cells were treated with the indicated drugs. 48 h post treatment cells were fixed and the distribution of the ganglioside GM1 (green), of the lysosomal marker LAMP1 (blue) and of the non-structural protein 5A (red, NS5A) was assessed by indirect immunofluorescence. Representative images are shown. The insets show magnifications of the area marked with a white rectangle. White or grey arrows label dilated or smaller LAMP1 positive structures, respectively. NS5A clusters are indicated with a yellow arrow. Scale bars represent 10 μm . (B) Quantification of the volume of filipin positive structures for each respective treatment condition. A minimum of 10 cells of a single experiment was analyzed, within which at least 155 individual structures were measured. The red bar indicates the mean of all measurements. (C) Degree of overlap of the NS5A and filipin signal. The Manders

correlation coefficient was determined for at least 13 cells of a single experiment. The background represents the Manders' coefficient measured in NS5A negative cells. (***, $p < 0.001$, **, $p < 0.01$, *, $p < 0.05$)

We further analyzed the degree of overlap of either lipid with the HCV non-structural protein 5a. In agreement with our previous results NS5A was found to partially colocalize with unesterified cholesterol in control cells. Mevastatin did not significantly affect the colocalization efficiency of the viral protein and the cholesterol marker filipin. However this colocalization was markedly reduced in presence of the cationic amphiphiles, suggesting a defect in cholesterol trafficking (Figure 3.35C). In contrast no overlap of GM1 and NS5A was detected in HCV infected cells and this was furthermore not altered by any of the drugs (Figure 3.36C).

Taken together our results indicate that treatment with cationic amphiphiles, but not with Mevastatin leads to the accumulation of free cholesterol and GM1 in lysosomal structures. This is furthermore concomitant with the decrease of NS5A and cholesterol signal overlap, which indicates an impaired traffic of cholesterol to NS5A positive sites.

3.2.5.2 Effect of sterol synthesis and trafficking inhibitors on HCV RNA replication

Sterol synthesis and trafficking inhibitors impair HCV RNA replication. Assuming that lipid traffic through the endo-/lysosomal pathway could serve to deliver plasma membrane derived lipids to the endoplasmic reticulum for the generation or maintenance of the HCV replication sites, we studied the drugs' antiviral potencies on viral RNA replication.

To this point genotype 2a and 1b stable *Firefly* luciferase reporter replicon cell lines were treated with different concentrations of the respective drug for 48 h. Effects of the 48 h drug treatment on viral RNA replication were assessed by measuring *Firefly* luciferase activity in cell lysates. Indeed RNA replication of the genotype 1b replicon was significantly inhibited by two-fold by all compounds tested (Figure 3.37A, B, C upper panel). In contrast, genotype 2a RNA replication was only decreased upon Ro 48-8071 treatment (Figure 3.37A, B, C lower panel). The observed changes in *Firefly* luciferase reporter activity were reflected by the NS5A protein levels determined by Western Blot (Figure 3.37D, E).

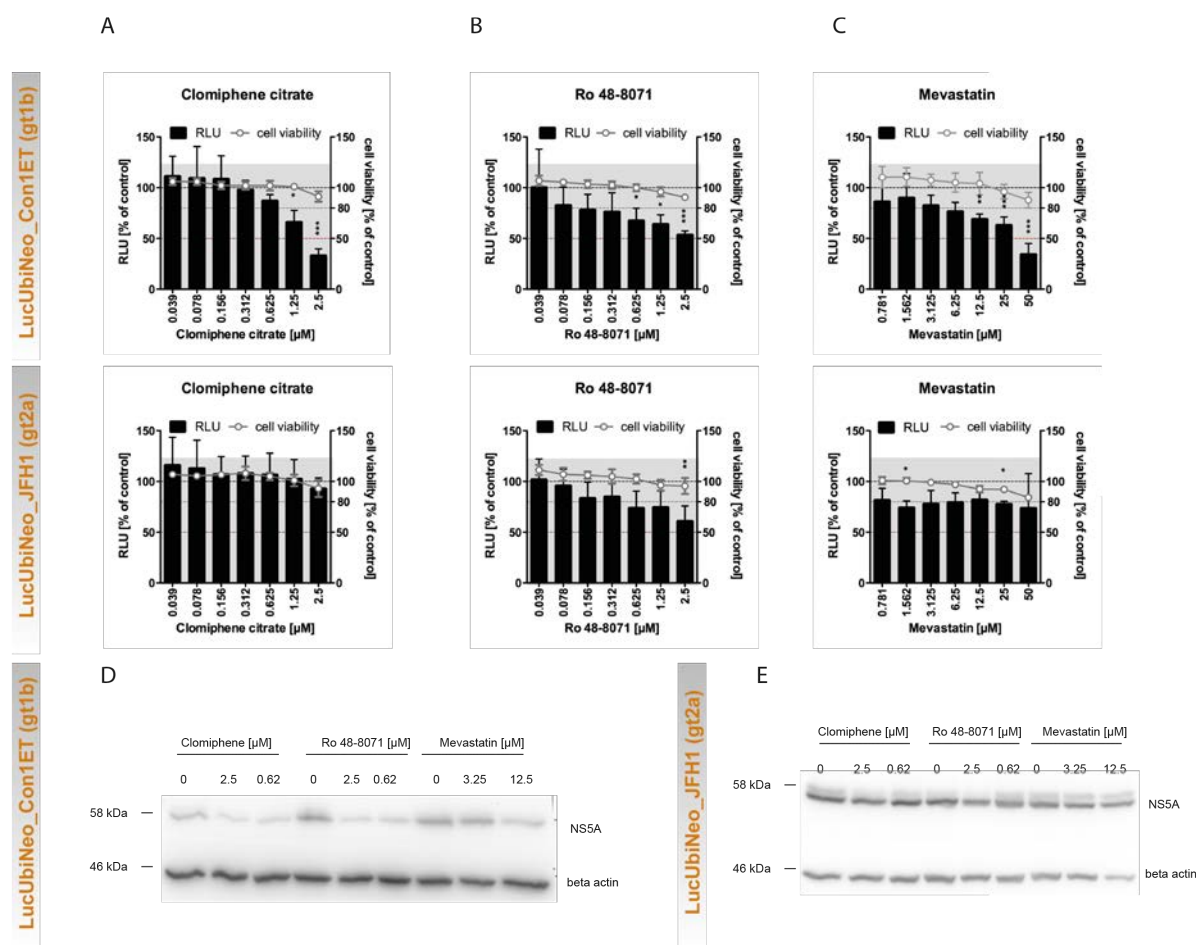
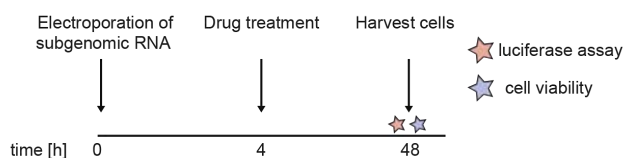


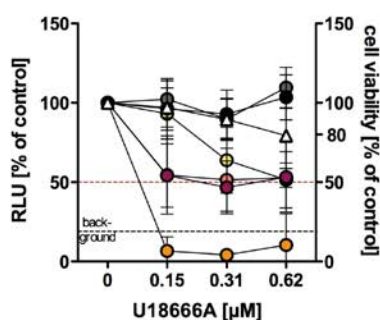
Figure 3.37 Effect of sterol synthesis and trafficking inhibitors on established viral genome replication. (A-C) Effect of treatment with clomiphene citrate, Ro 48-8071, and Mevastatin on the RNA replication of *gt1b* and *2a* stable replicon cell lines. LucUbiNeo_Con1ET (*gt1b*) or LucUbiNeo_JFH1 (*gt2a*) stable *Firefly* luciferase reporter replicon cells were treated for 48 h with different concentrations of the corresponding drug or the respective control. Effect of drug treatment on replication was determined by measuring the *Firefly* luciferase in cell lysates, the respective relative light units (RLU) are depicted. Additionally cell viability was determined by cell titer glo assay and only concentrations that did not cause cell cytotoxicity are shown. The mean and standard deviation of 4 independent experiments, measured in triplicates are shown. Experiments were performed in triplicates (***, $p < 0.001$, **, $p < 0.01$, *, $p < 0.05$). (D-E) Effect of drug treatment on NS5A protein levels of *gt2a* or *1b* stable replicon cell lines. Cell lysates were subjected to NS5A and beta-actin protein detection by Western Blot. Results of a single experiment are shown.

Our previous results showed that HCV RNA replication of genotype 1b was more sensitive towards knockdown of NPC1 or treatment with sterol synthesis inhibitors as compared to genotype 2a (Figure 3.30D and Figure 3.34D). Thus, we decided to test the sensitivity of subgenomic *Firefly* luciferase reporter replicons of different genotypes (1a, 1b, 2a, 3a, 4a, 5a, Figure 3.38) towards treatment with cationic amphiphiles or with Mevastatin. The results of these experiments revealed variances in the sensitivity of each replicon towards treatment with the given compounds. Generally *gt1b* replication (except of in case of Mevastatin treatment) was most strongly reduced, while *gt4a* and *5a* replicons were almost unaffected by either drug. RNA replication of *gt1a*, *2a* and *3a* was partially diminished depending on the drug used (Figure 3.38B-E). Surprisingly clomiphene citrate appeared to enhance viral RNA replication of *gt1a*.

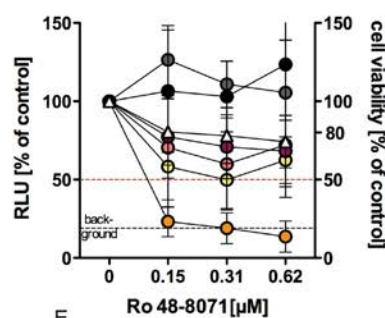
A



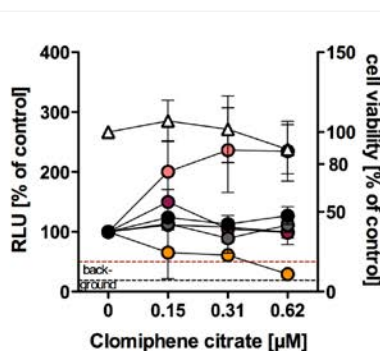
B



C



D



E

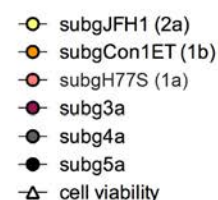
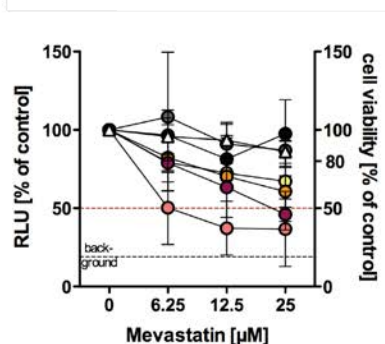


Figure 3.38 Effect of sterol synthesis and trafficking inhibitors on RNA replication of subgenomic replicons of different genotypes. (A) Schematic representation of the experimental setup. Huh7/Lunet cells were electroporated with *in vitro* transcripts of subgenomic *Firefly* luciferase reporter replicons of different genotypes: subgH77 (gt1a) subgCon1ET (gt1b), subgJFH1 (gt2a), subg3a, subg4a, subg5a. For background determination replication deficient replicons were included. 4 h later cells were treated with the respective drug or control. 48 h post electroporation, RNA replication was measured by determining the *Firefly* luciferase activity in cell lysates. (B-E) Cell viability (cell titer glo) as well as *Firefly* luciferase activity was measured in cell lysates and is presented as percentage of control. The mean and standard deviation of at least four independent experiments are shown. Background replication was determined by measuring *Firefly* luciferase activity in cell lysates transfected with the replication deficient replicons. Background is presented as percentage of the replication of genotype 4a and 5a replicons, which harbored the lowest replication efficiency and indicated by the black line. Experiments were performed in triplicates.

3.2.5.3 Effect of sterol synthesis and trafficking inhibitors on the transcript levels of major regulators of sterol homeostasis

No effect of sterol synthesis and trafficking inhibitors on the transcript levels of LDLR, HMGCoAR and ABCA1. With U18666A, Ro 48-8071, Clomiphene citrate and Mevastatin being inhibitors of the sterol synthesis pathway [285, 286], treatment with these compounds potentially induces long term changes in the regulation of the cellular cholesterol metabolism and thus in the absolute levels of cellular free cholesterol. Their main enzymatic targets

within the sterol synthesis pathway are depicted in Figure 3.39A. In general the cellular cholesterol content is controlled by i) LDL receptor mediated lipid uptake ii) by *de novo* synthesis catalyzed by the rate-limiting enzyme the HMGCoA reductase and iii) by cholesterol efflux mediated through cholesterol efflux pumps, the ATP binding cassette transporters ABCA1 and ABGC1. For long-term control the abundance of these proteins is regulated on a transcriptional level, whereas acute modulations occur via protein degradation [215].

We next asked whether the aberrant distribution of free cholesterol and the reduction of viral RNA replication induced by CA drug treatment was linked to the compounds potential to inhibit the sterol synthesis pathway and thus to alter cellular cholesterol homeostasis. Due to experimental limitations that did not allow us to measure the overall free or esterified cholesterol content in drug treated cells, we argued that any drug-induced imbalance in cholesterol homeostasis would potentially be counterbalanced by the above mentioned cellular pathways. Therefore we determined the transcript levels of the three major regulators: the HMGCoA reductase, the LDL receptor and ABCA1 upon drug treatment. To this point cells were treated with the respective concentration of the compounds that had already successfully been used in earlier experiments. We examined the transcript levels of the respective target gene in HCV infected cells, treated with the drug or the control, in comparison to the respective levels in non-infected cells (Figure 3.39B). Virus infection appeared to mildly increase the transcript levels of the HMGCoA reductase or the LDL receptor, while not affecting ABCA1 expression (Figure 3.39B, black bars “control”). Long-term treatment (48 h) at the given concentrations with none of the compounds led to a significant change in the amount of either transcript (Figure 3.39B).

In summary, our results showed that treatment with amphiphilic drugs modified cellular cholesterol and GM1 distribution and concomitantly impaired HCV RNA replication. The latter was also compromised by Mevastatin, which in turn did not induce major changes in the cellular lipid landscape. Although all compounds are (also) inhibitors of the sterol synthesis pathway, no change in the transcript levels of the key regulators was observed upon long-term drug treatment. This indicates that under the given experimental setup, treatment with the cationic amphiphiles might mainly alter cholesterol distribution and does not induce major changes in the intracellular cholesterol concentration.

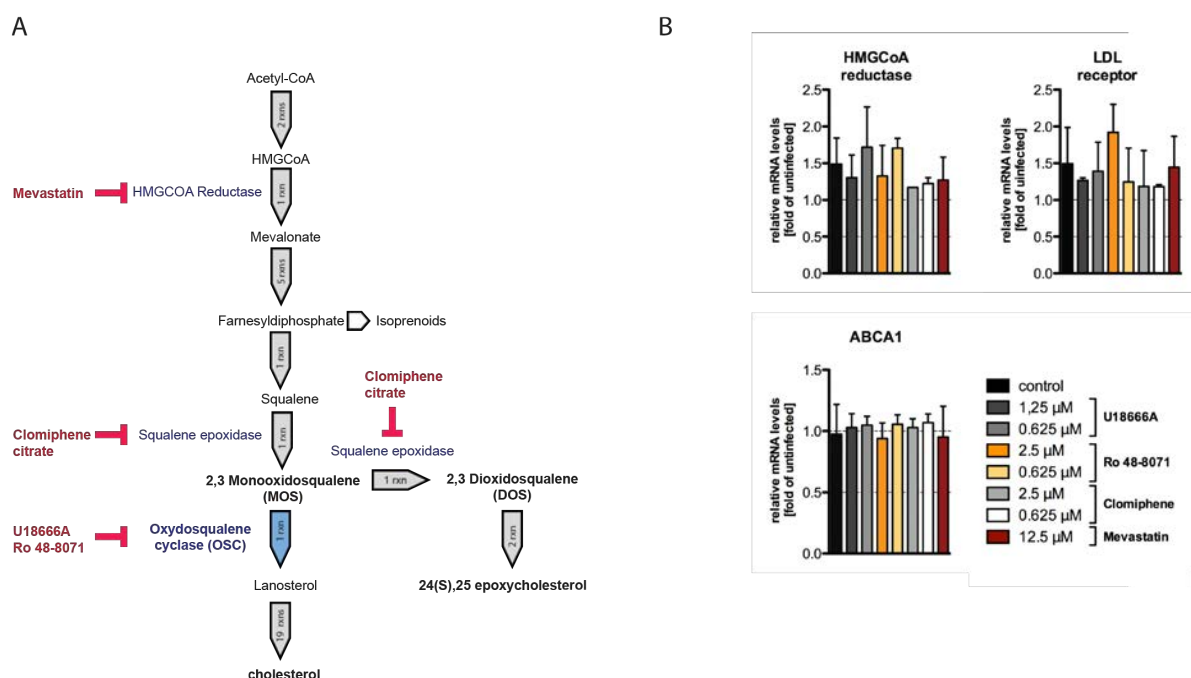


Figure 3.39 Effect of sterol synthesis and trafficking inhibitors on transcript levels of HMGCoA reductase (HMGCoAR), LDLR Receptor (LDLR) and the ATP binding cassette sub-family A member 1 (ABCA1) (A) Schematic representation of enzymes involved in the cholesterol synthesis pathway. The enzymatic targets (blue lettering) of the respective drugs (red lettering) are indicated. In case of U18666A 3 enzymes within the cholesterol synthesis pathway are targeted, but only the one most upstream in the pathway is shown [282, 285]. (B) Effect of drug treatment on the transcript levels of HMGCoA reductase, LDLR and ABCA1. Huh7.5 cells were infected with full-length virus Jc1 (MOI5). 6 h post infection the viral inoculum was removed and media either containing U18666A, Ro 48-8071, Clomiphene, Mevastatin or the control was added. Total cellular RNA was harvested 48 h post infection. The transcript levels of the HMGCoA reductase, LDLR and ABCA1 were determined by RT-qPCR. They were normalized to mRNA levels of GAPDH and are presented as fold of the uninfected control. The mean and standard deviation of two independent experiments performed in duplicates are shown.

3.2.6 Elucidating the biological relevance of endosomal lipid traffic in HCV replication

Given our previous results that indicate the importance of a functional lipid transport through the endosomal pathway in HCV replication, we aimed at elucidating in more detail its' biological relevance for the virus. Our immunofluorescence studies on the distribution of cholesterol upon treatment with CAs indicated a reduced degree of colocalization of NS5A and the lipid marker in presence of the drug (Figure 3.33, Figure 3.35). This suggests an impaired transport of cholesterol to sites of RNA replication. Thus we wondered whether altering the lipids' distribution in cells by treatment with CAs would limit the access of HCV replication sites to plasma membrane derived cholesterol. For this reason we investigated the dynamics of TFC in cells treated with U18666A, the most potent candidate amongst the compounds tested before.

3.2.6.1 Effect of U18666A treatment on Topfluor-Cholesterol dynamics

U18666A treatment alters the distribution of TFC but has no impact on the fluorescent lipid's recruitment velocity. In a first set of experiments we assessed whether U18666A treatment alters the distribution of TFC similarly to what we had observed for endogenous cholesterol. To this end, cells were treated with 1.25 μM U18666A for approximately 48 h. Importantly, U18666A was added to the cells 24 h before the onset of imaging and kept in the supernatant throughout the entire experiment. Given our previous results indicating that U18666A was most effective when added early in replication, we assessed the drug's effect on TFC distribution when added at early as compared to late stages in viral replication. (Figure 3.34E, Figure 3.40).

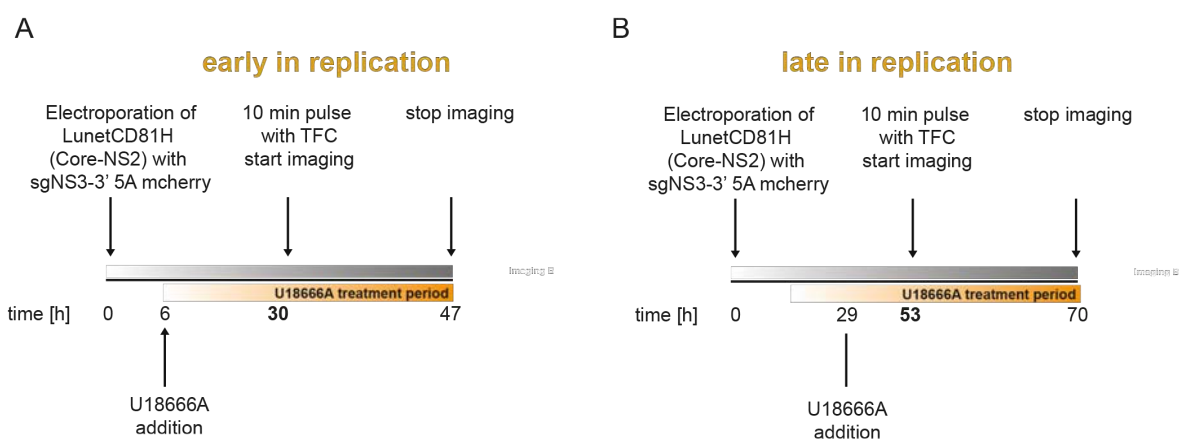


Figure 3.40 Experimental setup of live cell imaging of Topfluor-Cholesterol (TFC) in U18666A treated cells early or late in HCV replication. (A-B) Schematic representation of the live cell imaging setup. Huh7/LunetCD81H cells expressing the viral proteins Core to NS2 were transfected with in vitro transcripts of subgenomic replicon containing mCherry tagged NS5A (sgNS3-3' 5A mCherry, gt2a). (A) "Early replication" setup. 6 h later cells were treated with 1.25 μM U18666A. 30 h post epo cells were pulsed with 1 μM of TFC for 10 min, followed by extensive washing. TFC dynamics were imaged every 15 min for 17 h. (B) "Late replication" setup. Cells were handled as described in (A), however drug treatment was started 29 h post epo and cells were pulsed with TFC 24 h later.

In untreated HCV transfected cells, TFC was observed to accumulate in the perinuclear region (Figure 3.41A, first and third row). Upon treatment with 1.25 μM U18666A TFC was almost exclusively present in large vesicular structures which was similar to the CA induced clustering of endogenous cholesterol (compare Figure 3.41A, second and fourth row and Figure 3.35, Figure 3.33). Although the pattern of TFC localization was altered upon drug treatment, there was no reproducible difference in the intracellular TFC accumulation rate between treated and control cells in early or late phases of replication (Figure 3.41B, C). This indicates that U18666A treatment has no impact on early events in TFC trafficking, but possibly impairs the lipid's egress from late endocytic compartment.

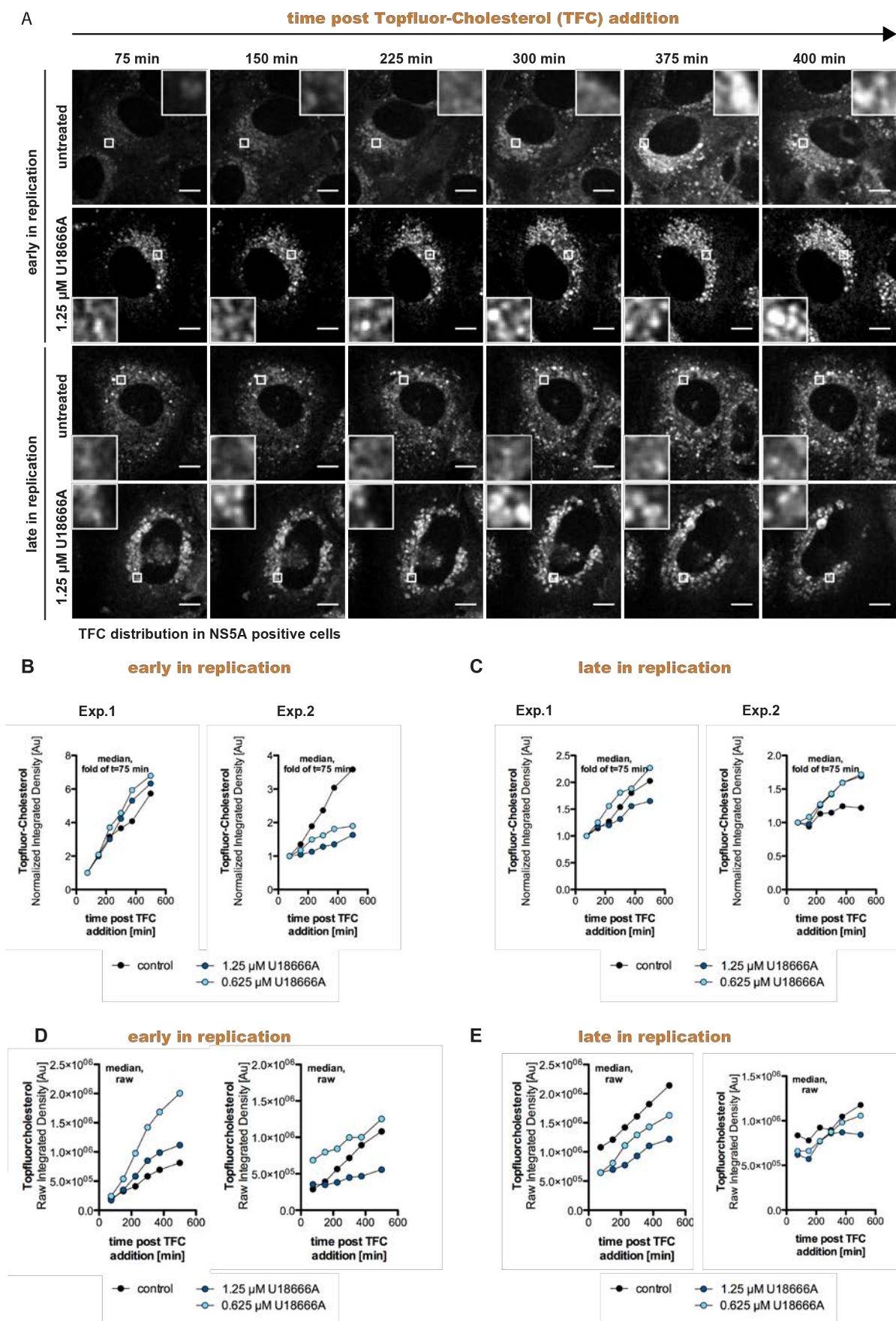


Figure 3.41 Live cell imaging of Topfluor-Cholesterol (TFC) in U18666A treated cells early or late in HCV replication. (A) TFC distribution over time in HCV replicating cells treated with 1.25 μM U18666A as described in Figure 3.40. Representative images of NS5A positive cells are shown indicating the TFC distribution within a single cell from 75 till 400 min post TFC addition. The insets show magnifications of the areas highlighted by the

white rectangle. The scale bars represent 10 μm . **(B-C)** *TFC recruitment velocity of cells treated with different concentrations of U18666A pulsed either early or late in replication.* TFC signal intensities at the perinuclear region were measured over time. The medians of at least 5 cells per condition are shown. The median is presented as fold of the value of the earliest time point of measurement. **(D-E)** *Raw values of the integrated density of intracellular TFC either added (D) early or (E) late in replication.* Results of the two independent experiments depicted in (B, C) are shown.

In agreement with this we observed that the raw signal intensities, early upon TFC addition, were elevated in cells treated with U18666A early in replication as compared to the control cells, indicating an intracellular accumulation of TFC (Figure 3.42D). However, this was not the case when TFC was added late in replication (Figure 3.42E).

Our previous studies in fixed cells revealed an exclusion of cholesterol from NS5A positive sites upon drug treatment. Thus we wondered whether U18666A treatment might interfere with the traffic of PM-derived TFC to NS5A positive sites. To this point we analyzed the degree of NS5A and TFC signal overlap over time (Figure 3.42). The assessment of NS5A protein levels indicated a slight decrease of NS5A signal intensity upon treatment early in replication, while they remained unaltered late in replication (Figure 3.42B). In untreated cells NS5A and TFC partially co-localized and the degree of signal overlap increased over time (Figure 3.42A, C, D). U18666A treatment did not cause an apparent alteration in the degree of signal overlap throughout the first 500 min of imaging (Figure 3.42C, D).

Taken together U18666A alters the partitioning of TFC inducing its accumulation in dilated vesicles. Nevertheless the exogenously added fluorescent cholesterol was found to be efficiently trafficked to NS5A positive sites irrespectively of the presence or absence of the drug.

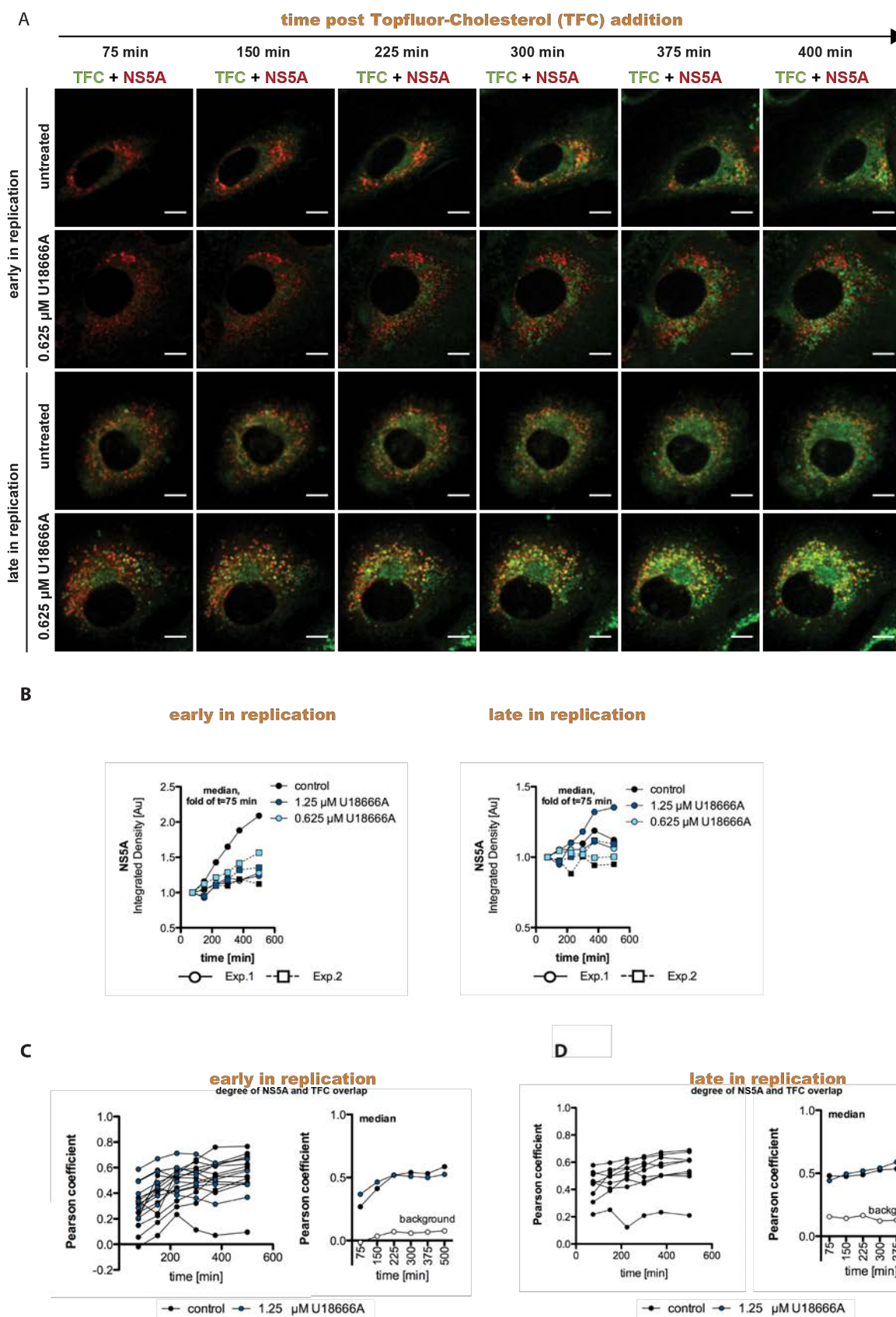


Figure 3.42 Live cell imaging of Topfluor-Cholesterol (TFC) and NS5AmCherry in U18666A treated cells early or late in HCV replication. (A) TFC and NS5A distribution over time in HCV replicating cells treated with 0.625 μM U18666A as described in Figure 3.40. Representative images are shown indicating the TFC and NS5A distribution within a single cell from 75 till 400 min TFC post addition. The scale bars represent 10 μm . (B) NS5A signal intensities of cells treated with different concentrations of U18666A and pulsed with TFC either early or late in replication. The medians of at least 5 cells per condition are shown. Two independent experiments are

depicted. The median is presented as fold of the value of the earliest time point of measurement. (C-D) *Degree of NS5A and TFC signal overlap over time.* The Pearson correlation coefficient (PCC) was determined over time starting from 75 min post TFC addition. The left of both panels represents the PCC determined in single cells over time, while the results are summarized in the right panel and the median of each condition is presented. Quantification of a single experiment is shown.

3.2.6.2 Effect of U18666A treatment on the ultrastructure of the HCV induced membranous web

U18666A treatment has no significant effect on DMV morphology. Functional studies on the role of cholesterol in HCV replication showed that its depletion causes a reduction in viral RNA replication and reduces the size of DMVs [79, 114]. Accordingly, our study suggests the importance of cholesterol traffic through the endo-/lysosomal pathway in viral replication with the lipid being transported from the plasma membrane to NS5A positive sites, thus potentially to DMVs. In order to address the question whether DMVs acquire cholesterol through the endo-/lysosomal pathway we analyzed the HCV induced membranous web by transmission electron microscopy upon U18666A treatment. Our previous results indicated a higher sensitivity of genotype 1b replication towards CA treatment as compared to genotype 2a (Figure 3.34 Figure 3.37 and Figure 3.38). For this reason we compared the drugs impact on the membranous web induced by the expression of the NS proteins of either genotype. To circumvent protein loss upon U18666A treatment when using a replication-based system, we made use of the T7-RNA polymerase-based expression system. This allowed us to study potential effects of U18666A on membranous web formation independently from its impact on viral replication and thus viral protein levels. To this end, Huh7/Lunet-T7 cells were pretreated for 24 h with U18666A. Next, they were transfected with the given expression constructs encoding the non-structural protein expression cassette (NS3-5B) derived from gt1b or 2a and cultured for another 24 h in presence of the drug (Figure 3.43A). To control for drug efficiency under the given experimental treatment conditions, the subcellular distribution of free cholesterol was analyzed by indirect immunofluorescence, which corroborated our previous findings of U18666A-induced vesicular accumulation of endogenous cholesterol (Supplementary figure 6, Figure 3.33, Figure 3.35) Furthermore NS5A protein levels were determined to ensure similar protein expression in the different samples (Figure 3.43B B). Indeed incubating the cells with the highest concentration (1.25 μ M U18666A) appeared to reduce NS5A protein levels as compared to the control, probably due to a diminished cell growth. In collaboration with Dr. I. Romero-Brey alterations of the membranous web morphology, namely in DMV size/diameter, were analyzed by using transmission electron microscopy. Our analysis indicated that treatment with the highest dose of 0.625 μ M U18666A that did not affect NS5A protein levels, did not have a significant

effect on DMV size, while the higher dose mildly increased vesicle diameter (Figure 3.43C-F).

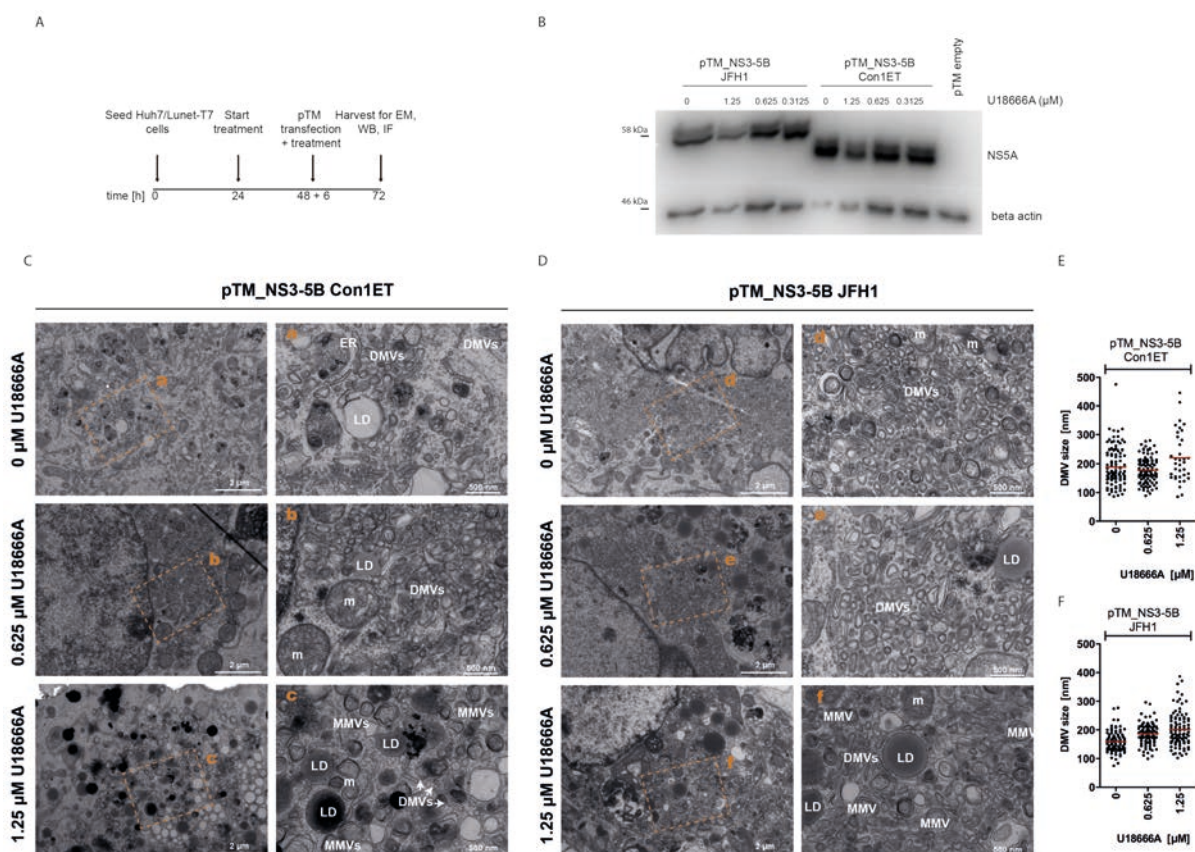


Figure 3.43 Effect of U18666A on HCV induced membranous web. (A) Scheme of experimental setup. Huh7/Lunet cells (Zeocin) were treated for 24 h with U18666A or the control prior to transfection of the pTM expression constructs encoding the NS3-5B expression cassette of genotype 2a (JFH1) or 1b (Con1ET). 6 h post transfection, the medium was replaced by drug containing medium. 24 h post transfection, cells were processed for immunofluorescence, Western Blot and transmission electron microscopy analysis. (B) NS5A protein levels as determined by Western Blot. Beta actin served as loading control. Protein levels were determined in cell lysates harvested at the end of the experiment. (C-D) Transmission electron microscopy analysis of the membranous web. Representative transmission electron microscopy pictures of cells expressing the nonstructural proteins NS3-5B of (C) Con1ET or (D) JFH1 in presence or absence of the drug. The yellow box indicates the area depicted in the adjacent picture. LD= lipid droplet, DMVs= double membrane vesicles, MMVs= multi membrane vesicles, m= mitochondria, ER= endoplasmic reticulum. (E-F): Quantification of DMV size. The results of a single experiment are shown.

Taken together, we observed that U18666A treatment caused an aberrant accumulation of (exogenously added) TFC in vesicular structures that clustered at the perinuclear region of the cytoplasm but it did not alter the colocalization of TFC with the viral protein NS5A. Additionally, CA treatment did not lead to a reduction in DMV size as determined by measuring DMV diameter.

4 Discussion

4.1 A comparative RNAi screen targeting potential LD-factors to study their implications in the replication cycle of HCV and DENV

4.1.1 RNAi screen analysis

Here we report for the **first** time of the performance of a **bipartite RNAi screen** that aimed at identifying host factors of human hepatoma cells involved in LD homeostasis and at unraveling their potential implication in the full replication cycle of the hepatotropic HCV and the related DENV. In our comparative RNAi screen the effect of gene knockdown on LD morphology was analyzed in a microscopy based approach, while the effect of gene silencing on the complete replication cycle of HCV and DENV was investigated using *Renilla* luciferase reporter viruses (Figure 3.1). Using this approach we were able to identify host factors potentially involved in the replication cycle of HCV and/or DENV as well as in the regulation of LD homeostasis in human hepatoma cells (Figure 3.5).

Analysis of the **performance of the controls** throughout the **primary screening** process revealed a robust performance of the screen (Figure 3.2). In line with this we were able to confirm the involvement of already established host factors such as members of the DEAD box RNA helicase family including DDX3 and DDX6, in early events of the replication cycle of HCV and DENV respectively, which highlights the reliability of the screen setup [154, 259]. In addition, our screen implicated a novel role of DDX3 in later stages of both viruses, which was the main focus of the herein presented follow-up studies.

A general major concern when analyzing RNAi data is inherent to the nature of RNAi itself that might cause the identification of false positives due to off-target effects [290]. These effects are caused by imperfect pairing of siRNA strands with sequence motifs within mRNAs that are not the intentional targets. Other off-target effects can be caused by innate immune responses to either the oligonucleotide or the delivery vehicle [290]. The use of oligo pools in addition to chemical modifications of the RNAi target sequence has been implemented to reduce the off-target effects caused by either way. In this study the primary LD and the LTP screen were performed with ON-TARGETplus® SMARTpools. According to the manufacturer these siRNA species are chemically modified in such a way that off-target effects are decreased, however cannot be ruled out completely [291]. Thus a common strategy to strengthen the reliability of RNAi screen data is the performance of a deconvolution screen, using four different oligos that are comprised in the siRNA pool of the primary screen [257]. Our **deconvolution screen** confirmed the importance of 67.6% of all primary hits in the replication cycle of either HCV or DENV. The hit recovery was largest for candidates

identified to be specific for HCV, highlighting the central role of LD-associated pathways in the HCV replication cycle (Figure 3.3). Interestingly, in case of HCV more candidates appeared to be involved in early as compared to late events of the HCV replication cycle (Figure 3.3A, Supplementary Table S 3). LDs are largely accepted to play a role in HCV assembly [116, 255], but their potential implication in earlier steps might so far have been underestimated. In fact, being storages of neutral lipids, such as cholesteryl esters and triacylglycerides [232], LDs could serve as sources of lipids to support the formation of the HCV induced membranous web. In addition HCV might usurp LDs in order to generate energy through beta-oxidation of fatty acids to support energy-demanding steps in viral replication. Interestingly, something similar has been reported for DENV [147]. The number of hit candidates affecting early or late steps of the DENV life cycle was similar (Figure 3.3A, Supplementary Table S 3).

Regarding the LD morphology RNAi screen, changes induced by Triacsin C (inhibitor of LD formation) or oleic acid treatment (stimulator of LD formation) were very well detected using our screen setup. However, in spite of this apparent good performance, candidates identified through this screen should be taken with caution. While our screen confirmed the involvement of 25.7% of all candidates tested in LD homeostasis in human hepatoma cells, the general impact of gene knockdown of these candidates on LD morphology was mild. Although a wide panel of LD morphology features was analyzed (Figure 3.1B, table) gene knockdown of hit candidates most often caused only mild alterations of a single feature (Supplementary Table S 2). Taken together this indicates, that while the controls were resulting in a profound „black and white phenotype“, smaller alterations in LD morphology upon gene knockdown were hardly detectable. Therefore siRNAs targeting host factors known to alter neutral lipid synthesis could represent a more appropriate measure for the sensitivity of our image-based readout. In fact our screen included siRNAs targeting ACAT (Acyl-coenzyme A: cholesterol acetyltransferase 2, catalyzing the esterification of cholesterol to cholesteryl esters [292]), DGAT1 (diacylglycerol O-acyltransferase 1, catalyzes the last step in triacylglycerol synthesis, [293]) both involved in the synthesis of neutral lipids, as well as the transcription factor SREBP and its co-factor SCAP, both known to regulate the expression of lipogenic genes [220]. One might expect that knockdown of these genes should affect the cellular neutral lipid content. However knockdown of either of these candidates did not alter LD morphology significantly in our RNAi screen (Supplementary Table S 2). Thus the herein presented image-based high content screen might not have been sensitive enough to detect small alterations in the cellular neutral lipid content. There are plenty of factors, such as a heterogeneous behavior of the cell population, differences in cell growth, RNAi transfection or infection efficiency and many more that influence the

outcome of RNAi screens and that render hit calling difficult. Especially in case of image-based readouts subtle differences in the handling of the samples might lead to substantial differences in the staining efficiency that cannot be easily controlled.

4.1.2 Potential role of COPI in HCV and DENV particle production as well as LD homeostasis

Bioinformatic analysis of our screen data revealed the involvement of the **Coat protein complex I**, of the nuclear ubiquitin-proteasome system, of the cell cycle control machinery, of the EIF3 translation initiation complex as well as of members of the spliceosome in the replication cycle of HCV and DENV and LD homeostasis (Figure 3.5). While the involvement of the coat protein complex I in HCV RNA replication has been reported earlier [258, 294] our screen results suggests a novel role of COPI function in particle production of both viruses (Figure 3.2A). Due to the 'housekeeping' nature of this macromolecular complex studying its involvement in the replication cycle of these viruses or LD homeostasis might be difficult. Indeed our attempts to gain a better insight into the role of the Coat protein complex I mediated trafficking in virus infection or LD morphology were substantially hampered by the essential role governed by this complex in cell survival and by a low reproducibility of the results using RNAi-mediated interference (Supplementary Figure 1). So far the function of COPI in the viral replication cycle of either virus has not been elucidated, but several hypotheses have been put forward.

Two independent studies reported that gene knockdown of specific **COPI subunits** or pharmacological inhibition of COPI function impairs **HCV genome replication** [258, 294]. Based on the observation that knockdown of factors involved in COPI recruitment caused a shift of NS5A from ER-like localization to LDs, which was concomitant to a reduction in viral RNA replication, Matto et al. hypothesized that COPI function might regulate the localization of NS proteins at the ER and LDs respectively [294]. According to another report COPI function might serve to remove the phosphatase Sac1 from PtdIns4P rich replication sites in order to maintain high local PtdIns4P levels and thus potentially the integrity of the membranous web [295]. The involvement of proteins of the secretory pathway in RNA replication and potentially in replication site formation has also been studied for the enterovirus Cocksackivirus B3 (CVB3) (*Picornaviridae* family). Some members of the *Picornaviridae* are known to cause substantial endomembrane remodeling, possibly membranes derived from the Golgi and the ER, to generate the viral replication organelles [130]. While one report suggested the involvement of components of the COPI trafficking machinery in the recruitment of the PI4KIIIbeta and the formation of the viral replication

organelles, this was refuted by a more recent study [296, 297]. Whether COPI could function in the generation or maintenance of the HCV induced membranous web remains to be elucidated. In line with this, our screen indicated that knockdown of several COPI components impaired early steps in the replication of HCV (Fig 3.2).

Intriguingly our screen data suggests a so far **novel role of COPI in restricting assembly and release of HCV and DENV particle production** (Figure 3.2A, Figure 3.6B). An interesting observation was made in *Drosophila* and HeLa cells, which showed that knockdown of COPI subunits caused a decreased localization of ATGL (adipose triglyceride lipase, catalyzes the first step in TAG hydrolysis) to the LD surface [237, 298]. Thus COPI function appears to regulate the association of proteins to LDs. This might further explain the observed over-storage of neutral lipids upon loss of COPI function [236, 237]. Hence one possibility could be that COPI alters the accessibility of cytosolic LDs through the HCV or DENV core/ capsid proteins. In case of HCV it was suggested that targeting of the viral core protein to LDs is of importance for the protein's stability and thus for infectious particle production [138, 299]. Similar could account for DENV. As mentioned earlier, gene knockdown or pharmacological inhibition of COPI function in *drosophila* cells has been reported to enhance neutral lipid storage, characterized by enlarged LDs [237]. In agreement with this, our screen identified COPI components as important regulators of neutral lipid storage in human hepatoma cells (Figure 3.2B, Figure 3.6B). One can only speculate about the importance of lipid storage induction in infectious particle production of either virus. It has been shown that ablation of LDs through Triacsin C treatment only mildly impaired HCV RNA replication but had a more profound negative effect on infectious particle production, potentially due to the concomitant decrease in core protein levels [299]. Thus enhancing neutral lipid storage might increase the LD-core interaction platform, thereby promoting the protein's stability and potentially its engagement in nucleocapsid formation. This is further supported by the observation that NS5A-mediated transfer of HCV genomic RNA from replication sites to core at LDs is essential for infectious particle production [71, 81]. In case of DENV, it is far less understood whether capsid at LDs is indeed involved in particle production [148]. Interestingly it has been reported that LDs could act as storage depots for excess proteins [300]. Accordingly COPI function could regulate the association of the viral core or capsid proteins with LDs and thereby their availability during the course of viral infection. Future studies could commence with the analysis of the dependence of the viral core/capsid protein's association with LDs on COPI function.

4.1.3 High hit rate of LD RNAi screen indicates central role of the lipid storage organelle in the replication cycles of LD-dependent viruses

Statistical analysis of the **hypothesis driven RNAi** screen data revealed that by targeting LD-associated pathways there was a high probability of affecting the replication of either one of the LD-dependent viruses. Indeed 57.8% of all candidates analyzed in the primary screen were important for either virus or both (Figure 3.4A). This hit rate is substantially higher when compared to the approximately 1% hit rate of other published high content screens [301] (Acosta and Fischl, unpublished) or to the 15 to 25% hit rate of two kinase screens performed for DENV or HCV respectively (Kumar and Cortese, unpublished) [77]. Of the genes identified to affect LD homeostasis in human hepatoma cells (Figure 3.4B), even 76.3% of the candidates were shown to be involved in the viral replication cycles. Interestingly more LD hits were specifically affecting HCV (23.7%) as compared to DENV (10.2%) (Figure 3.4C). This indicates that LD related pathways are of central importance especially for the highly liver-tropic HCV and are potentially less relevant for DENV. Indeed, almost every step in the HCV replication cycle is tightly linked to the lipid metabolism of hepatocytes, the latter process possibly being influenced by cellular LDs [302]. In line with this it is suggested that cytosolic LDs might serve as platforms that support the assembly of infectious virions. This hypothesis is supported by the findings that the recruitment of the viral core protein and replicase components to cytosolic LDs is essential for particle assembly, as well as by the observation of LDs being present at close proximity of the membranous web and of particle-like structures [81, 113, 136]. HCV was shown to hijack the VLDL synthesis pathway for infectious particle production, whose lipids might ultimately derive from ER-luminal LDs. It could be at sites of luminal LDs, where viral particle production merges with VLDL synthesis [116]. Additionally HCV infection has been linked to steatosis, characterized by an increased fat (neutral lipid) content of the liver, possibly attributed to the presence of the viral core protein [303]. Taken together it is not surprising that targeting LD-related pathways strongly alters the replication cycle of the liver-tropic hepatitis C virus. In case of DENV, the role of LDs is far less understood and discussed controversially. While some reports suggest a virus induced autophagy-dependent degradation of LDs for energy supply, others reported enhanced neutral lipid storage upon DENV infection [146, 147]. The function of DENV capsid recruitment to LDs remains enigmatic, but could promote the coordination of viral RNA replication and particle production by sequestering the capsid protein to prevent unscheduled RNA encapsidation [146, 148]. As mentioned before, our screen data suggests, that DENV is far less dependent on the cellular lipid metabolism of human hepatocytes as compared to HCV. This is in line with the fact that while HCV is mainly liver-tropic, DENV targets mainly inflammatory cells such as dendritic cells (DCs), monocytes and macrophages as well as other various tissues including spleen, kidney, liver and lung [144].

Interestingly, numerous other pathogens usurp LDs during their replication cycle. Rotaviruses (family *Reoviridae*, genus *Rotavirus*) were shown to depend on LD components for the formation of viroplasms, the sites of early viral morphogenesis and viral RNA replication [304]. Orthoreovirus (family *Reoviridae*, genus *Orthoreovirus*) outer capsid protein μ 1 was reported to bind to LDs, mitochondria and the ER through amphipathic helices at the protein's C-terminus which appears to be linked to the induction of apoptosis [230, 305]. Besides their role in cellular lipid metabolism, LDs have been implicated in innate immune signaling. For instance the cellular protein viperin (virus inhibitory protein ER associated interferon inducible) potentially exerts its antiviral activity against HCV through its interaction with NS5A at LDs and at the viral replication sites [306]. In contrast, the localization of viperin to LDs is dispensable for its antiviral activity against DENV [307].

Taken together, the so far neglected lipid storage organelle appears to be of central importance for multiple human pathogens. Given the importance of LDs not only in cellular lipid homeostasis, but also in the regulation of inflammatory responses, a better understanding of the intimate link between pathogens and LDs is essential in order to exploit this knowledge for the generation of antiviral therapeutics. Unravelling the mechanisms that control LD function, such as the potential involvement of COPI-mediated regulation of the LD protein coat, could pave the path for novel strategies to fight pathogen mediated infections. Several pharmaceutical companies developed and tested DGAT1 inhibitors in mice that showed that administration of these inhibitors led besides others to weight loss and to a reduction in serum and liver triacylglycerides. Thus these inhibitors could represent useful candidates for the treatment of metabolic disorders [308]. Intriguingly DGAT1 catalyzes the last step in triacylglycerol synthesis and has been shown to be an important dependency factor for HCV infectious particle production [139]. Therefore, targeting LD function through DGAT1 might represent a valuable tool to fight HCV infection. Unfortunately, the above-mentioned DGAT1 inhibitors had severe adverse effects in humans, which was suggested to be caused by the build-up of diacylglycerols and fatty acids upon DGAT1 inhibition [308]. In conclusion, while identifying host factors involved in the regulation of LD function could open new routes for the development of therapeutics, targeting an organelle of key importance in cellular lipid metabolism might remain challenging.

4.1.4 Studying the role of the DEAD box RNA helicase 3 in the replication cycle of HCV and DENV

Additional to the already described involvement of DDX3 in early events of the HCV replication cycle [76, 154] our screen implicated a novel function in particle morphogenesis of HCV and DENV.

4.1.4.1 Evaluation of the involvement of DDX3 in the full replication cycle of HCV or DENV

A set of siRNA-mediated knockdown experiments aimed to re-evaluate the screen results (Figure 3.7, Figure 3.8, Figure 3.9). We were able to confirm the proviral role of **DDX3 in early events** of the **HCV replication cycle**. Indeed, gene knockdown of DDX3 caused a significant reduction of entry and replication of genotype 2a HCV reporter virus (Figure 3.7B). This is in line with a previous siRNA screen that identified the role of DDX3 in early events of full-length reporter virus replication of the same genotype [76]. Ariumi et al. were the first to describe a potential involvement of this RNA helicase in HCV genome replication by the use of stable genotype 1b replicon cell lines [154]. Interestingly our results revealed that the replication of a genotype 2a replicon was not altered upon DDX3 gene knockdown while genotype 1b replication was mildly reduced. The fact that, under the experimental conditions tested, DDX3 gene knockdown strongly impaired early events of the replication cycle of genotype 2a reporter virus, but had no impact on replication of a stable genotype 2a replicon, could imply that this **DEAD box RNA helicase is mainly involved in virus entry** prior to RNA translation and replication or **in the early post-entry events** leading to the establishment of replication. In a recent RNAi screen follow-up study, multiple *in vitro* HCV model systems were applied (i.e. HCV_{pp}, HCV_{cc}, subgenomic replicons) in order elaborate the precise step in the viral replication cycle affected by selected host factors. This revealed the importance of DDX3 in entry of HCV_{pp} (clathrin-dependent entry) but also of the unrelated VSV_{pp} (Vesicular stomatitis, clathrin-dependent entry) and MLV_{pp} (Murine leukemia virus, clathrin-independent entry) [157] possibly indicating a more general role of DDX3 in endocytic events. The same study further reported the importance of DDX3 in replication of a genotype 2a subgenomic replicon. Thus an involvement of **DDX3 in viral RNA replication** is likely, although we were not able to recapitulate this, which could possibly be due to an inefficient sustained gene knockdown by transient siRNA transfection. Nevertheless it seems that the viral subgenomic replicons used in this study (Con1_ET (gt1b) and JFH1 (gt2a)) differ in their sensitivity towards DDX3 gene knockdown. In this respect it is interesting to note, that throughout our studies on host factors and their implications in the viral replication

cycle we repeatedly observed a higher sensitivity of the cell culture adapted Con1_ET replicon (three replication enhancing mutations in NS3 (T1280I and E1202G) and NS4B (K1846T) [86]) towards manipulation of the cellular environment when compared to the genotype 2a counterpart (Figure 3.20, Figure 3.34, Figure 3.37, Figure 3.38). Early after the establishment of genotype 1b and 2a replicon systems, with the latter one being capable of high RNA replication without the need of replication enhancing mutations, it was observed that genotype 2a replication was more robust towards IFN α treatment when compared to genotype 1b [309]. The molecular mechanism that could account for this discrepancy and whether this is due to the diverging genomic sequences remains elusive. A very recent report documented that the over-expression of a specific host factor (Sec14L2) allowed the replication of *wild-type* replicons of various genotypes (gt1a, 1b, 2a (J6), 3a, 4a, 5a) in human hepatoma cells, which usually requires the presence of adaptive mutations. In contrast the respective cell culture adaptive mutant replicons and the JFH1 replicon were only moderately influenced by Sec14L2 expression [310]. This could be a mechanism by which cell culture adapted mutants acquire the ability to cope with the lack of a proviral factor or to circumvent the negative effects of a restriction factor present in human hepatoma cells. This could further point to a differential dependency of distinct genotypes (including their *wild-type* or cell culture adapted mutant variants) on host factors and therefore could account for the different sensitivities of subgenomic Con1ET or JFH1 RNA replication towards DDX3 gene silencing.

In conclusion **DDX3 is likely to be involved in virus entry and genomic RNA replication** of HCV. So far the precise role in either step has not been elucidated. Initial data on Human Cytomegalovirus indicated a proviral involvement of DDX3 in virus spread and its incorporation into the virion [311]. Similarly, DDX3 was found to interact with HBV polymerase (Pol) and to become incorporated into HBV nucleocapsids. In this context, DDX3 was suggested to act as host restriction factor of HBV possibly inhibiting viral reverse transcription. [312, 313]. Whether DDX3 is also incorporated into the infectious HCV particle remains to be determined. Indeed, DDX3 was shown to bind the 3' NTR of the viral (+) RNA and could thus become part of the assembled particles [314].

DDX3 is a multifunctional protein implicated in several processes involving RNA (RNA splicing, mRNA export, transcriptional and translational regulation, ribosome biogenesis), cell cycle control and apoptosis [151]. Its pleiotropic functions in RNA metabolism might be usurped by HCV. Some reports claim that DDX3 suppresses cap-dependent translation but in turn enhances translation of highly structured 5' NTRs. Details on the underlying mechanisms are ambiguous and it remains unclear whether DDX3 can indeed regulate the

translation of specific transcripts and whether this would also apply to HCV IRES mediated RNA translation [315].

Our screen further indicated a **novel proviral role of DDX3 in particle production of DENV**, which we were not able to recapitulate in our transient siRNA knockdown experiments (Figure 3.2, Figure 3.7C). Not much is known about the role of DDX3 in the DENV replication cycle. It was reported that DDX3 interacts with the viral RdRp NS5 and that interference with DDX3 protein expression impairs steps in viral RNA replication in Huh7.5 cells [153]. However, a more recent report showed that DDX3 gene silencing promotes viral replication in interferon competent HEK293T cells, which contain in contrast to Huh7.5 cells a functional RIG-I mediated interferon pathway. These results indicated an antiviral role of the cellular RNA helicase, possibly by modulating the antiviral innate signaling and the induction of type I IFN production in response to DENV infection [316]. Given that our silencing experiments were performed using the interferon defective cell line Huh7.5FLuc we may have missed the antiviral effect of DDX3. This issue will be discussed in more detail later in context of the role of DDX3 in HCV infections. Taken together present data on the role of DDX3 in the DENV replication cycle is ambiguous.

4.1.4.2 Studying the implication of DDX3 recruitment by the HCV core protein in the viral replication cycle

In addition to the already described role of DDX3 in early events of HCV replication, our screen described a novel proviral function of this host factor in HCV particle production (Figure 3.2). Indeed transient DDX3 gene knockdown by siRNA transfection revealed a slight but significant reduction in infectious particle production (Figure 3.9).

Studying the **cellular localization of DDX3** in HCV or DENV infected cells we observed a relocalization of the cytosolic protein pool to core covered lipid droplets in HCV but not in DENV infected cells (Figure 3.10). Thus, one might argue that HCV- or DENV-induced changes of the LD protein coat, i.e. through the association of the viral core/ capsid proteins to LDs, do not contribute to the recruitment of the cellular helicase. Instead, DDX3 relocalization may result from a specific recruitment of the RNA helicase through determinants inherent to HCV proteins present at LDs. In line with earlier publications we identified the HCV core protein as sole determinant for DDX3 relocalization (Figure 3.11). [154]. However, we cannot exclude the involvement of other cellular proteins or of cellular or viral RNA acting as linker between both RNA binding proteins. When comparing the localization of DDX3 in cells transfected with the low assembly competent JFH1 or the

assembly deficient Jc1 Δ E1E2 or with the highly assembly competent Jc1 we observed a correlation of LD core coverage with the DDX3 relocalization efficiency (Figure 3.12). In line with an earlier report we could observe a prominent localization of the JFH1 core as well of the Jc1 core of the assembly mutant (Jc1 Δ E1E2) at LDs, while the Jc1 core labeled only few LDs (Figure 3.12) [264]. Concomitantly, DDX3 was relocalized in almost all cells replicating JFH1 or Jc1 Δ E1E2, while in case of Jc1 transfected cells, only few cells showed a profound relocalization of the cellular RNA helicase (Figure 3.12). This is not surprising, given that the viral core protein was found to be the prime determinant causing the relocalization of DDX3 (Figure 3.11).

Earlier studies showed that disrupting the DDX3-core interaction by the Y35A point mutation in HCV core had no significant effect on the viral replication cycle of JFH1 (genotype 2a) [260]. In contrast, others reported that the expression of core peptides capable of binding DDX3 were interfering with genotype 1b RNA replication, which could be rescued by the overexpression of DDX3. The same study further reported that the introduction of such core peptides did not alter the full replication cycle of genotype 2a virus [261]. This points to a varying importance of DDX3 in the replication cycle of distinct HCV genotypes. Therefore we wondered whether there are genotype-specific sensitivities towards disrupting the relocalization of DDX3 to LDs. In fact, we were curious to elucidate whether there might be differences in the virus's sensitivities towards the loss of DDX3 recruitment that could be correlated with the apparent differences in the virion production efficiencies.

To this end, **two single point mutations** (Y35A or F24A) were introduced into the HCV core protein of different inter/intra-genotypic chimeras. These point mutations have earlier been described to interfere with the interaction of the viral core protein with the cellular DEAD box RNA helicase 3 [260]. By the use of inter/intra-genotypic chimeras we aimed to compare their sensitivity towards loss of DDX3 recruitment. These chimeras share similar sequence of the replicase module (NS3-5B) of JFH1 (genotype 2a) and replicate to similar extent (Figure 3.17C). However, the assembly module, the core-NS2 sequence, derives from isolates of different genotypes and subtypes (2a, 1a, 1b). The J6/JFH1 chimera results in the production of the highest titers, Con1/JFH1 and H77/JFH1 show intermediate particle production efficiencies, while JFH1 (*wild-type*) produces only low levels of infectious particles (Figure 3.13) [262]. Using this approach, we were able to confirm that both mutations **caused a loss in DDX3 relocalization**, which in turn remained evenly distributed in the cytosol of cells transfected with the mutant virus (Figure 3.14, Figure 3.16).

We next aimed to elucidate whether infectious particle production of these chimeras was differentially sensitive towards loss of DDX3 recruitment by analyzing the impact of the selected point mutations on the viral replication cycle. We found that **disrupting the localization of DDX3 to HCV core at LDs had no significant impact on steps of viral RNA replication of the different inter/intra-genotypic chimeras** (Figure 3.15, Figure 3.17). This stands in agreement with an earlier report that showed that the core-DDX3 interaction was dispensable for RNA replication of JFH1 (genotype 2a) [260]. Note, that the viral chimeras used in this study share the replicase cassette of genotype 2a. As mentioned before, others reported that the expression of a core peptide capable of binding DDX3 impaired subgenomic RNA replication of a genotype 1b replicon [261]. Given this discrepancy one might speculate that the importance of **DDX3 recruitment to LDs by the HCV core protein in viral RNA replication might depend on the viral genotype** studied.

A considerable drawback in our study on the **effect of disrupting DDX3 localization to HCV core at LDs on HCV particle production** was the partially reduced level of mutant core proteins. In fact, all Y35A core mutants, but only some of the F24A mutants showed reduced core protein levels when compared to their respective *wild-type* counterparts. This could account for the impaired production in infectious particles. Nevertheless there was no good correlation between the reduced amounts of core protein levels with the extent of impairment of infectious particle production, what makes it difficult to unambiguously conclude that the lower titers are a direct consequence of the lower expression of core (Figure 3.15, Figure 3.17).

Finally we observed that **DDX3 gene knockdown impaired infectious particle production of F24A mutant chimeras to similar extent as compared to the corresponding wild-type virus** (Figure 3.19). Thus we conclude that inhibiting DDX3 recruitment to LDs does not affect its ability to support HCV particle production. In turn, changing the intrinsic properties of the core protein through the insertion of either one of the two studied point mutations might be the reason for the impairment in infectious particle production (Figure 3.17C). This has several implications for the understanding of the role of DDX3 *per se* and of its recruitment to LDs by the viral core protein in the HCV replication cycle.

First, it appears that the **recruitment of DDX3 to lipid droplets by the HCV core protein is dispensable** for its function in the **full replication cycle of HCV in the human hepatoma cell line Huh7/Lunet** used in this study. Nevertheless this function might be important in a more authentic cell system. As mentioned before, human hepatoma Huh7 cells were shown to have a low type I interferon (IFN) production in response to viral infection and also to

respond only poorly to IFNs [317]. The herein used Huh7/Lunet cells are derived from Huh7 cells, that were cured from the replication of a subgenomic replicon, and represent a highly permissive cell line for HCV RNA replication [239]. There are several reports describing the involvement of DDX3 in type I IFN induction but the protein's exact functions are unknown. Being a DEAD box RNA helicase DDX3 could potentially act as viral RNA sensor. However the protein lacks of a signaling domain similar to the one found in the innate immune receptors RIG-I (retinoic acid inducible gene) or MDA-5 (melanoma differentiation antigen 5) [150, 318]. DDX3 was found to contribute to type I IFN induction and act at different levels of the signaling cascade. It was reported that DDX3 binds to MAVS and thereby upregulates the RIG-I mediated IFN β promoter induction [319]. DDX3 was further suggested to act more downstream in the signaling cascade as signaling intermediate [152] or even as transcriptional activator of the IFN β promoter [319]. All in all, while the precise mechanism remains elusive, DDX3 supports type I IFN production upon viral infection. Given that the cell line used in this study induces type I IFN only to very low levels upon viral infection, it could be that a possible benefit of recruiting DDX3 to LDs is only relevant in an immunocompetent environment. Thus one could hypothesize that HCV core-mediated sequestration of DDX3 at LDs aids to remove it from sites of innate induction and thus serves to counteract the cellular antiviral response. Whether this hypothesis holds true or not remains to be determined in a more authentic immunocompetent cell system. Intriguingly, studies based on overexpression of DDX3, MAVS and the JFH1 core protein indicated that the viral protein interferes with the DDX3 mediated promotion of MAVS-induced IFN β promoter activity [320].

Deregulation of DDX3 has also been ascribed to tumorigenesis. In breast cancer, DDX3 is suggested to act as oncogene, while in case of hepatocellular carcinoma (HCC) (in particular of HBV positive patients) DDX3 has been found to be downregulated. The underlying mechanisms appear to be different but possibly include the transcriptional control of genes promoting or suppressing tumorigenesis by DDX3 [151]. Sequestration of DDX3 through the binding to the viral core protein might thus represent a strategy of the virus to interfere with the protein's tumorsuppressive activity and could promote HCC.

Given the results obtained so far, the purpose of the core-dependent DDX3 recruitment to LDs remains obscure. Additionally it is still unclear whether DDX3 (or its recruitment to LDs) might be (if at all) of different importance for the replication cycle of distinct genotypes. Our initial question whether DDX3 recruitment to LDs could contribute to the different efficiencies in HCV particle production observed for distinct genotypes or isolates still remains unanswered.

Second, our DDX3 knockdown experiments suggest an involvement of the DEAD box RNA helicase in early and late events of the HCV replication cycle. Thus either the remaining cytosolic (non-relocalized) fraction of DDX3 is supporting steps in the viral replication cycle or these functions are independent of the protein's localization. A very recent report suggested that DDX3 might serve as a sensor of HCV RNA, which concomitantly leads to the induction of the expression of lipogenic genes. This in turn could enhance the intracellular levels of neutral lipids, thus of LDs, and thereby resulting in a positive effect on HCV particle production [158]. As the HCV core protein is capable of binding viral RNA [31], we wondered whether the recognition of HCV RNA and subsequent induction of lipogenic genes by DDX3 was dependent on the proteins recruitment to the LDs by the viral core protein. We showed that the relocalization of DDX3 by the core protein does most likely not contribute to the protein's potential ability to induce lipogenesis. Although cells replicating core mutant virus of genotype 2a (JFH1) showed a reduced neutral lipid stain compared to cells replicating the *wild-type* virus (Figure 3.18), this could be attributed to the reduced core protein levels (Figure 3. 17E). Considering that the expression of core protein has been linked to the occurrence of steatosis in transgenic mice as well as the fact that HCV core protein was shown to induce SREBP cleavage [37, 321], it could be that the observed difference in the cellular neutral lipid content is caused by the different expression levels of mutant and *wild-type* core protein.

Third, DDX3 recruitment by the HCV core protein might **be unspecific**. Recently the cellular Y-box binding protein YB-1 was described to regulate the balance between viral replication and particle production possibly by interacting with HCV NS3 [322]. Interestingly, an interactome of YB-1 in human hepatoma cells indicated the protein's interaction with several host factors including DDX3. Similar to the DEAD box RNA helicase 3, YB-1 was found to associate to LDs in a core dependent manner. Intriguingly YB-1 appeared to regulate the localization of its interaction partners including DDX3 to LDs, arguing that these factors might act in a functional complex [322]. Nevertheless, it could be that DDX3 is accidentally co-shuttled with YB-1 to LDs, while not being of any relevance for the virus. This is supported by the fact that knockdown of YB-1 and its interaction partners significantly reduced viral RNA replication, while stimulating infectious particle egress, highlighting their functional link. In marked contrast, DDX3 knockdown did not influence particle release. Although DDX3 was found to be a part of this protein complex (including YB-1 and its interaction partners), it did not act in a similar fashion [322]. Thus the role of its recruitment by the HCV core protein to LDs, possibly as part of a larger protein complex, in the viral replication cycle remains unresolved.

In conclusion our results indicate that DDX3 is important for early and late events of the HCV replication cycle in human hepatoma cells (Huh7.5, Huh7/Lunet), which is most likely independent of its relocalization through the HCV core protein. This interaction might however play a role in a more authentic cell system. Being a protein involved in a multitude of cellular pathways HCV might depend but possibly also restrict several cellular functions of DDX3. It is not surprising that this DEAD box RNA helicase plays an important role, either as restriction or dependency factor in the replication cycle of several other viruses, namely vaccinia virus, DENV or HIV [151, 153]. One might argue that this host factor could be a good target for the development of broad-spectrum antivirals. However a far better understanding of its multiple actions in the viral replication cycles is required in order to specifically target DDX3 function while not affecting cell homeostasis [151].

4.1.4.3 Effect of the single point mutation Y35A or F24A in the HCV core protein on core protein stability and infectious particle production

In the course of this study, we observed that the two core point mutations Y35A or F24A reduced core protein levels of distinct HCV genotypes to different extent (Figure 3.15, Figure 3.17).

Core protein stability has been reported to depend on its **recruitment to LDs** which is mediated by two amphipathic helices in domain 2 at the protein's C-terminus [35]. Our immunofluorescence analysis revealed that the Y35A or F24A mutation did not interfere with the protein's localization to LDs (Figure 3.14). However whether the amount of mutant core protein at LDs reflects the exact *wild-type* condition needs to be determined. Nevertheless, considering that both point mutations are present at the protein's N-terminus (domain I) it is unlikely that they substantially alter the membrane targeting of the viral core protein.

The N-terminus of the HCV RNA core coding region however, has been predicted to fold into four **highly conserved RNA structures**, of which the two most N-terminal stem-loop structures (SL47 and SL87) were suggested to **contribute to RNA translation** [323]. Indeed, the herein used core point mutations are present within SL47. However, whether a single point mutation would disrupt the stem-loop structure and could cause a defect in viral RNA translation is not known. Given our observation that only the HCV core protein levels but neither the amounts of NS5A or NS3 nor the RNA replication efficiency were reduced in the context of either point mutation argues for a core specific defect unrelated to viral RNA translation (Figure 3.5, Figure 3.17).

We were able to identify two core mutations that in the context of the full-length virus (Jc1F24A, Con1F24A/JFH1) did not cause reduced core protein levels but a significant reduction in infectious particle production (Figure 3.17). The N-terminal domain (domain I) of the HCV core protein is suggested to be involved in RNA binding as well as core oligomerization. Both are possibly dependent on the presence of positively charged amino acids, and thus on the net charge of domain I [31, 32, 34]. Whether the mutation of the uncharged amino acid Tyrosine (Y) or Phenylalanine (F) could have any impact on these steps and thus could account for the observed defect in infectious particle production remains open. It could be that these amino acid residues mediate the interaction with other cellular proteins important for infectious particle production.

4.2 Studying the role of lipid transfer protein mediated cholesterol transport in the HCV replication cycle

Similar to other plus-strand RNA viruses, HCV induces a massive rearrangement of cellular endomembranes, generating the so-called membranous web that predominately consists of DMVs. There is increasing evidence that these DMVs represent the sites of viral RNA replication and are most likely generated by a concerted action of viral and host factors [113, 130, 265]. However the precise lipid composition as well as the source of the respective lipids remains elusive. It has been shown that HCV alters the expression of lipogenic genes [37, 131], which could provide lipids for the generation of DMVs through *de novo* lipogenesis or enhanced lipid uptake from the extracellular space. In addition HCV might cause changes in the distribution of endogenous lipids and induce their specific recruitment to sites of viral RNA replication. In this study we focused on HCV induced alterations of the free cholesterol landscape. The fact that viral replicase components were found to be associated with detergent resistant membranes, suggests a specific lipid environment of the replication organelles [127, 128]. Indeed several studies point to unesterified cholesterol as well as sphingomyelin as important components of the viral replication factories and as being important for viral RNA replication [79, 114, 324].

4.2.1 Studying the distribution of free cholesterol in HCV infected cells

In a set of microscopy-based experiments we studied the **fate of free cholesterol in HCV replicating cells** and could show that endogenous and exogenously added free cholesterol was recruited to NS5A positive sites at the perinuclear region of HCV replicating cells (Figure 3.20A, E, Figure 3.23A, B). In addition, we observed an increased intracellular accumulation of endogenous unesterified cholesterol in infected as compared to mock cells, which suggests that HCV alters cholesterol homeostatic pathways such as the lipid's trafficking to specifically recruit it to sites of viral replication (Figure 3.20C, Figure 3.20F). The fact that in mock cells a substantial amount of cellular unesterified cholesterol was present at the plasma membrane, which was largely decreased in HCV infected cells, prompted us to analyze the fate of PM-derived (exogenously added) free cholesterol (Figure 3.20 A, B).

Using fluorescently labeled free cholesterol (TFC) we aimed at unraveling whether HCV was able to recruit plasma membrane derived cholesterol to sites of viral RNA replication. In addition, given that cholesterol might represent an important structural component of the DMVs [79, 114], we wondered whether we could observe differences in the recruitment efficiency of TFC to the potential viral replication factories, when TFC was added at early as compared to late time points in replication (replication establishment vs steady state

replication). To this point we analyzed the **dynamics and distribution of exogenously added TFC** in HCV replicating cells, which was further supported by **biochemical analysis of NS4B membrane fractions, the DMVs**, purified from TFC pulsed cells.

Of note, we and others showed that TFC incorporates into the plasma membrane from which it may become endocytosed and distributed throughout the cell (Figure 3.22B, C) [267]. Nevertheless we cannot exclude that TFC possibly interacts with lipoproteins present in the cell culture media and is taken up by receptor-mediated endocytosis, i.e. through the LDL receptor. Importantly, in either case free cholesterol will be trafficked through the endosomal pathway to its intracellular targets such as the PM or the ER [214].

Analysis on the **dynamics of exogenously added TFC in HCV replicating** cells showed no significant differences in the recruitment velocity between HCV replicating and “mock” cells (Figure 3.23C). However, it needs to be mentioned that these “mock” cells expressed the viral core to NS2 proteins and thus do not represent authentic uninfected cells. In fact the viral core protein has been described to induce SREBP activity [37], thus enhancing the expression of lipogenic genes, which might in turn alter lipid trafficking. Moreover, while HCV replication might or might not affect the uptake velocity of excess plasma membrane derived cholesterol the virus could exploit additional mechanisms, such as the inhibition of cholesterol esterification, in order to trap the lipid at viral replication sites.

Assuming that free cholesterol might be of need for the generation or maintenance of the membranous web, we argued that cholesterol could be of particular importance at early time-points when the viral replication organelles are about to be established. To this end, we studied the **TFC recruitment velocity** when added **early or late in replication**. Our results did not indicate a significant difference in the rate of TFC accumulation when added during the establishment of replication or at times of steady state replication (Figure 3.22, Figure 3.23C, Figure 3.24C). There are several reasons that could account for this. Studies on the course of DMV accumulation throughout HCV infection showed a rapid increase in the occurrence of DMVs from 16 to 24 h post infection which remained steady in number until 48 h post infection (Jc1, gt2a) [113]. Given the experimental limitations we pulsed the cells with TFC at 30 h post electroporation, the earliest time point possible. So far we cannot exclude that at this time the majority of viral replication sites is already established. Another possibility is that the cell might cope, irrespectively of the presence of the virus, with excess plasma membrane cholesterol by triggering the lipid's endocytosis, its traffic to the ER and possibly its esterification and storage in LDs. Indeed, free cholesterol alters membrane structure and function [325] and thus the membrane's cholesterol content needs to be tightly regulated. In

the end, there might also be no differential recruitment of cholesterol throughout the course of a HCV infection. For instance, it could be that during steady state replication a high DMV turnover rate causes a continuous biogenesis of DMVs, which might resemble the *de novo* biogenesis early in infection.

While we were not able to observe differences in the recruitment velocity of TFC to the perinuclear region between HCV replicating and mock cells, we observed that TFC accumulated in a diffuse web (Figure 3.23B, Figure 3.24B) or in dot-like structures (Figure 3.23A, Figure 3.24A) at the perinuclear region in HCV replicating cells. In comparison to mock cells, TFC appeared to accumulate to larger extent at the perinuclear region, at least when added late in replication. This is in line with our previous results on the distribution of endogenous cholesterol upon HCV infection that showed an enrichment of free cholesterol at the perinuclear region in HCV replicating as compared to mock cells (Figure 3.20D, F, Figure 3.24D). Importantly we observed a significant colocalization of endogenous and exogenous cholesterol with the HCV NS5A, which we used as a potential marker for the viral replication sites. These results suggest that HCV might actively induce the recruitment of plasma membrane cholesterol to sites of viral RNA replication. To corroborate this further, the localization of unesterified cholesterol in respect to other viral non-structural proteins, or best to newly synthesized RNA, as a marker for active RNA replication, should be analyzed. Performing elaborate NS4B-HA pulldown experiments we were able to show that TFC is recovered in NS4B-associated membrane fractions, which have previously been reported to be DMVs and the putative sites of RNA replication (Figure 3.26) [114]. Using this biochemical approach it will be interesting to elucidate, whether inhibition of endosomal transport of PM derived/ extracellular cholesterol (i.e. through NCP1 knockdown or CA treatment) influences the incorporation of TFC or of endogenous cholesterol into DMVs.

Taken together we show first evidence that plasma membrane derived cholesterol is likely incorporated into the viral replication organelles, the DMVs. This is in line with a recent study that reported the recruitment of TFC to NS5A positive sites in HCV replicating cells as well as the enhanced association of TFC with DRMs in HCV replicating cells [79]. In this context, it will be interesting to investigate whether the addition of exogenous cholesterol, such as TFC, stimulates HCV RNA replication by for instance promoting DMV formation.

As indicated earlier, HCV may not only induce the active recruitment of cholesterol to sites of viral replication, but could also exploit other mechanisms in order to efficiently retain the lipid at sites of need. This could be achieved by preventing cholesterol esterification and its storage in LDs. This may be addressed by measuring the degree of TFC recruitment to LDs, which could serve as an indicator for the TFC esterification rate.

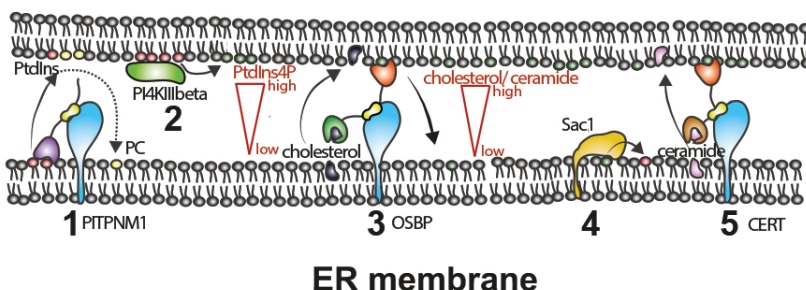
In conclusion, we showed that the distribution of endogenous and exogenous free cholesterol is altered in HCV infected cells, suggesting that the virus hijacks pathways in order to reorganize the cellular cholesterol landscape. In times of immediate need the plasma membrane cholesterol pool can serve as readily available pool [326]. We suggest that HCV usurps the plasma membrane cholesterol pool and recruits the lipid to sites of viral RNA replication, where it could contribute to the formation of the double membrane vesicle or support viral RNA replication by other means. Details on the underlying mechanisms that allow the virus to specifically enrich cholesterol at sites of need are still scarce and most likely involve a concerted action of vesicular and non-vesicular lipid traffic.

4.2.2 Evaluating the role of LTPs implicated in direct lipid transfer in the replication cycle of HCV and DENV

Being an obligate intracellular pathogen, HCV hijacks cellular pathways to promote genome replication and infectious virus production. We observed that HCV induces alterations in the cellular distribution of free cholesterol, with the lipid being recruited to the potential sites of RNA replication (Figure 3.20, Figure 3.26). This is in line with increasing evidence suggesting that the positive-strand RNA virus does not simply reshape ER membranes for the generation of the membranous web, but instead creates a membrane microenvironment of specific lipid composition [79, 129, 280]. Despite the ER being the site where cellular cholesterol levels are controlled through anabolic and catabolic processes, the ER exhibits only low cholesterol levels as compared to the PM. In fact, about 65% of total free cholesterol are suggested to be present at the PM, while only 1-2% are found in the ER [162]. Thus the question arises of how cholesterol becomes specifically enriched at the viral replication factories that most likely derive from ER membranes [113]. The virus could exploit several mechanisms in order to accumulate cholesterol at its replication sites. In addition to on-site *de novo* synthesis, or to a reduced esterification of free cholesterol or enhanced liberation of cholesterol from LD storages, HCV might hijack the vesicular and non-vesicular lipid transport machinery in order to recruit and to enrich cholesterol at specific sites. In this study we aimed to evaluate the **contribution of LTP-mediated cholesterol traffic to HCV replication**, in particular to the generation of the membranous web. We argued that the virus might hijack the function of these LTPs in order to generate local membrane enrichment in cholesterol and potentially other lipid species such as sphingolipids. Indeed some LTPs that exhibit a pleckstrin-homology domain mediating PtdIns4P binding and a VAP binding domain, the FFAT motif, seem to be attractive targets for viral manipulation.

uninfected cell

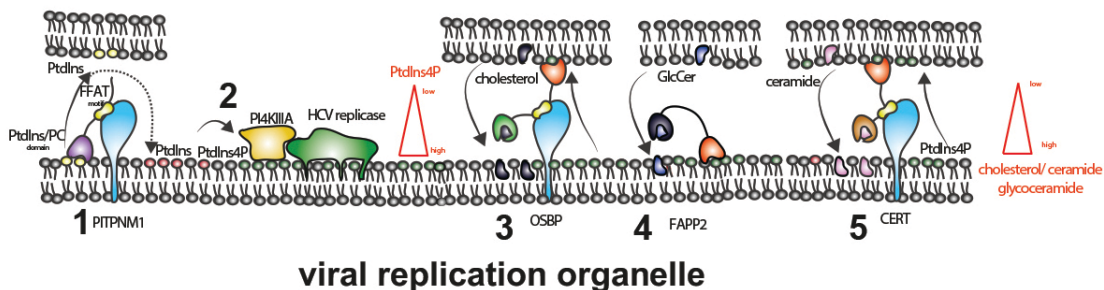
Golgi membrane



ER membrane

HCV infected cell

unknown donor membranes



viral replication organelle

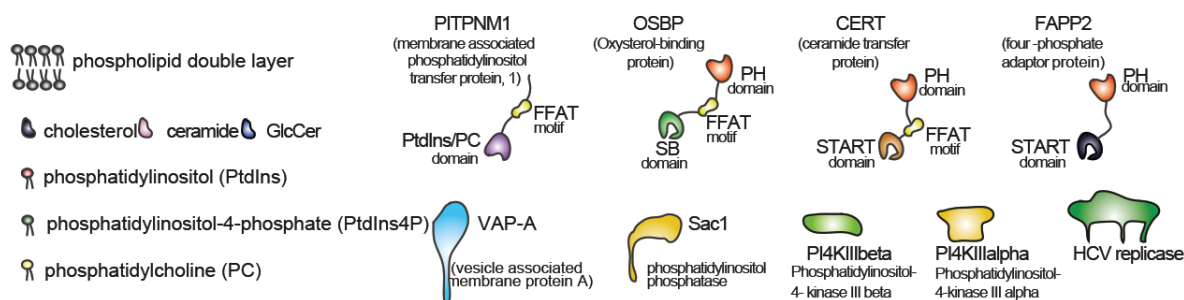


Figure 4.1 Possible model of lipid transfer through the concerted action of lipid transfer proteins at ER/Golgi contact sites. *Upper panel: uninfected cell.* The lipid transfer proteins PITPNM1, OSBP and CERT are recruited to the ER through their interaction with present VAP proteins. (1) PITPNM1 shuttles the exchange of PtdIns and PC between ER and Golgi membranes. (2) PtdIns can serve as substrate of the PI4KIIIbeta for PtdIns4P production. (3) (5) This generates a PtdIns4P gradient that drives the counter-transport of PtdIns4P with the respective lipids targeted by OSBP (free cholesterol) or CERT (ceramide). This in turn leads to an accumulation of cholesterol and ceramide at Golgi membranes. (4) The phosphatase Sac1 at the ER dephosphorylates PtdIns4P in order to maintain the PtdIns4P gradient. *Lower panel: HCV infected cell.* The LTPs (except of FAPP2) are recruited to the viral replication sites via interaction with present VAP proteins. (1) (2) PITPNM1 function might be hijacked in order to provide PtdInsP for the subsequent generation of PtdIns4P by the PI4KIIIalpha at the viral replication organelles. The local high PtdIns4P levels then promote the delivery of (3) cholesterol by OSBP and (5) ceramide by CERT. (4) FAPP2 is potentially recruited to the viral replication sites via

its binding to PtdIns4P and delivers GlcCer. These actions could allow an accumulation of specific lipid species at the viral replication organelles. PITPNM1: membrane associated phosphatidylinositol transfer protein 1, OSBP: oxysterol-binding protein, CERT: ceramide transfer protein, FAPP2: four phosphate adaptor protein 2, VAP-A/B: vesicle associated membrane protein A/B, PtdIns: Phosphatidylinositol, PtdIns4P: Phosphatidylinositol-4-Phosphate, PC: Phosphatidylcholine.

There is increasing evidence that HCV might co-opt these LTPs by recruiting them to the viral replication sites, possibly through their binding with VAP proteins, the latter shown to be present in DMVs [114]. HCV was shown to recruit the PI4KIII α to sites of viral replication and to stimulate the protein's kinase activity, which leads to the generation of high local PtdIns4P levels [77]. This allows the establishment of a PtdIns4P concentration gradient which then might drive the counter-transport of PtdIns4P and cholesterol or glycosphingolipid precursors, and finally leads to the enrichment of the raft lipids at the replication organelles (Figure 4.1, HCV infected cell) [79, 129]. A similar mechanism was proposed for the replication of other plus-strand RNA viruses such as several members of the *Picornaviridae*, known to depend on the PI4KIII β dependent PtdIns4P induction [187, 327]. The positive single-stranded RNA Tombus virus has been suggested to co-opt sterol transfer proteins through direct interaction with one of the replicase proteins thereby recruiting sterols to the viral replication site [328]. In the context of HCV, present studies mainly focused on OSBP, while OSBP-related/like proteins (ORP/OSBPLs) have been vastly neglected [79]. Nevertheless given that they share a similar domain structure (C-terminal sterol binding domain and in most cases a N-terminal FFAT motif and subsequent PH domain) it is likely that OSBPLs might act in a concerted fashion or even redundantly. Therefore we evaluated the role of several members of the OSBPL family but also of other protein families implicated in non-vesicular sterol transfer, such as of the START domain protein family or the NPC proteins in the replication cycle of HCV and DENV (Figure 3.27 table, references therein). In addition to the already known HCV life cycle regulators OSBP [79, 280, 329], COL4A3BP [280, 329] and PLEKHA8 [129], we here report for the first time of the involvement of the membrane associated phosphatidylinositol transfer protein 1 (PITPNM1) in the replication cycle of HCV (Figure 3.29C). The beforehand mentioned proteins act at ER/Golgi membrane contact sites, which highlights the importance of their concerted action mediating the lipid exchange between these two cellular compartments in the viral replication cycle. A model describing their potential mode of action in HCV infected cells is presented in Figure 4.1 (infected cell). PITPNM1 is a phosphatidylinositol (PtdIns) / phosphatidylcholine (PC) transfer protein. In uninfected cells PITPNM1 exchanges PtdIns from the ER with PC of the Golgi. The Golgi localized PI4KIII β subsequently phosphorylates PtdIns to PtdIns4P. The thereby generated PtdIns4P concentration gradient (PtdIns4P concentrations are low at ER but high at the Golgi) drives the counter-transport of PtdIns4P and cholesterol or ceramide by OSBP or CERT respectively [181] (Figure 4.1). Upon HCV infection high PtdIns4P levels at the replication organelles might drive the LTP-dependent delivery of free cholesterol and

ceramide to the replication sites. In this context, PITPNM1 could promote the local induction of high PtdIns4P levels by the cellular PI4KIII α through its transfer of PtdInsP to the viral replication sites. In line with this, we observed that knockdown of PITPNM1 impaired early events of viral infection (Figure 3.29C). The involvement of PITPNM1 in HCV RNA replication such as its contribution to the virus induced elevated PtdIns4P levels should be addressed in future studies.

In addition our screen results indicated an important role of OSBPL3, OSBPL9/11, described to function at ER/PM or Golgi/endosome membrane contact sites, in the HCV replication cycle. Furthermore LTPs (NPC1, STARD3, OSBPL1A/1B) involved in lipid traffic through the late endosomal/ lysosomal pathway appeared to be of relevance for the virus (Figure 3.28A, B, E) [179, 196, 274, 275, 279]. This **highlights the importance of LTPs present at several membrane contact sites** and at the **LE/LY organelles** in the viral replication cycle. This further suggests that **HCV might usurp several lipid sources** to acquire lipids, in particular cholesterol or sphingolipids.

It is intriguing to note, that only two of all LTPs tested were of relevance for the replication cycle of the related Dengue virus (Figure 3.28C, D). This implies that the latter is possibly far less dependent on cellular cholesterol for viral replication or uses different cellular pathways as compared to HCV. HCV replication supposedly occurs at DMVs, which are protrusions of the ER, while DENV genome replication is suggested to involve virus induced ER invaginations [113, 114, 149]. Given their distinct morphology it is likely that the viruses co-opt different cellular host factors and pathways for their generation and maintenance. In fact, DENV replication is independent of PI4KIII α /beta mediated PtdIns4P induction, which stands in contrast to HCV and several members of the *Picornaviridae*, known to induce high local PtdIns4P levels, that are suggested to drive the LTP-mediated lipid traffic at the ER/Golgi interface (see Figure 4.1). Accordingly, the dependency of HCV and DENV on PtdIns4P binding proteins, such as most of the ORP family members, correlates well with their dependence on PtdIns4P induction through PI4Kinases [77, 79, 129, 187, 327].

4.2.3 The role of LTP-assisted cholesterol traffic through the endosomal vesicular pathway in HCV replication

Although there is increasing evidence that supports the notion of HCV co-opting LTPs in order to generate a specific lipid microenvironment at its replication sites, the lipid's source membrane remains unknown. In case of OSBP, PITPNM1, CERT and FAPP2 this could be the Golgi compartment [79, 129, 181]. With the PM being highly enriched in cholesterol,

endocytosis of PM cholesterol or direct cholesterol transfer at PM/ER contact sites possibly mediated through OSBPL3 [274] could promote viral replication (Figure 3.28A, E). An additional major source of cellular cholesterol is the receptor-mediated uptake of LDL and subsequent hydrolysis of cholesterol esters in endosomal compartments, from which unesterified cholesterol is then transported from LE/LY to the PM or ER [162]. Several proteins have been implicated to mediate the sterol's export from late endosomes and lysosomes, namely NPC1 and 2 and STARD3 [194, 207]. In addition OSBPL1A was shown to regulate the positioning of late endosomes depending on their cholesterol content [188]. Intriguingly, we were able to show that NPC1, STARD3 and OSBPL1A function is important for early events in HCV infection (Figure 3.29C).

4.2.3.1 Studying the involvement of NPC1 in cholesterol traffic and HCV replication

Here we report of a **yet undescribed role of NPC1 in early events of the HCV but not the DENV replication cycle**. We showed that gene knockdown of NPC1 impaired steps in viral RNA replication of genotype 2a and 1b stable replicons, but could possibly have an additional role in HCV entry (Figure 3.30). NPC1 is a transmembrane protein present in the limiting membrane of late endosomes and lysosomes [204]. According to this we found NPC1 in lysosomal, but also yet undefined vesicular structures (Fig 3.32A). Defects in NPC1 function have been reported to cause tremendous accumulation of unesterified cholesterol in lipid lamellae, which bear late endosomal and lysosomal markers [201, 330]. In agreement with this, gene knockdown of NPC1 in human hepatoma cells led to an accumulation of unesterified cholesterol in large vesicles of lysosomal origin, irrespective of the presence or absence of the virus (Figure 3.32). So far, the precise role of NPC1 in cholesterol export from late endosomes remains elusive, but most likely involves several other LE proteins like NPC2 and additional cholesterol efflux exporter [207].

We showed that **NPC1 knockdown indeed caused an intracellular accumulation of free cholesterol in lysosomal structures**, which was concomitant to a **reduction in viral RNA replication**. So far we cannot rule out that NPC1 function might additionally be important for **entry of HCV** (Figure 3.31B, D). There are two possible scenarios of how NPC1 could affect the viral replication cycle. First, the virus eventually depends on a function of NPC1 independent of the protein's involvement in lipid trafficking. Second, one might argue that NPC1-mediated cholesterol egress from LE/LY compartments is substantial for HCV. In case of HCV entry, the viral fusogenicity with endosomal membranes was reported to be influenced by the target membrane's lipid composition [111]. Thus accumulation of high cholesterol amounts upon loss of NPC1 function could impair viral fusion events. On the

other hand, similar to Ebola virus entry, NPC1 might directly control viral escape from endosomal membranes by interacting with one of the viral glycoproteins [281, 331]. In addition, given that HCV RNA replication depends on the presence of unesterified cholesterol [79], the NPC1-mediated export of cholesterol from LE/LY compartments might be essential to promote HCV RNA replication.

4.2.3.2 Chemical inhibition of cholesterol traffic through the endosomal pathway and its impact on viral replication

Considering that the uptake of LDL and its subsequent processing in endosomal compartments represents one of the major sources of cellular free cholesterol, it is likely that HCV usurps this pathway in order to recruit specific lipid species. Indeed, in HCV infected hepatoma cells, the cell surface expression of the LDLR receptor is enhanced [332]. In line with this we observed a slight increase in LDLR transcript levels in HCV infected cells (Figure 3.39B). Thus HCV could promote the uptake of LDL in order to recruit LDL derived cholesterol to its replication organelles. In addition to this, HCV could usurp the PM-cholesterol pool and induce the endocytosis of cholesterol-rich microdomains of the plasma membrane.

Several **cationic amphiphiles (CA)** (U18666A, Ro 48-8071, clomiphene citrate) have been described to **block endosomal cholesterol** transport, while their mode of action is unknown [285]. The most prominent and frequently used CA is U18666A, reported to phenocopy NPC1 loss of function [282]. Accordingly we observed that U18666A treatment of HCV infected human hepatocytes resulted in an aggregation of free cholesterol in large vesicular structures in close proximity to the nucleus. Likewise, Ro 48-8071 or clomiphene citrate treated cells showed a profound accumulation of free cholesterol in bloated lysosomal organelles, which were significantly enlarged as compared to the control condition (Figure 3.33A, B, D, Figure 3.35A, B). Intriguingly, the aberrant **aggregation of endogenous free cholesterol** was **concomitant to a decrease in the lipid's colocalization with NS5A** (Figure 3.33C, Figure 3.35B). This suggests that free cholesterol present in LE/LY is transferred to NS5A positive sites, and thus potentially to the viral replication sites, which is inhibited upon CA treatment. In line with this we observed that, HCV **RNA replication** of several genotypes was **impaired** by treatment with the cationic amphiphiles (Figure 3.37, Figure 3.38).

Several hypotheses have been put forward to explain the underlying mechanism of CA induced lipidosis. In case of U18666A it has been reported that overexpression of NPC1

reduced the impact of the drug, indicating that NPC1 function might be targeted by U18666A [285]. We were not able to corroborate this (Supplementary Figure 5). However given the compound's structural similarity to cholesterol (Supplementary Figure 5A) it might directly interfere with NPC1 function, which is known to bind cholesterol [333]. Furthermore, CA were observed to accumulate in lysosomes where they can bind a specific lipid species forming a non-digestible lipid complex that subsequently aggregates in lysosomal lamellar bodies. On the other hand, CA might directly change the lysosomal membrane properties and thereby alter the function of membrane-associated proteins. In addition, CA-mediated inhibition of lysosomal enzymes could cause the accumulation of non-degraded lipid species [334]. The latter also accounts for the Niemann-Pick Disease Type A and B which are characterized by the accumulation of sphingomyelin, caused by a defective acid sphingomyelinase [199].

The herein used CA were reported to cause a vesicular accumulation of free cholesterol similar to NPC1 loss of function [285], which was confirmed by our studies (Figure 3.35). Given that cholesterol preferentially associates with raft lipids [335], it is likely that defects in cholesterol egress convert into trafficking defects of other lipids such as of sphingolipids. In line with this we showed that CA treatment did not only result in the entrapment of free cholesterol in dilated lysosomal bodies, but also caused an accumulation of GM1 therein, indicating that egress of several lipids is hampered (Figure 3.35 and Figure 3.36). However in contrast to endogenous free cholesterol, GM1 did not colocalize with NS5A in untreated cells (Figure 3.36). It remains to be elucidated which lipids are transferred in addition to unesterified cholesterol from LE/LY storage to the viral replication factories. In this regard characterizing the lipid content of lamellar bodies of CA treated cells could give a further hint to the lipid species promoting viral replication.

Taken together we hypothesize that **the transport of specific lipids such as cholesterol from LE/LY to the replication organelles is important for viral RNA replication.**

Nevertheless, it should not be neglected that a general defect in LE/LY function that could alter traffic of cargo internalized by endocytosis [167] might contribute to the impairment of viral replication. Indeed lysosomal function is necessary for the degradation of macromolecules and for providing nutrients to the cell [336]. To corroborate whether the CA-induced defect in cholesterol traffic causes the observed reduction in viral RNA replication, one could try to rescue viral RNA replication by the addition of exogenous cholesterol. Indeed our live-cell imaging analysis on the impact of CA treatment on TFC trafficking showed that exogenously added TFC was able to somehow overcome CA induced lipid trafficking defects and was efficiently transported to NS5A positive sites (Figure 3.42). Yet it is unclear whether TFC can rescue the CA induced impairment in viral RNA replication.

The inhibition of free cholesterol egress from LE/LY upon CA treatment or NPC1 knockdown might manifest, besides its apparent impact on the lipid's distribution, in less obvious changes in cellular cholesterol homeostasis. While LDL derived free cholesterol at the ER can initiate cholesterol homeostatic regulatory mechanisms, such as the reduction of HMGCoAR expression, this regulatory function is blocked upon treatment with the amphiphile U18666A [282]. Furthermore CA are inhibitors of several enzymes catalyzing the biosynthesis of cholesterol which potentially alters intracellular cholesterol levels (Figure 3.39A) [282, 285]. Therefore the CA induced inhibitory effect on viral RNA replication might be due to either (i) a defect in the lipid's trafficking or (ii) caused by alterations in total un-/esterified cholesterol levels as a consequence of changes in regulatory mechanisms, such as cholesterol synthesis through HMGCoAR or (iii) a result of both. We argued that CA induced changes in cholesterol homeostasis most likely manifest in alterations of the transcript levels of the major regulators such as LDLR, HMGCoAR and ABCA1. Our analysis revealed that neither CA nor Mevastatin treatment altered the transcript levels of LDLR, ABCA1 or HMGCoAR (Figure 3.39) [286]. Although this is unexpected at first, it could be that under the drug concentration tested, the local cholesterol levels at the ER are still sufficient to retain the SREBP-SCAP-Insig complex and inhibit SREBP mediated lipogenic gene expression (i.e. HMGCoAR). On the other hand one might speculate that in presence of HCV, suggested to induce SREBP activity [37], the SREBP-SCAP-Insig complex loses its sensitivity towards the regulation through ER localized free cholesterol. Given the rather indirect read-out the true effect of CA treatment on cellular levels of free and esterified cholesterol remains to be determined using biochemical assays.

In conclusion one might argue that under the herein tested conditions **CA mainly provoked an intracellular accumulation of cholesterol in late endosomes/ lysosomes**, while most likely the overall cellular cholesterol levels remained unaffected. Interestingly, Mevastatin treatment did not alter the localization of cholesterol or GM1 (Figure 3.35, Figure 3.38). This suggests that the CA induced changes in filipin and GM1 distribution are independent of the drugs' potential inhibitory effects on sterol synthesis. In agreement with reports of others [133] we showed that Mevastatin reduced viral RNA replication (Figure 3.37C,D, Figure 3.38). Being an inhibitor of the HMGCoAR which promotes sterol but also isoprenoid synthesis, it has been suggested that the impairment of HCV RNA replication is most likely due to defects in isoprenoid synthesis rather than to defects in the generation of cholesterol [135].

Taken together we suggest that **HCV RNA replication depends on the shuttling of unesterified cholesterol through the endosomal pathway**. This is based on our

observation that (i) HCV induces the reorganization of PM derived cholesterol and most likely causes the recruitment of this lipid to the viral replication organelles (Figure 3.20A, B, Figure 3.25, Figure 3.26) (ii) HCV RNA replication is significantly hampered when endosomal cholesterol traffic is inhibited either by targeting important LTPs or by CA treatment (Figure 3.29C, Figure 3.30, Figure 3.32, Figure 3.33, Figure 3.34, Figure 3.35, Figure 3.36, Figure 3.37) (iii) which is concomitant to a decreased localization of endogenous unesterified cholesterol to NS5A positive sites (Figure 3.33, Figure 3.35). Using a similar approach a recent study showed that several members of the Picornaviridae depend on endosomal cholesterol homeostasis to maintain viral replication with the lipid most likely acting as a structural component of the replication organelles [337].

4.2.3.3 Relevance of endosomal lipid traffic for HCV replication

The **precise role of cholesterol** delivered through the endosomal pathway in **viral RNA replication** remains unknown. A recent study showed that the OSBP-dependent recruitment of cholesterol to PtdIns4P rich replication compartments contributes to the establishment of the membranous web (Figure 4.1 infected cell) [79]. This is further supported by the observation of cholesterol being an important structural component of the DMVs [114, 127]. Thus HCV most likely usurps plasma membrane derived cholesterol for the generation of its replication organelles. Cholesterol could, by forming membrane rafts, serve as platform of the replicase machinery within the vesicular structures or serve to provide membrane rigidity. While we were able to show that exogenously added plasma membrane derived cholesterol (TFC) colocalized with NS5A and was readily incorporated into NS4B membrane fractions, presumably the DMVs (Figure 3.25, Figure 3.26), we were not able to observe an inhibition of this colocalization upon CA treatment (Figure 3.42A, C, D, E). This stands in contrast with our data obtained on the distribution of endogenous free cholesterol. In case of the latter, we showed that CA treatment induced cholesterol entrapment in lysosomal compartments which was concomitant to its decrease at NS5A positive sites, thus potentially at viral replication factories (Figure 3.35C). It appears that the addition of excess cholesterol can overcome the inhibitory effect of CA treatment. It is likely that upon the addition of excessive cholesterol and upon the lipid's transport to LE/LY compartments the cell may use alternative pathways to remove excessive intracellular LE/LY cholesterol. For instance the activity of other LE/LY resident cholesterol transporters such as STARD3 could be induced.

In agreement with our previous observations we were able to observe a strong intracellular accumulation of large TFC positive vesicles, which clustered around the nucleus upon CA treatment (Figure 3.33, Figure 3.41A). In line with the report of others these vesicles appeared static and immobile [210]. The loss of mobility of late endocytic compartments and

their aggregation at the perinuclear region has also been reported for cells lacking functional NPC1 [201]. It is suggested that either the accumulation of high cholesterol levels impair LE dynamics or the latter might be directly regulated by NPC1 function [188, 211, 338].

Although we were able to show that plasma membrane cholesterol is recruited to the potential site of viral replication, which most probably involves its transport through the endosomal pathway and export by LTPs such as NPC1, the role of PM-derived cholesterol in viral replication remains enigmatic. Given that CA treatment was most effective when added early in replication (Figure 3.34 E) it is **likely that cholesterol is needed** for early events such as the **establishment of the MW**. Therefore lack of cholesterol might manifest in changes in MW morphology. Indeed earlier reports showed that changes in the lipid composition of the replication organelles, such as reduced PtdIns4P or cholesterol levels, caused a reduction in DMV size which was concomitant to a defect in viral RNA replication [77, 79, 114]. To our surprise we were not able to observe such changes in the DMV morphology upon CA treatment at concentrations that had earlier been proven to impair the recruitment of this lipid to NS5A positive sites as well as to impair viral RNA replication (Figure 3.43). It could be that U18666A treatment causes only subtle changes in the cholesterol content of the viral replication factories that do not become apparent in the size of DMVs. This could possibly be addressed by analyzing the cholesterol content of purified DMVs from HCV replicon cells in presence or absence of CA [114]. Additionally, heterogeneity in the phenotype might impede the analysis. In order to rule out that endo-lysosomal cholesterol traffic is indeed dispensable for DMV morphology, one could use correlative light electron microscopy to ease the search for cells showing a strong vesicular cholesterol accumulation upon drug treatment and to correlate this phenotype with potential changes in DMV morphology.

Besides of being a structural component **cholesterol could regulate the proviral action of cellular factors** or of the **enzymatic activity of the viral replicase**, e.g. in a similar fashion as compared to the allosteric control of enzymes. Several viral proteins have been reported to associate with distinct lipid species. The viral RdRp NS5B is able to bind sphingomyelin and inhibition of sphingolipid synthesis impairs viral RNA replication. The role of sphingomyelin association to NS5B needs to be clarified, but could mediate the membrane raft association of the protein [339]. The interaction of FASN with NS5B was reported to enhance the viral RdRp activity, however most likely independent of FASN enzymatic activity [340]. The recruitment of FASN to the viral replication sites in turn might support the local synthesis of phospholipids and could potentially contribute to palmitoylation of viral proteins [341]. Although NS4B was believed to be palmitoylated, very recent studies reported no

evidence for palmitoylation of the viral protein [342]. The most prominent cholesterol interaction motifs found in the transmembrane domains of membrane proteins are the CRAC (Cholesterol Recognition/ interaction Amino acid Consensus sequence) or the CARC motif, the latter exhibiting the opposite orientation of the CRAC motif [343]. Whether such motifs are present in the viral non-structural proteins and could mediate the association with cholesterol is unknown. Finally it would be intriguing to elucidate, whether cholesterol or other lipids have a direct stimulatory effect on the enzymatic function of the viral replicase. This could be addressed by studying the *in vitro* RNA replicase activity of crude replication complexes (CRCs) purified from replicon cells [344] in dependency of the addition of lipids such as free cholesterol.

5 Conclusion and perspectives

The herein presented data allows us to put forward several hypotheses on the interplay of HCV and (A) LD-associated pathways and (B) the cellular cholesterol landscape.

(A) HCV and LD-associated pathways

The high hit rate of our hypothesis driven LD RNAi screen highlights the central role of LDs in the replication cycle of the two LD-dependent viruses, HCV and DENV. We found that several major cellular pathways are acting as central nodes and are involved in all three processed analyzed, such as the COPI trafficking machinery and the proteasomal degradation pathway. It would be intriguing to study whether these pathways link the viral replication cycles to LD homeostasis. Moreover gaining a better understanding of the link between HCV, DENV and the lipid storage organelle might reveal novel promising targets for antiviral therapy. Studying the function of the DEAD box RNA helicase 3 in HCV replication we were able to confirm its involvement in several steps of the viral replication cycle. Our data further suggests that the recruitment of the protein to LDs by the HCV core protein is dispensable for its proviral function in human hepatoma cells. As discussed earlier this should be re-evaluated in a more authentic immune competent cellular system.

(B) HCV and the cellular cholesterol landscape

We were able to show that **HCV reshapes the cellular cholesterol landscape**, which became apparent in our imaging analysis of endogenous and exogenous plasma membrane derived cholesterol. This reshaping might involve vesicular but also non-vesicular mechanisms and thus the action of lipid transfer proteins. In line with this we identified several LTPs that are implicated in direct lipid transfer at membrane contact sites of the ER/PM, ER/ Golgi and possibly the ER and late endosomal/ lysosomal compartments.

Our data suggests that **cholesterol from late endocytic compartments**, possibly derived from the PM or from LDL uptake, **is trafficked to NS5A positive sites**. This most likely involves the function of host factors, such as NPC1 that could act as cholesterol efflux pump at late endosomes. Pharmacological inhibition of lipid transport through the endosomal/ lysosomal pathway was shown to impair HCV RNA replication and the delivery of cholesterol to NS5A positive sites, thus possibly to the sites of RNA replication. Nevertheless we cannot exclude, that a general defect in LE/LY function caused by either NPC1 knockdown or CA treatment might provoke the impairment of HCV RNA replication.

HCV might take advantage of several cholesterol storage compartments, possibly depending on their availability. While the plasma membrane cholesterol pool represents a 'ready to use' pool for immediate supply, HCV could in addition induce the uptake of LDL or

the mobilization of cholesterol from LDs. Some Rhinoviruses were recently reported to mobilize cholesterol from LD pools and by recruiting it to the viral replication factories promoting replication on Golgi derived membranes [327]. Whether HCV usurps other cholesterol sources should be addressed in future studies.

We showed that **HCV takes advantage of NPC1-mediated cholesterol traffic** through the endosomal pathway, however knowledge on the details of the underlying mechanism is scarce. It is still enigmatic how cholesterol is shuttled from lysosomal compartments to its intracellular target membranes such as the PM or the ER. This post-lysosomal transport most likely involves cytosolic receptors and/ or vesicular traffic of LE/LY. In fact knockdown of the ER-resident OSBPL5 was shown to cause an accumulation of cholesterol in the limiting membrane of LE/LY, while NPC1 loss of function manifests in the accumulation of free cholesterol within these vesicular structures [190, 345]. For this reason one might argue that OSBPL5 acts as cytosolic receptor of cholesterol exported from LE/LY through the function of NPC1. Although OSBPL5 was also included in our LTP RNAi screen we were not able to establish an importance of this protein in the viral replication cycle so far (Figure 3.27). Nevertheless it would be worthwhile to include OSBPL5 into future studies. Another member of the OSBPL family, namely OSBPL1A has been reported to regulate the positioning of LE according to their cholesterol content, and to regulate the establishment of LE/ ER contact sites through its interaction with ER-resident VAP proteins [188]. We observed that knockdown of OSBPL1A/1B impaired early events in viral replication (Figure 3.29C). In line with this it would be intriguing to elucidate, whether HCV hijacks the function of OSBPL1A or OSBPL5 in order to recruit cholesterol loaded LE/LY to the viral replication sites. Future studies should further implement the function of other LTPs, such as STARD3, and ABCA1 that act as cholesterol export shuttles at the LE/LY [193, 271]. Intriguingly STARD3 was recently described to contribute to the formation of ER/LE membrane contact sites possibly by acting with the ER resident VAP proteins [346], which might support the delivery of LE cargo to the ER. In conclusion, HCV might take advantage of the function of OSBPL1A and STARD3 in order to establish membrane contact sites between cholesterol loaded LE/LY and the viral replication factories. Furthermore HCV could possibly recruit OSBPL5 (or other OSBPLs such as OSBP) to sites of viral replication in order to enrich for cholesterol that is delivered from LE/LY through the action of NPC1 and additional LTPs such as NPC2, ABCA1 and STARD3 (Figure 5.1). In line with this it would be intriguing to study the dynamics of NPC1 positive vesicles in HCV infected cells as well as the localization of OSBPL1A, STARD3 and OSBPL5 in respect to the viral replication sites.

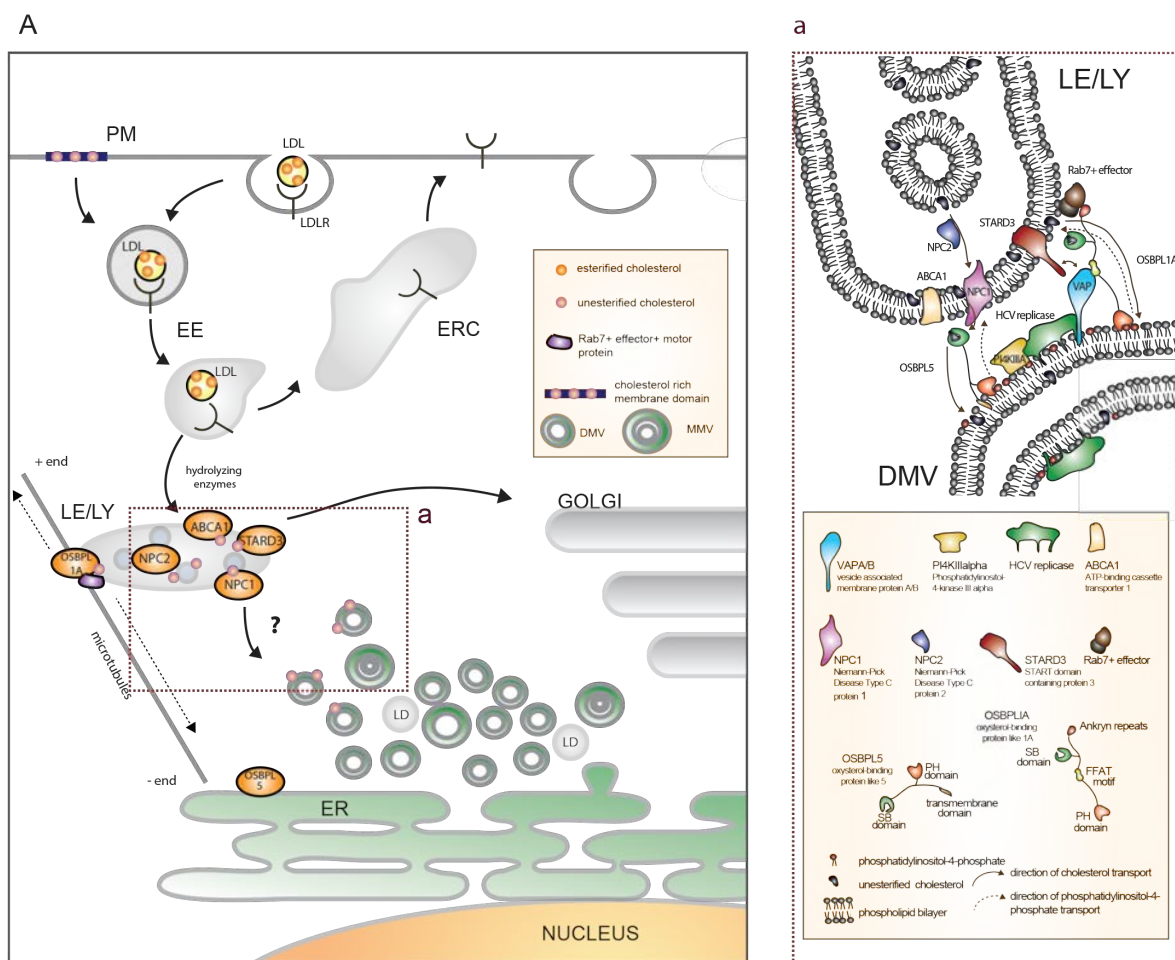


Figure 5.1 Hypothetical model of LTP-assisted cholesterol transport through the endocytic pathway to the viral replication sites. (A) Upon LDL receptor-mediated uptake of low-density lipoproteins, LDL is targeted to LE/LY for degradation, while the receptor is recycled back to the PM. Cholesterol esters are hydrolyzed by acid lipases present in lysosomes but also in earlier endocytic compartments. In addition cholesterol rich plasma membrane microdomains are endocytosed and deliver free cholesterol to late endocytic compartments [217]. How free cholesterol is then leaving the LE/LY compartments is not understood, but might involve vesicular mechanisms as well as the action of LTPs such as of NPC1/2, STARD3, OSBPL5, OSBPL1A and ABCA1. OSBPL1A tethers LE/LY compartments depending on their cholesterol content to the vesicle transport machinery. LE of low cholesterol content are scattered throughout the cell periphery, while LE of high cholesterol content are transported to the microtubule minus ends. OSBPL1A further mediates the formation of LE/ER contact sites through its interaction with ER-resident VAP proteins [188]. OSBPL5 is an ER-resident protein that might act as cytosolic acceptor of cholesterol delivered through the action of NPC1/2 or other cholesterol efflux pumps [190]. **(a)** HCV might recruit OSBPL1A to the viral replication sites (the DMVS) through OSBPL1A interaction with VAP proteins. The interaction of OSBPL1A with Rab7 and its effectors at LE through the protein's N-terminal ankyrin repeats could then allow the establishment of LE/DMV contact sites. This could support the export of free cholesterol from LE/LY compartments through the action of several LTPs. NPC1, possibly in a concerted action with NPC2 and/or ABCA1, catalyzes the egress of cholesterol from the endocytic compartment [207] and could transfer it onto a cytosolic acceptor such as OSBPL5. The ER resident OSBPL5 might then catalyze the counter transport of cholesterol and phosphatidylinositol-4-phosphate (PtdIns4P). The directionality of the transport is given by the high PtdIns4P levels at the DMVs. In addition STARD3 could act as LE/LY cholesterol exporter but might also help to establish LE/DMV contact sites by its interaction with VAP proteins [346]. In conclusion, HCV might hijack the function of several LTPs in order to recruit cholesterol or other lipids to its sites of replication.

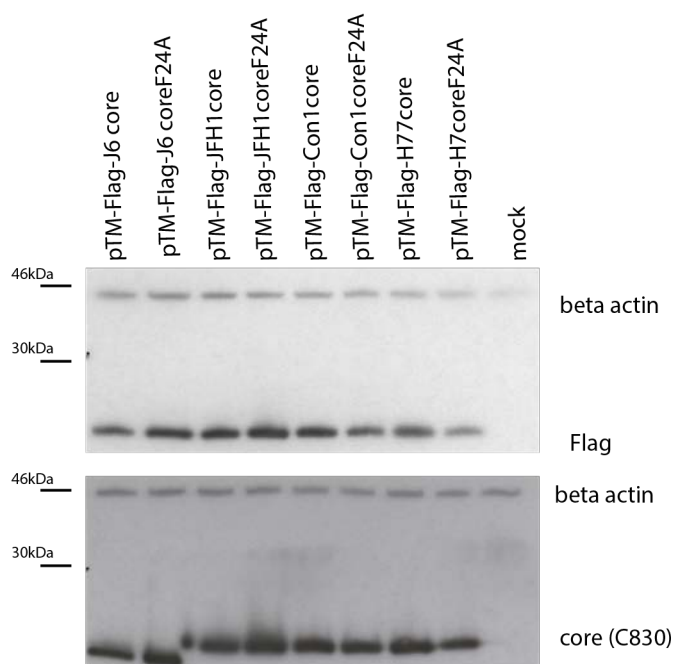
While we were able to recover PM derived cholesterol from NS4B associated DMVs, the **function of cholesterol** at these sites **remains enigmatic**. The lipid possibly acts as structural component [114] contributing to the formation of lipid rafts that might serve as platform of the viral replicase. In addition cholesterol could have a direct stimulatory effect on the HCV RNA replicase activity. This open question should be tackled in future studies and

might shed novel insight into the intimate connection between HCV and the host cellular lipid metabolism.

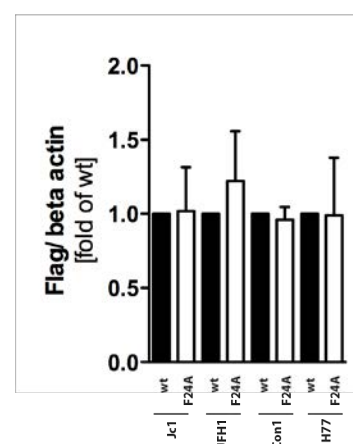
In this study we mainly focused on the contribution of cholesterol transport to early events of the HCV replication cycle such as viral RNA replication and the establishment or maintenance of the viral replication factories, the DMVs. Given that multiple steps of the viral replication cycle, such as infectious particle production are linked to cellular lipid metabolism [302, 347], it would be intriguing to study the implication of LTP-mediated endosomal cholesterol transport in infectious particle production. Indeed, we observed the recruitment of free cholesterol to NS5A positive sites, which might not only mark the sites of viral RNA replication, but given the protein's role in particle production could indicate sites of progeny virus assembly [81]. The fact that viral particle resembles very-low- and low-density – lipoproteins highly enriched in cholesteryl esters [120] further supports the notion that directed cholesterol transport could be of importance for the assembly of infectious particles.

6 Supplement

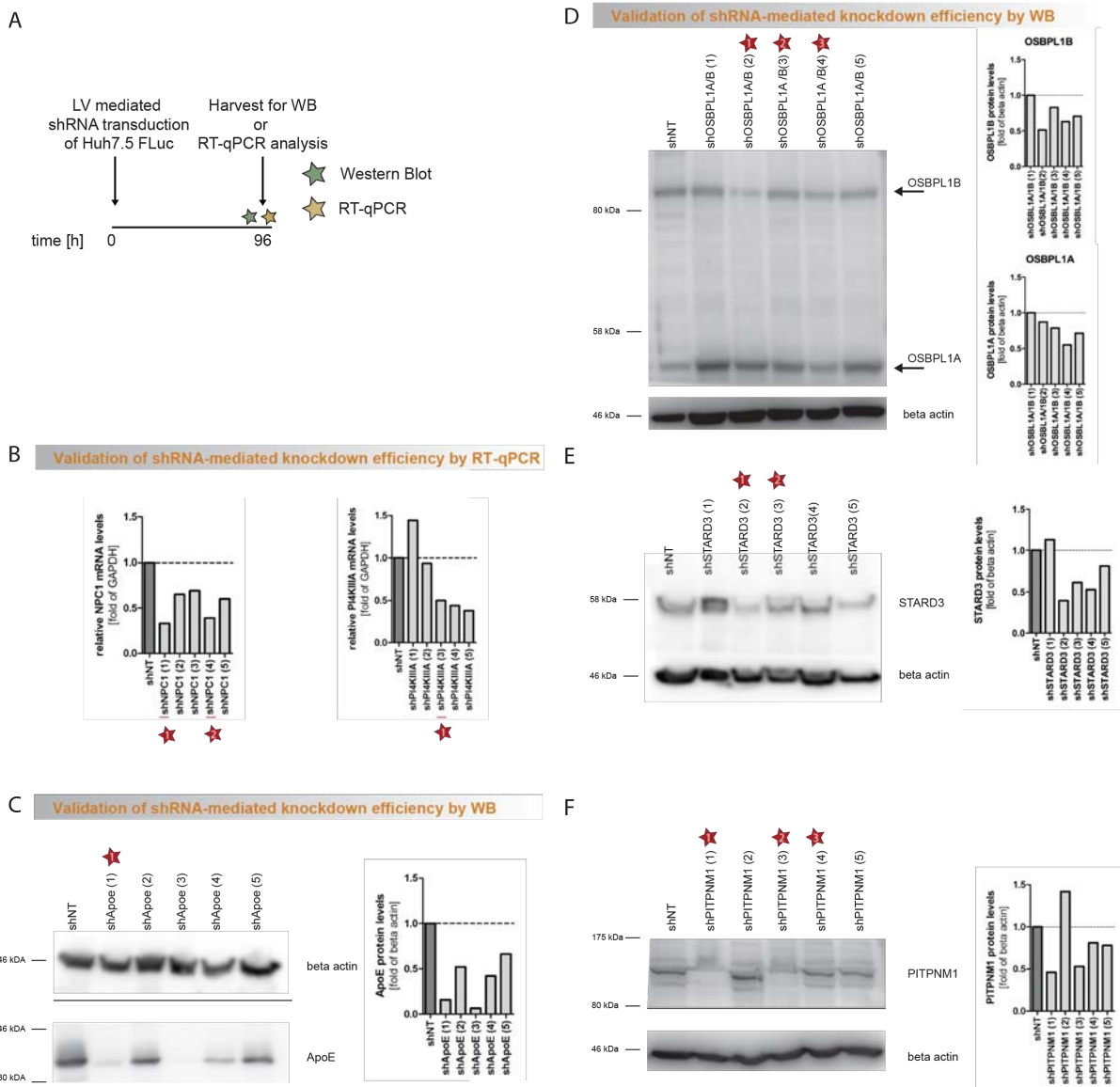
A



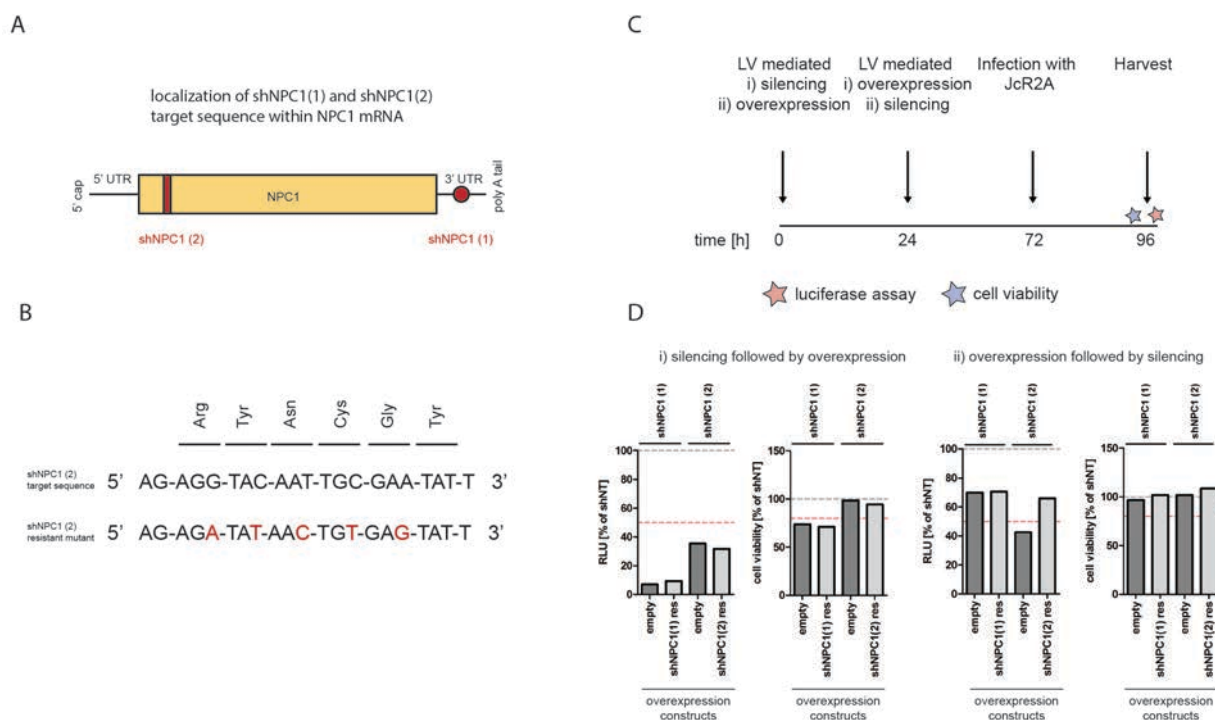
B



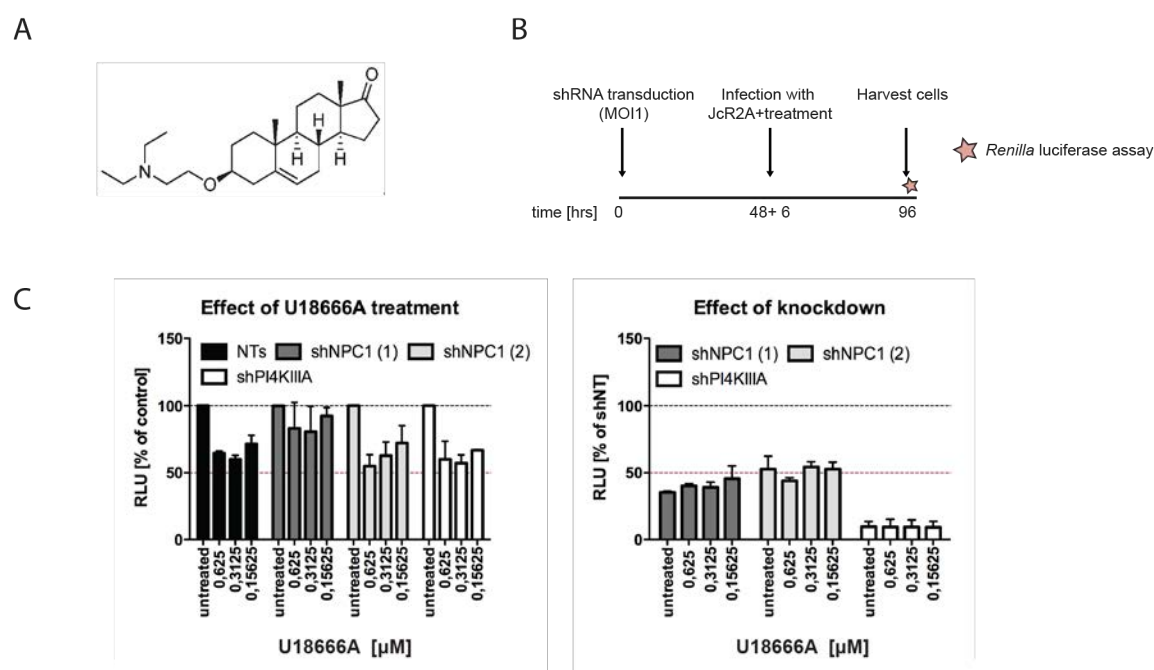
Supplementary Figure 2 Detection of Flag tagged *wild-type* and F24A mutant core of different genotypes by the core specific C830 antibody as well as Flag tag specific antibody. (A) Huh7/Lunet-T7 cells were transfected with the respective pTM overexpression constructs encoding the *wild-type* or F24A mutant core with a N-terminal Flag tag. 24 h later the protein levels of Flag tagged HCV core were analyzed in parallel with antibodies against the Flag tag as well as against the HCV core protein. Beta actin is depicted as loading control. A representative image is shown. (B) Quantification of the Flag signal intensities of the respective conditions. The Flag signal was normalized to the beta actin loading control. Mean and standard deviation of two independent experiments are shown.



Supplementary Figure 3 Validation of shRNA-mediated knockdown efficiency. (A) Huh7.5FLuc cells were transduced with Lentivirus at an approximate MOI of 2. Cells were kept under puromycin selection (1 μ g/ ml) for 96 h. Cells were then harvested for the determination of the knockdown efficiency. (B) In case of no working antibody available, knockdown was measured by determining the transcript levels of the gene of interest by RT-qPCR. They were normalized to mRNA levels of the housekeeping gene GAPDH. The means of triplicates are presented as fold of the non-targeting shRNA control. (C-F) When possible, protein levels were determined by Western Blot. For quantification of the knockdown efficiency target protein levels were normalized to beta actin and are presented as fold of the non-targeting shRNA control. In case of OSBPL1A/1B the protein levels are presented as fold of shOSBPL1A/1B (1). Data of a single experiment is shown.

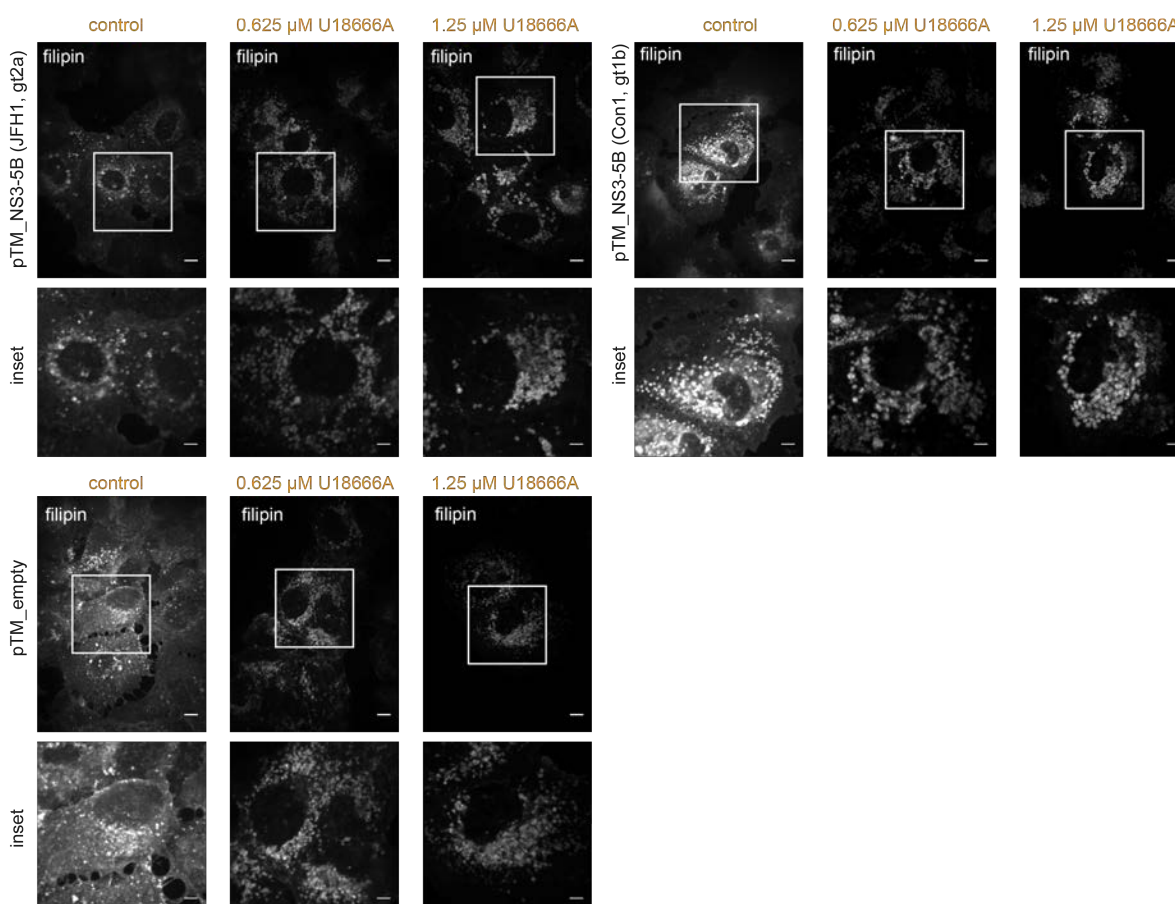


Supplementary Figure 4 Attempt of rescuing NPC1 silencing by overexpression of shRNA resistant NPC1 constructs. (A) Scheme indicating the localization of the target sequence of shNPC1 (1) and shNPC1 (2) within NPC1 mRNA. shNPC1 (1) targets the 3' UTR, while shNPC1 (2) targets a sequence within the coding region. (B) shNPC1 (2) target sequence and the encoded amino acids. For the generation of a shNPC1 (2) resistant expression construct 5 silent point mutations were introduced into the target sequence. (C) Setup of NPC1 rescue experiments. Cells were transduced with lentivirus for either i) gene silencing followed by NPC1 overexpression or ii) overexpression and subsequent gene silencing. Next, cells were infected with *Renilla* luciferase reporter HCV (JcR2A) for 48 h. (D i, ii) Effect of combined silencing and overexpression on the early phase of JcR2A replication (measurement of *Renilla* luciferase activity in cell lysates) as well as on cell viability (cell titer glo assay) is shown. Data is presented as percentage of the non-targeting shRNA. The mean relative life units (RLU) of triplicates of a single experiment are shown.



Supplementary Figure 5 Combination of NPC1 knockdown and U18666A treatment. (A) Chemical structure of U18666A. (B) Experimental setup. Huh7.5 cells were transduced with shRNA containing Lentivirus at a MOI of 1. 48 h later cells were infected with *Renilla* luciferase reporter virus (MOI 0.5). After removal of the viral inoculum cells were treated with different concentrations of U18666A. 48 h post infection cells were lysed and viral

replication was determined by measuring the *Renilla* luciferase activity in cell lysates. (C) *Effect of shRNA mediated knockdown of NPC1 or PI4KIII α combined with U18666A treatment.* The same results are shown in both panels. Upper panel: Effect of U18666A treatment in knockdown cells. Lower panel: Effect of knockdown in drug treated cells. The mean relative light units (RLU) and standard deviation of two independent experiments are shown. Experiments were performed in triplicates.



Supplementary Figure 6 Free cholesterol distribution upon U18666A treatment of cells expressing the non-structural proteins NS3-5B of JFH1 (gt2a) or Con1Et (gt1b). Huh7/Lunet-T7 cells were treated with different concentrations of U18666A for 24 h followed by transfection of the respective pTM expression constructs in presence of the drug. 6 h later medium was replaced by fresh drug containing medium. 24 h post transfection cells were fixed and free cholesterol was visualized using filipin. The white boxes highlight the areas shown in the enlargements below. Scale bars represent 10 μ m or 5 μ m respectively.

6.2 Supplementary Tables

Supplementary Tables are provided on CD.

Supplementary Table S 1: Dharmacon RNAi library

Supplementary Table S 2: Primary screen results (z-scores)

Supplementary Table S 3: Primary screen hits (HCV and DENV)

Supplementary Table S 4: Primary LD morphology screen hit list

Supplementary Table S 5: Deconvolution screen hit list

6.3 Supplementary Movies

Supplementary Movies are provided on CD.

Supplementary Movie 1: Live cell imaging of Huh7/LunetCD81H cells transfected with the subgenomic replicon containing mCherry tagged NS5A and pulsed with 4 μ M Topfluor-Cholesterol. Representative pictures are shown in Figure 3.21.B, upper panel.

Supplementary Movie 2: Live cell imaging of Huh7/LunetCD81H cells transfected with the subgenomic replicon containing mCherry tagged NS5A and pulsed with 1 μ M Topfluor-Cholesterol. Representative pictures are shown in Figure 3.21.B, lower panel.

Supplementary Movie 3: Live cell imaging of Huh7/LunetCD81H cells transfected with the subgenomic replicon containing mCherry tagged NS5A and pulsed with 1 μ M Topfluor-Cholesterol (TFC) early in replication. Dynamics of TFC and NS5A-mcherry are shown. Representative pictures are shown in Figure 3.23A.

Supplementary Movie 4: Live cell imaging of Huh7/LunetCD81H cells transfected with the subgenomic replicon containing mCherry tagged NS5A and pulsed with 1 μ M Topfluor-Cholesterol (TFC) late in replication. Dynamics of TFC and NS5A-mcherry are shown. Representative pictures are shown in Figure 3.23B.

Supplementary Movie 5: Live cell imaging of Huh7/LunetCD81H cells transfected with the subgenomic replicon containing mCherry tagged NS5A and pulsed with 1 μ M Topfluor-Cholesterol (TFC) early in replication. Dynamics of TFC and NS5A-mcherry are shown. Representative pictures early upon TFC addition are shown in Figure 3.24A.

Supplementary Movie 6: Live cell imaging of Huh7/LunetCD81H cells transfected with the subgenomic replicon containing mCherry tagged NS5A and pulsed with 1 μ M Topfluor-Cholesterol (TFC) late in replication. Dynamics of TFC and NS5A-mcherry are shown. Representative pictures early upon TFC addition are shown in Figure 3.24B.

Supplementary Movie 7 - Live tracking of Topfluor-Cholesterol (TFC, green) and NS5A-mCherry (red) in Huh7/LunetCD81H cells transfected with the subgenomic replicon containing mCherry tagged NS5A and pulsed with 1 μ M Topfluor-Cholesterol early in replication. Dynamics of TFC and NS5A-mcherry are shown. A movie depicting the overlap of NS5A (red) and TFC (green) is presented. Representative pictures are shown in Figure 3.25.A.

Supplementary Movie 8 - Live tracking of Topfluor-Cholesterol (TFC, green) and NS5A-mCherry (red) in Huh7/LunetCD81H cells transfected with the subgenomic replicon containing mCherry tagged NS5A and pulsed with 1 μ M Topfluor-Cholesterol late in replication. Dynamics of TFC and NS5A-mcherry are shown. A movie depicting the overlap of NS5A (red) and TFC (green) is presented. Representative pictures are shown in Figure 3.25.B.

Supplementary Movie 9 - Live tracking of Topfluor-Cholesterol (TFC) in Huh7/LunetCD81H cells transfected with the subgenomic replicon containing mCherry tagged NS5A, pulsed with 1 μ M Topfluor-Cholesterol early in replication and treated or not with 1.25 μ M U18666A. Dynamics of TFC and NS5A-mcherry in control or U18666A treated cells are shown. In addition a movie showing the pictures depicted in Figure 3.41A is presented.

Supplementary Movie 10 - Live tracking of Topfluor-Cholesterol (TFC) in Huh7/LunetCD81H cells transfected with the subgenomic replicon containing mCherry

tagged NS5A, pulsed with 1 μ M Topfluor-Cholesterol late in replication and treated or not with 1.25 μ M U18666A. Dynamics of TFC and NS5A-mcherry in control or U18666A treated cells are shown. In addition a movie showing the pictures depicted in Figure 3.41A is presented.

Supplementary Movie 11 - Live tracking of Topfluor-Cholesterol (TFC) and NS5A-mCherry in Huh7/LunetCD81H cells transfected with the subgenomic replicon containing mCherry tagged NS5A, pulsed with 1 μ M Topfluor-Cholesterol early in replication and treated or not with 1.25 μ M U18666A. Dynamics of TFC and NS5A-mcherry in control or U18666A treated cells are shown. A movie showing the overlap of the TFC and NS5A signal is presented. Pictures of the first 400 min post TFC pulse are depicted in 3.42A.

Supplementary Movie 12 - Live tracking of Topfluor-Cholesterol (TFC) and NS5A-mCherry in Huh7/LunetCD81H cells transfected with the subgenomic replicon containing mCherry tagged NS5A, pulsed with 1 μ M Topfluor-Cholesterol late in replication and treated or not with 1.25 μ M U18666A. Dynamics of TFC and NS5A-mcherry in control or U18666A treated cells are shown. A movie showing the overlap of the TFC and NS5A signal is presented. Pictures of the first 400 min post TFC pulse are depicted in 3.42A.

7 References

1. Mosby, *Mosby's medical dictionary*. Elsevier Health, 2013. **9th edition**.
2. WHO, *Fact sheet N°328, N°204, N°164, N°280*. 2015.
3. Ke, P.Y. and S.S. Chen, *Hepatitis C virus and cellular stress response: implications to molecular pathogenesis of liver diseases*. *Viruses*, 2012. **4**(10): p. 2251-90.
4. Poynard, T., et al., *A comparison of fibrosis progression in chronic liver diseases*. *J Hepatol*, 2003. **38**(3): p. 257-65.
5. Feinstone, S.M., et al., *Transfusion-associated hepatitis not due to viral hepatitis type A or B*. *N Engl J Med*, 1975. **292**(15): p. 767-70.
6. Choo, Q.L., et al., *Isolation of a cDNA clone derived from a blood-borne non-A, non-B viral hepatitis genome*. *Science*, 1989. **244**(4902): p. 359-62.
7. A. M. Q. King, M.J.A., E. J. Lefkowitz, *Virus Taxonomy: Classification and Nomenclature of viruses: Ninth Report of the International Committee on Taxonomy of Viruses*. Elsevier, Academic Press, 2011.
8. Bukh, J., R.H. Miller, and R.H. Purcell, *Genetic heterogeneity of hepatitis C virus: quasispecies and genotypes*. *Semin Liver Dis*, 1995. **15**(1): p. 41-63.
9. Simmonds, P., *Genetic diversity and evolution of hepatitis C virus--15 years on*. *J Gen Virol*, 2004. **85**(Pt 11): p. 3173-88.
10. Murphy, D.G., et al., *Hepatitis C virus genotype 7, a new genotype originating from central Africa*. *J Clin Microbiol*, 2015. **53**(3): p. 967-72.
11. Bartenschlager, R., V. Lohmann, and F. Penin, *The molecular and structural basis of advanced antiviral therapy for hepatitis C virus infection*. *Nat Rev Microbiol*, 2013. **11**(7): p. 482-96.
12. WHO, *Factsheet N°164*. 2015.
13. Lavanchy, D., *Evolving epidemiology of hepatitis C virus*. *Clin Microbiol Infect*, 2011. **17**(2): p. 107-15.
14. Averhoff, F.M., N. Glass, and D. Holtzman, *Global burden of hepatitis C: considerations for healthcare providers in the United States*. *Clin Infect Dis*, 2012. **55 Suppl 1**: p. S10-5.
15. Perz, J.F., et al., *The contributions of hepatitis B virus and hepatitis C virus infections to cirrhosis and primary liver cancer worldwide*. *J Hepatol*, 2006. **45**(4): p. 529-38.
16. Frank, C., et al., *The role of parenteral antischistosomal therapy in the spread of hepatitis C virus in Egypt*. *Lancet*, 2000. **355**(9207): p. 887-91.
17. Mohamed, A.A., et al., *Hepatitis C virus: A global view*. *World J Hepatol*, 2015. **7**(26): p. 2676-80.
18. Messina, J.P., et al., *Global distribution and prevalence of hepatitis C virus genotypes*. *Hepatology*, 2015. **61**(1): p. 77-87.
19. Pearlman, B.L. and N. Traub, *Sustained virologic response to antiviral therapy for chronic hepatitis C virus infection: a cure and so much more*. *Clin Infect Dis*, 2011. **52**(7): p. 889-900.
20. Rupp, D. and R. Bartenschlager, *Targets for antiviral therapy of hepatitis C*. *Semin Liver Dis*, 2014. **34**(1): p. 9-21.
21. Scheel, T.K. and C.M. Rice, *Understanding the hepatitis C virus life cycle paves the way for highly effective therapies*. *Nat Med*, 2013. **19**(7): p. 837-49.
22. Wyles, D.L., *Antiviral resistance and the future landscape of hepatitis C virus infection therapy*. *J Infect Dis*, 2013. **207 Suppl 1**: p. S33-9.
23. Ip, P.P., et al., *Therapeutic vaccination against chronic hepatitis C virus infection*. *Antiviral Res*, 2012. **96**(1): p. 36-50.

24. Liu, Y., E. Wimmer, and A.V. Paul, *Cis-acting RNA elements in human and animal plus-strand RNA viruses*. *Biochim Biophys Acta*, 2009. **1789**(9-10): p. 495-517.
25. Niepmann, M., *Internal translation initiation of picornaviruses and hepatitis C virus*. *Biochim Biophys Acta*, 2009. **1789**(9-10): p. 529-41.
26. Murray, C.L., C.T. Jones, and C.M. Rice, *Architects of assembly: roles of Flaviviridae non-structural proteins in virion morphogenesis*. *Nat Rev Microbiol*, 2008. **6**(9): p. 699-708.
27. McLauchlan, J., et al., *Intramembrane proteolysis promotes trafficking of hepatitis C virus core protein to lipid droplets*. *EMBO J*, 2002. **21**(15): p. 3980-8.
28. Moradpour, D., F. Penin, and C.M. Rice, *Replication of hepatitis C virus*. *Nat Rev Microbiol*, 2007. **5**(6): p. 453-63.
29. Kopp, M., et al., *Genetic analysis of the carboxy-terminal region of the hepatitis C virus core protein*. *J Virol*, 2010. **84**(4): p. 1666-73.
30. Gawlik, K. and P.A. Gallay, *HCV core protein and virus assembly: what we know without structures*. *Immunol Res*, 2014. **60**(1): p. 1-10.
31. Fan, Z., et al., *Specific in vitro association between the hepatitis C viral genome and core protein*. *J Med Virol*, 1999. **59**(2): p. 131-4.
32. Santolini, E., G. Migliaccio, and N. La Monica, *Biosynthesis and biochemical properties of the hepatitis C virus core protein*. *J Virol*, 1994. **68**(6): p. 3631-41.
33. Boulant, S., et al., *Hepatitis C virus core protein is a dimeric alpha-helical protein exhibiting membrane protein features*. *J Virol*, 2005. **79**(17): p. 11353-65.
34. Nakai, K., et al., *Oligomerization of hepatitis C virus core protein is crucial for interaction with the cytoplasmic domain of E1 envelope protein*. *J Virol*, 2006. **80**(22): p. 11265-73.
35. Boulant, S., et al., *Structural determinants that target the hepatitis C virus core protein to lipid droplets*. *J Biol Chem*, 2006. **281**(31): p. 22236-47.
36. Xu, Z., et al., *Synthesis of a novel hepatitis C virus protein by ribosomal frameshift*. *EMBO J*, 2001. **20**(14): p. 3840-8.
37. Waris, G., et al., *Hepatitis C virus induces proteolytic cleavage of sterol regulatory element binding proteins and stimulates their phosphorylation via oxidative stress*. *J Virol*, 2007. **81**(15): p. 8122-30.
38. Park, C.Y., et al., *Hepatitis C virus nonstructural 4B protein modulates sterol regulatory element-binding protein signaling via the AKT pathway*. *J Biol Chem*, 2009. **284**(14): p. 9237-46.
39. Dubuisson, J., F. Penin, and D. Moradpour, *Interaction of hepatitis C virus proteins with host cell membranes and lipids*. *Trends Cell Biol*, 2002. **12**(11): p. 517-23.
40. Op De Beeck, A., et al., *The transmembrane domains of hepatitis C virus envelope glycoproteins E1 and E2 play a major role in heterodimerization*. *J Biol Chem*, 2000. **275**(40): p. 31428-37.
41. Petracca, R., et al., *Structure-function analysis of hepatitis C virus envelope-CD81 binding*. *J Virol*, 2000. **74**(10): p. 4824-30.
42. Flint, M., et al., *Functional analysis of cell surface-expressed hepatitis C virus E2 glycoprotein*. *J Virol*, 1999. **73**(8): p. 6782-90.
43. Carrere-Kremer, S., et al., *Subcellular localization and topology of the p7 polypeptide of hepatitis C virus*. *J Virol*, 2002. **76**(8): p. 3720-30.
44. Wozniak, A.L., et al., *Intracellular proton conductance of the hepatitis C virus p7 protein and its contribution to infectious virus production*. *PLoS Pathog*, 2010. **6**(9): p. e1001087.

45. Pavlovic, D., et al., *The hepatitis C virus p7 protein forms an ion channel that is inhibited by long-alkyl-chain iminosugar derivatives*. Proc Natl Acad Sci U S A, 2003. **100**(10): p. 6104-8.
46. Nieva, J.L., V. Madan, and L. Carrasco, *Viroporins: structure and biological functions*. Nat Rev Microbiol, 2012. **10**(8): p. 563-74.
47. Steinmann, E., et al., *Hepatitis C virus p7 protein is crucial for assembly and release of infectious virions*. PLoS Pathog, 2007. **3**(7): p. e103.
48. Jones, C.T., et al., *Hepatitis C virus p7 and NS2 proteins are essential for production of infectious virus*. J Virol, 2007. **81**(16): p. 8374-83.
49. Jirasko, V., et al., *Structural and functional characterization of nonstructural protein 2 for its role in hepatitis C virus assembly*. J Biol Chem, 2008. **283**(42): p. 28546-62.
50. Santolini, E., et al., *The NS2 protein of hepatitis C virus is a transmembrane polypeptide*. J Virol, 1995. **69**(12): p. 7461-71.
51. Grakoui, A., et al., *A second hepatitis C virus-encoded proteinase*. Proc Natl Acad Sci U S A, 1993. **90**(22): p. 10583-7.
52. Jirasko, V., et al., *Structural and functional studies of nonstructural protein 2 of the hepatitis C virus reveal its key role as organizer of virion assembly*. PLoS Pathog, 2010. **6**(12): p. e1001233.
53. Ma, Y., et al., *Hepatitis C virus NS2 protein serves as a scaffold for virus assembly by interacting with both structural and nonstructural proteins*. J Virol, 2011. **85**(1): p. 86-97.
54. Bartenschlager, R., et al., *Complex formation between the NS3 serine-type proteinase of the hepatitis C virus and NS4A and its importance for polyprotein maturation*. J Virol, 1995. **69**(12): p. 7519-28.
55. Morikawa, K., et al., *Nonstructural protein 3-4A: the Swiss army knife of hepatitis C virus*. J Viral Hepat, 2011. **18**(5): p. 305-15.
56. Gwack, Y., et al., *Characterization of RNA binding activity and RNA helicase activity of the hepatitis C virus NS3 protein*. Biochem Biophys Res Commun, 1996. **225**(2): p. 654-9.
57. Paul, D., V. Madan, and R. Bartenschlager, *Hepatitis C virus RNA replication and assembly: living on the fat of the land*. Cell Host Microbe, 2014. **16**(5): p. 569-79.
58. Ma, Y., et al., *NS3 helicase domains involved in infectious intracellular hepatitis C virus particle assembly*. J Virol, 2008. **82**(15): p. 7624-39.
59. Li, K., et al., *Immune evasion by hepatitis C virus NS3/4A protease-mediated cleavage of the Toll-like receptor 3 adaptor protein TRIF*. Proc Natl Acad Sci U S A, 2005. **102**(8): p. 2992-7.
60. Li, X.D., et al., *Hepatitis C virus protease NS3/4A cleaves mitochondrial antiviral signaling protein off the mitochondria to evade innate immunity*. Proc Natl Acad Sci U S A, 2005. **102**(49): p. 17717-22.
61. Brass, V., et al., *Structural determinants for membrane association and dynamic organization of the hepatitis C virus NS3-4A complex*. Proc Natl Acad Sci U S A, 2008. **105**(38): p. 14545-50.
62. Phan, T., et al., *The acidic domain of hepatitis C virus NS4A contributes to RNA replication and virus particle assembly*. J Virol, 2011. **85**(3): p. 1193-204.
63. Lindenbach, B.D., et al., *The C terminus of hepatitis C virus NS4A encodes an electrostatic switch that regulates NS5A hyperphosphorylation and viral replication*. J Virol, 2007. **81**(17): p. 8905-18.
64. Lundin, M., et al., *Topology of the membrane-associated hepatitis C virus protein NS4B*. J Virol, 2003. **77**(9): p. 5428-38.

65. Gouttenoire, J., F. Penin, and D. Moradpour, *Hepatitis C virus nonstructural protein 4B: a journey into unexplored territory*. Rev Med Virol, 2010. **20**(2): p. 117-29.
66. Egger, D., et al., *Expression of hepatitis C virus proteins induces distinct membrane alterations including a candidate viral replication complex*. J Virol, 2002. **76**(12): p. 5974-84.
67. Gosert, R., et al., *Identification of the hepatitis C virus RNA replication complex in Huh-7 cells harboring subgenomic replicons*. J Virol, 2003. **77**(9): p. 5487-92.
68. Paul, D., et al., *NS4B self-interaction through conserved C-terminal elements is required for the establishment of functional hepatitis C virus replication complexes*. J Virol, 2011. **85**(14): p. 6963-76.
69. Jones, D.M., et al., *The hepatitis C virus NS4B protein can trans-complement viral RNA replication and modulates production of infectious virus*. J Virol, 2009. **83**(5): p. 2163-77.
70. Macdonald, A. and M. Harris, *Hepatitis C virus NS5A: tales of a promiscuous protein*. J Gen Virol, 2004. **85**(Pt 9): p. 2485-502.
71. Appel, N., T. Pietschmann, and R. Bartenschlager, *Mutational analysis of hepatitis C virus nonstructural protein 5A: potential role of differential phosphorylation in RNA replication and identification of a genetically flexible domain*. J Virol, 2005. **79**(5): p. 3187-94.
72. Elazar, M., et al., *Amphipathic helix-dependent localization of NS5A mediates hepatitis C virus RNA replication*. J Virol, 2003. **77**(10): p. 6055-61.
73. Moradpour, D., et al., *Insertion of green fluorescent protein into nonstructural protein 5A allows direct visualization of functional hepatitis C virus replication complexes*. J Virol, 2004. **78**(14): p. 7400-9.
74. Appel, N., et al., *Essential role of domain III of nonstructural protein 5A for hepatitis C virus infectious particle assembly*. PLoS Pathog, 2008. **4**(3): p. e1000035.
75. Masaki, T., et al., *Interaction of hepatitis C virus nonstructural protein 5A with core protein is critical for the production of infectious virus particles*. J Virol, 2008. **82**(16): p. 7964-76.
76. Randall, G., et al., *Cellular cofactors affecting hepatitis C virus infection and replication*. Proc Natl Acad Sci U S A, 2007. **104**(31): p. 12884-9.
77. Reiss, S., et al., *Recruitment and activation of a lipid kinase by hepatitis C virus NS5A is essential for integrity of the membranous replication compartment*. Cell Host Microbe, 2011. **9**(1): p. 32-45.
78. Berger, K.L., et al., *Hepatitis C virus stimulates the phosphatidylinositol 4-kinase III alpha-dependent phosphatidylinositol 4-phosphate production that is essential for its replication*. J Virol, 2011. **85**(17): p. 8870-83.
79. Wang, H., et al., *Oxysterol-binding protein is a phosphatidylinositol 4-kinase effector required for HCV replication membrane integrity and cholesterol trafficking*. Gastroenterology, 2014. **146**(5): p. 1373-85 e1-11.
80. Evans, M.J., C.M. Rice, and S.P. Goff, *Phosphorylation of hepatitis C virus nonstructural protein 5A modulates its protein interactions and viral RNA replication*. Proc Natl Acad Sci U S A, 2004. **101**(35): p. 13038-43.
81. Zayas, M., et al., *Coordination of Hepatitis C Virus Assembly by Distinct Regulatory Regions in Nonstructural Protein 5A*. PLoS Pathog, 2016. **12**(1): p. e1005376.
82. Behrens, S.E., L. Tomei, and R. De Francesco, *Identification and properties of the RNA-dependent RNA polymerase of hepatitis C virus*. EMBO J, 1996. **15**(1): p. 12-22.

83. Moradpour, D., et al., *Membrane association of the RNA-dependent RNA polymerase is essential for hepatitis C virus RNA replication*. J Virol, 2004. **78**(23): p. 13278-84.
84. Bartenschlager, R., *Hepatitis C virus replicons: potential role for drug development*. Nat Rev Drug Discov, 2002. **1**(11): p. 911-6.
85. Lohmann, V., et al., *Replication of subgenomic hepatitis C virus RNAs in a hepatoma cell line*. Science, 1999. **285**(5424): p. 110-3.
86. Lohmann, V., et al., *Viral and cellular determinants of hepatitis C virus RNA replication in cell culture*. J Virol, 2003. **77**(5): p. 3007-19.
87. Blight, K.J., A.A. Kolykhalov, and C.M. Rice, *Efficient initiation of HCV RNA replication in cell culture*. Science, 2000. **290**(5498): p. 1972-4.
88. Blight, K.J., J.A. McKeating, and C.M. Rice, *Highly permissive cell lines for subgenomic and genomic hepatitis C virus RNA replication*. J Virol, 2002. **76**(24): p. 13001-14.
89. I. Woerz, V.L., R. Bartenschlager, *Hepatitis C virus replicons: dinosaurs still business=*. Journal of viral hepatology, 2009. **16**(1): p. 1-9.
90. Peng, B., et al., *Development of robust hepatitis C virus genotype 4 subgenomic replicons*. Gastroenterology, 2013. **144**(1): p. 59-61 e6.
91. Saeed, M., et al., *Efficient replication of genotype 3a and 4a hepatitis C virus replicons in human hepatoma cells*. Antimicrob Agents Chemother, 2012. **56**(10): p. 5365-73.
92. Wose Kinge, C.N., et al., *Hepatitis C virus genotype 5a subgenomic replicons for evaluation of direct-acting antiviral agents*. Antimicrob Agents Chemother, 2014. **58**(9): p. 5386-94.
93. Yi, M. and S.M. Lemon, *Adaptive mutations producing efficient replication of genotype 1a hepatitis C virus RNA in normal Huh7 cells*. J Virol, 2004. **78**(15): p. 7904-15.
94. Bukh, J., et al., *Mutations that permit efficient replication of hepatitis C virus RNA in Huh-7 cells prevent productive replication in chimpanzees*. Proc Natl Acad Sci U S A, 2002. **99**(22): p. 14416-21.
95. Pietschmann, T., et al., *Production of infectious genotype 1b virus particles in cell culture and impairment by replication enhancing mutations*. PLoS Pathog, 2009. **5**(6): p. e1000475.
96. Bartosch, B. and J. Dubuisson, *Recent advances in hepatitis C virus cell entry*. Viruses, 2010. **2**(3): p. 692-709.
97. Bartosch, B., J. Dubuisson, and F.L. Cosset, *Infectious hepatitis C virus pseudo-particles containing functional E1-E2 envelope protein complexes*. J Exp Med, 2003. **197**(5): p. 633-42.
98. Steinmann, E., et al., *Efficient trans-encapsidation of hepatitis C virus RNAs into infectious virus-like particles*. J Virol, 2008. **82**(14): p. 7034-46.
99. Wakita, T., et al., *Production of infectious hepatitis C virus in tissue culture from a cloned viral genome*. Nat Med, 2005. **11**(7): p. 791-6.
100. Pietschmann, T., et al., *Construction and characterization of infectious intragenotypic and intergenotypic hepatitis C virus chimeras*. Proc Natl Acad Sci U S A, 2006. **103**(19): p. 7408-13.
101. Blaising, J. and E.I. Pecheur, *Lipids: a key for hepatitis C virus entry and a potential target for antiviral strategies*. Biochimie, 2013. **95**(1): p. 96-102.
102. Agnello, V., et al., *Hepatitis C virus and other flaviviridae viruses enter cells via low density lipoprotein receptor*. Proc Natl Acad Sci U S A, 1999. **96**(22): p. 12766-71.

103. Barth, H., et al., *Cellular binding of hepatitis C virus envelope glycoprotein E2 requires cell surface heparan sulfate*. J Biol Chem, 2003. **278**(42): p. 41003-12.
104. Pileri, P., et al., *Binding of hepatitis C virus to CD81*. Science, 1998. **282**(5390): p. 938-41.
105. Scarselli, E., et al., *The human scavenger receptor class B type I is a novel candidate receptor for the hepatitis C virus*. EMBO J, 2002. **21**(19): p. 5017-25.
106. Evans, M.J., et al., *Claudin-1 is a hepatitis C virus co-receptor required for a late step in entry*. Nature, 2007. **446**(7137): p. 801-5.
107. Ploss, A., et al., *Human occludin is a hepatitis C virus entry factor required for infection of mouse cells*. Nature, 2009. **457**(7231): p. 882-6.
108. Blanchard, E., et al., *Hepatitis C virus entry depends on clathrin-mediated endocytosis*. J Virol, 2006. **80**(14): p. 6964-72.
109. Meertens, L., C. Bertaux, and T. Dragic, *Hepatitis C virus entry requires a critical postinternalization step and delivery to early endosomes via clathrin-coated vesicles*. J Virol, 2006. **80**(23): p. 11571-8.
110. Garry, R.F. and S. Dash, *Proteomics computational analyses suggest that hepatitis C virus E1 and pestivirus E2 envelope glycoproteins are truncated class II fusion proteins*. Virology, 2003. **307**(2): p. 255-65.
111. Haid, S., T. Pietschmann, and E.I. Pecheur, *Low pH-dependent hepatitis C virus membrane fusion depends on E2 integrity, target lipid composition, and density of virus particles*. J Biol Chem, 2009. **284**(26): p. 17657-67.
112. Jopling, C.L., K.L. Norman, and P. Sarnow, *Positive and negative modulation of viral and cellular mRNAs by liver-specific microRNA miR-122*. Cold Spring Harb Symp Quant Biol, 2006. **71**: p. 369-76.
113. Romero-Brey, I., et al., *Three-dimensional architecture and biogenesis of membrane structures associated with hepatitis C virus replication*. PLoS Pathog, 2012. **8**(12): p. e1003056.
114. Paul, D., et al., *Morphological and biochemical characterization of the membranous hepatitis C virus replication compartment*. J Virol, 2013. **87**(19): p. 10612-27.
115. Andre, P., et al., *Characterization of low- and very-low-density hepatitis C virus RNA-containing particles*. J Virol, 2002. **76**(14): p. 6919-28.
116. Bartenschlager, R., et al., *Assembly of infectious hepatitis C virus particles*. Trends Microbiol, 2011. **19**(2): p. 95-103.
117. Vieyres, G., J. Dubuisson, and T. Pietschmann, *Incorporation of hepatitis C virus E1 and E2 glycoproteins: the keystones on a peculiar virion*. Viruses, 2014. **6**(3): p. 1149-87.
118. Thomssen, R., S. Bonk, and A. Thiele, *Density heterogeneities of hepatitis C virus in human sera due to the binding of beta-lipoproteins and immunoglobulins*. Med Microbiol Immunol, 1993. **182**(6): p. 329-34.
119. Nielsen, S.U., et al., *Association between hepatitis C virus and very-low-density lipoprotein (VLDL)/LDL analyzed in iodixanol density gradients*. J Virol, 2006. **80**(5): p. 2418-28.
120. Merz, A., et al., *Biochemical and morphological properties of hepatitis C virus particles and determination of their lipidome*. J Biol Chem, 2011. **286**(4): p. 3018-32.
121. Chang, K.S., et al., *Human apolipoprotein e is required for infectivity and production of hepatitis C virus in cell culture*. J Virol, 2007. **81**(24): p. 13783-93.
122. Pecheur, E.I., *Lipoprotein receptors and lipid enzymes in hepatitis C virus entry and early steps of infection*. Scientifica (Cairo), 2012. **2012**: p. 709853.

123. Out, R., et al., *Scavenger receptor class B type I is solely responsible for the selective uptake of cholesteryl esters from HDL by the liver and the adrenals in mice.* J Lipid Res, 2004. **45**(11): p. 2088-95.
124. Albecka, A., et al., *Role of low-density lipoprotein receptor in the hepatitis C virus life cycle.* Hepatology, 2012. **55**(4): p. 998-1007.
125. Sainz, B., Jr., et al., *Identification of the Niemann-Pick C1-like 1 cholesterol absorption receptor as a new hepatitis C virus entry factor.* Nat Med, 2012. **18**(2): p. 281-5.
126. Aizaki, H., et al., *Critical role of virion-associated cholesterol and sphingolipid in hepatitis C virus infection.* J Virol, 2008. **82**(12): p. 5715-24.
127. Aizaki, H., et al., *Characterization of the hepatitis C virus RNA replication complex associated with lipid rafts.* Virology, 2004. **324**(2): p. 450-61.
128. Shi, S.T., et al., *Hepatitis C virus RNA replication occurs on a detergent-resistant membrane that cofractionates with caveolin-2.* J Virol, 2003. **77**(7): p. 4160-8.
129. Khan, I., et al., *Modulation of hepatitis C virus genome replication by glycosphingolipids and four-phosphate adaptor protein 2.* J Virol, 2014. **88**(21): p. 12276-95.
130. Paul, D. and R. Bartenschlager, *Architecture and biogenesis of plus-strand RNA virus replication factories.* World J Virol, 2013. **2**(2): p. 32-48.
131. Blackham, S., et al., *Gene expression profiling indicates the roles of host oxidative stress, apoptosis, lipid metabolism, and intracellular transport genes in the replication of hepatitis C virus.* J Virol, 2010. **84**(10): p. 5404-14.
132. Diamond, D.L., et al., *Temporal proteome and lipidome profiles reveal hepatitis C virus-associated reprogramming of hepatocellular metabolism and bioenergetics.* PLoS Pathog, 2010. **6**(1): p. e1000719.
133. Delang, L., et al., *Statins potentiate the in vitro anti-hepatitis C virus activity of selective hepatitis C virus inhibitors and delay or prevent resistance development.* Hepatology, 2009. **50**(1): p. 6-16.
134. Greenwood, J., L. Steinman, and S.S. Zamvil, *Statin therapy and autoimmune disease: from protein prenylation to immunomodulation.* Nat Rev Immunol, 2006. **6**(5): p. 358-70.
135. Ye, J., et al., *Disruption of hepatitis C virus RNA replication through inhibition of host protein geranylgeranylation.* Proc Natl Acad Sci U S A, 2003. **100**(26): p. 15865-70.
136. Miyanari, Y., et al., *The lipid droplet is an important organelle for hepatitis C virus production.* Nat Cell Biol, 2007. **9**(9): p. 1089-97.
137. Boulant, S., et al., *Hepatitis C virus core protein induces lipid droplet redistribution in a microtubule- and dynein-dependent manner.* Traffic, 2008. **9**(8): p. 1268-82.
138. Boulant, S., P. Targett-Adams, and J. McLauchlan, *Disrupting the association of hepatitis C virus core protein with lipid droplets correlates with a loss in production of infectious virus.* J Gen Virol, 2007. **88**(Pt 8): p. 2204-13.
139. Herker, E., et al., *Efficient hepatitis C virus particle formation requires diacylglycerol acyltransferase-1.* Nat Med, 2010. **16**(11): p. 1295-8.
140. Lehner, R., J. Lian, and A.D. Quiroga, *Luminal lipid metabolism: implications for lipoprotein assembly.* Arterioscler Thromb Vasc Biol, 2012. **32**(5): p. 1087-93.
141. Huang, H., et al., *Hepatitis C virus production by human hepatocytes dependent on assembly and secretion of very low-density lipoproteins.* Proc Natl Acad Sci U S A, 2007. **104**(14): p. 5848-53.

142. Perlemuter, G., et al., *Hepatitis C virus core protein inhibits microsomal triglyceride transfer protein activity and very low density lipoprotein secretion: a model of viral-related steatosis*. *FASEB J*, 2002. **16**(2): p. 185-94.
143. Lee, J.Y., et al., *Apolipoprotein E likely contributes to a maturation step of infectious hepatitis C virus particles and interacts with viral envelope glycoproteins*. *J Virol*, 2014. **88**(21): p. 12422-37.
144. Acosta, E.G., A. Kumar, and R. Bartenschlager, *Revisiting dengue virus-host cell interaction: new insights into molecular and cellular virology*. *Adv Virus Res*, 2014. **88**: p. 1-109.
145. (ed.), R.B., *Hepatitis C virus: From Molecular Virology to Antiviral Therapy*. Current Topics in Microbiology and Immunology 369, Springer-Verlag, 2013.
146. Samsa, M.M., et al., *Dengue virus capsid protein usurps lipid droplets for viral particle formation*. *PLoS Pathog*, 2009. **5**(10): p. e1000632.
147. Heaton, N.S. and G. Randall, *Dengue virus-induced autophagy regulates lipid metabolism*. *Cell Host Microbe*, 2010. **8**(5): p. 422-32.
148. Fischl, W. and R. Bartenschlager, *Exploitation of cellular pathways by Dengue virus*. *Curr Opin Microbiol*, 2011. **14**(4): p. 470-5.
149. Welsch, S., et al., *Composition and three-dimensional architecture of the dengue virus replication and assembly sites*. *Cell Host Microbe*, 2009. **5**(4): p. 365-75.
150. Rocak, S. and P. Linder, *DEAD-box proteins: the driving forces behind RNA metabolism*. *Nat Rev Mol Cell Biol*, 2004. **5**(3): p. 232-41.
151. Schroder, M., *Human DEAD-box protein 3 has multiple functions in gene regulation and cell cycle control and is a prime target for viral manipulation*. *Biochem Pharmacol*, 2010. **79**(3): p. 297-306.
152. Schroder, M., M. Baran, and A.G. Bowie, *Viral targeting of DEAD box protein 3 reveals its role in TBK1/IKKepsilon-mediated IRF activation*. *EMBO J*, 2008. **27**(15): p. 2147-57.
153. Khadka, S., et al., *A physical interaction network of dengue virus and human proteins*. *Mol Cell Proteomics*, 2011. **10**(12): p. M111 012187.
154. Ariumi, Y., et al., *DDX3 DEAD-box RNA helicase is required for hepatitis C virus RNA replication*. *J Virol*, 2007. **81**(24): p. 13922-6.
155. Owsianka, A.M. and A.H. Patel, *Hepatitis C virus core protein interacts with a human DEAD box protein DDX3*. *Virology*, 1999. **257**(2): p. 330-40.
156. Mamiya, N. and H.J. Worman, *Hepatitis C virus core protein binds to a DEAD box RNA helicase*. *J Biol Chem*, 1999. **274**(22): p. 15751-6.
157. Li, Q., et al., *Integrative functional genomics of hepatitis C virus infection identifies host dependencies in complete viral replication cycle*. *PLoS Pathog*, 2014. **10**(5): p. e1004163.
158. Li, Q., et al., *Hepatitis C virus infection activates an innate pathway involving IKK-alpha in lipogenesis and viral assembly*. *Nat Med*, 2013. **19**(6): p. 722-9.
159. Upadya, M.H., J.J. Aweya, and Y.J. Tan, *Understanding the interaction of hepatitis C virus with host DEAD-box RNA helicases*. *World J Gastroenterol*, 2014. **20**(11): p. 2913-26.
160. Diaz-Rohrer, B., K.R. Levental, and I. Levental, *Rafting through traffic: Membrane domains in cellular logistics*. *Biochim Biophys Acta*, 2014. **1838**(12): p. 3003-3013.
161. Holthuis, J.C. and A.K. Menon, *Lipid landscapes and pipelines in membrane homeostasis*. *Nature*, 2014. **510**(7503): p. 48-57.
162. Hullin-Matsuda, F., et al., *Lipid compartmentalization in the endosome system*. *Semin Cell Dev Biol*, 2014. **31**: p. 48-56.

163. Di Paolo, G. and P. De Camilli, *Phosphoinositides in cell regulation and membrane dynamics*. Nature, 2006. **443**(7112): p. 651-7.
164. Bissig, C. and J. Gruenberg, *Lipid sorting and multivesicular endosome biogenesis*. Cold Spring Harb Perspect Biol, 2013. **5**(10): p. a016816.
165. Sasaki, T., et al., *Mammalian phosphoinositide kinases and phosphatases*. Prog Lipid Res, 2009. **48**(6): p. 307-43.
166. Holthuis, J.C. and T.P. Levine, *Lipid traffic: floppy drives and a superhighway*. Nat Rev Mol Cell Biol, 2005. **6**(3): p. 209-20.
167. Mukherjee, S. and F.R. Maxfield, *Role of membrane organization and membrane domains in endocytic lipid trafficking*. Traffic, 2000. **1**(3): p. 203-11.
168. Lev, S., *Non-vesicular lipid transport by lipid-transfer proteins and beyond*. Nat Rev Mol Cell Biol, 2010. **11**(10): p. 739-50.
169. Lee, A.G., *Lipid sorting: lipids do it on their own*. Curr Biol, 2005. **15**(11): p. R421-3.
170. Roux, A., et al., *Role of curvature and phase transition in lipid sorting and fission of membrane tubules*. EMBO J, 2005. **24**(8): p. 1537-45.
171. Brugger, B., et al., *Evidence for segregation of sphingomyelin and cholesterol during formation of COPI-coated vesicles*. J Cell Biol, 2000. **151**(3): p. 507-18.
172. Ikonen, E., *Mechanisms for cellular cholesterol transport: defects and human disease*. Physiol Rev, 2006. **86**(4): p. 1237-61.
173. Helle, S.C., et al., *Organization and function of membrane contact sites*. Biochim Biophys Acta, 2013. **1833**(11): p. 2526-41.
174. Flis, V.V. and G. Daum, *Lipid transport between the endoplasmic reticulum and mitochondria*. Cold Spring Harb Perspect Biol, 2013. **5**(6).
175. Funato, K. and H. Riezman, *Vesicular and nonvesicular transport of ceramide from ER to the Golgi apparatus in yeast*. J Cell Biol, 2001. **155**(6): p. 949-59.
176. Lev, S., *Nonvesicular lipid transfer from the endoplasmic reticulum*. Cold Spring Harb Perspect Biol, 2012. **4**(10).
177. Schulz, T.A., et al., *Lipid-regulated sterol transfer between closely apposed membranes by oxysterol-binding protein homologues*. J Cell Biol, 2009. **187**(6): p. 889-903.
178. Levine, T.P. and S. Munro, *The pleckstrin homology domain of oxysterol-binding protein recognises a determinant specific to Golgi membranes*. Curr Biol, 1998. **8**(13): p. 729-39.
179. Ngo, M. and N.D. Ridgway, *Oxysterol binding protein-related Protein 9 (ORP9) is a cholesterol transfer protein that regulates Golgi structure and function*. Mol Biol Cell, 2009. **20**(5): p. 1388-99.
180. Hanada, K., et al., *Molecular machinery for non-vesicular trafficking of ceramide*. Nature, 2003. **426**(6968): p. 803-9.
181. Peretti, D., et al., *Coordinated lipid transfer between the endoplasmic reticulum and the Golgi complex requires the VAP proteins and is essential for Golgi-mediated transport*. Mol Biol Cell, 2008. **19**(9): p. 3871-84.
182. Mesmin, B., et al., *A four-step cycle driven by PI(4)P hydrolysis directs sterol/PI(4)P exchange by the ER-Golgi tether OSBP*. Cell, 2013. **155**(4): p. 830-43.
183. Lev, S., *The role of the Nir/rdgB protein family in membrane trafficking and cytoskeleton remodeling*. Exp Cell Res, 2004. **297**(1): p. 1-10.
184. Prinz, W.A., *Non-vesicular sterol transport in cells*. Prog Lipid Res, 2007. **46**(6): p. 297-314.

185. Lehto, M. and V.M. Olkkonen, *The OSBP-related proteins: a novel protein family involved in vesicle transport, cellular lipid metabolism, and cell signalling*. Biochim Biophys Acta, 2003. **1631**(1): p. 1-11.
186. Olkkonen, V.M., et al., *The OSBP-related proteins (ORPs): global sterol sensors for co-ordination of cellular lipid metabolism, membrane trafficking and signalling processes?* Biochem Soc Trans, 2006. **34**(Pt 3): p. 389-91.
187. Strating, J.R., et al., *Itraconazole inhibits enterovirus replication by targeting the oxysterol-binding protein*. Cell Rep, 2015. **10**(4): p. 600-15.
188. Rocha, N., et al., *Cholesterol sensor ORP1L contacts the ER protein VAP to control Rab7-RILP-p150 Glued and late endosome positioning*. J Cell Biol, 2009. **185**(7): p. 1209-25.
189. Johansson, M., et al., *The oxysterol-binding protein homologue ORP1L interacts with Rab7 and alters functional properties of late endocytic compartments*. Mol Biol Cell, 2005. **16**(12): p. 5480-92.
190. Du, X., et al., *A role for oxysterol-binding protein-related protein 5 in endosomal cholesterol trafficking*. J Cell Biol, 2011. **192**(1): p. 121-35.
191. Olkkonen, V.M., *OSBP-Related Protein Family in Lipid Transport Over Membrane Contact Sites*. Lipid Insights, 2015. **8**(Suppl 1): p. 1-9.
192. Clark, B.J., *The mammalian START domain protein family in lipid transport in health and disease*. J Endocrinol, 2012. **212**(3): p. 257-75.
193. Strauss, J.F., 3rd, et al., *START domain proteins and the intracellular trafficking of cholesterol in steroidogenic cells*. Mol Cell Endocrinol, 2003. **202**(1-2): p. 59-65.
194. Zhang, M., et al., *MLN64 mediates mobilization of lysosomal cholesterol to steroidogenic mitochondria*. J Biol Chem, 2002. **277**(36): p. 33300-10.
195. Mesmin, B., et al., *STARD4 abundance regulates sterol transport and sensing*. Mol Biol Cell, 2011. **22**(21): p. 4004-15.
196. Ioannou, Y.A., *Guilty until proven innocent: the case of NPC1 and cholesterol*. Trends Biochem Sci, 2005. **30**(9): p. 498-505.
197. Liscum, L., R.M. Ruggiero, and J.R. Faust, *The intracellular transport of low density lipoprotein-derived cholesterol is defective in Niemann-Pick type C fibroblasts*. J Cell Biol, 1989. **108**(5): p. 1625-36.
198. Vanier, M.T., *Niemann-Pick disease type C*. Orphanet J Rare Dis, 2010. **5**: p. 16.
199. M. Patterson, M.V., K. Suzuki, J.A. Morris, E. Carstea, E. Neufeld, J. Blanchette-Mackie, P. Pentchev, *Niemann-Pick Disease Type C: A lipid trafficking disorder*. Gene Reviews, 2013.
200. Pentchev, P.G., et al., *A defect in cholesterol esterification in Niemann-Pick disease (type C) patients*. Proc Natl Acad Sci U S A, 1985. **82**(23): p. 8247-51.
201. Ikonen, E. and M. Holtta-Vuori, *Cellular pathology of Niemann-Pick type C disease*. Semin Cell Dev Biol, 2004. **15**(4): p. 445-54.
202. Sturley, S.L., et al., *The pathophysiology and mechanisms of NP-C disease*. Biochim Biophys Acta, 2004. **1685**(1-3): p. 83-7.
203. Holtta-Vuori, M. and E. Ikonen, *Endosomal cholesterol traffic: vesicular and non-vesicular mechanisms meet*. Biochem Soc Trans, 2006. **34**(Pt 3): p. 392-4.
204. Strauss, J.F., 3rd, et al., *Sterols and intracellular vesicular trafficking: lessons from the study of NPC1*. Steroids, 2002. **67**(12): p. 947-51.
205. Neufeld, E.B., et al., *The Niemann-Pick C1 protein resides in a vesicular compartment linked to retrograde transport of multiple lysosomal cargo*. J Biol Chem, 1999. **274**(14): p. 9627-35.

206. Millard, E.E., et al., *The sterol-sensing domain of the Niemann-Pick C1 (NPC1) protein regulates trafficking of low density lipoprotein cholesterol*. J Biol Chem, 2005. **280**(31): p. 28581-90.
207. Infante, R.E., et al., *NPC2 facilitates bidirectional transfer of cholesterol between NPC1 and lipid bilayers, a step in cholesterol egress from lysosomes*. Proc Natl Acad Sci U S A, 2008. **105**(40): p. 15287-92.
208. Millard, E.E., et al., *Niemann-pick type C1 (NPC1) overexpression alters cellular cholesterol homeostasis*. J Biol Chem, 2000. **275**(49): p. 38445-51.
209. Yu, X.H., et al., *NPC1, intracellular cholesterol trafficking and atherosclerosis*. Clin Chim Acta, 2014. **429**: p. 69-75.
210. Ko, D.C., et al., *Dynamic movements of organelles containing Niemann-Pick C1 protein: NPC1 involvement in late endocytic events*. Mol Biol Cell, 2001. **12**(3): p. 601-14.
211. Lebrand, C., et al., *Late endosome motility depends on lipids via the small GTPase Rab7*. EMBO J, 2002. **21**(6): p. 1289-300.
212. Zervas, M., K. Dobrenis, and S.U. Walkley, *Neurons in Niemann-Pick disease type C accumulate gangliosides as well as unesterified cholesterol and undergo dendritic and axonal alterations*. J Neuropathol Exp Neurol, 2001. **60**(1): p. 49-64.
213. Tabas, I., *Consequences of cellular cholesterol accumulation: basic concepts and physiological implications*. J Clin Invest, 2002. **110**(7): p. 905-11.
214. Ikonen, E., *Cellular cholesterol trafficking and compartmentalization*. Nat Rev Mol Cell Biol, 2008. **9**(2): p. 125-38.
215. Sharpe, L.J., et al., *The UPS and downs of cholesterol homeostasis*. Trends Biochem Sci, 2014. **39**(11): p. 527-35.
216. Trapani, L., M. Segatto, and V. Pallottini, *Regulation and deregulation of cholesterol homeostasis: The liver as a metabolic "power station"*. World J Hepatol, 2012. **4**(6): p. 184-90.
217. Soccio, R.E. and J.L. Breslow, *Intracellular cholesterol transport*. Arterioscler Thromb Vasc Biol, 2004. **24**(7): p. 1150-60.
218. Brown, A.J., et al., *Cholesterol addition to ER membranes alters conformation of SCAP, the SREBP escort protein that regulates cholesterol metabolism*. Mol Cell, 2002. **10**(2): p. 237-45.
219. Radhakrishnan, A., et al., *Switch-like control of SREBP-2 transport triggered by small changes in ER cholesterol: a delicate balance*. Cell Metab, 2008. **8**(6): p. 512-21.
220. Yang, T., et al., *Crucial step in cholesterol homeostasis: sterols promote binding of SCAP to INSIG-1, a membrane protein that facilitates retention of SREBPs in ER*. Cell, 2002. **110**(4): p. 489-500.
221. Horton, J.D., et al., *Combined analysis of oligonucleotide microarray data from transgenic and knockout mice identifies direct SREBP target genes*. Proc Natl Acad Sci U S A, 2003. **100**(21): p. 12027-32.
222. Sugii, S., et al., *Distinct endosomal compartments in early trafficking of low density lipoprotein-derived cholesterol*. J Biol Chem, 2003. **278**(29): p. 27180-9.
223. Accad, M. and R.V. Farese, Jr., *Cholesterol homeostasis: a role for oxysterols*. Curr Biol, 1998. **8**(17): p. R601-4.
224. Boadu, E., R.C. Nelson, and G.A. Francis, *ABCA1-dependent mobilization of lysosomal cholesterol requires functional Niemann-Pick C2 but not Niemann-Pick C1 protein*. Biochim Biophys Acta, 2012. **1821**(3): p. 396-404.

225. Chen, W., et al., *Preferential ATP-binding cassette transporter A1-mediated cholesterol efflux from late endosomes/lysosomes*. J Biol Chem, 2001. **276**(47): p. 43564-9.
226. Lehmann, J.M., et al., *Activation of the nuclear receptor LXR by oxysterols defines a new hormone response pathway*. J Biol Chem, 1997. **272**(6): p. 3137-40.
227. Venkateswaran, A., et al., *Control of cellular cholesterol efflux by the nuclear oxysterol receptor LXR alpha*. Proc Natl Acad Sci U S A, 2000. **97**(22): p. 12097-102.
228. Bartz, R., et al., *Lipidomics reveals that adiposomes store ether lipids and mediate phospholipid traffic*. J Lipid Res, 2007. **48**(4): p. 837-47.
229. Guo, Y., et al., *Lipid droplets at a glance*. J Cell Sci, 2009. **122**(Pt 6): p. 749-52.
230. Saka, H.A. and R. Valdivia, *Emerging roles for lipid droplets in immunity and host-pathogen interactions*. Annu Rev Cell Dev Biol, 2012. **28**: p. 411-37.
231. Martin, S. and R.G. Parton, *Lipid droplets: a unified view of a dynamic organelle*. Nat Rev Mol Cell Biol, 2006. **7**(5): p. 373-8.
232. Farese, R.V., Jr. and T.C. Walther, *Lipid droplets finally get a little R-E-S-P-E-C-T*. Cell, 2009. **139**(5): p. 855-60.
233. Fujimoto, T. and R.G. Parton, *Not just fat: the structure and function of the lipid droplet*. Cold Spring Harb Perspect Biol, 2011. **3**(3).
234. Bickel, P.E., J.T. Tansey, and M.A. Welte, *PAT proteins, an ancient family of lipid droplet proteins that regulate cellular lipid stores*. Biochim Biophys Acta, 2009. **1791**(6): p. 419-40.
235. Bulankina, A.V., et al., *TIP47 functions in the biogenesis of lipid droplets*. J Cell Biol, 2009. **185**(4): p. 641-55.
236. Guo, Y., et al., *Functional genomic screen reveals genes involved in lipid-droplet formation and utilization*. Nature, 2008. **453**(7195): p. 657-61.
237. Beller, M., et al., *COPI complex is a regulator of lipid homeostasis*. PLoS Biol, 2008. **6**(11): p. e292.
238. Graham, F.L., et al., *Characteristics of a human cell line transformed by DNA from human adenovirus type 5*. J Gen Virol, 1977. **36**(1): p. 59-74.
239. Friebe, P., et al., *Kissing-loop interaction in the 3' end of the hepatitis C virus genome essential for RNA replication*. J Virol, 2005. **79**(1): p. 380-92.
240. Koutsoudakis, G., et al., *Characterization of the early steps of hepatitis C virus infection by using luciferase reporter viruses*. J Virol, 2006. **80**(11): p. 5308-20.
241. Jo, J., et al., *Analysis of CD8+ T-cell-mediated inhibition of hepatitis C virus replication using a novel immunological model*. Gastroenterology, 2009. **136**(4): p. 1391-401.
242. Backes, P., et al., *Role of annexin A2 in the production of infectious hepatitis C virus particles*. J Virol, 2010. **84**(11): p. 5775-89.
243. Shaner, N.C., et al., *Improving the photostability of bright monomeric orange and red fluorescent proteins*. Nat Methods, 2008. **5**(6): p. 545-51.
244. Mosca, J.D. and P.M. Pitha, *Transcriptional and posttranscriptional regulation of exogenous human beta interferon gene in simian cells defective in interferon synthesis*. Mol Cell Biol, 1986. **6**(6): p. 2279-83.
245. C., S., *The method of right and wrong cases (Constant stimuli) without Gauss's formulae*. British Journal of Psychology, 1908. **2**(227-242).
246. Whittaker, R., et al., *Identification of MicroRNAs that control lipid droplet formation and growth in hepatocytes via high-content screening*. J Biomol Screen, 2010. **15**(7): p. 798-805.

247. Parent, R., et al., *The heat shock cognate protein 70 is associated with hepatitis C virus particles and modulates virus infectivity*. Hepatology, 2009. **49**(6): p. 1798-809.
248. Szymanski, K.M., et al., *The lipodystrophy protein seipin is found at endoplasmic reticulum lipid droplet junctions and is important for droplet morphology*. Proc Natl Acad Sci U S A, 2007. **104**(52): p. 20890-5.
249. Eastman, S.W., M. Yassaee, and P.D. Bieniasz, *A role for ubiquitin ligases and Spartin/SPG20 in lipid droplet turnover*. J Cell Biol, 2009. **184**(6): p. 881-94.
250. Berger, K.L., et al., *Roles for endocytic trafficking and phosphatidylinositol 4-kinase III alpha in hepatitis C virus replication*. Proc Natl Acad Sci U S A, 2009. **106**(18): p. 7577-82.
251. Schroeder, F., J.F. Holland, and L.L. Bieber, *Fluorometric evidence for the binding of cholesterol to the filipin complex*. J Antibiot (Tokyo), 1971. **24**(12): p. 846-9.
252. Muller, C.P., et al., *Filipin as a flow microfluorometry probe for cellular cholesterol*. Cytometry, 1984. **5**(1): p. 42-54.
253. Holtta-Vuori, M., et al., *Modulation of cellular cholesterol transport and homeostasis by Rab11*. Mol Biol Cell, 2002. **13**(9): p. 3107-22.
254. Berger, C., et al., *Daclatasvir-like inhibitors of NS5A block early biogenesis of hepatitis C virus-induced membranous replication factories, independent of RNA replication*. Gastroenterology, 2014. **147**(5): p. 1094-105 e25.
255. Filipe, A. and J. McLauchlan, *Hepatitis C virus and lipid droplets: finding a niche*. Trends Mol Med, 2015. **21**(1): p. 34-42.
256. Fujimoto, Y., et al., *Involvement of ACSL in local synthesis of neutral lipids in cytoplasmic lipid droplets in human hepatocyte HuH7*. J Lipid Res, 2007. **48**(6): p. 1280-92.
257. Amberkar, S., et al., *High-throughput RNA interference screens integrative analysis: Towards a comprehensive understanding of the virus-host interplay*. World J Virol, 2013. **2**(2): p. 18-31.
258. Tai, A.W., et al., *A functional genomic screen identifies cellular cofactors of hepatitis C virus replication*. Cell Host Microbe, 2009. **5**(3): p. 298-307.
259. Ward, A.M., et al., *Quantitative mass spectrometry of DENV-2 RNA-interacting proteins reveals that the DEAD-box RNA helicase DDX6 binds the DB1 and DB2 3' UTR structures*. RNA Biol, 2011. **8**(6): p. 1173-86.
260. Angus, A.G., et al., *Requirement of cellular DDX3 for hepatitis C virus replication is unrelated to its interaction with the viral core protein*. J Gen Virol, 2010. **91**(Pt 1): p. 122-32.
261. Sun, C., et al., *Hepatitis C virus core-derived peptides inhibit genotype 1b viral genome replication via interaction with DDX3X*. PLoS One, 2010. **5**(9).
262. Woerz, I., *Improvement of the Hepatitis C Virus cell culture system and application for a siRNA-based human kinome screen*. PhD Thesis, 2010.
263. Linder, P. and E. Jankowsky, *From unwinding to clamping - the DEAD box RNA helicase family*. Nat Rev Mol Cell Biol, 2011. **12**(8): p. 505-16.
264. Shavinskaya, A., et al., *The lipid droplet binding domain of hepatitis C virus core protein is a major determinant for efficient virus assembly*. J Biol Chem, 2007. **282**(51): p. 37158-69.
265. Ferraris, P., et al., *Sequential biogenesis of host cell membrane rearrangements induced by hepatitis C virus infection*. Cell Mol Life Sci, 2013. **70**(7): p. 1297-306.
266. Ferraris, P., E. Blanchard, and P. Roingeard, *Ultrastructural and biochemical analyses of hepatitis C virus-associated host cell membranes*. J Gen Virol, 2010. **91**(Pt 9): p. 2230-7.

267. Holtta-Vuori, M., et al., *BODIPY-cholesterol: a new tool to visualize sterol trafficking in living cells and organisms*. Traffic, 2008. **9**(11): p. 1839-49.
268. Neef, A.B. and C. Schultz, *Selective fluorescence labeling of lipids in living cells*. Angew Chem Int Ed Engl, 2009. **48**(8): p. 1498-500.
269. Wolk, B., et al., *A dynamic view of hepatitis C virus replication complexes*. J Virol, 2008. **82**(21): p. 10519-31.
270. D'Angelo, G., et al., *Glycosphingolipid synthesis requires FAPP2 transfer of glucosylceramide*. Nature, 2007. **449**(7158): p. 62-7.
271. Boadu, E. and G.A. Francis, *The role of vesicular transport in ABCA1-dependent lipid efflux and its connection with NPC pathways*. J Mol Med (Berl), 2006. **84**(4): p. 266-75.
272. Hynynen, R., et al., *OSBP-related protein 2 is a sterol receptor on lipid droplets that regulates the metabolism of neutral lipids*. J Lipid Res, 2009. **50**(7): p. 1305-15.
273. Jansen, M., et al., *Role of ORPs in sterol transport from plasma membrane to ER and lipid droplets in mammalian cells*. Traffic, 2011. **12**(2): p. 218-31.
274. Lehto, M., et al., *Targeting of OSBP-related protein 3 (ORP3) to endoplasmic reticulum and plasma membrane is controlled by multiple determinants*. Exp Cell Res, 2005. **310**(2): p. 445-62.
275. Zhou, Y., et al., *OSBP-related protein 11 (ORP11) dimerizes with ORP9 and localizes at the Golgi-late endosome interface*. Exp Cell Res, 2010. **316**(19): p. 3304-16.
276. Mesmin, B. and F.R. Maxfield, *Intracellular sterol dynamics*. Biochim Biophys Acta, 2009. **1791**(7): p. 636-45.
277. Nissila, E., et al., *ORP10, a cholesterol binding protein associated with microtubules, regulates apolipoprotein B-100 secretion*. Biochim Biophys Acta, 2012. **1821**(12): p. 1472-84.
278. Lehto, M., et al., *Subfamily III of mammalian oxysterol-binding protein (OSBP) homologues: the expression and intracellular localization of ORP3, ORP6, and ORP7*. Cell Tissue Res, 2004. **315**(1): p. 39-57.
279. Apy, F., et al., *The steroidogenic acute regulatory protein homolog MLN64, a late endosomal cholesterol-binding protein*. J Biol Chem, 2001. **276**(6): p. 4261-9.
280. Amako, Y., G.H. Syed, and A. Siddiqui, *Protein kinase D negatively regulates hepatitis C virus secretion through phosphorylation of oxysterol-binding protein and ceramide transfer protein*. J Biol Chem, 2011. **286**(13): p. 11265-74.
281. Carette, J.E., et al., *Ebola virus entry requires the cholesterol transporter Niemann-Pick C1*. Nature, 2011. **477**(7364): p. 340-3.
282. Cenedella, R.J., *Cholesterol synthesis inhibitor U18666A and the role of sterol metabolism and trafficking in numerous pathophysiological processes*. Lipids, 2009. **44**(6): p. 477-87.
283. Harmala, A.S., et al., *Cholesterol transport from plasma membranes to intracellular membranes is inhibited by 3 beta-[2-(diethylamino)ethoxy]androst-5-en-17-one*. Biochim Biophys Acta, 1994. **1211**(3): p. 317-25.
284. Ohgami, N., et al., *Binding between the Niemann-Pick C1 protein and a photoactivatable cholesterol analog requires a functional sterol-sensing domain*. Proc Natl Acad Sci U S A, 2004. **101**(34): p. 12473-8.
285. Shoemaker, C.J., et al., *Multiple cationic amphiphiles induce a Niemann-Pick C phenotype and inhibit Ebola virus entry and infection*. PLoS One, 2013. **8**(2): p. e56265.
286. Endo, A., *The discovery and development of HMG-CoA reductase inhibitors*. J Lipid Res, 1992. **33**(11): p. 1569-82.

287. Simons, K. and E. Ikonen, *Functional rafts in cell membranes*. *Nature*, 1997. **387**(6633): p. 569-72.
288. Van Heyningen, W.E., S. Van Heyningen, and C.A. King, *The nature and action of cholera toxin*. *Ciba Found Symp*, 1976(42): p. 73-88.
289. Yachi, R., et al., *Subcellular localization of sphingomyelin revealed by two toxin-based probes in mammalian cells*. *Genes Cells*, 2012. **17**(8): p. 720-7.
290. Jackson, A.L. and P.S. Linsley, *Recognizing and avoiding siRNA off-target effects for target identification and therapeutic application*. *Nat Rev Drug Discov*, 2010. **9**(1): p. 57-67.
291. Healthcare, G., *Off-target Effects: Disturbing the silence of RNA interference (RNAi)*. Tech-Note, 2014.
292. Chang, T.Y., et al., *Acyl-coenzyme A:cholesterol acyltransferases*. *Am J Physiol Endocrinol Metab*, 2009. **297**(1): p. E1-9.
293. Liu, Q., et al., *Acyl-CoA:diacylglycerol acyltransferase: molecular biology, biochemistry and biotechnology*. *Prog Lipid Res*, 2012. **51**(4): p. 350-77.
294. Matto, M., et al., *Role for ADP ribosylation factor 1 in the regulation of hepatitis C virus replication*. *J Virol*, 2011. **85**(2): p. 946-56.
295. Li, H., et al., *Hepatitis C virus NS5A hijacks ARFGAP1 to maintain a phosphatidylinositol 4-phosphate-enriched microenvironment*. *J Virol*, 2014. **88**(11): p. 5956-66.
296. Hsu, N.Y., et al., *Viral reorganization of the secretory pathway generates distinct organelles for RNA replication*. *Cell*, 2010. **141**(5): p. 799-811.
297. Dorobantu, C.M., et al., *Recruitment of PI4KIIIbeta to coxsackievirus B3 replication organelles is independent of ACBD3, GBF1, and Arf1*. *J Virol*, 2014. **88**(5): p. 2725-36.
298. Soni, K.G., et al., *Coatomer-dependent protein delivery to lipid droplets*. *J Cell Sci*, 2009. **122**(Pt 11): p. 1834-41.
299. Liefhebber, J.M., et al., *Modulation of triglyceride and cholesterol ester synthesis impairs assembly of infectious hepatitis C virus*. *J Biol Chem*, 2014. **289**(31): p. 21276-88.
300. Cermelli, S., et al., *The lipid-droplet proteome reveals that droplets are a protein-storage depot*. *Curr Biol*, 2006. **16**(18): p. 1783-95.
301. Poenisch, M., et al., *Identification of HNRNPK as regulator of hepatitis C virus particle production*. *PLoS Pathog*, 2015. **11**(1): p. e1004573.
302. Felmler, D.J., et al., *Hepatitis C virus, cholesterol and lipoproteins--impact for the viral life cycle and pathogenesis of liver disease*. *Viruses*, 2013. **5**(5): p. 1292-324.
303. Negro, F., *Hepatitis C virus-induced steatosis: an overview*. *Dig Dis*, 2010. **28**(1): p. 294-9.
304. Cheung, W., et al., *Rotaviruses associate with cellular lipid droplet components to replicate in viroplasm, and compounds disrupting or blocking lipid droplets inhibit viroplasm formation and viral replication*. *J Virol*, 2010. **84**(13): p. 6782-98.
305. Coffey, C.M., et al., *Reovirus outer capsid protein micro1 induces apoptosis and associates with lipid droplets, endoplasmic reticulum, and mitochondria*. *J Virol*, 2006. **80**(17): p. 8422-38.
306. Helbig, K.J., et al., *The antiviral protein viperin inhibits hepatitis C virus replication via interaction with nonstructural protein 5A*. *Hepatology*, 2011. **54**(5): p. 1506-17.
307. Helbig, K.J., et al., *Viperin is induced following dengue virus type-2 (DENV-2) infection and has anti-viral actions requiring the C-terminal end of viperin*. *PLoS Negl Trop Dis*, 2013. **7**(4): p. e2178.

308. DeVita, R.J. and S. Pinto, *Current status of the research and development of diacylglycerol O-acyltransferase 1 (DGAT1) inhibitors*. J Med Chem, 2013. **56**(24): p. 9820-5.
309. Miyamoto, M., et al., *Comparison between subgenomic replicons of hepatitis C virus genotypes 2a (JFH-1) and 1b (Con1 NK5.1)*. Intervirology, 2006. **49**(1-2): p. 37-43.
310. Saeed, M., et al., *SEC14L2 enables pan-genotype HCV replication in cell culture*. Nature, 2015. **524**(7566): p. 471-5.
311. Cavnignac, Y., et al., *The Cellular Proteins Grb2 and DDX3 Are Increased upon Human Cytomegalovirus Infection and Act in a Proviral Fashion*. PLoS One, 2015. **10**(6): p. e0131614.
312. Wang, H., S. Kim, and W.S. Ryu, *DDX3 DEAD-Box RNA helicase inhibits hepatitis B virus reverse transcription by incorporation into nucleocapsids*. J Virol, 2009. **83**(11): p. 5815-24.
313. Ko, C., et al., *DDX3 DEAD-box RNA helicase is a host factor that restricts hepatitis B virus replication at the transcriptional level*. J Virol, 2014. **88**(23): p. 13689-98.
314. Harris, D., et al., *Identification of cellular factors associated with the 3'-nontranslated region of the hepatitis C virus genome*. Mol Cell Proteomics, 2006. **5**(6): p. 1006-18.
315. Ariumi, Y., *Multiple functions of DDX3 RNA helicase in gene regulation, tumorigenesis, and viral infection*. Front Genet, 2014. **5**: p. 423.
316. Li, G., et al., *DEAD-box RNA helicase DDX3X inhibits DENV replication via regulating type one interferon pathway*. Biochem Biophys Res Commun, 2015. **456**(1): p. 327-32.
317. Keskinen, P., et al., *Impaired antiviral response in human hepatoma cells*. Virology, 1999. **263**(2): p. 364-75.
318. Ahmad, S. and S. Hur, *Helicases in Antiviral Immunity: Dual Properties as Sensors and Effectors*. Trends Biochem Sci, 2015. **40**(10): p. 576-85.
319. Soulat, D., et al., *The DEAD-box helicase DDX3X is a critical component of the TANK-binding kinase 1-dependent innate immune response*. EMBO J, 2008. **27**(15): p. 2135-46.
320. Oshiumi, H., et al., *DEAD/H BOX 3 (DDX3) helicase binds the RIG-I adaptor IPS-1 to up-regulate IFN-beta-inducing potential*. Eur J Immunol, 2010. **40**(4): p. 940-8.
321. Moriya, K., et al., *Hepatitis C virus core protein induces hepatic steatosis in transgenic mice*. J Gen Virol, 1997. **78 (Pt 7)**: p. 1527-31.
322. Chatel-Chaix, L., et al., *A host YB-1 ribonucleoprotein complex is hijacked by hepatitis C virus for the control of NS3-dependent particle production*. J Virol, 2013. **87**(21): p. 11704-20.
323. Vassilaki, N., et al., *Role of the hepatitis C virus core+1 open reading frame and core cis-acting RNA elements in viral RNA translation and replication*. J Virol, 2008. **82**(23): p. 11503-15.
324. Hirata, Y., et al., *Self-enhancement of hepatitis C virus replication by promotion of specific sphingolipid biosynthesis*. PLoS Pathog, 2012. **8**(8): p. e1002860.
325. Brown, D.A. and E. London, *Structure and function of sphingolipid- and cholesterol-rich membrane rafts*. J Biol Chem, 2000. **275**(23): p. 17221-4.
326. Field, F.J., E. Born, and S.N. Mathur, *Triacylglycerol-rich lipoprotein cholesterol is derived from the plasma membrane in CaCo-2 cells*. J Lipid Res, 1995. **36**(12): p. 2651-60.
327. Roulin, P.S., et al., *Rhinovirus uses a phosphatidylinositol 4-phosphate/cholesterol counter-current for the formation of replication compartments at the ER-Golgi interface*. Cell Host Microbe, 2014. **16**(5): p. 677-90.

328. Barajas, D., et al., *Co-opted oxysterol-binding ORP and VAP proteins channel sterols to RNA virus replication sites via membrane contact sites*. PLoS Pathog, 2014. **10**(10): p. e1004388.
329. Amako, Y., et al., *Role of oxysterol binding protein in hepatitis C virus infection*. J Virol, 2009. **83**(18): p. 9237-46.
330. Mukherjee, S. and F.R. Maxfield, *Lipid and cholesterol trafficking in NPC*. Biochim Biophys Acta, 2004. **1685**(1-3): p. 28-37.
331. Cote, M., et al., *Small molecule inhibitors reveal Niemann-Pick C1 is essential for Ebola virus infection*. Nature, 2011. **477**(7364): p. 344-8.
332. Syed, G.H., et al., *Hepatitis C virus stimulates low-density lipoprotein receptor expression to facilitate viral propagation*. J Virol, 2014. **88**(5): p. 2519-29.
333. Lu, F., et al., *Identification of NPC1 as the target of U18666A, an inhibitor of lysosomal cholesterol export and Ebola infection*. Elife, 2015. **4**.
334. Anderson, N. and J. Borlak, *Drug-induced phospholipidosis*. FEBS Lett, 2006. **580**(23): p. 5533-40.
335. Simons, K. and R. Ehehalt, *Cholesterol, lipid rafts, and disease*. J Clin Invest, 2002. **110**(5): p. 597-603.
336. Schulze, H. and K. Sandhoff, *Lysosomal lipid storage diseases*. Cold Spring Harb Perspect Biol, 2011. **3**(6).
337. Albulescu, L., et al., *Cholesterol shuttling is important for RNA replication of coxsackievirus B3 and encephalomyocarditis virus*. Cell Microbiol, 2015. **17**(8): p. 1144-56.
338. Zhang, M., et al., *Cessation of rapid late endosomal tubulovesicular trafficking in Niemann-Pick type C1 disease*. Proc Natl Acad Sci U S A, 2001. **98**(8): p. 4466-71.
339. Sakamoto, H., et al., *Host sphingolipid biosynthesis as a target for hepatitis C virus therapy*. Nat Chem Biol, 2005. **1**(6): p. 333-7.
340. Huang, J.T., et al., *Hepatitis C virus replication is modulated by the interaction of nonstructural protein NS5B and fatty acid synthase*. J Virol, 2013. **87**(9): p. 4994-5004.
341. Yu, G.Y., et al., *Palmitoylation and polymerization of hepatitis C virus NS4B protein*. J Virol, 2006. **80**(12): p. 6013-23.
342. Paul, D., R. Bartenschlager, and C. McCormick, *The predominant species of nonstructural protein 4B in hepatitis C virus-replicating cells is not palmitoylated*. J Gen Virol, 2015. **96**(Pt 7): p. 1696-701.
343. Fantini, J. and F.J. Barrantes, *How cholesterol interacts with membrane proteins: an exploration of cholesterol-binding sites including CRAC, CARC, and tilted domains*. Front Physiol, 2013. **4**: p. 31.
344. Quinkert, D., R. Bartenschlager, and V. Lohmann, *Quantitative analysis of the hepatitis C virus replication complex*. J Virol, 2005. **79**(21): p. 13594-605.
345. Du, X. and H. Yang, *Endosomal cholesterol trafficking: protein factors at a glance*. Acta Biochim Biophys Sin (Shanghai), 2013. **45**(1): p. 11-7.
346. Alpy, F., et al., *STARD3 or STARD3NL and VAP form a novel molecular tether between late endosomes and the ER*. J Cell Sci, 2013. **126**(Pt 23): p. 5500-12.
347. Alvisi, G., V. Madan, and R. Bartenschlager, *Hepatitis C virus and host cell lipids: an intimate connection*. RNA Biol, 2011. **8**(2): p. 258-69.

8 Publications and presentations

8.1 Publications

Ji-Young Lee, Eliana G. Acosta, **Ina K. Stoeck**, Gang Long, Marie-Sophie Hiet, Stephanie Kallis, Francois Penin and Ralf Bartenschlager *Apolipoprotein E likely contributes to a maturation step of infectious hepatitis C virus particles and interacts with viral envelope glycoproteins*. J Virol, 2014. **88**(21): p. 12422-37.

8.2 Oral Presentations

27th international conference on Antiviral Research (ICAR). Raleigh, NC, US 12-16 May 2014: Identification of Host Factors Involved in Lipid Droplet Homeostasis and the Replication of Hepatitis C and Dengue Virus by RNAi Screening. **Ina K. Stoeck**, Gualtiero Alvisi, Sandeep Amberkar, Narsis Kiani, Christoph Sommer, Wolfgang Fischl, Marion Poenisch, Fred A. Hamprecht, Giorgio Palu, Lars Kaderali, Ralf Bartenschlager

8.3 Poster presentations

27th international conference on Antiviral Research (ICAR). Raleigh, NC, US 12-16 May 2014: Identification of Host Factors Involved in Lipid Droplet Homeostasis and the Replication of Hepatitis C and Dengue Virus by RNAi Screening. **Ina K. Stoeck**, Gualtiero Alvisi, Sandeep Amberkar, Narsis Kiani, Christoph Sommer, Wolfgang Fischl, Marion Poenisch, Fred A. Hamprecht, Giorgio Palu, Lars Kaderali, Ralf Bartenschlager
(winner of 2nd poster prize, category “Graduate Students”)

22nd International Symposium on HCV and Related Viruses. Strasbourg, 9-13 October 2015: *The role of lipid transfer proteins in Hepatitis C virus replication*. **Ina K. Stoeck**, David Paul, Ines Romero-Brey, Marion Poenisch, Lars Kaderali, Ralf Bartenschlager

